DEVELOPMENT OF POROSITY GRADIENT BIOGLASS CERAMIC SCAFFOLD

A Thesis Submitted in Partial Fulfillment of the

Requirements for the Degree of

MASTER OF TECHNOLOGY (RESEARCH)

In

CERAMIC ENGINEERING

By

EZHIL VENUSWARAN.R.R.

(Roll No: 611CR301)

Under the guidance of

Prof. SUMIT KUMAR PAL

Department of Ceramic Engineering
National Institute of Technology, Rourkela

AUGUST 2015

I would like to dedicate

this research thesis

to my parents

NATIONAL INSTITUTE OF TECHNOLOGY

Rourkela – 769008

CERTIFICATE

This is to certify that the thesis entitled, "**Porosity Gradient Bioglass Ceramic Scaffold**" submitted by **Mr. Ezhil Venuswaran.R.R**. in partial fulfillment of the requirement for the award of **Master of Technology (Research) Degree** in **Ceramic Engineering**, from the Department of Ceramic Engineering, National Institute of Technology Rourkela is an authentic work carried out by him under my supervision and guidance.

To the best of my knowledge, the matter embodied in this thesis has not submitted in any other University/Institute for the award of any degree or diploma.

Date:

Prof. SUMIT KUMAR PAL
Department of Ceramic Engineering
National Institute of Technology
Rourkela - 769008

Declaration

I declare that this thesis is my own work and has not submitted in any form for another degree or diploma at any university or any other institution of tertiary education. Information derived from the published and unpublished work of others has been acknowledged in the text and the list of references had been enclosed.

Date: (EZHIL VENUSWARAN.R.R.)

ABSTRACT

In order to cure critical size bone defects, three dimensional scaffolds are required. The bone has a functionally graded structure, with the outer cortical bone having with 10-15% of porosity and inner cancellous bone possess 50-90% of porosity. Thus functionally graded scaffolds, fabricated with Class A biomaterial can be the better therapeutic design for curing critical size bone defects. In this work, an attempt had been made to develop porosity gradient bioglass scaffold. 45S5 bioglass and other two glasses, viz. 2P (with 2 wt.% P_2O_5) & 4P (with 4 wt.% P_2O_5) had been chosen to fabricate the scaffold. The bioactive glasses had been synthesized by melt quench method. Differential Scanning Calorimetry and Dilatometric study had been carried out to observe the thermal and sintering behavior of these bioactive glasses. Cytotoxicity, Haemocompatibility and Protein Absorption studies had been carried out on bioactive glasses as well as on sintered glass product. Porous scaffold preparation has been achieved using naphthalene as a pore former (0 wt.%, 30 wt.% & 50 wt.%), shaping by uniaxial pressing followed by sintering. Initially, single layer porous scaffolds had been fabricated and sintered at 800°C, 850°C & 900°C. Apparent porosity and bulk density had been measured for those single layer scaffolds and XRD phase analysis had been carried out. Diametral Tensile strength and flexural strength of those single layer scaffolds had been evaluated. Functionally graded scaffolds had been fabricated by incorporating 0wt.% naphthalene on outer layer and 30 wt.% & 50wt.% naphthalene on the inner layer, which had been sintered at 800°C, 850°C & 900°C. Apparent porosity and bulk density had been measured for the entire FGM system and graded layers separately. Splitting tensile strength had been calculated for the functionally graded scaffolds. Cell viability had been evaluated on those functionally graded scaffolds. The functionally graded scaffolds had been soaked in SBF for 1, 4, 7 & 14 days to observe the carbonated hydroxyapatite layer formation.

ACKNOWLEDGEMENTS

I wish to express my sincere thanks and regards to my supervisor Prof. Sumit Kumar Pal for his continuous guidance and support throughout my M.Tech (Research) program. I have to thank scholars of my research group Hara Prasad Murthy, Pinky Dey & Aishwarya Dash, with whom I had joined hands and solved many technical problems during the course of my research project.

I wish to convey my greetings to Prof. B.B.Nayak, Head of the department, Department of Ceramic Engineering, NIT Rourkela, who had provided full-fletched infrastructure to carry out my research experiments. It's inevitable to thank the faculty members of my department, Prof.Santanu Bhattacharya, Prof.Japes Bera, Prof.R.Sarkar, Prof.S.K.Behera, Prof.S.K.Prathihar, Prof.Sunipa Bhattacharya, Prof.Sudip Dasgupta, Prof.R.Mazumdar, Prof.Arun Choudary, Prof.Arindham Paul & Prof.Partha Saha, who had been my support for my each and every proceedings. The most importantly, the non-teaching staffs, Bapi Sir, Arvind, Sushil Sir, G.Behera Sir & Subhabrata Sir, who had been with me especially during the instrumental problems.

I would wish to thank Mr.K.Senthil Guru (Phd Scholar) & Prof. Indrarnil Banerjee, from Department of Biotechnology and Medical Engineering, NIT Rourkela, who had spent their time and resources for the biological characterization carried out in my project. Since I'm from non-Material science background, during crisis I felt great because I received lot of helping hands form the senior research scholars, Sarat Kumar Rout, Subrat Kumar Mohanty, Sanjay Kumar Swain, Smrithi Rekha Dash & Ganesh Kumar Sahoo.

A lot of stimulating discussions had been carried out with my research colleagues Abhishek Choudary, Sreenivasalu, Venkatesh, Raju Mula, Jayarao Gorinta, Akilesh Singh, & Kanchan Maji. I have to thank my friends of my department, Denny, Mandvi, Uttam, Subham, Tiny, Gaurav, Prativa & Badolia who had created many delightful moments. I never forget my sweet memories with Vignesh, KK, Kuppu, Arif, Elias, Rahul, Shaibu, Rajeev, Srikrishnan, Gurumoorthi, Uvanesh, Gautham.H.N, Gautham, Gokul, Leonard, Inigo, Kamal, Siddharth & Yuvaraj. I have a great hope that some of my friends won't feel bad since their names are not mentioned here.

EZHIL VENUSWARAN.R.R.

TABLE OF CONTENTS

LIST OF FIGURES

LIST OF TABLES

CHAPTER 1

INTRODUCTION

1.1 GENERAL INTRODUCTION

Bone is a complex organ formed by the combined work of bone (osseous) tissue, cartilage, dense connective tissues, epithelium, adipose tissue and nervous tissue **[1]**. Bone tissues are predominately called as living dynamic tissue, since they continuously engaged in the bone remodeling process: new bone building and deterioration of old bones. In other words, remodeling is a mechanism with a combination of both resorption and re-deposition of minerals on itself. Apart from blood cells, the regeneration capability of bone tissue had been more vital when compared to the skin tissues, neurons and muscle tissues **[2]**. Excluding the larger bone defects, some of the bone defects will get healed spontaneously during the bone remodeling process itself. But at certain times, this bone wound healing eventually failed on the critical size defects (CSD). In the recent years, CSD had been technically defined as the intraosseous wound which would not heal spontaneously without any surgical intervention **[3]**.

Before analyzing the bone healing mechanism, it is required to observe the anatomical features of bone. Bones comprises with outer cortical and inner cancellous /spongy bone layers **(refer Fig 1.1)**. The outer cortical bone layer acts as a protective layer to the spongy bone, during proliferation or at any stage of remodeling. The cortical bone possesses around 10-15% of porosity, where the pores act as attachment points for the tendons and muscular tissues. The cancellous or spongy bone layer is highly vascularized porous structure, where the macroscopic spaces had been filled with red bone marrow and yellow bone marrow. It contains 50-90% of porosity, where the pores present in the spongy bone structure acts as pathways for various mechanisms. The production of blood cells, nutrient transport, storage and release of mineral salts had been carried out within the spongy bone. Table 1.1 illustrates the mechanical properties of cortical and cancellous bone layer of the human bone.

Table 1.1- Summary of mechanical properties of the human bone **[4]**

	Compressive Strength (MPa)	Flexural Strength (MPa)	Tensile Strength (MPa)	Modulus (GPa)	Fracture Toughness ($MpA\text{-}m^{1/2}$)	Porosity (%)
Cortical or compact bone	100 - 150	135 – 193	50 – 151	10 – 20	2 – 12	5 – 10
Cancellous or Spongy bone	2-12	10 - 20	1 - 5	0.1 - 5	0.1 – 0.8	50 – 90

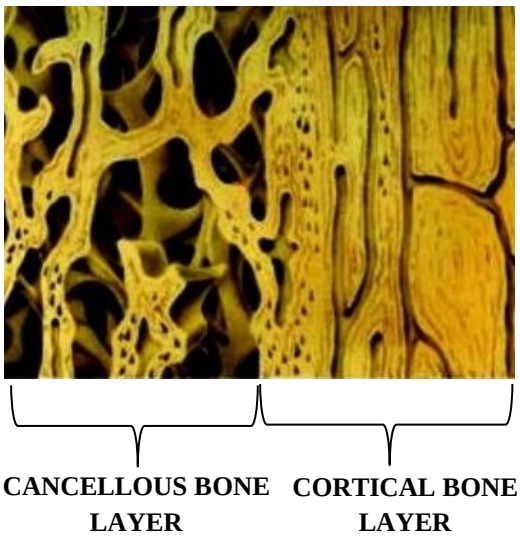

Fig 1.1(a)

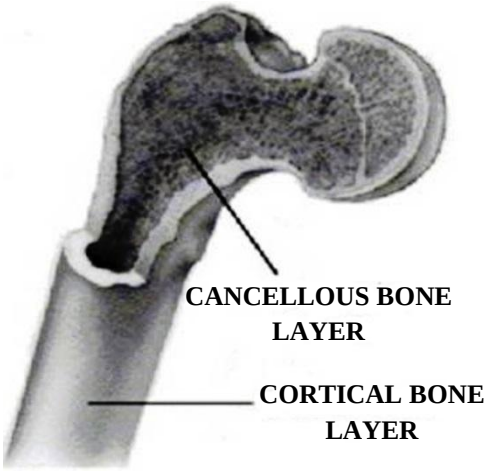

Fig 1.1(b)

Fig 1.1 (a) Cortical and cancellous bone layer showing the graded structure **[1]**
Fig 1.1(b) macroscopic view of the bone showing cortical and cancellous bone layer **[1]**

As the porosity decreases from the outer layer to the core, bones can be called as porosity gradient structure. Support, protection, associating in movement, mineral storage, production of red bone marrow and triglyceride storage are some of the major functions of bone. Since each layer of the bone performs a specific function, the bone is said to be functionally graded material (FGM). Thus, the bone alternatives with the similar architecture of the bone may attain enhanced biological recognition.

1.2 Therapeutics for bone defects

In general, either larger or small bone defects, the treatment towards the bone defects had been initiated during the pre-historic age itself. Almost several centuries ago, when a tissue is damaged or diseased, with minor medication, the offending parts were generally removed for the betterment of patient's life. As the diseased part or damaged tissue interrupts various biological mechanisms and contaminate the surrounding tissues, a partial improvement had been achieved by the removal of those tissues **[5]**. During the last century, surgeons demanded tissue replacements and bone fillers for the spaces created during the removal of tissues. Several investigations had been carried out and finally two alternative options had been emerged out: (1) transplant (2) implant.

The initial days of implantation had flourished with the reunion of damaged bones which had been done by using metal plates and screw fixation. Depends on the condition of the patient, the metal plates and screws had been fixed externally and sometimes internally too **(Fig 1.1)**. When entire bone was damaged or diseased, these fixation devices were unhelpful. During this situation, surgeons preferred metallic implants, which is actually the commencement of the first generation of synthetic / man-made or biomaterials. Simultaneously, on the other side of the shore, various investigations had been progressed for the development of transplants. Harvesting a tissue from a donor and transplanting to a host is the simple phenomena for transplantation procedure. If the donor and the patient are the same individual, then they are called as Autografts **[6]**. When the donor and the recipient are different individuals, then they are called as allografts. Heterografts or Xenografts are harvested from the other species, which had been considered as the last option for tissue replacements.

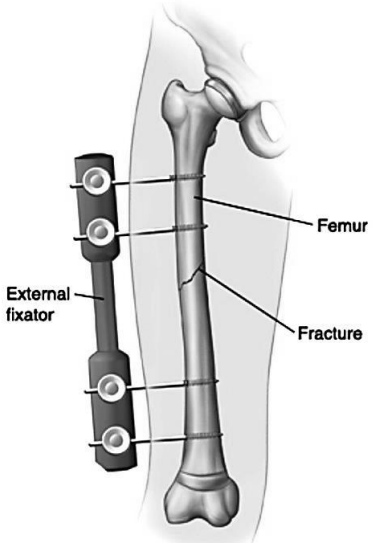

Fig – 1.2 (a)

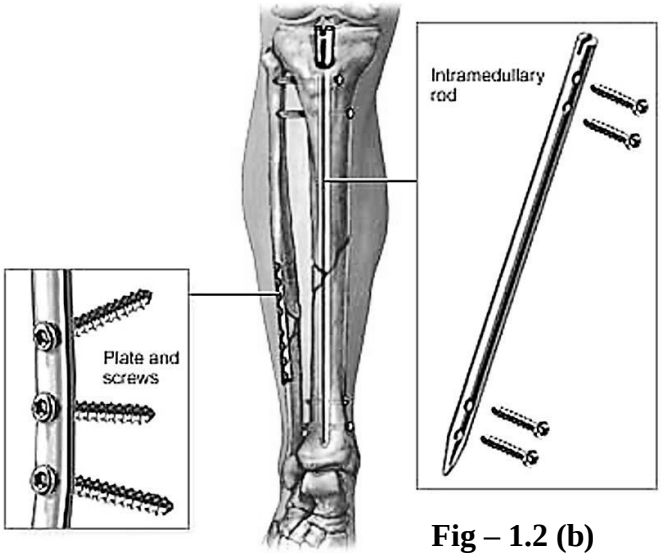

Fig – 1.2 (b)

Fig – 1.2 Treatment methods with metal plates and screws by fixing (a) externally (b) internally **[7,8]**

This grafting technology had many times focused on the critical size bone defects. But a wide range of limitations had been associated along with these Autografts and allografts. The former created additional pain since the donor and the recipient are from the same individual. The major consequence faced by the allografts is the rejection of donor tissues by the recipient tissue, majorly due to disease transfer and other contamination evolved while executing the grafting protocols **[9]**.

Due to the scarcity of the donors, graft pieces had been procured from the graft bank. Non-availability of fresh graft pieces sometimes created cell adhesions and inflammation surrounding the recipient site. These problems had been overcome by the implants, with the synthetic / man made biomaterials.

1.3 Metallic implants

As mentioned earlier, the first generation of biomaterials had been commenced with the metallic implants. Except minor inflammation and cell damage during adhesions, no major critical issues had been raised from the patient's side, when the trauma cases had been treated by external fixation. When the physicians opted for internal fixation of broken bones, they faced several problems during post-surgical periods. Either to support for bone healing or replacement of entire tissue, metallic implants had created problems by post-surgical inflammation and certain times by leaching out or releasing toxic metal ions.

It is a widely accepted fact that the metallic implants are the best alternative for load bearing positions. But it lacks biological recognition at the implant-host interface, which had triggered the material scientist and ortho-surgeons to explore another compatible solution. Since bio-incompatibility was the serious issue with the metallic implants, they expected a material which completely behaves as bio-inert as far as possible **[10]**. In the year 1975, α- Al_2O_3 had been identified as the first bio-inert material, by which the surgeons thought to utilize as artificial hip prosthesis instead of metallic implants. Low wear and elastic modulus of around 380 GPa are the properties observed with α- Al_2O_3 as a hip prosthesis. These alumina based implants had partially performed the functions of metallic implants and had drastically created a biocompatible environment by its bio-inert nature. As a result, these α- Al_2O_3 ceramic implants had discarded various metallic implants as bone alternatives. **[11]**.

It was a big astonishment that ***L.L.Hench*** **[12]** broke the incompatibility barrier with his 45S5 bioglass in the year 1970 itself, even before the discovery of α- Al_2O_3. In order to preserve the mechanical properties of metals within the implant and also to afford biocompatible environment, bioglass coatings had been provided on the metallic surfaces **[13]**. Our human body fluid comprises a combination of various metal ions. Furthermore, the optimum level of metal ions leached out from the metallic implants can take part in the bone remodeling process. The role of different metal ions in bone remodeling process had been illustrated in table 1.2.

Table 1.2 Metal ions and its role in various mechanisms **[14]**

S.No	Metal ions	Role
1.	Li^{+}	Osteogenesis
2.	Zn^{2+}	Osteogenesis
3.	Mg^{2+}	Angiogenesis
4.	Sr^{2+}	Osteogenesis
5.	Cu^{+}	Angiogenesis
6.	Co^{2+}	Angiogenesis
7.	B^{3+}	Osteogenesis / Angiogenesis
8.	Mn^{2+} & Mn^{3+}	Osteogenesis
9.	Si^{4+}	Osteogenesis / Angiogenesis

Angiogenesis is the formation of new blood vessel and osteogenesis is the formation of osteoblast (bone cells). These two mechanisms can be considered as constructive stages of the bone remodeling process. In spite of various disadvantage from the biological perspective, many metallic implants had been used still for bone alternatives. The most commonly utilized metallic implants are stainless steel 316 L (ASTM F138), Cobalt based alloys (mainly ASTM F75, and ASTM F799) and titanium alloys. In the case of titanium alloys, Ti-6Al-4V (ASTM F67 and F136) are frequently preferred as fixation devices. Table – 1.3 provides the list of metallic implants and its corresponding orthopedic applications.

Table -1.3 Metallic Implants and its orthopedic applications **[15]**

METAL IMPLANTS	ORTHOPEDIC APPLICATIONS
Stainless steel (316, 316L)	Fracture plates, screws, hip nails
Co-Cr-Mo alloys	Prostheses stems, load bearing positions in total joint replacements
HA coated Ti alloys	Hip and knee prostheses, screws and pins for fixation
Ti6Al4V	Prostheses stems
NiTi	Internal fixator for long bone shafts, spinal correctors, vertebral spacers anchoring prostheses and staples

Fabrication of metallic implants and machining according to the required size of the bone defect will be a challenging task. Since the biological system demands a porous structure, incorporating porous architecture is highly difficult. Due to its ductile nature, metallic implants may tend to get fractured, when these metallic materials had been forced to organize itself in a porous architecture. And the processing techniques for the fabrication of porous metallic scaffold are also highly complex.

This critical situation had catalyzed the search of a new group of materials. In order to solve the CSD, it is necessary to optimize the implants from the powder stage itself. Acquiring a desired phase, feasibility of machining and achieving desired porous architecture are the major features required for repairing CSD. It had been proposed that scaffold based materials are the appropriate bone alternative for repairing critical size bone defects **[16]**. As the inability of metals had been mentioned already for this kind of application, it is adequate to utilize scaffolds made of ceramic materials.

1.4 Bio ceramic implants

Alumina based ceramics had been recognized as the first bioinert material (refer section 1.3), which had been widely used in the load bearing positions due to its better mechanical properties. For a better enhancement in mechanical properties, material research professionals had made investigations with zirconia, which was also considered as another promising bioceramic material for hip replacements. Various bio ceramic materials and its corresponding orthopedic applications had been illustrated in table 1.4.

Table 1.4 – Illustration of bio ceramic materials and its orthopedic applications **[15]**

BIO CERAMIC MATERIALS	ORTHOPEDIC APPLICATIONS
Bio inert Materials	
High alumina ceramics	Orthopedic load bearing positions
ISO alumina standard 6747	Dental implants
PSZ	Alveolar ridge augmentation, otolaryngological coatings for tissue ingrowth, maxillofacial reconstruction
Bioresorbable Materials -	
Calcium phosphate cement	
R cement	Cleft palate, apical barrier
H cement	Periodontal pockets, filling periapical
Biopex	Alveolar bone augmentation, bony defects
Bonesource	Periodontal osseous defects, repair of large periodefects

Table – 1.4 contd.

BIOGLASSES	
45S5 BG, 45S5.4F BG	Maxillofacial reconstruction
45B15S5 BG	Middle ear reconstruction, dental implants
52S4.6 BG	Percutaneous access devices, junction of spinal vertebrae
GLASS CERAMICS	
KGC ceravital, KGS ceravital, KGy 213 ceravital	Dental implants, maxillofacial reconstruction
AW/GC	Vertebral prosthesis devices
MB GC, Bioverit	Iliac crest prostheses

Apart from these materials, calcium phosphate based ceramics like hydroxyapatite and β-tricalcium phosphate had been widely preferred for bone repairing applications. These calcium phosphate based materials had shown better bioresorbable and bioactivity since they closely resemble the mineral phase of the human bone. As alone, these bioresorbable materials were unable to execute or take part in the osteoinductive mechanism and also it resorb very slowly. Polymer – ceramics bioresorbable composites may reduce this problem by its better degradation, but inducing the osteoblast cells will be still slow. It is required to accelerate the bioresorbability process to proceed further with a new bone mineral formation. Thus the bioactive materials, which had been categorized under the third generation of biomaterials, had been predominantly preferred to carry out tissue regeneration.

1.5 Polymer based implants

As the third generation of biomaterials majorly focused on biodegradation and tissue regeneration, comparatively biopolymers are the better candidates for biodegradation. A controlled biodegradation should be carried out to provide better stability during bone healing. It is necessary because scaffolds are not permanent implants. They have to degrade and allow the cells to produce their own extra cellular matrix. In other words, it can be said that degradation rate of the polymers should match the neo tissue formation rate **[17]**. Not all the polymers are biodegradable, at certain times, few synthetic polymers exhibit biologically non-degradable behavior.

Polymers had been broadly classified as naturally derived polymers and synthetic polymers. Most of the natural polymers are biodegradable, like starch, collagen, cellulose and gelatin. Synthetic polymers had been sub-classified into biodegradable and non-biodegradable polymers **[18]**. Table 1.5 illustrates some of the polymers used in bone tissue engineering applications.

As a single component, polymers fail most of the time due to its low mechanical strength. This issue had been solved by using bio ceramic and metal fillers into the polymer matrix. These types of design enact the concept of reinforcement to upgrade the mechanical properties of polymer based scaffolds. Fig – 1.3 shows illustrates the mechanical properties of different biomaterials used for bone tissue engineering applications.

Table 1.5 – Applications of polymers in bone tissue engineering procedures **[15]**

POLYMER MATERIALS	ORTHOPEDIC APPLICATIONS
Polymethacrylic acid (PMMA)	Acrylic bone cements, anchoring of hip prostheses, vertebroplasties & kyphoplasties
Polyethylene (PE)	Liner of acetabular cups in hip arthoplasties
	Tibial insert and patellar components in total knee arthoplasties
Polydimethylsulphoxide (PDMS)	Replacement of small joints in hand and foot
Polypropylene (PP)	Bone fixation devices
Polysulphone (PS)	Bone fixation devices, total joint arthoplasties
Polycarbonate (PC)	Bio absorbable fixation devices and bone regeneration, drug delivery
Polyglycolic acid	Bio absorbable fixation devices and bone regeneration
Polylactic acid (PLA)	Drug delivery
Polycaprolactone (PCL)	
Polydioxanone (PDS)	

1.6 Bioglass

1.6.1 Biocompatibility of bioglass

Prof. L.L.Hench had shattered the concept of bio incompatibility by his revolutionary 45S5 bioactive glass **[12]**. It is a glass composition with 45 wt. % of SiO_2, 24.5 wt. % of Na_2O, 24.5 wt. % of CaO & 6 wt. % of P_2O_5, by which he had strong belief that it has the capability of bonding with the bone tissues. By collaborating with ***Dr. T.K.Greenlee*** **[19]**, he had conducted in vivo experiments on a rat femoral model, which proved the bone bonding capability of 45S5 bioactive glass. Furthermore, they had ensured that this 45S5 bioactive glass composition has the capability of forming new bone tissue. By invitro analysis, they had clearly confirmed the presence of carbonated hydroxyapatite phase on the surface of the 45S5 bioactive glass. The initial intention of Hench and co-workers was to promote the bioresorbable behavior of 45S5 bioglass. But their invitro results had clearly proved that the 45S5 bioglass had the capability to exhibit neo tissue formation. An additional to that, their invitro analysis had been undertaken as a complete guide to draft the detailed invitro mechanism of 45S5 bioactive glass immersed in Simulated Body Fluid (SBF) **[20]**.

Simulated Body Fluid (SBF) is an artificially synthesized body fluid, which possesses the close, resembles of the ions present in the human body. This ionization reaction had been clearly illustrated in the Fig -.1.3. The 45S5 bioglass exhibits SiO_2 - CaO - Na_2O - P_2O_5 as its glass system. When the scaffolds fabricated based on this glass system, it undergoes around eight steps for the formation of carbonated hydroxyapatite phase in invitro SBF medium **[21]**.

- In the first step, the Na^+ and Ca^{2+} ions had been leached out from the glass composition, which had been replaced by H^+ and H_3O^+ ions respectively. Since the ion exchange rate of Ca^{2+} ions will be comparatively lower than Na^+ ions, Na^+ ions degrade first from the glass system. At this situation, the scaffold will be holding Si-OH, Si-O-Si and Si-O-P as its major bonds.
- The second step of this ionization mechanism will be the attachment of H_2O molecules on the above-mentioned network. Here these H_2O molecules break the Si-O-Si and Si-O-P bonds and forms completely with Si-OH bonds.
- The excess soluble silanols [$Si(OH)_4$] leached out of the scaffold mixed with the SBF. The breaking of Si-O-P bonds results with PO_4^{3-} ions which go out in the search of Ca^{2+} ions.

- The fourth step will be the formation of sandwich gel-like structures, which will be in a combination of soluble silanols and glass with Si-OH bonds.
- This complex structure leads to the initiation of polymerization and condensation of a rich silica layer with a bunch of Si-OH bonds.
- The next step will be the attachment of Ca^{2+} and PO_4^{3-} ions in a form of clusters. The heavy deposition of the Calcium Phosphate clusters leads to the breaking of Si-OH bonds of the rich silica layer.
- Amorphous calcium phosphate (ACP) will be formed when complete silanols had been leached from the network. Later on OH^- and CO_3^{2-} ions will get adhered on the surface of the amorphous calcium phosphate.
- OH^- ions hydrate the ACP and CO_3^{2-} ions crystallize the same for the formation of carbonated hydroxyapatite.

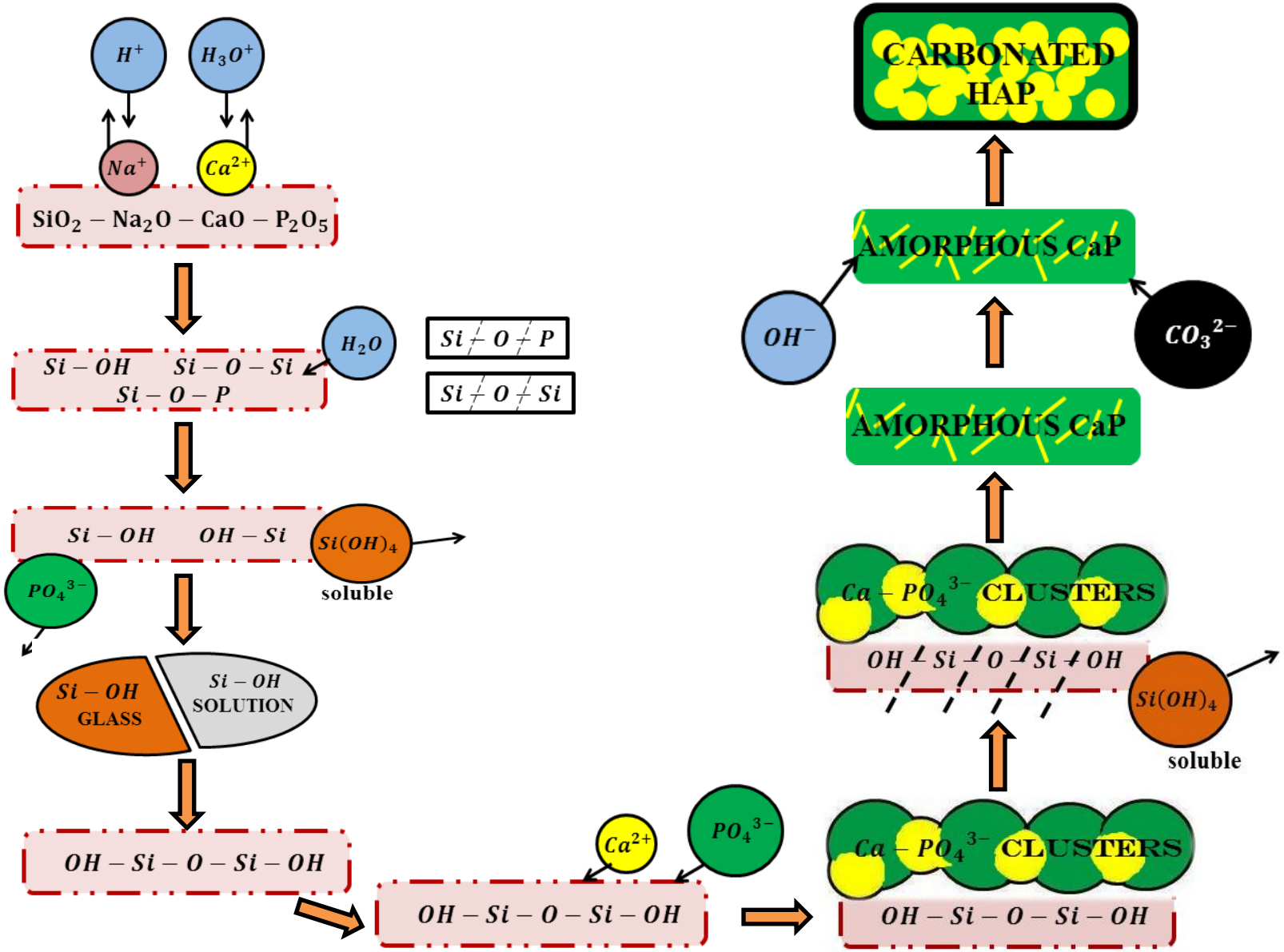

Fig – 1.3 Invitro mechanism of bioglass scaffold in Simulated Body Fluid (SBF)

Later on the macrophage cells disseminate the degraded minerals from the scaffolds and the adsorption of proteins had been carried out. The next stage will be the attachment and differentiation of stem cells, further leads to the HA matrix formation. A cell seeded bioactive glass scaffolds undergoes these reaction kinetics. The reaction mechanism will be the same, but the rate of kinetics differs according to the crystallinity and density of the bioglass scaffold **[22]**.

1.6.2 Formulation of Bioglass composition

Prof. L.L.Hench had been driven by a hypothesis that the implant material along with calcium and phosphate minerals would not be rejected by the human body unless it forms a Hydroxyapatite layer during in vivo analysis **[23]**. In order to confirm the hypothesis, ***L.L.Hench*** had formulated the 45S5 glass composition (refer section 1.6.1) by adapting the compositional phase diagram of Na_2O-SiO_2-CaO ternary system (refer fig 1.4). He had utilized a large amount of CaO along with little of P_2O_5 to blend into the Na_2O-SiO2 matrix. Apart from this 45S5 glass composition, he had tested bioactivity on various other glass compositions which had been illustrated in the fig 1.5. It has to be noted that P_2O_5 had been kept constant as 6 wt. % for all the cases. As shown in the fig 1.5, the glass compositions fall under the region A exhibit better bone bonding. Whereas in the case of glass compositions from the regions B,C, & D, non-bone bonding had been observed. The reactivity of the glass compositions from the regions B & C are too low and too high respectively. But the region D had been filled with non-glass forming compositions. The glass compositions from the region S exhibit better bone bonding ability even with the soft tissues. These glass compositions can be called as Class A biomaterials. And finally the 45S5 glass composition had been marked as E. The bioactivity of these glass compositions had been evaluated in terms of the index of bioactivity (I_B). The region F represents the Apatite – Wollastonite glass ceramic compositions with variable P_2O_5.

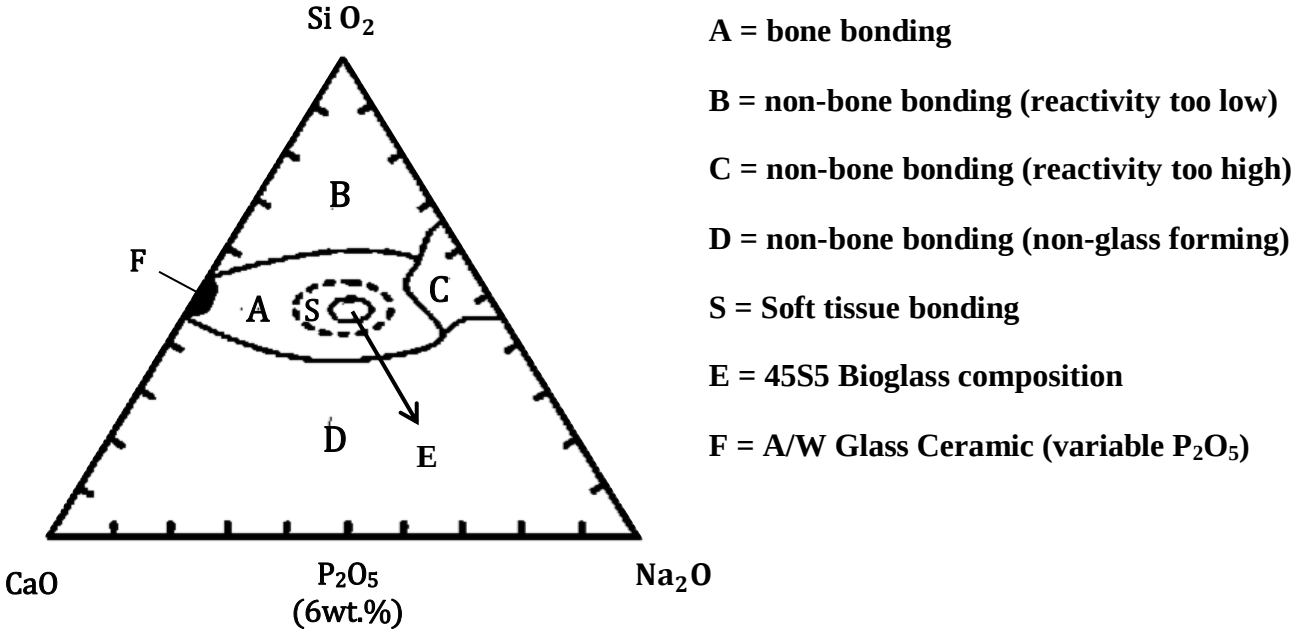

Fig – 1.4 Compositional diagram of glass compositions representing bone bonding ability **[23]**

Index of bioactivity is the time required for 50% of the implant's surface to bond bone. By using the equation below, all the glass compositions had been characterized **[24]**.

$$\textit{Index of Bioactivity}, \qquad _B = \left[\frac{100}{t_{0.5}}\right] (days^{-1})$$

This evaluation had laid a platform for categorizing the Class A and Class B biomaterials for bone tissue engineering applications. From the compositional diagram, it should be noted that not all the glass compositions are bioactive materials. Glass compositions with 36wt. % to 52wt. % of silica were observed to have better bone bonding ability and falls under Class A biomaterials. Beyond that, the compositions will be completely inert and also at certain times they even lose glass forming ability. The properties of Class A and Class B biomaterials had been already discussed in section 1.2. But another aspect is Class A biomaterials have the ability to bond both hard tissues as well as soft tissues. In the case of Class B biomaterials, they have the ability to bond only with hard tissues. Various biomaterials and its index of bioactivity had been illustrated in table 1.6.

Table 1.6 – Biomaterials and its index of bioactivity **[5]**

Biomaterial	Index of bioactivity (I_B)	Class of bioactivity
45S5 Bioactive glass	12.5	A
5254.6 Bioactive glass	10.5	A
A/W Bioactive glass ceramic	6	B
Ceravital glass ceramic	5.6	B
5554.3 Bioactive glass	`3.7	B
Hydroxyapatite ceramic	3.1	B
Ceravital K6X	2.3	B
Alumina	0	0

In this index of bioactivity evaluation, 45S5 bioglass tops the chart with higher bioactivity and acquires the ability to bond both hard and soft tissues. Even though 5554.3 glass composition is also a bioactive glass, it acquires low index of bioactivity and had been categorized under Class B Biomaterials. This had happened since in its composition it has 55 wt. % of silica, which is not favorable as per the compositional diagram (refer fig 1.1). Hydroxyapatite based ceramics has the index of bioactivity of 3.1 which is 4 times lower than the 45S5 bioglass, even though HA is the major mineral in the bone matrix. This is due to the slow degradation rate of hydroxyapatite which happened due to a high percentage of crystallinity. Alumina being an inert material exhibits no bioactivity. Thus bioglass (45S5) may be considered as a better bioactive material than any other ceramic materials.

1.6.3 Synthesis of Bioglass powders

The traditional approach of preparation of glass powders is the melt quench method. The first prepared bioglass powders are also carried out by melt quench method. While L.L.Hench was formulating the bioglass composition, he had included Na_2O in the 45S5 glass system to reduce the melting point of bioglass batch. As the 45S5 glass composition also fell close to the eutectic point, he was able to melt the glasses easily.

This temperature depends upon the alkali flux used in the glass system like Na_2O, K_2O and B_2O_3 etc. High-quality phosphates, quartz or silica and carbonates are required for the preparation of melt derived glasses **[25]**. Glasses can also be prepared by using sol-gel method. By liquid precursors and with a combination of hydrolysis and condensation reactions, sol-gel glass had been prepared. The first sol-gel based silica had been synthesized in 1844 by Ebelmen. Commercially, sol-gel coatings to the flat glass had been done during the early sixties **[26]**. Later on, in 1981, 'the First International workshop on glass and ceramics from gels' had proudly announced the possibility of bioglass synthesis at low temperature. Apart from low-temperature synthesis, high homogeneity, high purity and short range of particle size are the other advantages of this method.

The major differences acquired between sol-gel derived glasses and melt quench glasses are the surface area and porosity rate of the glasses, in general, the textural properties **[27]**. The surface area of sol-gel derived glasses will be high when compared to the melt quench glasses. Apparently the particle size of the melt derived glasses will be in micron range whereas in the case of sol-gel glasses, it will be in the nano range. These changes majorly influence the biological properties by expecting higher ionic exchange with sol-gel derived glasses than the melt derived glasses. Kinetically this leads to rapid formation of larger amount of apatite layer in sol-gel derived than the melt derived glasses. In spite of various advantages of sol-gel glasses over melt derived glasses, melt derived glasses had been preferred due to its low-cost raw materials and feasibility for bulk production.

1.6 Scaffold architecture

The self-assembly technique of skeletal tissues, namely the bones and cartilages, leads to the formation of 3D skeletal structural framework **[28]**. In order to repair complex bone fractures or any other bone based disorders, it is necessary to obtain a scaffold, whose architecture has to be optimized into 3D structural units. Since the anatomy of bone represents itself as a highly vascularized porosity gradient structure, the implant material should mimic the same to attain better growth mechanism and bone healing. This can be possible only with the 3D scaffolds which had been widely accepted during the discovery of bioglass itself. Thus, the entire field of bone tissue engineering broadly relies on the usage of porous 3D scaffolds for better proliferation. From the material scientist's perspective, scaffolds are supporting structures, with optimized 3D architecture, which take part in bone healing mechanism. But in a biological perspective, scaffolds can be called as templates, where cells had been seeded, which facilitate tissue formation on it **[29]**.

Occasionally along with cells, growth factors are also incorporated into the scaffolds, which enhance tissue regeneration. These mechanisms will be successfully carried out unless and until proper diffusion of biological fluid and cell viability took place. For better diffusion and cell viability, it is necessary to provide optimum pore size with interconnected pore structure to the scaffolds. The osteoinducible minerals from the biomaterial scaffold degrade and structural minerals from the scaffold will get stimulated to form new bone **[30]**.

The biomaterial 3D scaffold should exhibit a controlled rate of degradation to execute these mineral exchange mechanisms successfully. This partly depends on the strength of the scaffold, i.e. the elastic modulus of the material utilized for scaffold fabrication. Different regions of the body demand scaffolds with different elastic modulus. Verifying the elastic modulus had been considered as one of the major criteria for material selection. Most of the cells, excluding the blood cells, reside as a solid matrix in the extra cellular matrix; the scaffolds have to contribute some mineral phase to it, which facilitates better bioactivity. Thus, the composition of the biomaterials used for scaffold fabrication plays a vital role in this mineral phase formation during bone remodeling. The biomolecules recognize these biomaterials as a foreign body and the level of toxicity varies according to the biocompatible properties of the scaffolds. By consolidating the above-mentioned facts, it had been realized that more investigations are required to analyze the chemistry of biomaterials. In short, including the architecture of the scaffold, the mechanical and biological properties have to be optimized to fabricate an ideal scaffold **[31]**. ***C.M.Agarwal et al*** **[32]** had clearly drafted the desirable properties of an ideal scaffold as follows:

1. Biocompatible in nature
2. Biodegradable and ability for remodeling
3. Biodegradability should be along with the repairing/regenerative process
4. It should contain optimum amount of porosity with interconnectivity
5. It should have high permeability to allow proper diffusion of biomolecules
6. Pore size should be comfortable for the encroachment of target cells
7. Adequate mechanical properties to establish micro stress environment for cells
8. Scaffold surface properties should enhance affinity of cell attachment
9. Contribution of subsequent minerals to ECM
10. It should be capable of carrying the growth factors

1.7 Significance of Functionally graded biomaterials

As discussed in section 1.1, functional gradation had been evolved within the bone tissue morphology. To be more specific, the gradient in porosity had been attained from the cortical bone to the cancellous bone layers. These pores are highly responsible for the attachment of extra cellular matrix, spreading of cells within the interconnected pore network and differentiation of cells. These mechanisms are the essential modules of tissue regeneration. Customized pore size and pore morphology acquires better cell affinity and viability. It can be concluded that mimicking or simulating the bone morphology into the scaffold design favors the enhancement of tissue regeneration. An additional to that several researchers had reported that the fractures of homogeneous scaffolds had been more viral than the fractures occurred in porosity gradient scaffolds. Thus, the fabrication of porosity gradient scaffolds will be highly inspired by the grafting area.

1.8 Scope of work

The above-mentioned facts clearly illustrate that bioglass is the better bioactive material than any other ceramic materials **(refer table 1.6)**. It had been clearly understood that scaffold based materials are the better solution for critical size bone defects. Since bones possess porosity gradient structure **(refer fig 1.1)**, it is required to achieve a porosity gradient structure in the scaffold architecture to attain better biological recognition. Thus it had been concluded that bioactive glass-ceramic scaffolds have to be designed with porosity gradient architecture **(refer section 1.6)**. These porosity gradient bioglass scaffolds may enhance better tissue regeneration and most importantly, they heal the critical size bone defects.

CHAPTER 2

LITERATURE REVIEW

2.1 Design of Tissue Engineered Scaffolds

Till now, the protocols of implant devices drafted by the material scientist and research professionals commenced with a module called 'selection of biomaterials'. A better understanding of the properties of biomaterials and its appropriate correlation with the clinical principles is required, which is considered as a prime factor in the entire design process. ***Felicity R. A. J. Rose et al*** **[33]** had given a better review about the strategies of tissue-engineered scaffold. The clinical needs, stem cell differentiation in a scaffold and growth factors are the major concepts discussed which completely rely on the architecture of the scaffold. His review highlights the significance of an osteoconductive and osteoinductive scaffold, which furthermore opens the gateway for angiogenesis*.

The scaffolds with porous architecture favor the angiogenesis had been observed by ***Kuboki Y et al*** **[34]**. They carried out experiments for Bone morphogenetic proteins (BMP-2) delivery to a rat ectopic model. A mixture of a solid and porous form of hydroxyapatite had been used for BMP delivery. No new bone had been formed in the dense regions whereas perfect osteogenesis* had been carried out in the porous regions. This gives the clear picture about the significance of porous scaffolds for bone tissue engineering applications.

As bone is already porosity gradient in structure (section 1.6), incorporation of optimum porosity on the scaffold paves the way for the biomimetic approach. Various fabrication techniques had been designed and executed by many people for porous materials. But all the techniques will have its own limitations on the optimization of pore morphology. A simple review had been given by ***Julian R. Jones & Larry L. Hench*** **[35]** about the regeneration of trabecular bone, i.e. the porous regions of a scaffold material. Direct foaming, with porogens, gel casting, sol-gel method, polymer replica and rapid prototyping are the methods had been discussed in that paper. Each method provides different pore morphology and pore size. They had concluded that complete biological characterization has to be carried out to understand the detailed invitro mechanism on the variation of pore morphology.

Fabrication technique of porous scaffolds, shape, pore size, porosity (%) and its corresponding appropriate biological application had been illustrated in the review of ***David Kaplan et al*** **[36]** and had been adapted here in the table 2.1 to 2.6.

Table 2.1 - Porosities and pore size of bio ceramic scaffolds – adapted from ***David Kaplan et al*** **[36]**

Material	Fabrication technique	Shape	Pore size(µm)	Porosity (%)	Biological Application
Hydroxyapatite 10(HAP)	Sintering	Scaffolds with honey comb pores	90-120, 100-200 and 350		BMP-2 delivery & ectopic bone formation in rats
		Scaffolds	366 and 444	38 & 44	Mandible defects
		Scaffolds	400 and 800	60 & 70	Goat bone marrow stromal cells ex-vivo and ectopic bone formation in goats
		Blocks	500	77	Ectopic bone formation in mice
		Cylinders	400- 600	80	Femoral defects in rats
		Blocks	100-200		BMP-2 delivery & ectopic bone formation in rats
		Blocks	106–212, 212–300, 300–400, 400–500, and 500–600		Ectopic bone formation in rats
		Particles	150 & 230	70 & 66	
		Rods	200 and 400		Ectopic bone formation in dogs
Tricalcium phosphate (TCP) cement	Salt leaching	Pellets	0.2 and 8.7	31 & 62	
Calcium metaphosphate	Sintering	Blocks	200		Rat bone marrow stromal cells ex-vivo and ectopic bone formation in goats
Natural coral	Sintering	Human mandibular condyle	150-200	36	Rabbit marrow mesenchymal cells ex vivo andectopic bone formation in mice
HAP/TCP	Sintering	Blocks	100-150	36	Femoral defects in dogs

Table 2.2 - Porosities and pore size of glass and glass ceramic scaffolds -

adapted from ***David Kaplan et al*** **[36]**

Material	**Fabrication technique**	**Pore size(µm)**	**Porosity (%)**	**Biological Application**
Glasses	sintering	100 – 200	5 40	Tibia defects in rabbits
Bioglass	Foaming	10 – 500		Primary human osteoblasts in vitro
	Sintering	100 – 600		Ectopic bone formation in dogs
Glass ceramics	Sintering	100 – 200		
	Phase transformation	10 – 300	51, 47 & 43	Femoral defects in rabbits

Table 2.3 - Porosities and pore size of natural polymer scaffolds –

adapted from ***David Kaplan et al*** **[36]**

Natural polymer	**Fabrication technique**	**Pore size(µm)**	**Porosity (%)**	**Biological Application**
Hyaluronic acid	Salt leaching	100 – 600	80 – 90	BMP-2 delivery and C3H10T1/2 cells in vitro
Collagen	Freeze drying	11-105 & 14-134		Tibia defects in rats
Collagen / Hyaluronate	Cross linking	45.7 & 35.4		Cranial defects in rats
Collagen / Hyaluronic acid (cross linked with EDC)	Freeze drying	84 (-196°C) 186(-70°C) 190(-20°C)	62(-196°C) 62(-70°C) 64(-20°C)	
Silk fibroin	Freeze drying	50(-20°C) 15(-80°C)	99	
	Salt leaching	202	84 – 98	Human bone marrow stromal cells in vitro
	Gas foaming	155	87 – 97	

Table 2.4 - Porosities and pore size of metallic scaffolds for bone regenerations - adapted from ***David Kaplan et al*** **[36]**

Porous surface technique	**Pore size(µm)**	**Porosity (%)**	**Biological Application**
Sintered titanium fiber meshes	250	86	Rat bone marrow stromal cells ex vivo and cranial defects in rats. TGF-b1 delivery in cranial defects in rabbits
Self-propagating high temperature synthesized nitinol implants	259 and 505 353, 218 & 179	66 and 47 43, 54 & 51	Femoral defects in rats Cranial defects in rabbits
Sintering	50-200	35	
Plasma spraying	200- 400	50 - 60 56 - 60	Femoral defects in dogs Femoral condyles in dogs
Diffusion	350	45	Hip arthoplasties in dogs
Laser texture	100, 200 & 300		Femoral defects in rabbits
Electrochemical oxidation	< 8	13 – 24	Tibia defects in rabbits
Machining	Submicron to 10		
Shot blasting	< 10	44 and 48	Mandible and femoral defects in dogs
Acid etching	Submicron to 1		Femoral defects in rabbits
Deposition through polystyrene latex beads	0.4, 13 and 40		Human bone derived cells in vitro

Table 2.5 - Porosities and pore size of chemically synthesized polymer scaffolds - adapted from ***David Kaplan et al*** **[36]**

Polymer	Fabrication technique	Pore size (μm)	Porosity (%)	Application
Poly(lactide)	Salt leaching	600		
Poly(lactide) / Poly(glycolide)	Molding	800		
Poly(L-lactide-co-D, L-lactide)	Porogen melting		58 and 80	
Poly (lactide-co-glycolide)	Sintering	72, 164, 101 and 210	>30	
	Consolidation by pressure drop	100	65	Teeth implants
	Sintering	187	31	
	Gas foaming	200		Human mesenchymal stem cells in vitro
	Electros pining	2 – 465	92	
Poly (lactide-co-glycolide) / Poly (ethylene glycol)	Porogen dissolving	300 – 500	`85	Periosteal cells in vivo
Poly (lactide-co-glycolide) / Poly (vinyl alcohol)	Salt leaching	200 – 300	90	Cranial defects in rabbits
Poly (multifunctional lactic acid based oligomer)	Salt leaching	45 – 150 and 300 – 600	80	
Poly (propylene fumarate)	Gas foaming with effervescent reaction (in vivo)	70	51	Tibia defects in rats
	Salt leaching	300 – 500	70	TGF – β1 delivery in cranial defects in rabbits
	Salt leaching		80	
	Salt leaching	300 – 500 and 600 – 800	57 – 75	Cranial defects in rabbits
Polyethylene terephthalate	Melt – blowing		93 – 97	Rat mesenchymal stem cells in vitro
Polymeric foams	Emulsion polymerisation	40 and 100		Rat osteoblasts in vitro
Poly (glycol-co-fumaric acid)	Gas foaming with effervescent reaction (in vivo)	100 – 500		Cortical defects in rats
Poly(desaminotyrosyl-tyrosine ethyl ester carbonate)	Salt leaching	500	80 – 87.5 (gradient)	Cranial defects in rabbits

Table 2.6 - Porosities and pore size of composite scaffolds - adapted from ***David Kaplan et al*** **[36]**

Composite	Fabrication technique	Pore size (μm)	Porosity (%)	Application
Hydroxyapatite / poly (ε caprolactone)	Sintering	150 – 200	87	
Hydroxyapatite / chitosan – gelatin	Freeze drying	300 – 500		Rat calvarial osteoblasts in vitro
Hydroxyapatite / β – TCP / chitosan	Sintering	300 – 600		
Collagen / hydroxyapatite	Freeze drying	30 – 100	85	Rabbit periosteal cells in vitro
	Freeze drying	50 – 300	49, 73 and 79	MC3T3- E1 osteoblasts in vitro
Titanium / calcium phosphate	Sintering	50 – 200 (surface coating)	35 (surface coating)	Femoral defects in rabbits
	Sintering	250 (porous meshes)	86 (porous meshes)	Ectopic bone formation in rats
	Soaking			Human osteoblasts in vitro
Titanium / polyvinyl alcohol (PVA)	Sintering	170	60	Femoral condyles in dogs
Titanium / boron	Self-propagating high temperature synthesis		15 – 55	Cranial defects in rats
Poly(L-lactide-co-D, L-lactide) / β – TCP	Salt leaching	125 – 150	80 – 87.5 (gradient)	Cranial defects in rabbits
Poly(propylene fumarate) / β – TCP	Salt leaching	150 – 300	69 and 74	
Poly(L-lactide)/bioglass	Phase separation	50 – 200		
silica / ceramic	Sintering	10 – 300	51, 47 and 43	Femoral defects in rabbits
Poly(lactide-co-glycolide)/ collagen/apatite	Salt leaching	325 – 425	87	

The table 2.1 to 2.6 reveals that each fabrication technique fetches different pore morphological parameters. Each grafting site demands different pore morphological specifications. The biomimetic approach of designing a tissue engineered scaffold becomes very complex due to these kinds of clinical facts. Apart from the scaffold architecture, surface chemistry, biodegradation mechanism, leached out mineral phases, regenerative capability and the mechanical properties of the scaffolds are the major challenges which have to be investigated for fabrication of an ideal scaffold.

2.2 Bioactive glass / glass ceramic based scaffolds

Bioactive glasses had been in demand as a scaffold material due to its high bioresorbability and regenerative capability. It had been widely accepted that scaffolds fabricated with bioactive glasses had a pronounced effect in stimulating the osteogenesis at genetic level **[37]**. In another perspective, the dissolution rate of amorphous materials will be high when compared with crystalline material:

Rate of dissolution of Amorphous HAP >> α – TCP >> β – TCP >> crystalline HA [38]

The above statement can be generalized and it can be concluded that rate of dissolution of bio-glasses will be more than the synthetic hydroxyapatite and other crystalline materials. This means the regenerative capability of bioactive glasses is higher than not only with hydroxyapatite but also with other biomaterials. Bioactive glasses had been synthesized by the conventional melt quench method and sol-gel method **[39-43]**. Due to the mesoporous structure of sol-gel derived glasses, they are highly bioactive than the melt quench glasses **[44]** But the necessity of preferring melt derived glasses had been briefly explained in the section 1.6.3.

As ***L.L. Hench et al*** discovered 45S5 bioglass on 1978 **[45]**, many material scientists started designing scaffolds with various bioactive glass compositions. The emergence and necessity of scaffolds too got highlighted only after the discovery of bioglass. It had been observed that bioglass possess poor mechanical property. Meanwhile by pronounced heat treatment, which by default incorporates crystalline phases, enhances the mechanical properties. The early research papers of L.L.Hench had discussed regarding this issue. Therefore, selection of a fabrication technique and optimizing better powder characteristics (starting material) are much important. Sol-gel processing, thermally bonding of particles or fibers, polymer foam replication, solid free form or rapid prototyping and freeze casting are some of the methods followed for the fabrication of bioactive glass scaffolds **[46]**.

Comparatively, better mechanical strength had been attained in most of the bioactive glass compositions than the biodegradable polymers **[47]**. Better mechanical properties of bioglass based scaffolds can be attained unless and until sintering has been done at higher temperatures. Sintering beyond the glass transition temperature leads to the formation of glass ceramic phases, which actually makes the scaffold inert **[48]**. But later on, ***Oscar P.F. et al*** **[49]** had observed with their 45S5 bioglass ceramic scaffolds, that bioactivity is restricted and not completely suppressed, due to crystallinity. Due to this ambiguous situation prevailed within the crystallization and mechanical properties of bioglass scaffolds, fabrication of bioglass based composites had been started. The approach towards the fabrication of bioglass based scaffolds had been varying in a wide range due to its capability of attaining tailored properties. ***Francesco Baino et al*** **[50]**, in their review, had described different methods used for the preparation of bioglass based scaffolds, till date. The entire description had been depicted in **table 2.7.**

R. Boccaccini et al **[51]** had fabricated porous 45S5 bioglass scaffolds by using sponge replica method. By dipping polyurethane foams in melt-derived bioglass slurry, the scaffolds had been fabricated and sintered at around 1000°C/1 hour. At around 89-92% of porosity and 0.42MPa of compressive strength had been obtained with these scaffolds. Keeping the trabecular bone regions in mind, this work had been executed.

Table 2.7 – Processing methods for the fabrication of bioactive glass based scaffolds [**50**]

S.No	Processing method	Description
1.	Coating methods	It provides a bioactive layer on the substrate of the major implant material. It is carried out from the suspensions of bioactive glass particulates. Thermal treatment is not applied to remove the organic phase. Sintering is not done for the densification of inorganic phase.
2.	Evaporation induced self-assembly [EISA]	This method offers mesoporous silica based glasses. With the metal alkoxide liquid precursors, surfactant is added for better solvent dispersion. Evaporation of ethanol increases the concentration of surfactant. Further the surfactants drive the silica molecules to organise into a mesophase structure. Calcination burnouts the surfactant and generate mesoporous glasses.

Table – 2.7 continued.

3.	H_2O_2 foaming	Bioactive glass powders and H_2O_2 solution is mixed homogeneously and the solvent had been casted into moulds. The casted bodies had been dried at 60°C in a dry air owen and foams had been generated. Further sintering of those casted bodies forms porous scaffolds.
4.	In-situ foaming	Sol-gel derived bioactive glass powders had been dispersed in liquid monomer batch. After polymerisation took place, sintering of glass particles had been carried out.
5.	Microsphere sintering	Glass polymer microsphere composites had been prepared by evaporation of emulsion solvent. Sintering of those microspheres results with porous 3D bioglass scaffolds
6.	Organic phase burn out	Bioactive glass powders had been mixed with organic polymers, either binder or pore formers, had been compacted with some optimum pressure and sintered at some optimum temperature.
7.	Sol gel method	This method is a combination of hydrolysis and condensation reactions. With metal alkoxide liquid precursors, glass formation had been carried out at low temperatures. Glass monoliths and coatings can be done with this method. Furthermore, production of glass nanomaterial can be done by this method.
8.	Sol gel foaming	Similar to the previous method, synthesis had been carried out liquid precursors. In additional to that, surfactants had been included for the formation of foams. Generated foams had been sintered for the formation of porous scaffolds.
9.	Solid free form fabrication	As per the computer aided design, 3D printing of scaffolds had been done.
10.	Solvent casting – particulate leaching	Polymer solution had been prepared and salt particles had been added into it. Bioactive glass particles had been added later and casted into moulds. On drying the solvent evaporates and leaves the salt behind. On treating them in a bath makes the salt particles to get leached out and leaves a porous structure.

As bioglass scaffolds degrade in a controlled manner, the targeted oxides, which had been incorporated into the glass system for a particular purpose, will release as metals ions and performs its function. The feasibility of tailoring a biomaterial is more in the glass system when compared to the other biomaterials.

2.3 Functionally graded scaffolds (FGS)

Identification of a utility of FGSs in the field of biomaterials is entirely a new scenario. The necessity of FGSs in the biological systems is purely of the responses stimulated by the morphology of the living tissues. The prominent and remarkable feature of biomaterials in invitro is the tendency to form hierarchical structures. The pathways of the cells and other micro fluids of biological systems are habituated with the hierarchical structures **[52]**. In order define the fabricated scaffolds as biomimetic scaffolds, and then it is necessary to obtain hierarchical architectures for the scaffolds. In the previous sections, it had been discussed that bone is a functionally graded material, with dense-cortical bone layer and porous – cancellous bone layer, which is the outer and inner layers of the bone respectively. Better bone ingrowth had been facilitated in the porous regions and dense regions restrict the physiological and mechanical stress generated within and surrounding the host tissue **[53]**. So, in particular, it is necessary to fabricate scaffolds with a porosity gradient structure to mimic the natural bone architecture.

Cevat Erisken et al **[54]** had fabricated functionally graded Polycaprolactone/β-TCP nanocomposite by using twin screw extrusion/electrospining process. This polymer blend had been incorporated along with β-TCP to mimic the bone and cartilage interface. The spatial distribution of calcium phosphate phase and organic polymer phase increases the feasibility of better proliferation of the osteoblast cells.

Young-Mi Soon et al **[55]** went beyond further for the reproduction of cortical/cancellous bone structure. In a material science perspective, it can be called as core and shell structures. Their scaffolds had been fabricated by using Camphene based freeze casting method, with different concentrations of hydroxyapatite slurries. The slurries had been casted on a graphite template and further it had been fired around 900°C for the removal of the same. Then the dried core/shell green structures had been sintered at around 1250°C. It had been observed that compressive strength of core/shell HA scaffolds is better than the ordinary porous (non-graded) HA scaffolds. Similar camphene based free casting method had been utilized by ***Changqing Hong et al*** **[56]** for fabrication of functionally graded alumina ceramics. Here slurries had been casted in silicone rubber die instead of graphite template.

Each layer of FGS possesses different characteristic features and can be fabricated individually. ***Y. H. Hsu et al*** **[57]** had fabricated cortical bone layer and cancellous bone layer separately and joined together.

Low porosity layer had been fabricated by vacuum impregnation method whereas high-porosity layer had been fabricated by using dipping method. Both of the microstructures partly depend on the templates used. Later on, both the layers had been joined by using press-fitting method. Illustration of this method had been given in the Fig – 2.1. .

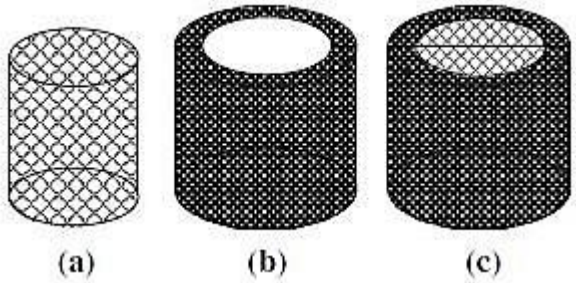

(a) High porous –spongy bone by dipping method

(b) Low porous – cortical bone layer by vacuum impregnation method

(c) Joined cortical and spongy bone layers by press-fitting method

Fig –2.1 Illustrations of cortical-cancellous bone layer fabrication ***[Y. H. Hsu et al]***

Gradient structures can also be generated by using a mixture of powders with different particle size. ***L.H.Wong et al*** **[58]** had prepared Fluoroapatite and TCP on different particle sizes. Their investigations reveal the comparative study of symmetric and non-symmetric FGM on before and after sintering. This had been clearly visualized in Fig – 2.2. In this work, the differential shrinkage had been considered as a major problem.

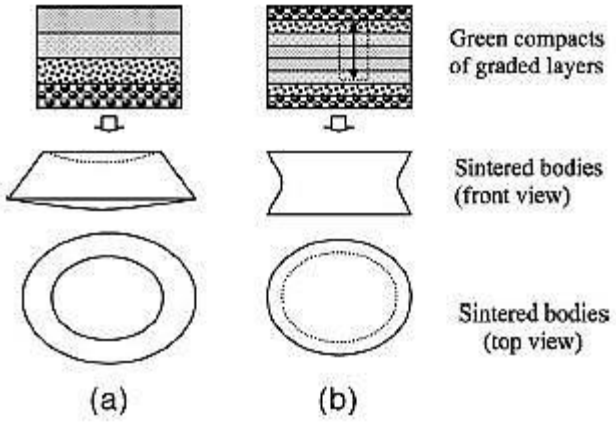

Fig – 2.2 Change in shape after sintering due to differential shrinkage (a) Non-symmetric FGM (b) Symmetric FGM ***[L.H.Wong et al]***

Chiara vitale-brovarone et al **[59]** had fabricated porosity gradient bioglass ceramic scaffold to mimic the cortical and cancellous bone structure. SiO_2(45 wt.%) – P_2O_5 (3 wt.%) – CaO (26 wt.%) – MgO (7wt.%) – Na_2O (15wt.%) – K_2O (4wt.%) glass system had been in this work, which is commercially called as CEL2 glass. For the processing of this FG-glass ceramic scaffold, they had proposed six methods (refer Fig – 2.3) and its features had been illustrated in the table – 2.7.

Table – 2.8 Characteristic feature of CEL 2 glass ceramic – porosity gradient sacaffold **[59]**

Method	**Preparation details**	**Scaffold structure**	**Coresspondence with the human bone**
A	PE burn-off	Multilayer structure	Cancellous bone
B	PE burn-off + glazing technique	Porous layer +compact layer	Cancellous/ cortical bone
C	Sponge replication	Porous double layer	Cancellous bone
D	Sponge replication + glass powders pressing	Porous double layer + compact layer	Cancellous/ cortical bone
E	Sponge replication + glazing technique	Porous double layer + compact layer	Cancellous/ cortical bone
F	Sponge replication + PE burn-off	Porous double layer	Cancellous bone
S-CEL2	Sintering of glass powder compacts	Bulk	Cortical bone

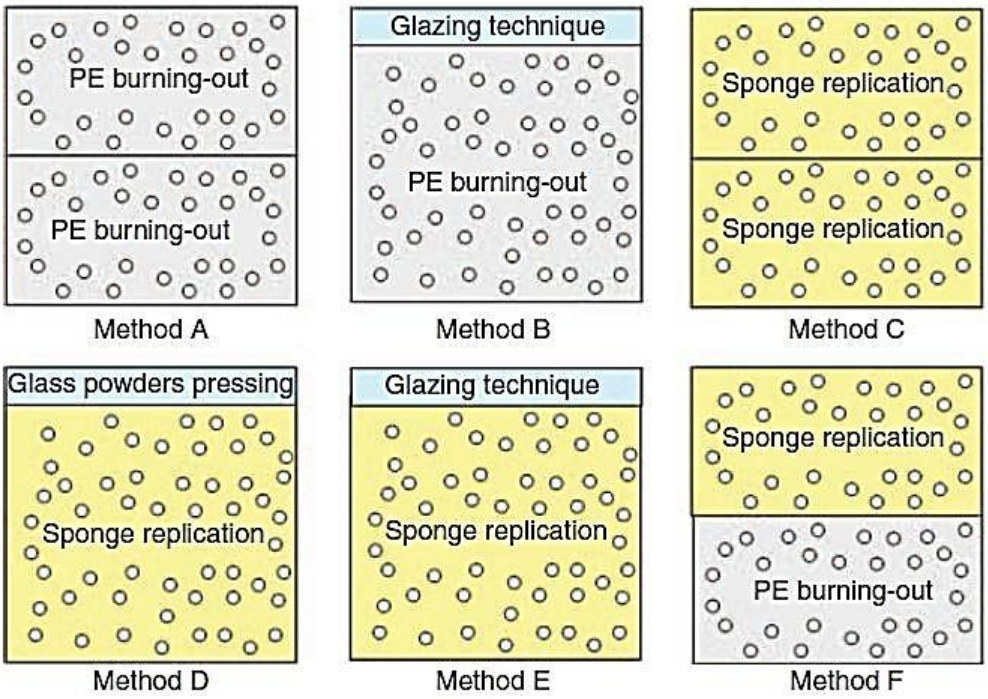

Fig – 2.3 Features of the proposed methods for the fabrication of FGS **[59]**

Jan Wernera et al **[60]** had developed graded HA matrices by multiple tape casting method as shown in the Fig – 2.4. Along with HA slurry, polybutylmethacrylate spheres, of diameters ranging from 100-200mm and in further heat treatment, leaves a pore size of about 70-200mm. The sintering temperature is the major criteria which influence more on the density and microstructure. It had been observed that a three-layer graded porous structure attains flexural strength higher than the homogeneous porous structure.

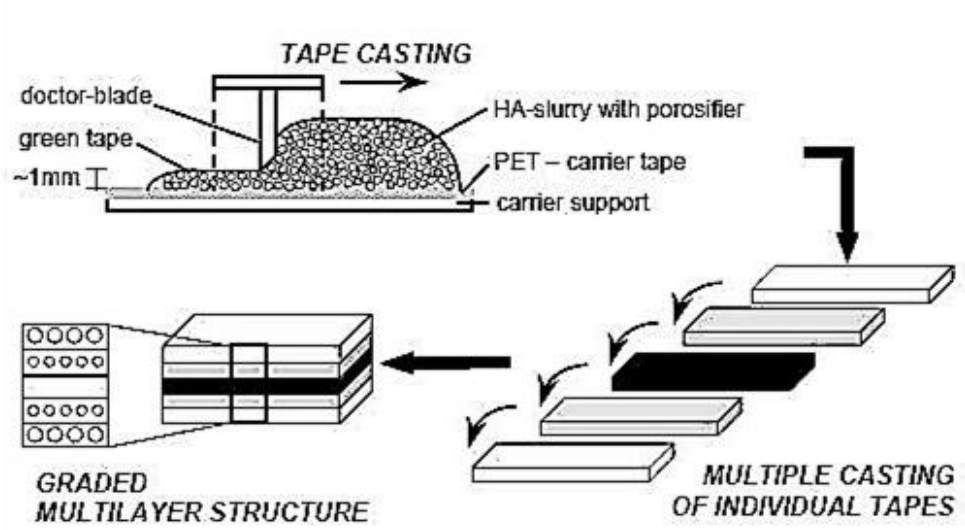

Fig – 2.4 Hydroxyapatite based FGS by multiple tape casting method **[60]**

2.4 Concluding Remarks from the literature

On the above findings from the literature, it can be observed that the fabrication of porosity gradient – functionally graded scaffold will fetch the exact architecture of the natural bone. Various processing techniques for the fabrication of functionally graded scaffold had been summarised in the above mentioned literatures. A distinct boundary conditions for the cortical and cancellous bone layers has to be applied in order to mimic the exact nature of the bone, which had not been optimized yet in the FGS design. The current work had been capitalised more on this problem, which had been tried to overcome by the uniaxial die pressing method. Morever, fabrication of functionally graded glass scaffolds are attempted by very few people. Its well known that FGS will create an exact mimicking of the biomodal structure of bone. Further more, FGS designed with glass materials fluorish more with an enhanced bioactivity, since these glasses topped the chart of index of bioactivity **(refer table – 1.6)**.

OBJECTIVE OF THE CURRENT WORK

Functionally graded scaffolds (FGS) prepared with Class A biomaterials can be the better alternative for bone substitutes. It is evident from the literature that the fabrication of functionally graded scaffolds had been carried out with highly complex protocols. It is necessary to propose a simple method for the fabrication of functionally graded scaffolds. In this current work, bioactive glass compositions 45S5 (6wt. % P_2O_5), 2P (2wt. % P_2O_5) and 4P (4wt. % P_2O_5) had been taken for the fabrication of functionally graded scaffolds. The compositions of these bioactive glasses had been illustrated in the table given below

BIOACTIVE GLASS	SiO_2 **(in wt%)**	Na_2O **(in wt%)**	CaO **(in wt%)**	P_2O_5 **(in wt%)**
45S5 Bioglass	45	24.5	24.5	6
2P	49.6	24.2	24.2	2
4P	48.4	23.8	23.8	4

But it is necessary to evaluate the performance of single layer scaffolds, before fabrication of functionally graded scaffolds. The featured investigations in this work had been designed as follows:

- Synthesis of bioactive glass compositions – 45S5, 2P and 4P by melt quench method.
- Study of thermal analysis and sintering behavior of Bioactive glass compositions
- Study of phase Analysis and FTIR analysis of bioactive glass and glass ceramics
- Haemocompatibility, protein adsorption and cell viability studies on bioactive glass and glass ceramics
- Fabrication of porous single layer bioactive glass ceramic scaffolds, incorporating naphthalene as a pore former, by using uniaxial pressed and sintering method
- Evaluation of Apparent Porosity, Bulk density, Diametral tensile strength & Flexural strength of porous single layer scaffolds
- Microstructure analysis of single layer – porous bioactive glass ceramic scaffolds
- Fabrication of porosity gradient bioactive glass ceramic scaffolds, incorporating naphthalene as a pore former, by uniaxial pressed and sintering method

- Evaluation of Apparent porosity and bulk density of entire FGS and layer by layer
- Brazilian disc analysis of functionally graded bioactive glass ceramic scaffolds
- Microstructure analysis of functionally graded bioactive glass ceramic scaffolds
- Invitro analysis of functionally graded bioactive glass ceramic scaffolds by using Simulated Body Fluid (SBF).
- Invitro analysis of functionally graded bioactive glass ceramic scaffolds by using MG-63 cell line.

CHAPTER 3

EXPERIMENTAL PROCEDURE

3.1 Bioactive glass composition and raw materials

The evaluation and performance of bioactive glasses mentioned in the SiO_2-CaO-Na_2O ternary phase diagram (refer fig – 1.4) had been carried out by keeping P_2O_5 as 6 wt.%. This had triggered to initiate the work by analysing bioactive glass compositions with varying wt.% of P_2O_5. The glass compositions selected in this current work had been given in table 3.1. The glass composition with 2 wt.% of P_2O_5 had been identified as 2P and similarly the glass composition with 4 wt.% P_2O_5 had been called as 4P.

Table 3.1 – Bioactive glass compositions used

BIOACTIVE GLASS	$\boldsymbol{SiO_2}$ **(in wt%)**	$\boldsymbol{Na_2O}$ **(in wt%)**	$\boldsymbol{CaO}$ **(in wt%)**	$\boldsymbol{P_2O_5}$ **(in wt%)**
45S5 Bioglass	45	24.5	24.5	6
4P **[61]**	48.4	23.8	23.8	4
2P **[61]**	49.6	24.2	24.2	2

In order to synthesize bulk and economic bioactive glass powders, melt quench route had been selected. The extra pure silica (40-150 mesh) - SiO_2, precipitated Calcium Carbonate (AR) – $CaCO_3$ and Anhydrous Diammonium Hydrogen Orthophosphate – $(NH_4)_2HPO_4$, purchased from Loba Chemie, Mumbai, India, had been used as raw materials for SiO_2, CaO and P_2O_5 in the glass system. Anhydrous Sodium Carbonate (AR), procured from RFCL, is used as a source for Na_2O. As mentioned in section 1.6.3, these raw materials are cheaper than the precursors used for sol-gel method.

3.2 Preparation of glass powders by melt quench method

Without further processing of raw materials, as per the batch calculation, the raw materials had been weighed and mixed homogeneously. The above mentioned glass compositions (Table-3.1) had been melted in sillimanite crucible as per the optimised melting profile shown in Fig 3.1. At 650°C, the glass batch had been soaked for 1hour and proceeds further to the decarbonation stage at 950°C. For the decomposition of carbonates present in Anhydrous Sodium Carbonate and Calcium Carbonate, the glass batch had been soaked for 5 hours at 950°C.

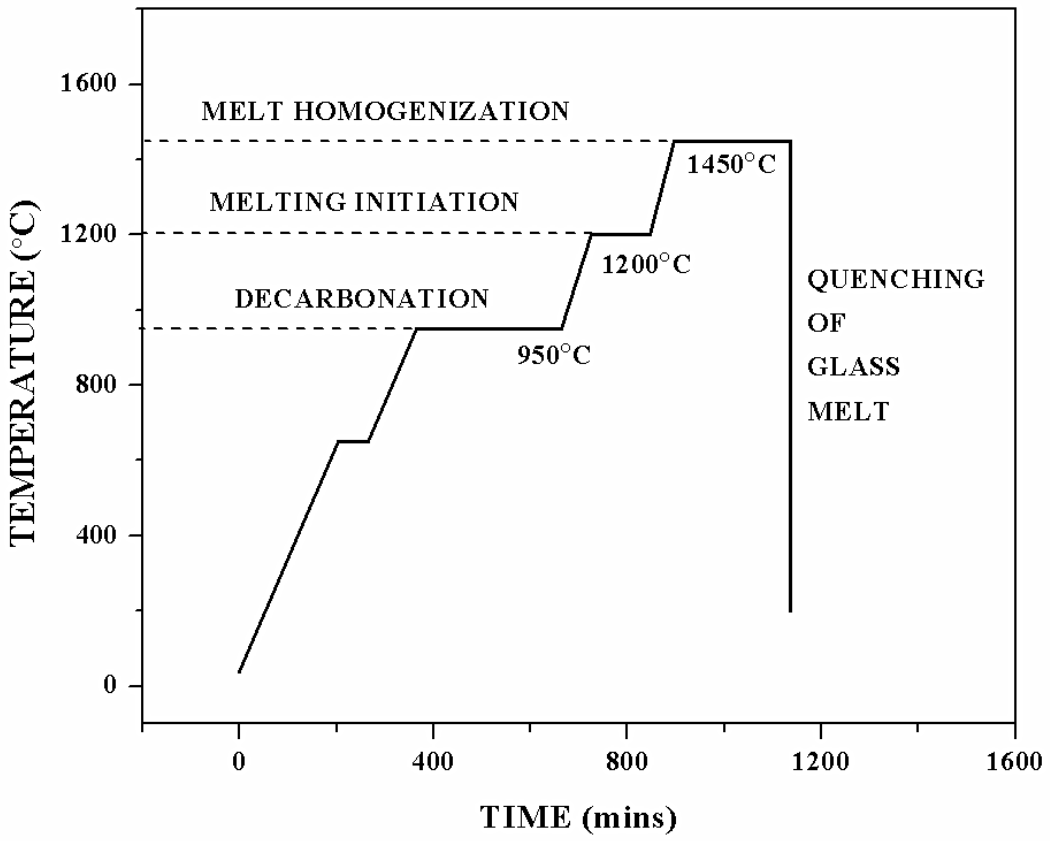

Fig – 3.1 Melting profile of bioactive glasses

The next soaking cycle had been carried out in the melt initiation stage at 1200°C for 2 hours. Finally, the glass batch had been melted at 1450°C for 4 hours. Sufficient holding time has to be provided at 1450°C to attain better homogeneity of the melt. Then the glass melt had been poured in a water bath for the formation of glass frits. The glass frits had been milled by using planetary milling with Silicon Nitride balls on a silicon nitride milling jars in a deionized water medium. The obtained glass frits had been milled for 8 hours at 350 rpm to make them into powder. Further, the powders are again milled for 13 hours at 380 rpm.

3.3 DSC-TG Analysis of Bioactive glass powders

Thermal Analysis of the bioactive glass powders had been carried out by using Netzsch STA/409C. Both Differential Scanning Calorimetry and Thermogravimetric analysis had been done with this equipment. The glass powders had been fired from room temperature to 950°C in Argon atmosphere. Heat flow (mW/mg) and Mass loss (%) had been observed with the corresponding temperature.

3.4 Dilatometric analysis of Bioactive glass samples

Sintering and shrinkage behavior of the bioactive glass green compacts had been studied by using NETZSCH dilatometer model DIL 402 C. Bar shaped (15mm x 6mm x 6mm) bioactive glass green compacts had been used for this investigation. The sintering and shrinkage behavior had been observed by firing the samples from room temperature to 900°C at a heating rate of 10°C/min, in Argon atmosphere.

3.5 BET surface area analysis

The Brunauer–Emmett–Teller (BET) surface area had been measured by using 5 point method analysis had been done by AUTOSORB 1, (Quantachrome) (Model No: Nova 1200 BET). The BET method is carried out by using monolayer of liquid nitrogen. The surface area had been calculated by using the following equation, which actually required the amount of nitrogen absorbed.

$$\textbf{BET Equation,} \qquad \left(\frac{\mathbf{1}}{\boldsymbol{V_g}}\right)\left(\frac{\boldsymbol{x}}{\mathbf{1}-\boldsymbol{x}}\right) = \left(\frac{(\boldsymbol{c}-\mathbf{1})}{\boldsymbol{cV_m}}\right)\boldsymbol{x} + \left(\frac{\mathbf{1}}{\boldsymbol{cV_m}}\right)$$

where, V_g = volume of gas adsorbed, V_m = volume of gas adsorbed at monolayer coverage, $x = P/P_o$, P = Ambient pressure, P_o= Total pressure, c = a constant that is related to the heat of adsorption. A plot of $\left[\left(\frac{1}{V_g}\right)\left(\frac{x}{(1-x)}\right)\right]$ versus x gives a straight line with slope, $m = \frac{(c-1)}{(cV_m)}$, Intercept, $g = \frac{1}{cV_m}$, The value of V_m and c are calculated, $V_m = \frac{1}{(slope+intercept)}$. This is normalized by the mass of particles tested to give a specific surface area (m^2/gm).

3.6 Cell Viability analysis of bioactive glass powders

Before designing and fabricating scaffolds, it is necessary to check the level of toxicity of the biomaterial used. The cytotoxicity analysis had been done on bioactive glass powders and bioactive glass ceramics (heat treated at 800°C, 850°C and 900°C) with MG-63 osteoblast cell line. The cell line had been procured from NCCS, Pune, India and the entire investigation had been carried out in the Department of Biotechnology & Medical Engineering, NIT Rourkela. The cells had been seeded, at a concentration of 10^4 MG-63 cells per well, along with 200 µl of Dulbecco's Modified Eagle Medium (DMEM), Himedia (high glucose), on a 96 well plate. The cell seeded well plate had been kept for incubation(5% CO_2 + 95% Humidity @ 37.5°C) for 1 day, in a CO_2 incubator for cell adherence.

10mg of bioactive glass and glass ceramic powders had been sterilized by heating at around 121 °C in an autoclave, at 15 psi pressure for 20 minutes. Then the sterlized glass and glass ceramic powders had been dispersed in a Phosphate Buffer Saline(PBS), Himedia, at a ratio of 1:9 **[62]**. After the cells had been adhered on the surface of the wells, the media had been removed from the wells. The 10µl of PBS-glass and 10µl of PBS-glass ceramic powder mixture had been added to the wells along with 190µl of fresh DMEM, had been kept for incubation.

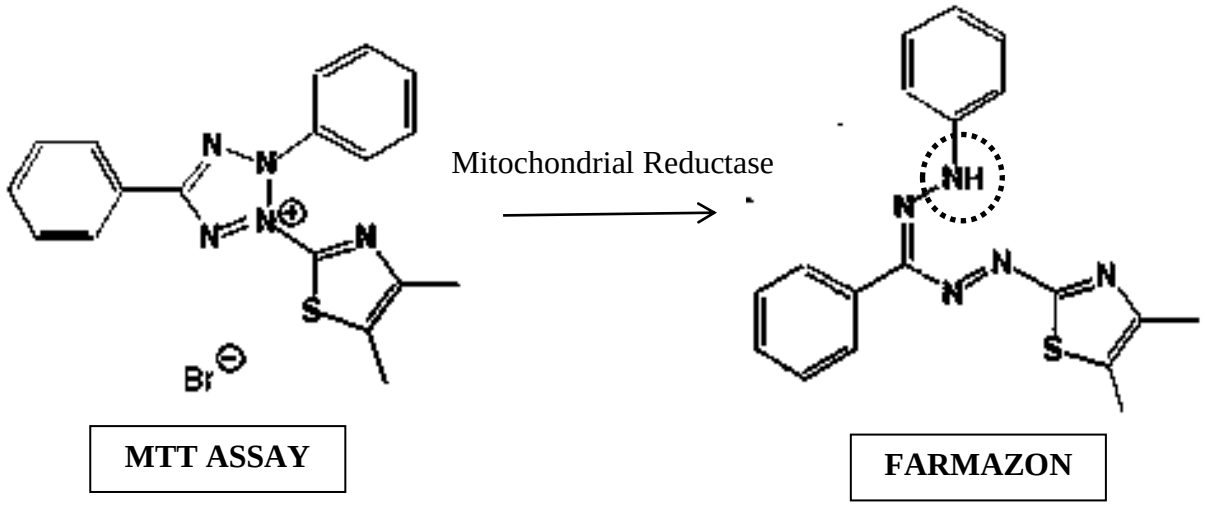

Fig – 3.2 Formation of Farmazon compounds during mitochondrial reduction

After 1 day incubation, the media (along with PBS-glass/glass ceramic mixture) had been removed from the wells. Then 1µl of MTT Assay, Himedia, and 9µl of DMEM added to the wells. MTT Assay is a complex bromide compound which undergoes mitochondrial reduction reaction with the viable cells present in the well, as shown below. During this reaction, viable mitochondria crystallizes the MTT, which leads to the formation of farmazon compound. The farmazon is an insoluble purple color precipitate which had been dissolved by Dimethyl sulfoxide (DMSO), Sigma Aldrich, Reagent Grade, 99%. The optical density of farmazon compound will be directly proportional to the cell viability. This had been evaluated by using Double beam UV Spectrophotometer, Systronicx 2203, by measuring the absorbance at 595nm **[63]**.

3.7 Protein Adsorption Studies of Bioactive glass powders

To attain better proliferation, protein absorption has to be carried out by these bioactive glass scaffold. While incorporating outer collagen layer to the bioglass scaffold, this protein adsorption studies plays the major role.

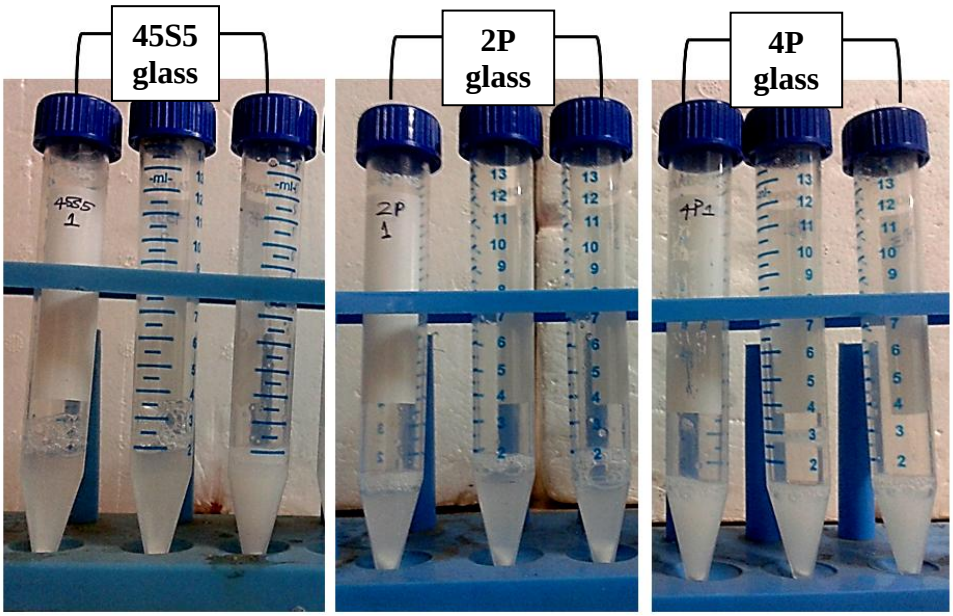

Fig – 3.3(a) Bioactive glass powders mixed with BSA aqueous solution

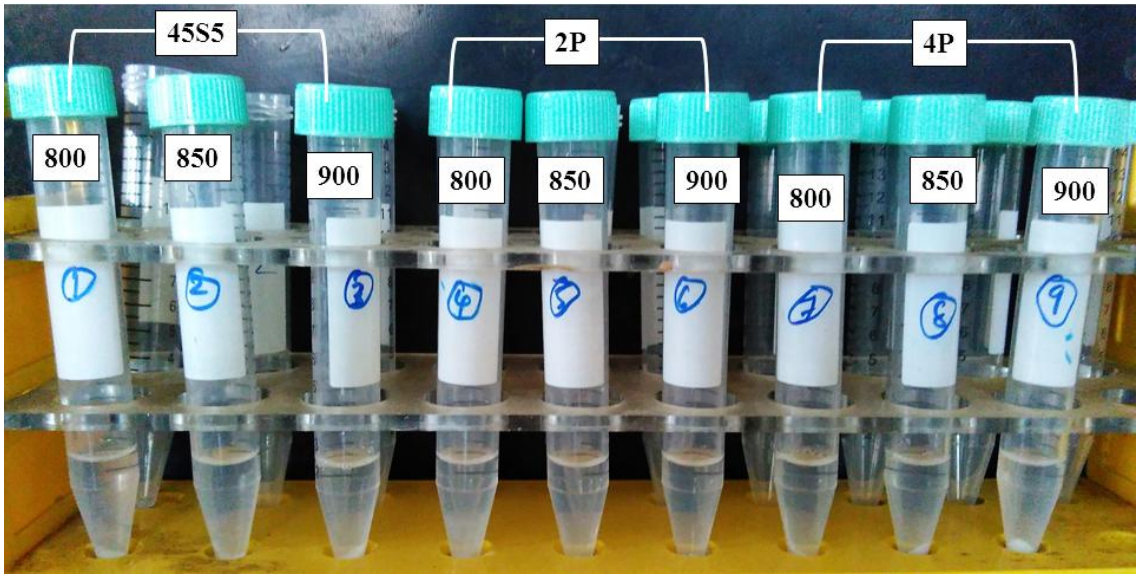

Fig – 3.3 (b) Bioactive glass ceramic powders – heat treated at 800°C, 850°C & 900°C, mixed with BSA solution

The entire investigation had been carried out in the Department of Biotechnology & Medical Engineering, NIT Rourkela. The protein adsorption studies had been carried by corelating the absorption capability of bioactive glass powders with Bovine Serum Albumin (BSA) **[64]**.

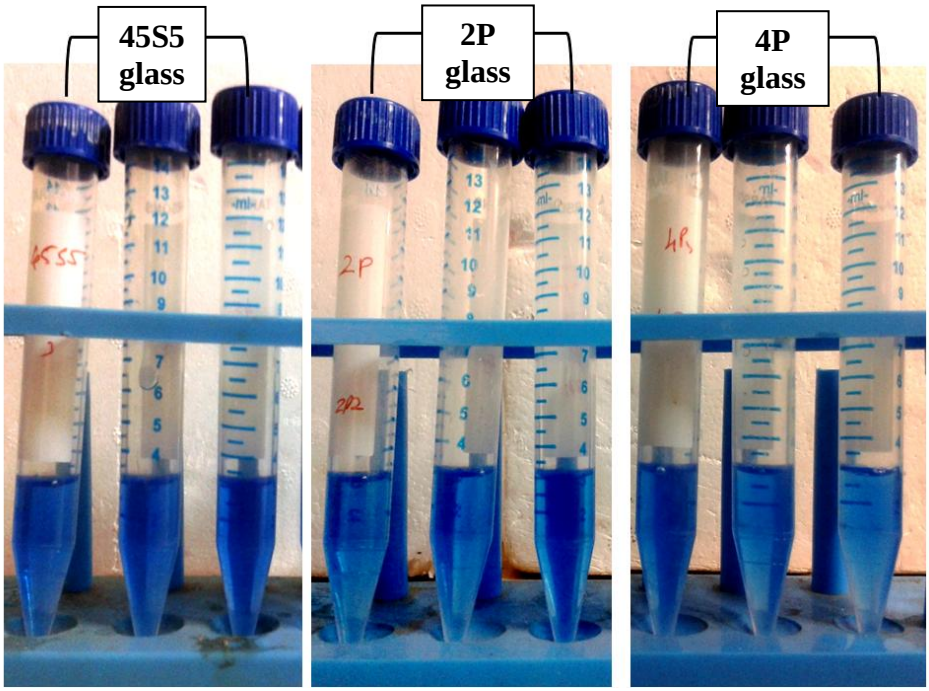

Fig – 3.3(c) BSA adsorbed Bioactive glass powders after addition of Bradd Ford Assay

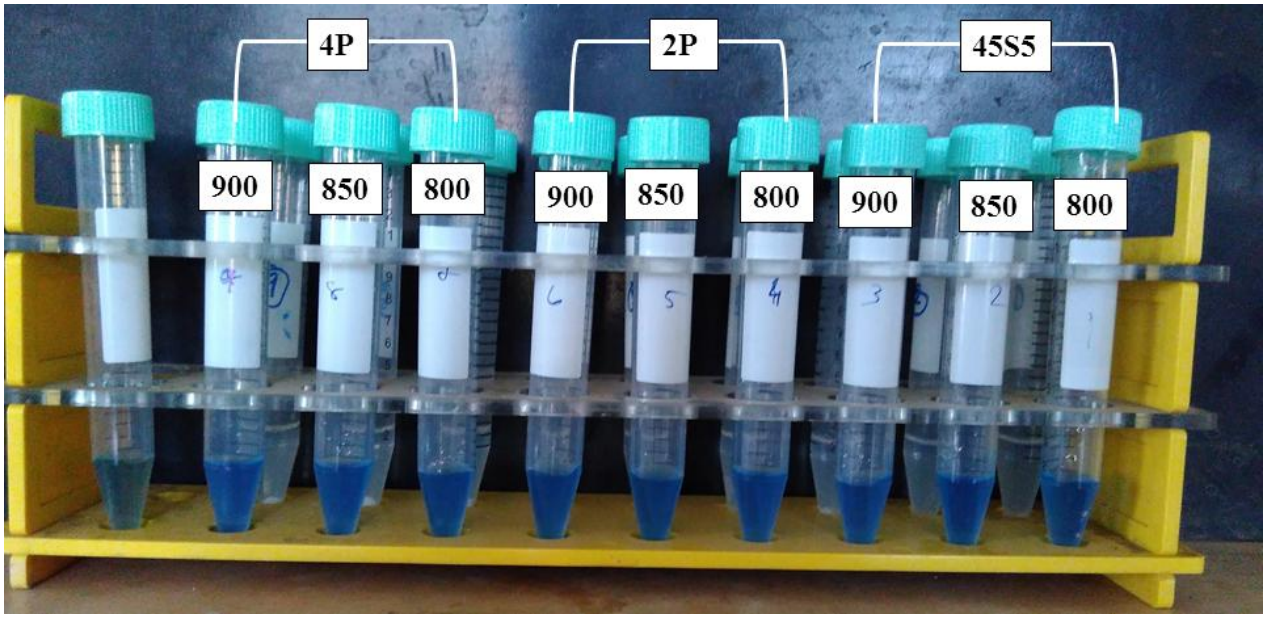

Fig – 3.3 (d) BSA adsorbed Bioactive glass ceramic powders – heat treated at 800°C, 850°C & 900°C, after addition of Bradd Ford Assay

BSA aqueous solution had been prepared at 1200µg/ml concentration. The protein adsorption studies had been carried out on triplicate samples of Bioactive glass powders and bioactive glass ceramics, which had been heat treated at 800°C, 850°C & 900°C. The samples had been sterilized (section 3.6) and added to these BSA aqueous solution at concentration of 10mg/ml [refer Fig – 3.3(a) & 3.3 (b)]. The samples had been kept for incubation for period of 24 hours for the adsorption of proteins. Then the samples had been centrifuged at 8000 rpm in a REMI Cooling Centrifuge **[65]**. The supernatant solvent had been collected separately and bradford Assay had been added for evaluation of left out protein present in the solvent **[66]**. The optical density measured at 595nm, by using Double beam UV Spectrophotometer, Systronicx 2203, had been deducted from the total amount of protein added. This gives the amount of protein adsorbed by the bioactive glass and glass ceramic powders.

3.8 Haemocompatibility analysis of bioactive glass powders

Blood compatibility or haemocompatibility of the bioactive glass and glass ceramic powders had been studied by using a fresh goat blood. The entire investigation had been carried out in the Department of Biotechnology & Medical Engineering, NIT Rourkela.

Fig – 3.4(a) Haemocompatibility analyses of bioactive glass and glass ceramic powders – before incubation

To prevent coagulation, tri-sodium citrate (3.8 g w/v %), Merk India, Reagent Grade, was added to the blood. The blood was diluted with normal saline (0.9 % NaCl), Merk India, in the ratio of 8:10 (v/v) as the working standard. 10 mg of the samples was taken in a clean test tube and 0.5ml of blood was added to it.

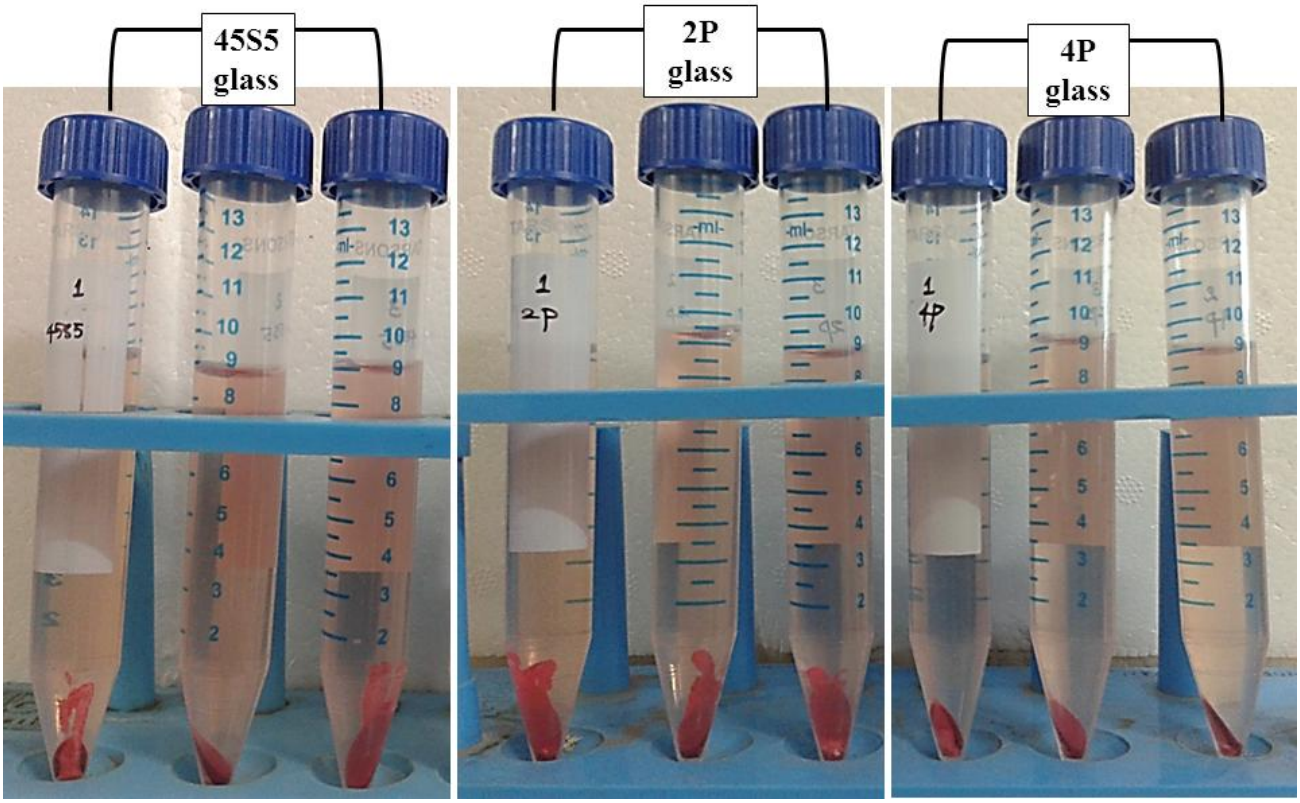

Fig – 3.4(b) Haemocompatibility analyses of bioactive glass powders – after incubation and centrifuge

The sample volume was made up to 10ml with normal saline (0.9 % NaCl) and kept at 37 °C for 1h. 0.5 ml of saline and 0.5 ml of 0.1 M HCl were taken as negative and positive controls respectively. After the incubation, the solutions were centrifuged at 4000 RPM for 10 min. Absorbance, in terms of optical density (O.D) of the supernatant was measured at 545 nm. The samples having percentage hemolysis less than 5 % are considered as highly hemocompatible and the samples having percentage hemolysis less than 10 % is hemocompatible. The samples which have percentage hemolysis more than 20 % are not hemocompatible **[67]**.

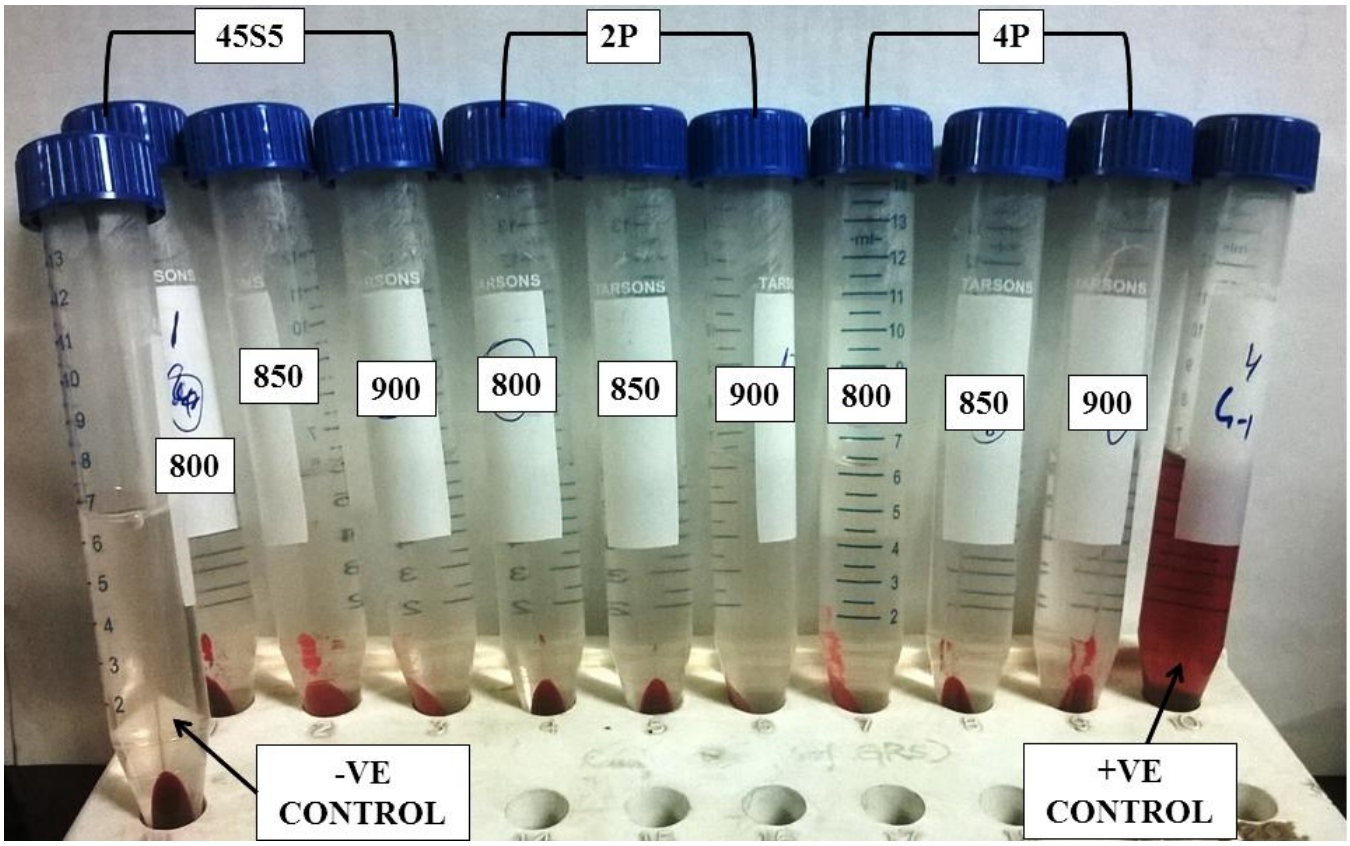

Fig – 3.4(c) Haemocompatibility analyses of bioactive glass ceramic powders – after incubation and centrifuge

The percentage hemolysis is given by equation,

$$\boldsymbol{Hemolysis}\ (\%) = \left(\frac{\boldsymbol{OD_{Test} - OD_{-ve}}}{\boldsymbol{OD_{+ve} - OD_{-ve}}}\right) * \mathbf{100}$$

Where OD_{Test} – Bioactive glass powders with blood sample

OD_{+ve} – 0.1M HCl with blood sample

OD_{-ve} – Saline with blood sample

Fig – 3.4(c) shows the Haemocompatibility analysis of bioactive glass ceramic powders. Apart from that positive control and negative control of the analysis had also been shown in the figure. The positive control, the 0.1M HCl solution along with blood sample shows 100% haemolysis and the negative control, Saline with blood sample, shows the 0% hemolysis.

3.9 Fabrication of porous single layer bioactive glass ceramic scaffolds

Porous bioactive glass scaffolds had been prepared by using uniaxially pressed and sintering method. Naphthalene had been used as a pore former. The glass powders (100, 70 & 50 wt.%) had been mixed with different wt.% of naphthalene (0, 30 & 50 wt.%) and had been binded with 3 wt.% PVA solution. The binded mixture had been uniaxially pressed in a hydraulic press, at 260MPa to form cylindrical pellets, approximately 12mm diameter. The green samples had been dried at around 90°C for 6 hours in a hot air owen, for the decomposition of naphthalene. Then the samples had been sintered at 800, 850 and 900°C for 2 hours.

3.10 Phase Analysis of bioactive glass and glass ceramic powders

The amorphous nature and the glass ceramic phases formed beyond the glass transition temperature had been investigated by using Philips X-ray Diffractometer with Ni filter Cu-K_α (λ=1.5418 Å). Along with the milled bioactive glass powders, glass powders sintered at 700°C, 800°C, 850°C and 900°C, had been kept for powder diffraction. The diffraction angle(2θ) measured from 15°C to 50°C at a scanning rate of 0.05°/min.

3.11 FTIR Analysis of bioactive glass powders

The structural analysis of bioactive glass and glass ceramic powders had been studied by using FTIR analysis. Bulk glass and glass ceramic powders had undergone transmission of infrared rays by using Shimadzu/IR prestige 21, in an ATR mode. The scanning range was around 600 – 1300 cm^{-1}.

3.12 Fabrication of porosity gradient bioactive glass ceramic scaffolds

As shown in the Fig – 3.6, the two concentric layers of bioactive glass scaffold may mimic the anatomy of the bone. The outer dense layer, represents the cortical bone layer and the inner porous layer mimics the cancellous bone layer. By uniaxially pressed and sintering, these porosity gradient scaffolds had been prepared. Mixing of napthalene, the pore former, into the glass powder had been done as given in the table 3.2.

Table 3.2 – Preparation of glass powder mixture for Porosity gradient bioactive glass scaffold

SAMPLE ID	OUTER LAYER		INNER LAYER	
	GLASS	NAPHTHALENE	GLASS	NAPHTHALENE
(030)	100 wt.%	0 wt.%	70wt.%	30 wt.%
(050)	100 wt.%	0 wt.%	50 wt.%	50 wt.%

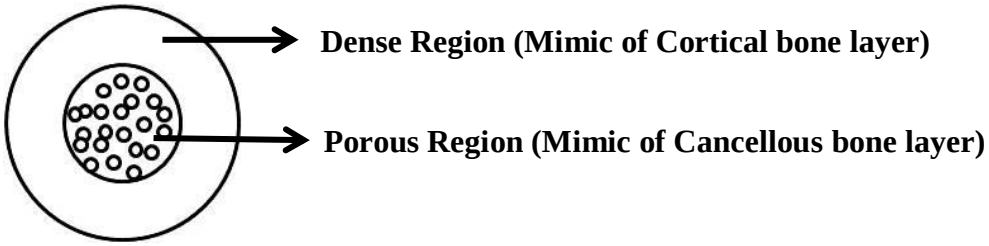

Fig – 3.5 Schematic representation of porosity gradient bioactive glass scaffold

It should be noted that napthalene, the pore former, had been added only to the mixture prepared for cancellous bone layer. Then 3 wt% PVA had been added as a binder to the above mentioned mixtures. Then the geometry had been fixed that the total diameter of the scaffold will be 30mm approx. and the inner layer diameter will be around 15mm. The fabrication procedure for the porosity gradient bioactive glass scaffold had been illustrated in the Fig – 3.6.

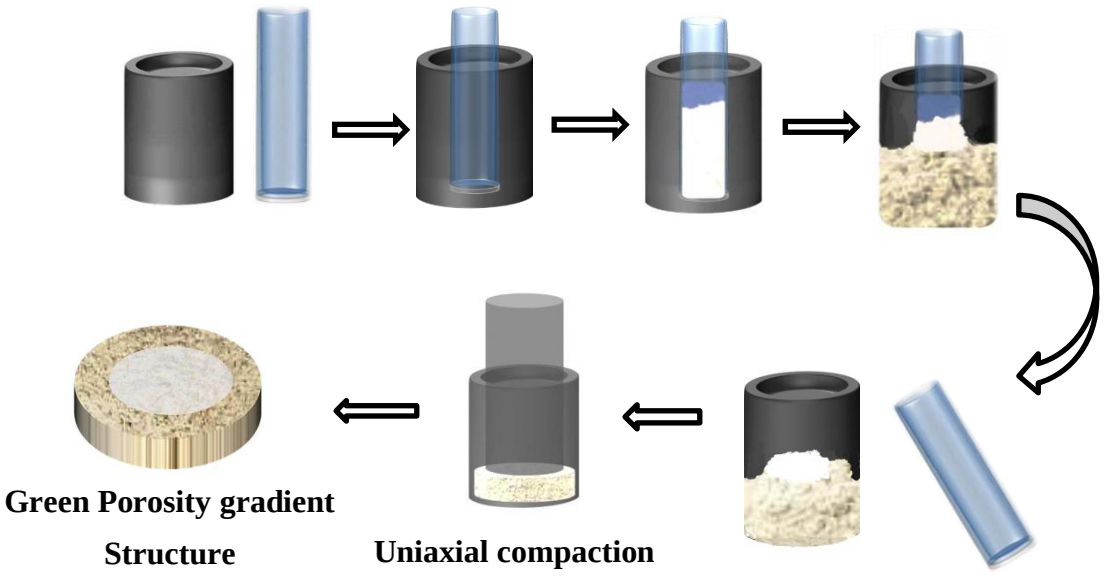

Fig – 3.6 Fabrication of porosity gradient bioactive glass scaffold

A hollow glass cylinder, approximately 15mm in diameter, had been kept inside the 30mm cylindrical die. It had been placed in such a way that it sits perfectly to the center of the die. The cortical bone layer mixture had been filled outside the glass hollow cylinder and cancellous bone layer mixture had been filled inside the hollow cylinder. After the powder mixture had been settled down within the cylindrical die by gentle tapping, the glass hollow cylinder had been taken out of the die. The entire mixture had been uniaxial pressed at around 100MPa. Then the green porosity gradient pellet had been dried at round 90°C for 6 hours. Later on, the samples had been sintered at 800, 850 and 900°C for 2 hours.

3.13 Apparent Porosity & Bulk density measurements

Bulk density and apparent porosity of the sintered scaffolds had been determined by using Archimedes principle. In this work, three types of specimens had been characterised.

1. Scaffolds with Individual / single layer (porous and dense)
2. Entire functionally graded scaffold
3. Outer and inner layer of scaffold

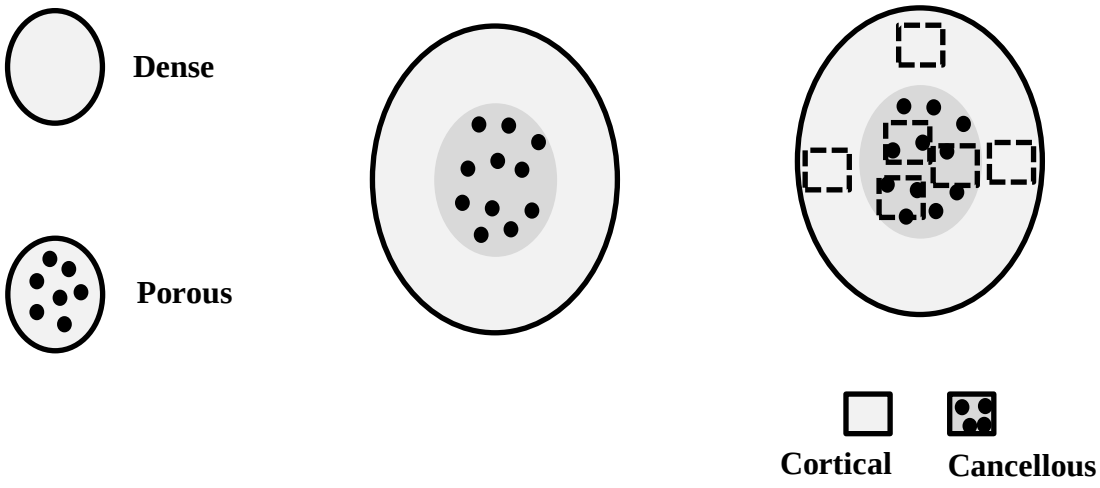

(a) Single layers scaffolds (b) FGS (c) Engraved out cortical and cancellous layers

Fig – 3.7 Specimens characterised for Apparent porosity & bulk density

Fig – 3.7(a) shows the individual layer or single layer scaffolds. Fig – 3.7(b) shows the porosity gradient scaffold (FGS) and Fig – 3.7(c) shows the cortical and cancellous bone layers. From the functionally graded scaffolds, the cortical and the cancellous bone layers had been cut out with help of a diamond tool. After the specimens had been prepared, the dry weight of the sample had been measured **(W_d)**. Then they had been immersed in kerosene and kept at vacuum for 1 hour in dessicator. This makes the kerosene to get penetrated into the pores. Then soaked weight **(W_s)** and suspended weight**(W_a)** of the sample had been measured. Finally the apparent porosity and bulk density of the samples had been measured by using the formulae as follows:

$$\boldsymbol{Bulk\ density, B.D = \left(\frac{W_d}{W_s - W_a}\right) * Density\ of\ kerosene}$$

$$\boldsymbol{Apparent\ porosity, A.P = \left(\frac{W_s - W_d}{W_s - W_a}\right) * 100}$$

3.14 Diametral Tensile strength measurements

In general, diametral tensile strength is a mechanical property used to evaluate the performance of brittle materials under tensile stress **[68]**. The individual layer or single layer scaffolds which had been sintered at 800, 850 & 900°C, had undergone diametral tensile strength measurement. The Diametric tensile strength had been calculated by using the formula,

$$\boldsymbol{Diametral\ tensile\ strength = \frac{2P}{\pi Dt}\ (MPa)}$$

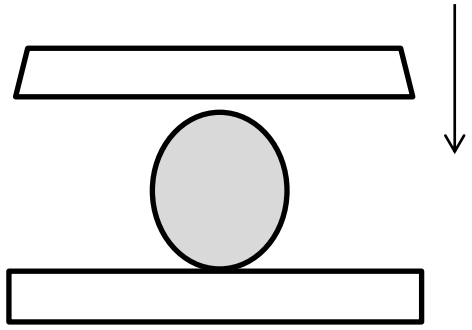

Fig – 3.8 Diametral tensile strength of individual / single layer scaffolds

3.15 Three point bending moment measurement

Porous single layer bioactive glass ceramics scaffolds of (60mm x 6mm x 6mm) size had been compacted at 100MPa and sintered at 800, 850 & 900°C. With a span of 45mm, the uniaxial loading had been given to the samples on 3point bending moment setup as shown in the Fig – 3.9. The flexural strength of the samples had been calculated by using the formula,

$$\boldsymbol{Flexural\ Strength, \sigma = \left(\frac{3FL}{2bd^2}\right)}$$

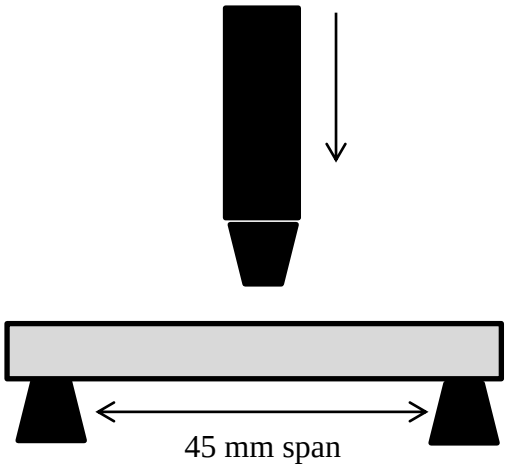

Fig – 3.9 Three point bending moment of dense bioactive glass ceramic scaffolds

3.16 Brazilian disc Analysis for FGS

In rock mechanics, splitting tensile strength is measure due to it gradient microstructures. Since the current work is also focussed on Functionally graded material, it is necessary to carry out splitting tensile test method. This method and its specimen preparation had been clearly drafted in the ASTM standards international, D3967-08 **[69]**. A lot of specifications has to be followed as per the ASTM standards in order to prepare brazilian disc specimens. Thickness to diameter (t/D) ratio should be between 0.2 to 0.75. The ends of the specimen had been cut to make it parallel to each other. Brazilian disc specimens had been prepared by using a diamond tool and the splitting tensile strength measurement had been measured as illustrated in Fig – 3.10.

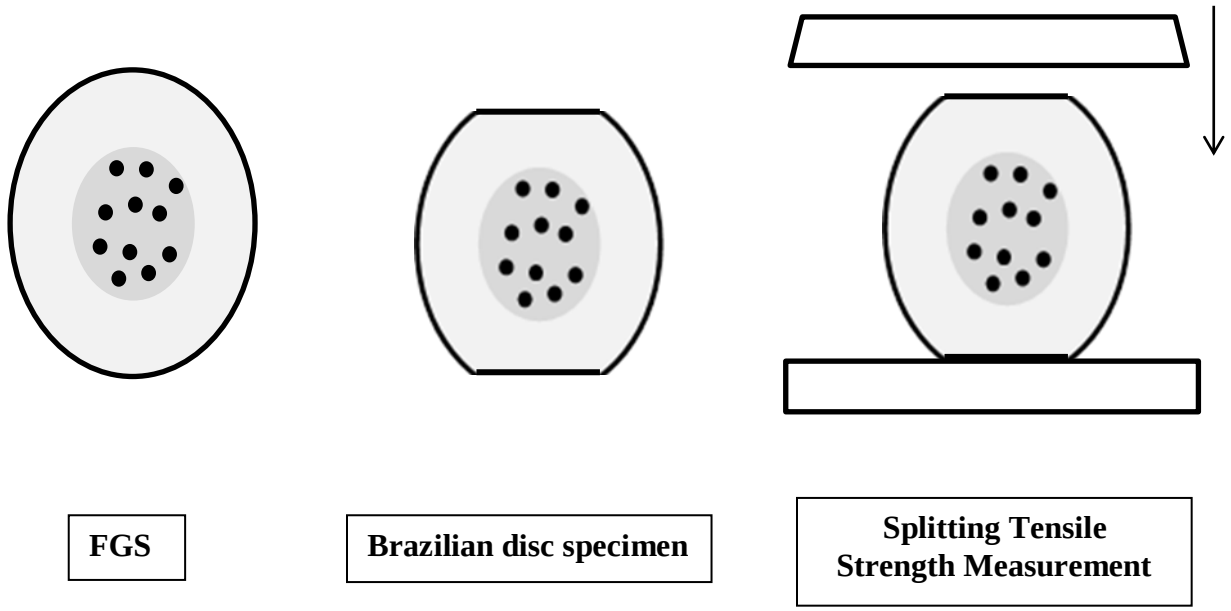

Fig – 3.10 illustration of splitting tensile strength measurement of FGS

3.17 Invitro analysis of FGS by using SBF

The bioactive glass scaffolds prepared had been immersed in Simulated Body Fluid to analyse the regeneration capacity. The complete mechanism of bioactive glass scaffolds in SBF had been illustrated clearly in the section 1.3.2. Kokubo **[70]** and many others had designed the SBF concentration in such a way that they closly mimic the ion concentrations present in the human blood plasma. Kokubo et al **[71]** had confirmed the formation of apatite layer by soaking the bioglass type scaffolds in SBF. The intention of this experiment in this current work is to see how the morphology of apatite layer had been differentiated between porous and dense layers of porosity gradient scaffolds. The Table – 3.3 depicts the close mimic of ionic concentrations of SBF and Human blood plasma designed by Kokubo et al **[71]**. The table – 3.4 gives the raw materials used and amount required for the preparation of 1000ml of SBF **[72]**. In a 2000ml Tarson Beaker, the reagents had been added as per the sequence in 700ml of deionised water. The reagents are not added unless the previous reagent had been dissolved in the solution. 1M HCl had been added to adjust the ph≈7.4 and the temperature maintained at 33°C. Then the solution had been adjusted to 1000ml by adding deoinised water.

Table – 3.3 Illustration of ionic concentration of SBF and Human blood plasma **[71].**

Ion	**Kukobo et al (mM)**	**Human Blood Plasma (mM)**
Na^+	142.0	142.0
Cl^-	147.8	103.3
HCO_3^-	34.2	27
K^+	5.0	5.0
Mg^{2+}	1.5	1.5
Ca^{2+}	2.5	2.5
HPO_4^{2-}	1.0	1.0
SO_4^{2-}	0.5	0.5

Table – 3.4 Raw materials used for preparation of SBF **[72]**

Order	**Reagent**	**Amount (gpl)**
1	NaCl	6.547
2	$NaHCO_3$	2.268
3	KCl	0.373
4	$Na2HPO_4.2H_2O$	0.178
5	$MgCl_2.6H_2O$	0.305
6	$CaCl_2.2H_2O$	0.368
7	Na_2SO_4	0.071
8	$(CH_2OH)_3CNH_2$	6.057

Then the 45S5(0,50), functionally graded bioglass scaffold, which had been sintered at 850°C, had been kept in a 30ml polysterene container. Almost 20ml of SBF had been poured into the container and kept for incubation. The invitro analysis had been carried out for 0,1,7and 14 days. After incubation, the scaffolds had been dried at around 70°C. Furthermore these scaffolds had undergone XRD and microstructural analysis to determine the Carbonated-hydroxyapatite formation.

3.18 Invitro analysis of FGS with MG-63 cell line

The purpose of fabricating Functionally graded scaffolds is to obtain a biomimetic approach. The outer dense region acts as a protective layer and inner porous region favours better proliferation. The level of proliferation will be more in the porous regions than the dense region. In order to determine the level of proliferation and cell viability, MG-63 osteoblast cell line had been seeded in to the FGS.

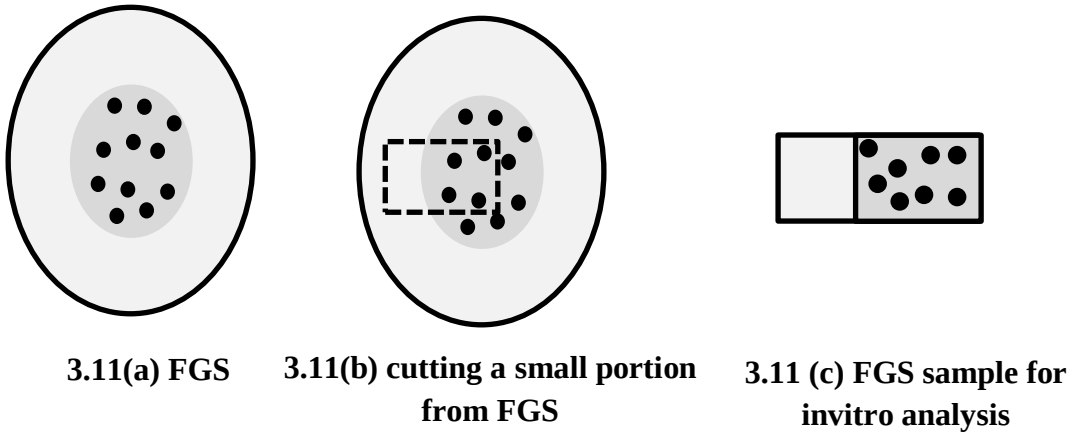

3.11(a) FGS **3.11(b) cutting a small portion from FGS** **3.11 (c) FGS sample for invitro analysis**

Fig – 3.11 FGS sample preparation for invitro analysis

It had been ensured that the sample prepared, by cutting a small portion from the FGS [refer Fig 3.12(c)], bears both dense region as well as porous region. 45S5 (0,50), 2P(0,50) & 4P(0,50) scaffolds, which had been sintered at 850°C, had been used for this investigation. The MG-63 cells had been seeded on two batches of FGS specimen, as per the protocol done for bioactive glass powders (refer 3.6). After incubation, MTT assay had been added to one batch of the specimen, to determine the cell viability. With the other batch, the cells had been fixed with 2.5% glutaraldehyde, Sigma Aldrich 25% SEM grade, for 2 hours at room temperature **[73]**. The cell fixed scaffolds had been dehydrated by series of concentrations of ethanol and vacuum drying had been done. Then the specimens had been carried for microscopic analysis.

CHAPTER 4

RESULTS, DISCUSSIONS

& CONCLUSIONS

4. RESULTS & DISCUSSIONS

4.1 SYNTHESIS OF BIOACTIVE GLASS POWDERS

The glass compositions, 45S5, 2P & 4P (refer table-3.1) had been synthesized by melt quench method. The quenched products had been obtained as glass frits which had been grounded and milled to make into glass powders. The XRD studies had been done for the milled glass powders which had been shown in the fig 4.1.

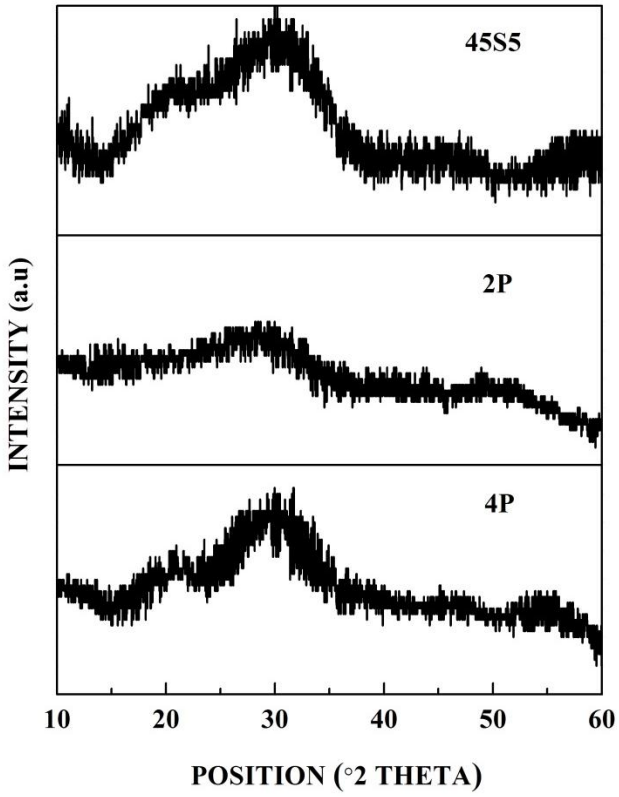

Fig 4.1 XRD of as Quenched Melt derived bioactive glass powders

This XRD spectrum shows that the powders are in the amorphous state and no crystallization interference had been taken place during rapid quenching of the melt in water bath. The collected glass frits from the water bath had undergone planetary ball milling. On equal milling time, the BET surface area of these three bioactive glass powders had been evaluated. The BET Surface Area of about 6.32 m^2/g, 1.16 m^2/g & 5.62 m^2/g had been attained for 45S5, 2P & 4P bioactive glasses respectively. The corresponding five point BET plots of 45S5, 2P & 4P bioactive glass powders had been given in the Fig 4.2 (a), 4.2(b) & 4.2(c) respectively.

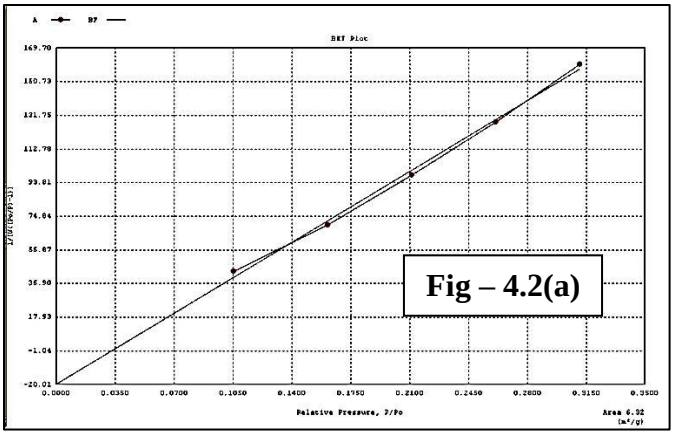

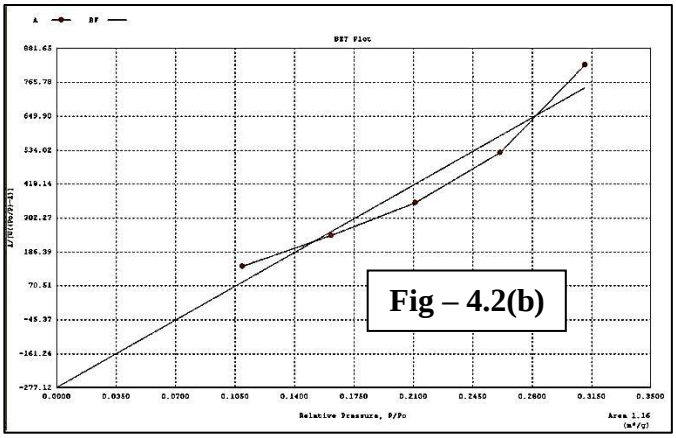

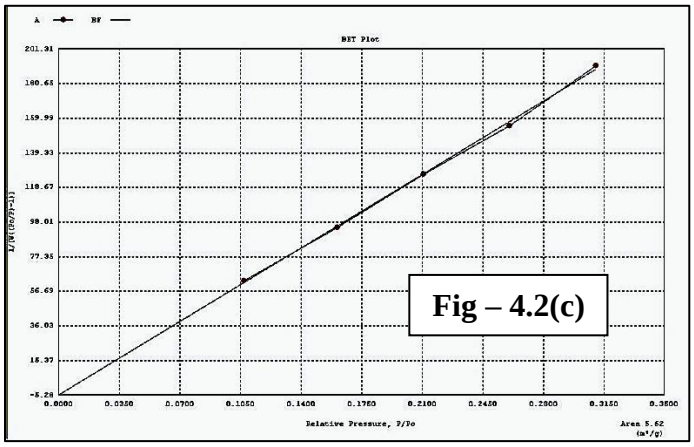

Fig- 4.2 Five point BET plots of (a) 45S5 (b) 2P (c) 4P

4.2 DSC-TG ANALYSIS

Different bioactive glass compositions mentioned in the compositional diagram (refer Fig – 1.4) had been designed by keeping the amount of P_2O_5 constant at 6 wt.%. Here in this current work, three bioactive glass compositions with different amount of P_2O_5 had been considered. The region S mentioned in the same compositional diagram consists of bioactive glass compositions with 36 – 52 wt. % of silica. Excluding P_2O_5 in the compositional diagram, the three bioactive glass compositions which had been taken in this work, lies in the region of S, which had been categorized as Class A biomaterial. Even though these bioactive glass compositions had been formulated within the short region of the composition diagram, there are great variations in the thermal behavior. Fig – 4.3(a) illustrates the DSC-TG curve for 45S5 bioactive glass powder.

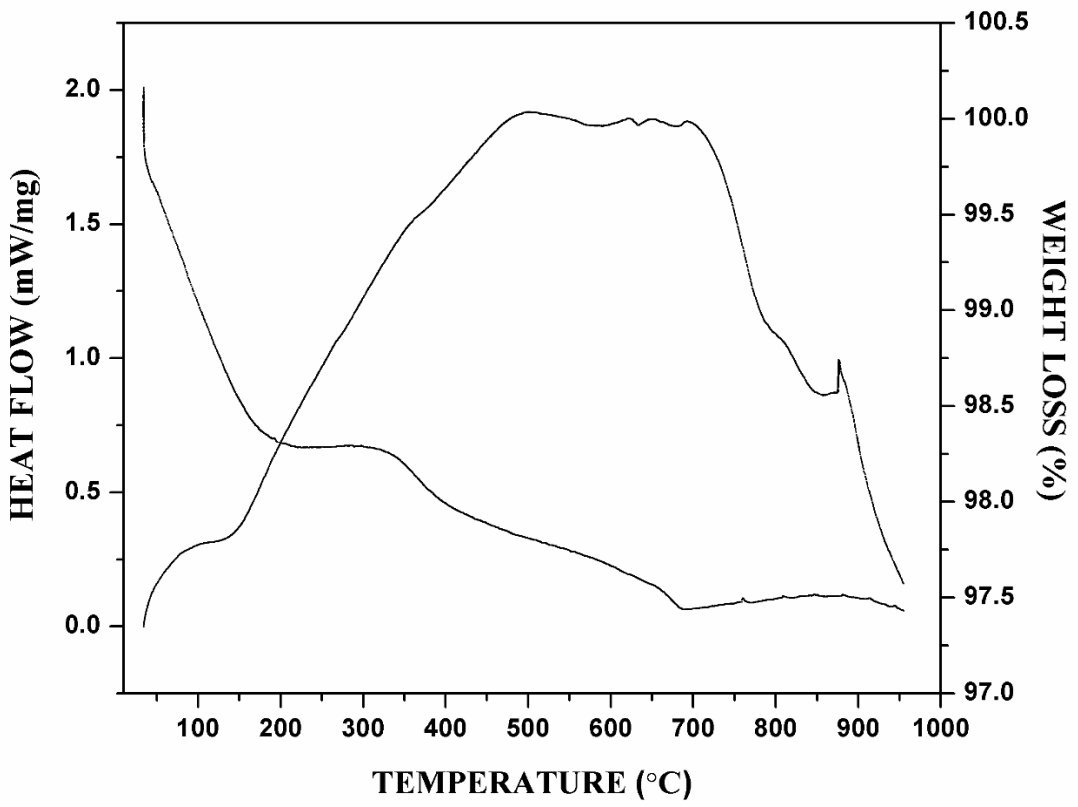

Fig – 4.3(a) DSC-TG analysis of 45S5 bioactive glass powder

Since the glass frits had been undergone planetary milling in water medium, there is possibility of weight loss. This is because silica has the better affinity towards –OH bonds present in the water molecules, which enters the network and forms Si-OH (silanols). Formation of silanols occurs because the water molecules either gets entrapped into the pores of the particles or physically adsorbed on the surface of the particles. The initial decomposition at around 175°C shows the decomposition of water molecules present on the surface of the glass particles. The decomposition at 317°C, 402°C & 645°C ensures the stage by stage release of –OH bonds from the silanols formed. A major exothermic peak occurs at 690°C due to the phase separation and liquid phase formation. A weak endothermic peak at 780°C represents the onset of crystallization or glass ceramic phase formation. The endothermic peak observed at 870°C indicates the major crystallization.

Fig – 4.3(b) illustrates the DSC-TG curve of 2P bioactive glass powder. Similar to 45S5 bioactive glass powders, 2P bioactive glass also registers some weight loss due to the release of –OH bonds from the silanols, till 609°C.

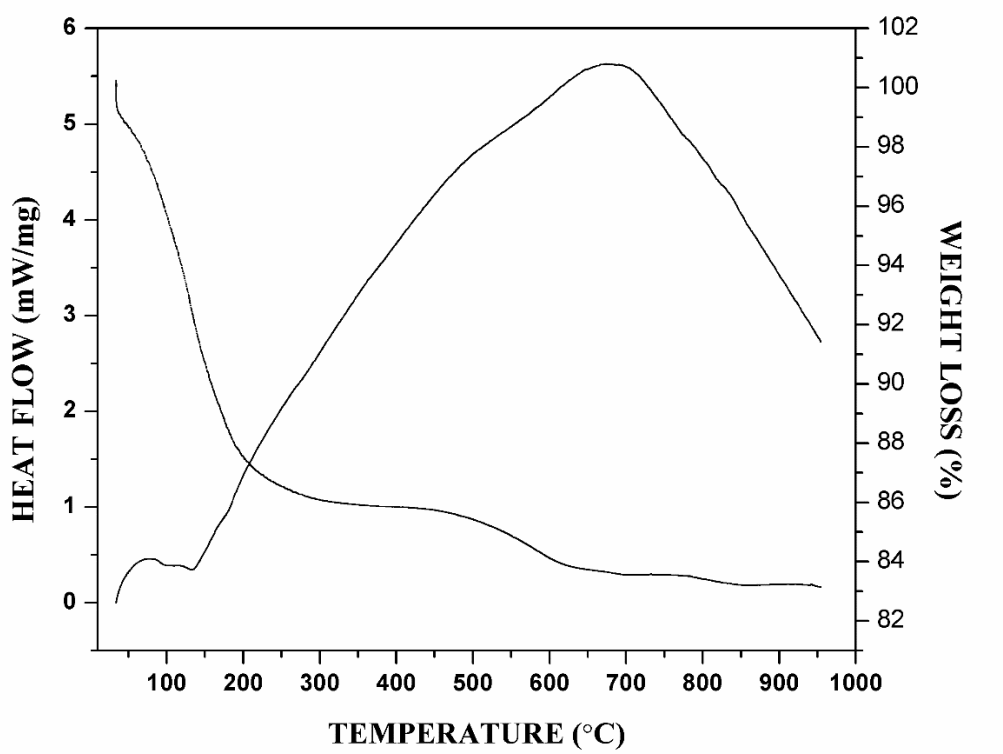

Fig – 4.3(b) DSC-TG analysis of 2P bioactive glass powder

The major exothermic reaction got initiated at 690°C which further proceeds with an endothermic peak at 770°C. As the exothermic reaction is predominantly interrupted by endothermic peak, this bioactive glass composition is pruned to crystallization beyond 800°C.

Fig – 4.3(c) shows the DSC-TG curve of 4P bioactive glass powder. The –OH bonds from the silanols formed from the 4P bioactive glass powders had been released at different amount on 93°C, 205°C, 288°C, 443°C, 667°C & 727°C. Beyond the major exothermic peak at 685°C, there initiates a slight endothermic peak at 725°C, which initiates the onset of crystallization of 4P bioactive glass. Beyond that there is consecutive fall in heat flow and emerges back with endothermic peaks at 785°C, 840°C, 875°C and a weak endothermic peak at 900°C. This shows the simultaneous reactions of phase separation and crystallizations at high temperatures. But the glass ceramic phase formation of 4P bioactive glass starts from the temperature of 725°C.

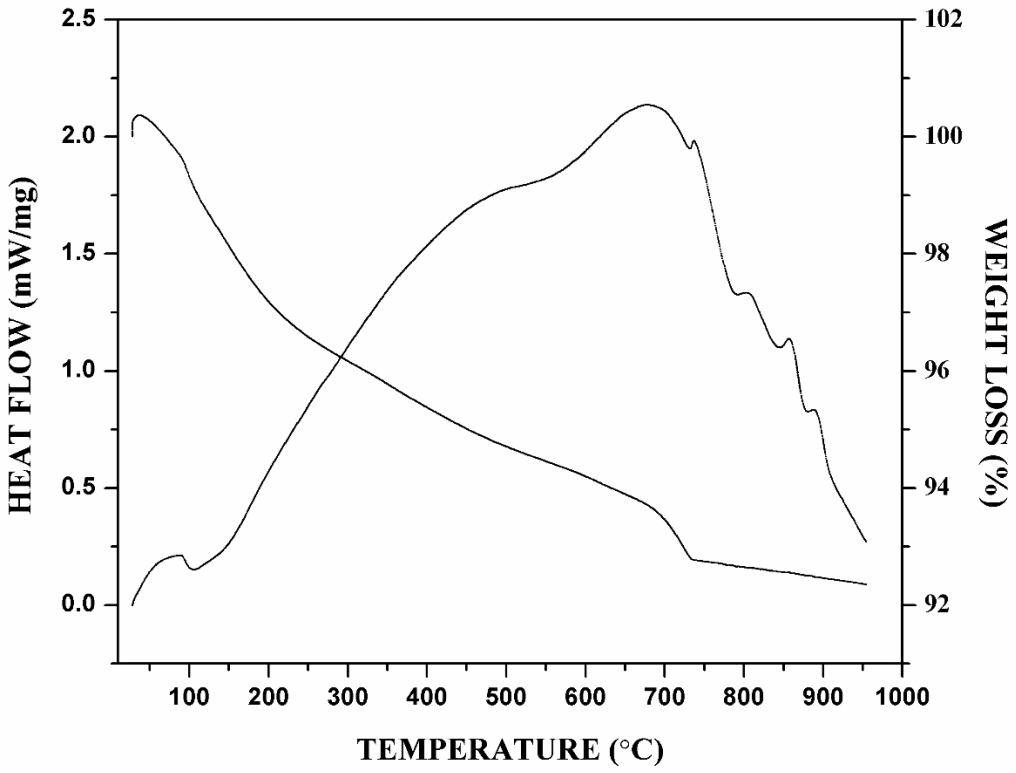

Fig – 4.3(c) shows the DSC-TG curve of 4P bioactive glass powder

When the thermal behavior of these three bioactive glass powders had been compared, it had been observed that the glass composition with least amount of P_2O_5 had utilized higher amount of heat flow to initiate the major exothermic peak. When the amount of P_2O_5 increases, the proportion of Q3 species had been increased, which further results with pronounced crystallization **[79]**. Thus apart from the other modifiers Na_2O and CaO, P_2O_5 plays a major role on the thermal behavior on the glass system.

4.3 DILATOMETRIC ANALYSIS

In order to understand the sintering behavior of bioactive glass scaffolds, it is necessary to undergo dilatometric analysis. The rectangular compacts had been fired in the dilatometric furnace under argon atmosphere.

The Fig – 4.4(a) illustrates the sintering behavior of 45S5 bioactive glass compacts. From 89°C to 181°C, there is a slight decrease in volume, which is due to the evaporation of water molecules associated with the binder.

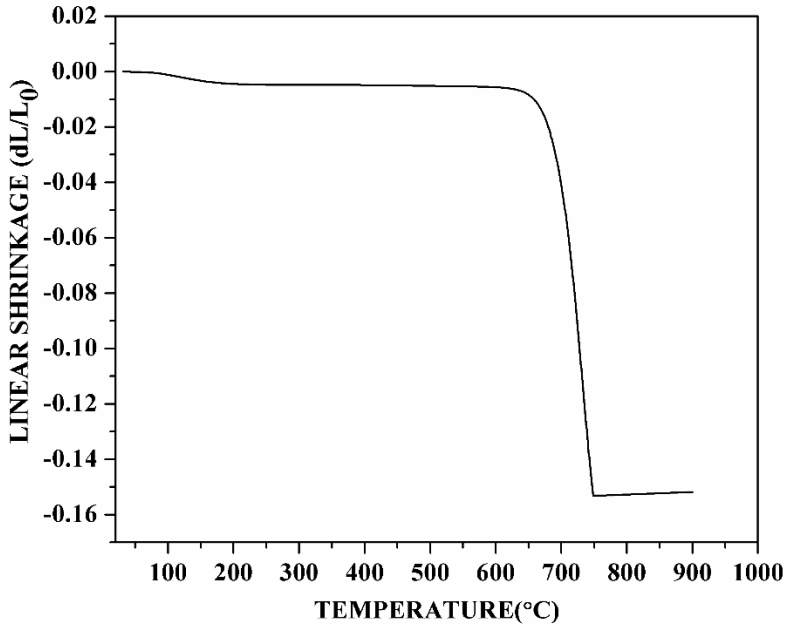

Fig – 4.4(a) – Dilatometric analysis of 45S5 bioactive glass green compacts

Till 607°C, there is no substantial linear shrinkage observed, which less than 0.6%. By a drastic fall at 607°C, sintering got initiated and proceeds till 745°C. This drastic fall indicates the liquid phase formation and phase separation. At 800°C, 850°C and 900°C, linear shrinkage of about 15.27%, 15.21% and 15.14% had been observed respectively.

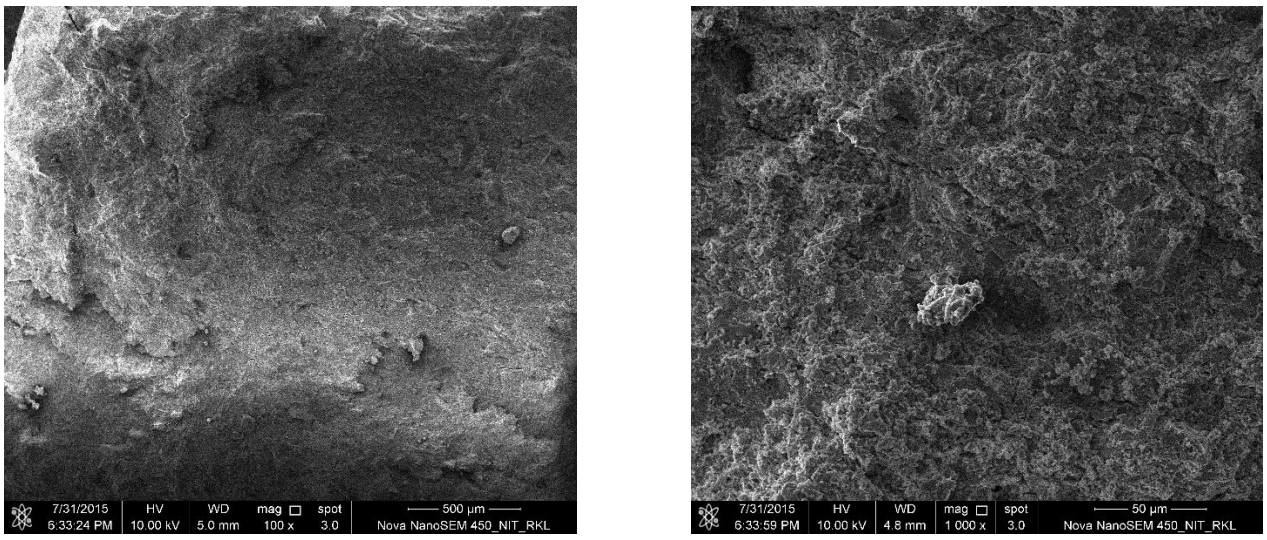

Fig – 4.4(b) Fractured surfaces of 45S5 glass ceramics sintered at 800°C (without pore former)

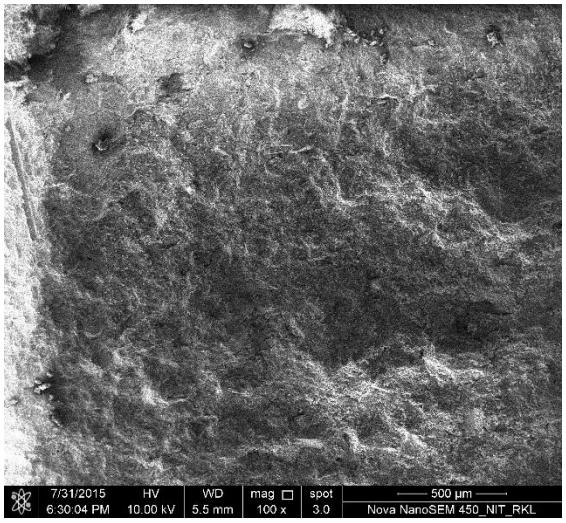

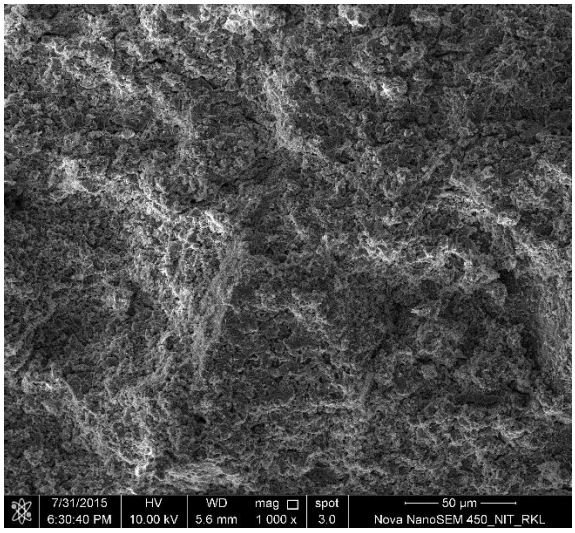

Fig – 4.4(c) Fractured surfaces of 45S5 glass ceramics sintered at 850°C (without pore former)

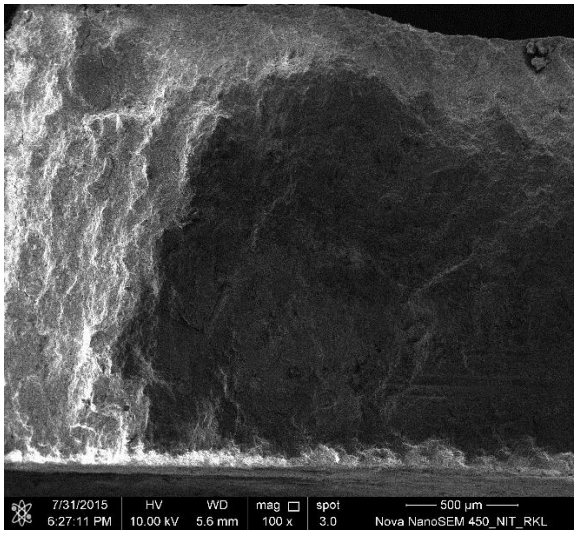

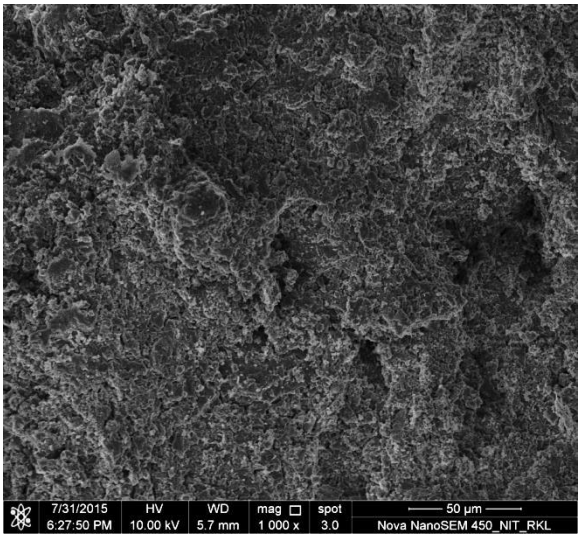

Fig – 4.4(d) Fractured surfaces of 45S5 glass ceramics sintered at 900°C (without pore former)

Fig – 4.4(b), Fig – 4.3(c) & Fig – 4.3(d) shows the microstructures of 45S5 glass ceramics sintered at 800°C, 850°C & 900°C respectively. The microstructures given in the Fig- Fig – 4.4(b), Fig – 4.3(c) & Fig – 4.3(d) shows that the efficient densification is not carried out. The simultaneous crystallization and phase separates retards the densification mechanism.

.

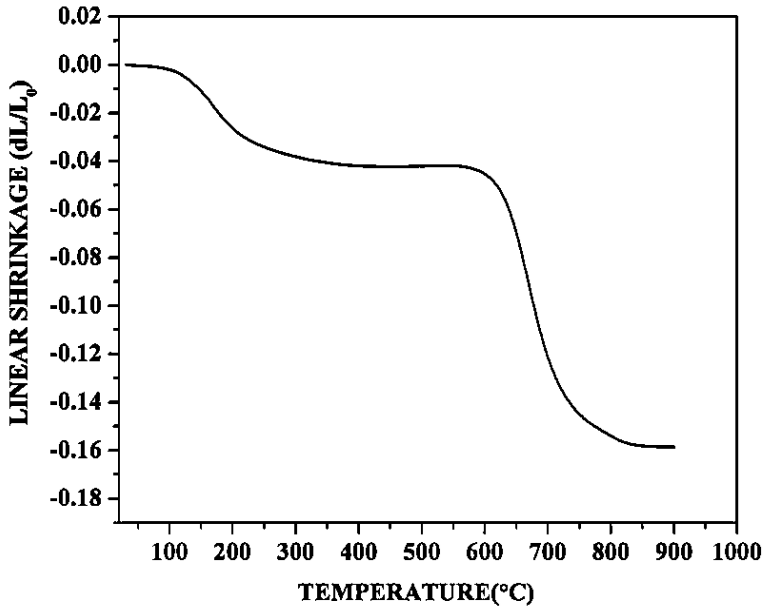

Fig – 4.4 (e) Dilatometric analysis of 2P bioactive glass green compacts

Fig–4.3(e) illustrates the sintering behavior of 2P bioactive glass compact. This composition undergoes two stages of sintering. During the first stage of sintering, the compact tends to contract from 91°C to 273°C, at a linear shrinkage of about 3.62%. Till 542°C, there is no significant increase in linear shrinkage. Beyond that temperature, the second stage of sintering took place, with a drastic fall till 705°C. At that temperature, the linear shrinkage was around 13.47%. Then reduction of volume got saturated when it reaches 800°C. For 2P bioactive glass compact, the linear shrinkage of about 15.44%, 15.76% & 15.84% had been recorded at the temperatures 800°C, 850°C & 900°C respectively.

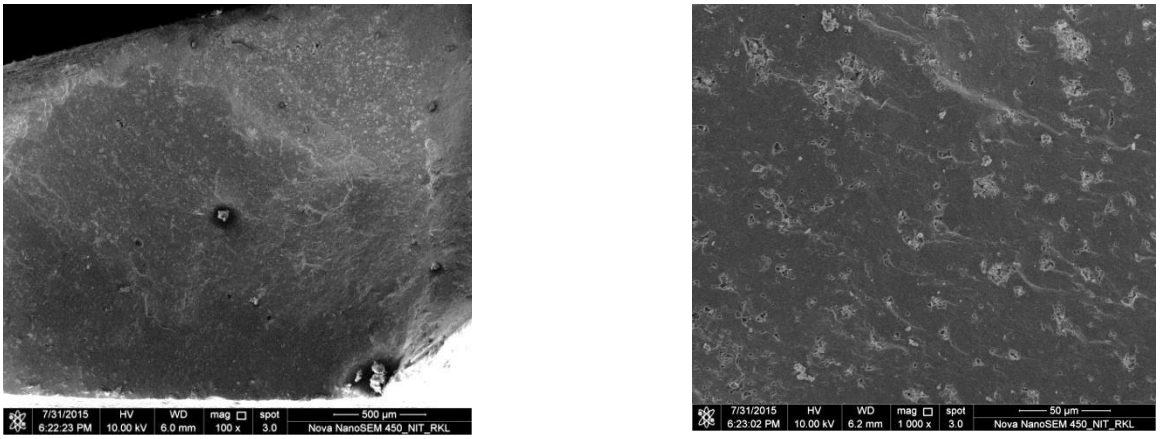

Fig – 4.4(f) Fractured surfaces of 2P glass ceramics sintered at 800°C (without pore former)

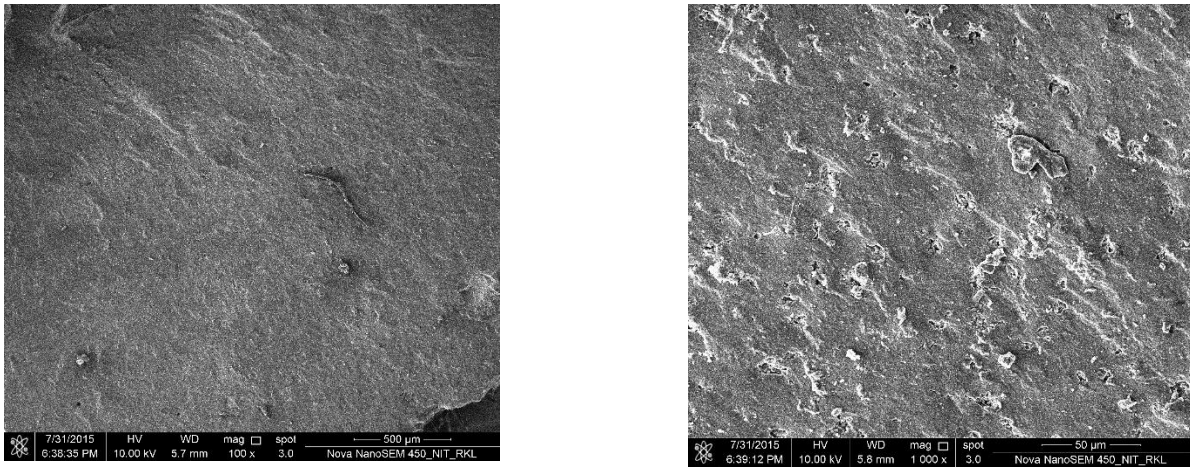

Fig – 4.4(g) Fractured surfaces of 2P glass ceramics sintered at 850°C (without pore former)

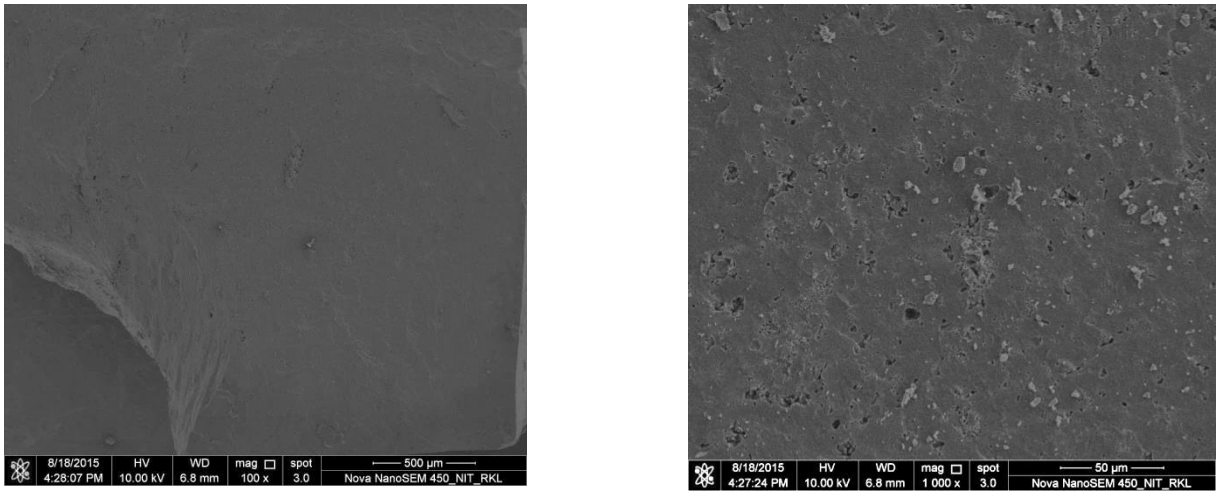

Fig – 4.4(h) Fractured surfaces of 2P glass ceramics sintered at 900°C (without pore former)

Fig – 4.4(f), Fig – 4.4(g) & Fig – 4.4(h) shows the microstructures of 2P glass ceramics sintered at 800°C, 850°C & 900°C. The microstructures clearly shows that the densification had been carried out efficiently within minimum amount of pores present.

Fig – 4.3(i) illustrates the sintering behavior of 4P bioactive glass compact. From 105°C to 217°C, there is a slight contraction due to the evaporation of water molecules and moisture present in the sample. At 615°C, the linear shrinkage was about 10.13%, which further leads to a drastic fall in volume till 800°C. At 800°C, the linear shrinkage was around 13.56%. There is a slight fall in volume again when the temperature proceeds to 850°C, where the linear shrinkage had been recorded as 14.38%.

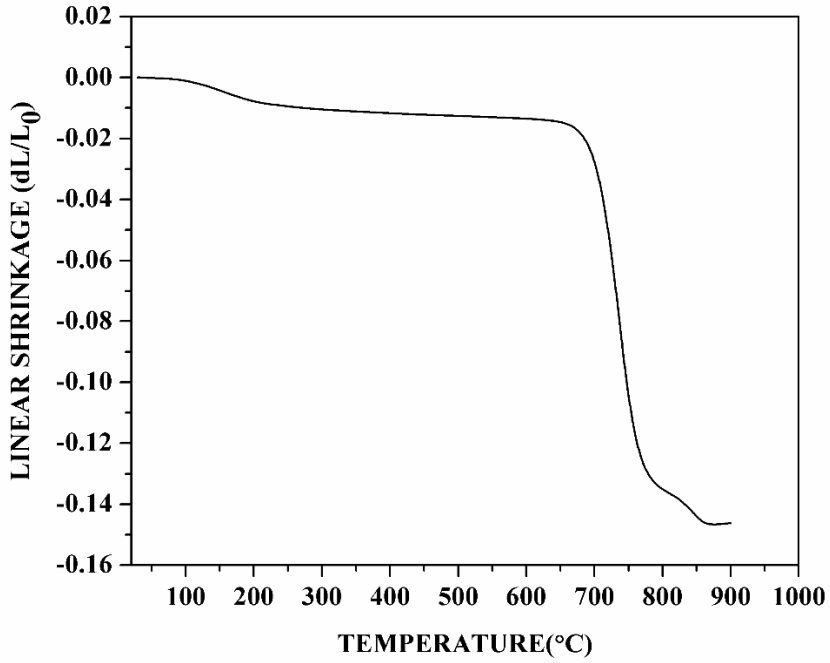

Fig – 4.4 (i) Dilatometric analysis of 4P bioactive glass green compacts

A little amount of contraction took place when the temperature proceeds towards 900°C, with a linear shrinkage of about 14.62%. The saturation of volume shrinkage had been reduced when the temperature is beyond 850°C. The Fig – 4.4 (j), 4.4 (k) & 4.4 (l) shows the microstructures of 4P bioactive glass ceramics at the fracture surfaces.

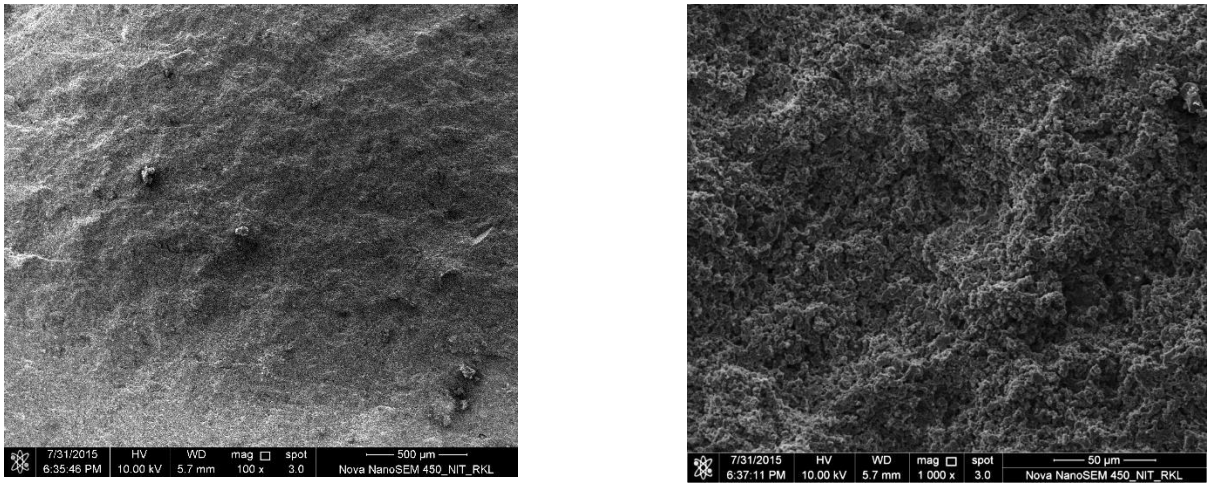

Fig – 4.4(j) Fractured surfaces of 4P glass ceramics sintered at 800°C (without pore former)

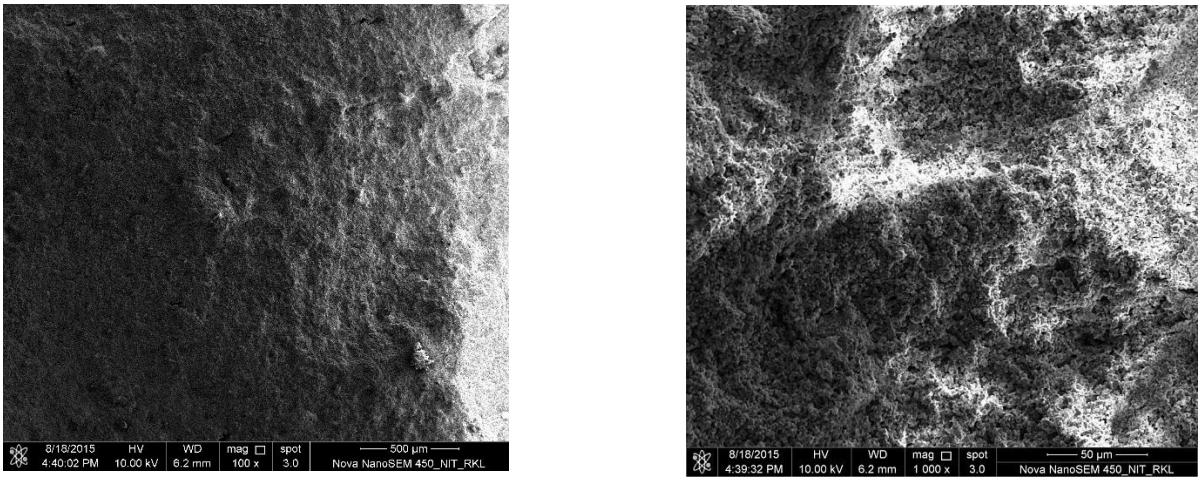

Fig – 4.4(k) Fractured surfaces of 4P glass ceramics sintered at 850°C (without pore former)

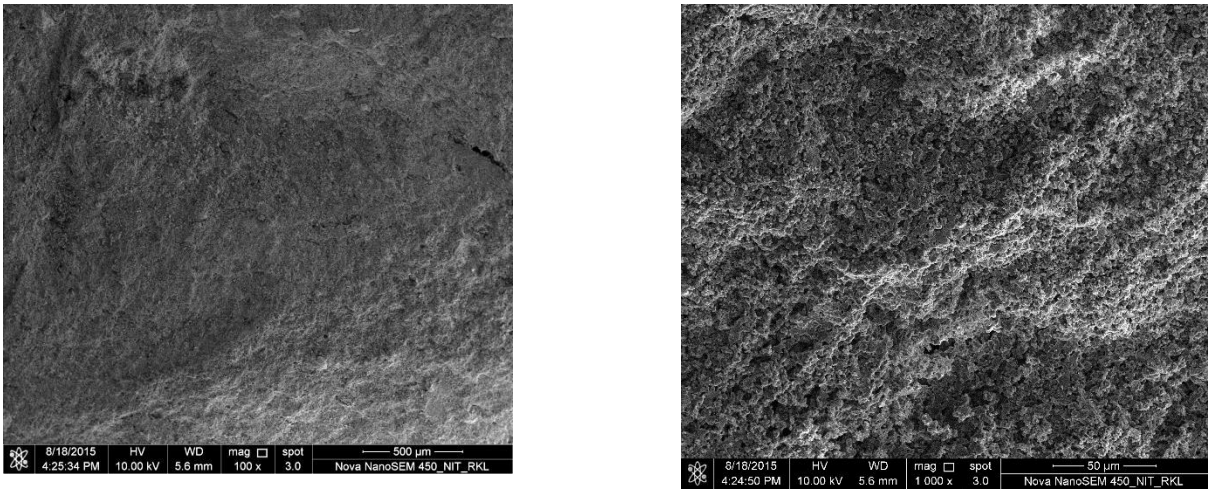

Fig – 4.4(l) Fractured surfaces of 4P glass ceramics sintered at 900°C (without pore former)

From the Fig – 4.4(j), Fig – 4.4(k) & Fig – 4.4(l), it shows that more amount inter particle voids had been observed even after sintering at 900°C. When compared to the other two glass ceramics, 4P glass ceramics shows higher amount of porosity on the fracture surface. On comparing the sintering behavior of these three bioactive glass composition, it had been observed that the saturation of linear shrinkage had been took place within the temperatures 800°C and 900°C. As discussed in the previous section, there will be corresponding increase in Q3 species when there is an increase in P_2O_5. Due to this reason, during the course of sintering, the average degree of polymerization of Si network had increased.

Thus the actual densification mechanism commences at higher temperature, if the amount of P_2O_5 increases. Since the linear shrinkage of the bioactive glass compacts got saturated within the temperature range of 800°C to 900°C, the sintering temperatures of bioactive glass scaffolds had been fixed as 800°C, 850°C & 900°C.

4.4 PHASE ANALYSIS OF BIOACTIVE GLASS CERAMIC POWDERS

For the fabrication of bioactive glass ceramic scaffolds, uniaxial pressing and sintering method had been utilized. From the previous section, it had been decided to sinter the bioactive glass ceramic scaffolds at 800°C, 850°C & 900°C. From the literatures it had been well understood that sintering of bioactive glass green scaffolds leads to crystallization and formation of glass ceramic phases. Therefore it is necessary to identify the glass ceramic phases formed on post sintering.

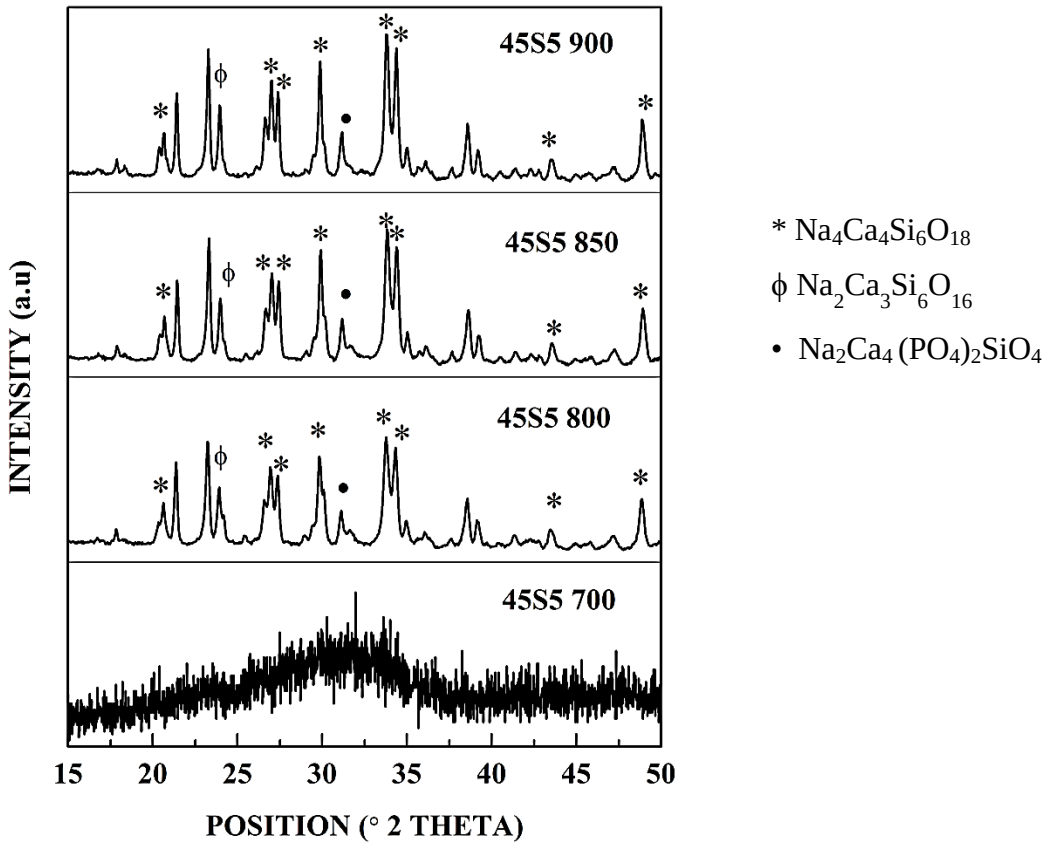

Fig – 4.5 (a) Phase Analysis of 45S5 Bioactive glass ceramics

Fig – 4.5(a) shows the phases formed by the sintered 45S5 bioactive glass ceramic. At 700°C, the 45S5 retains its amorphous state and crystallization had been observed from 800°C. This shows that glass ceramic phase formation had occurred within the temperatures 700°C and 800°C. Sodium Calcium Silicate – $Na_4Ca_4Si_6O_{18}$ is the major phase formed at 800°C, which had been matched by its reference pattern 75-1686. $Na_2Ca_3Si_6O_{16}$ (77-0386) is the secondary phase formed and Na_2Ca_4 $(PO_4)_2SiO_4$ (33-1229) appears as a minor phase. Similar phases had been formed when the 45S5 glass fired at 850°C and 900°C. No major phase transformations occurred with the 45S5 glass ceramics when the sintering temperature proceeds towards 850°C and 900°C.

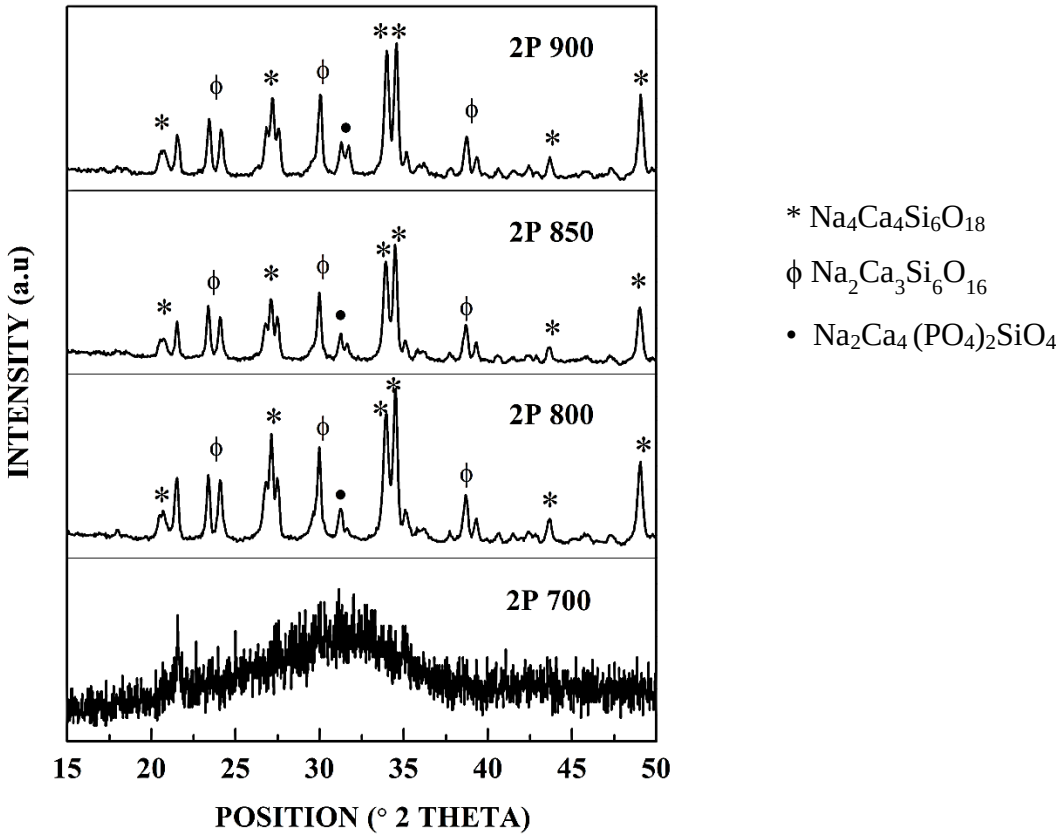

Fig – 4.5 (b) Phase Analysis of 2P Bioactive glass ceramics

Fig – 4.5(b) illustrates the phase formation of 2P bioactive glass ceramic at the temperatures 700°C, 800°C, 850°C and 900°C. Similar to 45S5 bioactive glass fired at 700°C, 2P bioactive glass also retains its amorphous state at 700°C. The major crystallization peak had been observed from $Na_4Ca_4Si_6O_{18}$.

The secondary phase $Na_4Ca_4Si_6O_{18}$ and $Na_2Ca_4(PO_4)_2SiO_4$ had been identified as secondary phase and minor phase of the 2P glass ceramic system. The initiation of phase separation of $Na_2Ca_4(PO_4)_2SiO_4$ had been observed, when the sintering temperature increases from 800°C to 850°C, due to less amount of P_2O_5 present in the glass composition. Excluding that no major phase transformation had been observed.

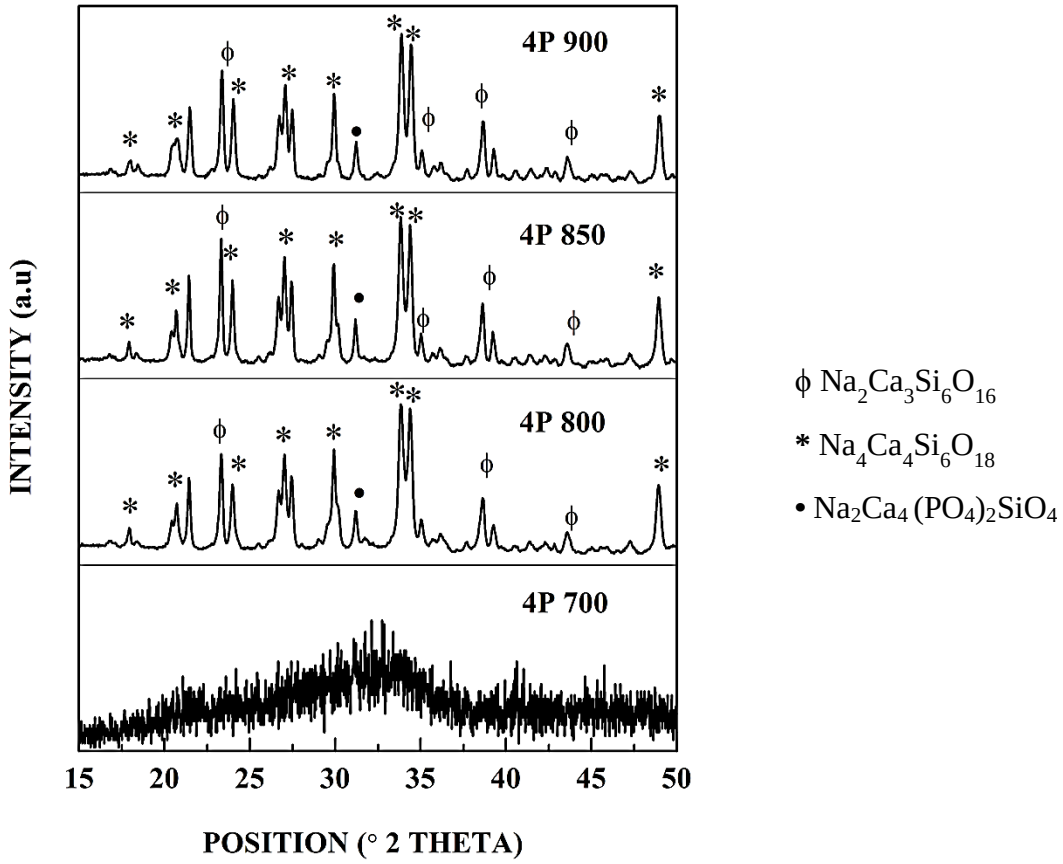

Fig – 4.5 (c) Phase Analysis of 4P Bioactive glass ceramic

Fig – 4.5(c) shows the glass ceramic phase formation on 4P bioactive glass ceramic. Even this composition retains its amorphous nature when fired at 700°C. $Na_4Ca_4Si_6O_{18}$ – 75-1686 is the major phase formed on 4P bioactive glass and $Na_2Ca_3Si_6O_{16}$ (77-0386) is the secondary phase. $Na_2Ca_4(PO_4)_2SiO_4$ had been identified as minor phase of the 4P glass ceramic system. In the temperature range of 800°C - 900°C, active crystallization had been carried out. But major transformation was not observed in all the glass compositions.

4.5 FTIR ANALYSIS

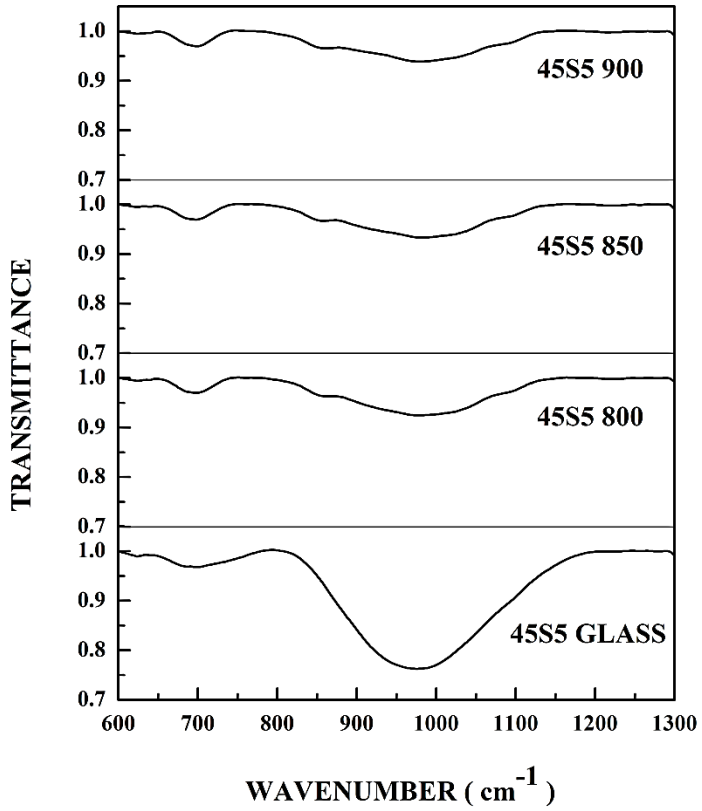

Fig- 4.6(a) FTIR spectra of 45S5 bioactive glass and glass ceramics

Fig – 4.6 (a) shows the FTIR spectra of 45S5 bioactive glass and glass ceramics sintered at 800°C, 850°C & 900°C. An asymmetric Si-O-Si stretching at 960 cm^{-1} and Si-O-Si bending at 760 cm^{-1} had been attributed to the 45S5 glass. On post sintering, due to crystallization, the Si-O-Si bond deflects for an asymmetric stretch of Si-O-NBO in Q_2 and Q_1 occurs at 860 cm^{-1}, which indicates the presence of bioactive glass ceramic phase formation. Further, the band at 950 cm^{-1} corresponds to the Si-O-Si stretching vibration mode of glass ceramics. A band at 640 cm-1 indicates P-O bending vibration and the band at 700 cm^{-1} corresponds to P-O-P unit stretching which indicates the presence of crystalline phosphate. **[74-79]**

Fig – 4.6(b) shows the FTIR spectra of 2P bioactive glass and glass ceramics sintered at 800°C, 850°C & 900°C.

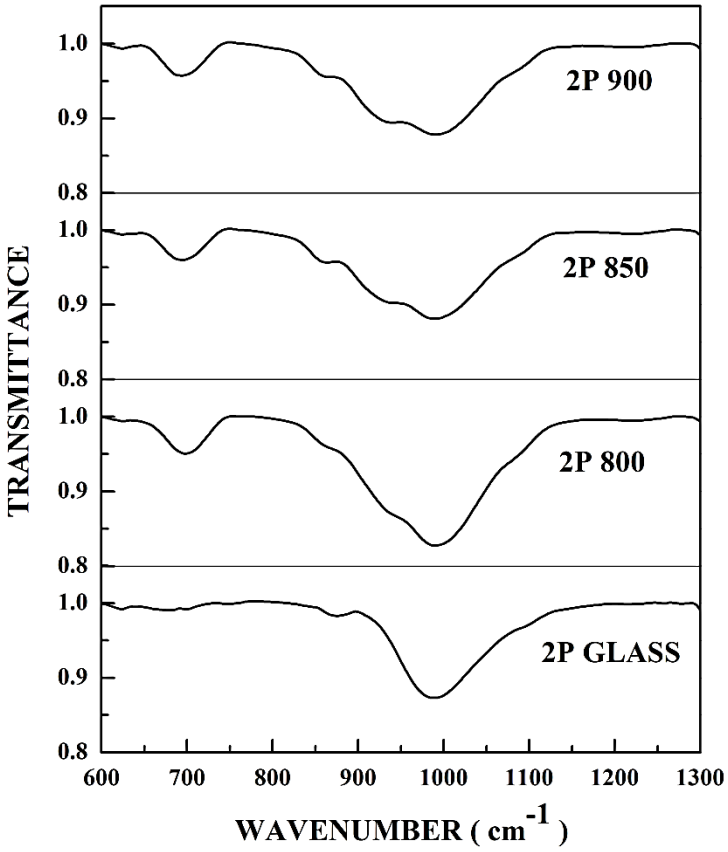

Fig- 4.6(b) FTIR spectra of 2P bioactive glass and glass ceramics

Due to less amount of P_2O_5 present in the 2P bioactive glass composition, P-O bending vibration occurred as a weak band at 640 cm^{-1}. A narrow Si-O-Si asymmetric stretching had been occurred at 990 cm^{-1}. On crystallization, Si-O-Si band deflects and Si-O-NBO stretches at 860 cm^{-1}, whereas 2P glass stretches at 870 cm^{-1}. Due to this strong asymmetric stretching, overlapping of PO_4 occurs. This results in P-O-P vibrations at 680 cm-1 and 690 cm-1 for 2P bioactive glass and glass ceramics respectively. **[74-79]**

Fig – 4.6(b) shows the FTIR spectra of 2P bioactive glass and glass ceramics sintered at 800°C, 850°C & 900°C.

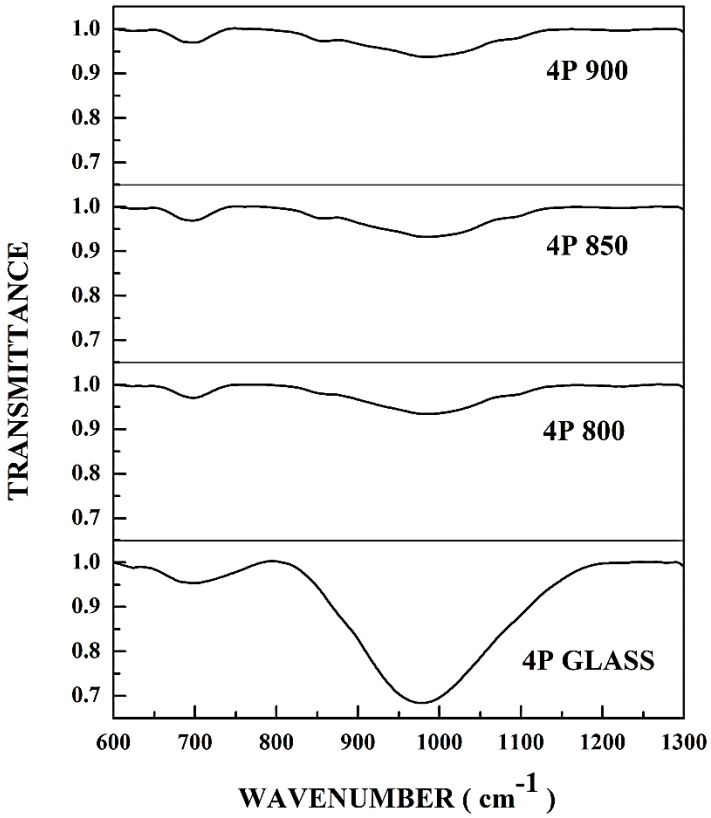

Fig- 4.6(c) FTIR spectra of 4P bioactive glass and glass ceramics

The band at 975cm^{-1} and 985cm^{-1} corresponds to the asymmetric Si-O-Si stretching of 4P bioactive glass and glass ceramics. The band at 690 cm^{-1} corresponds to the P-O-P unit stretching of Q3 in Q2 and Q1. On crystallization, the Si-O-Si stretching vibration mode at 1100 cm^{-1} had been observed. On post sintering, due to crystallization, the Si-O-Si bond deflects for an asymmetric stretch of Si-O-NBO in Q_2 and Q_1 occurs at 850 cm^{-1}. **[74-79]**

On a comparison of 45S5, 4P and 2P bioactive glass compositions, the structural features of 45S5 and 4P are similar. But due to less P_2O_5 in 2P glass composition, a strong Si-O-Si stretching had been incurred by the glass system.

4.6 CELL VIABILITY OF BIOACTIVE GLASS AND GLASS CERAMICS

The MG-63 cell line had been seeded to the bioactive glass and glass ceramics as per the protocol prescribed in the section 3.6. On sintering, since the bioactive glasses transforms into glass ceramics, it is necessary to evaluate the cell viability on glass ceramics. In this experiment, including the bioactive glasses, 45S5, 2P & 4P, its corresponding glass ceramics, which had been fired at 800°C, 850°C & 900°C, had also tested. Fig – 4.7 (a) shows the phase contrast microscopic images of MG-cell seeded bioactive glasses.

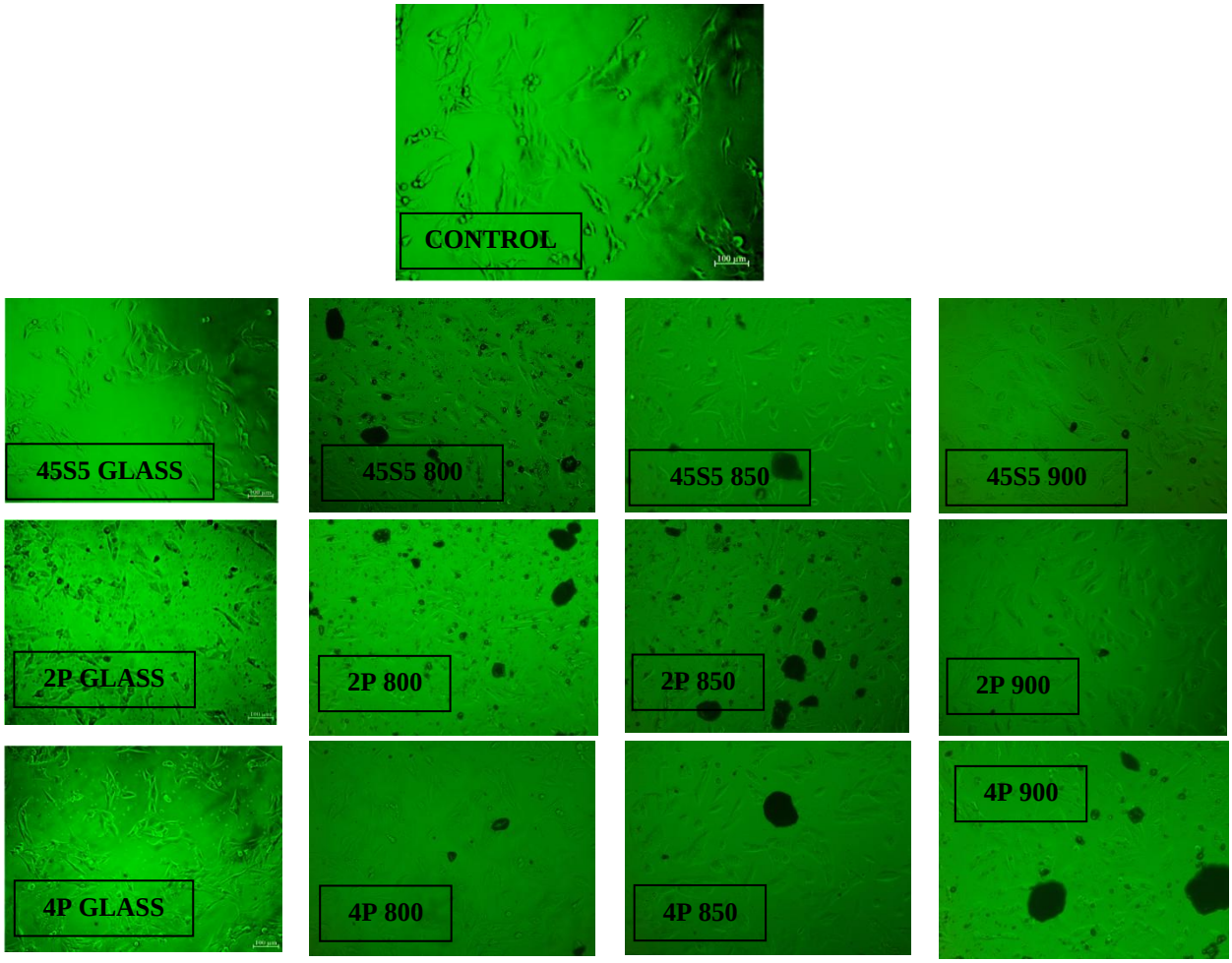

Fig-4.7 (a) Phase contrast microscopic image of cell seeded bioactive glass and glass ceramics after 1 day incubation

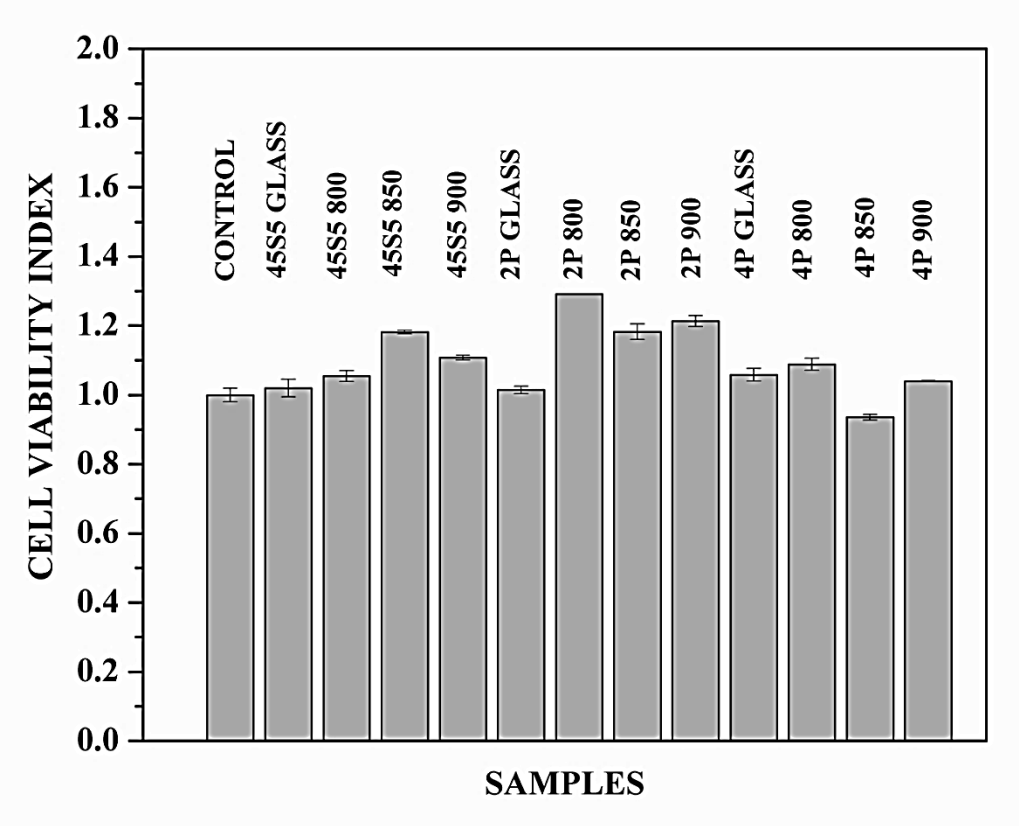

Fig-4.7 (b) MTT Cell viability of Bioactive glasses and glass ceramics

After one day incubation, by using MTT Assay, the cell viability index had been evaluated for bioactive glass and glass ceramics, which had been illustrated in the Fig – 4.7(b). Since all the samples have the cell viability index of more than 0.7, it had been ensured that all the samples are biocompatible. Except 4P 850, all the samples are having cell viability index more than the control. Cell viability index of 2P 850 is less when compared with 2P 800 & 2P 900. Similarly cell viability index of 4P 850 is less when compared with 4P 800 & 4P 900. This feature is not seen with 45S5 glass and its glass ceramics. Except 4P 850, the cell viability of all the glasses are less than the cell viability of its corresponding glass ceramic. On an overall comparative study it had been concluded that 2P based bioactive glass ceramics induces more proliferation than 45S5 and 4P based glass and glass ceramics. 2P bioactive glass composition has higher silica content (49.5wt. %) than the other two glass compositions. Since Si^{4+} ions are responsible for osteogenesis and angiogenesis (refer table 1.2), it had been concluded that 2P based bioactive glass ceramics are highly biocompatible than the 45S5 and 4P based glass and glass ceramics.

4.7 HAEMOCOMPATIBILITY OF BIOACTIVE GLASS AND GLASS CERAMICS

Hemolysis study can be interpreted for the evaluation of blood compatibility of the bioactive glass and glass ceramics. Fig – 4.8 shows the % hemolysis of bioactive glass and glass ceramics.

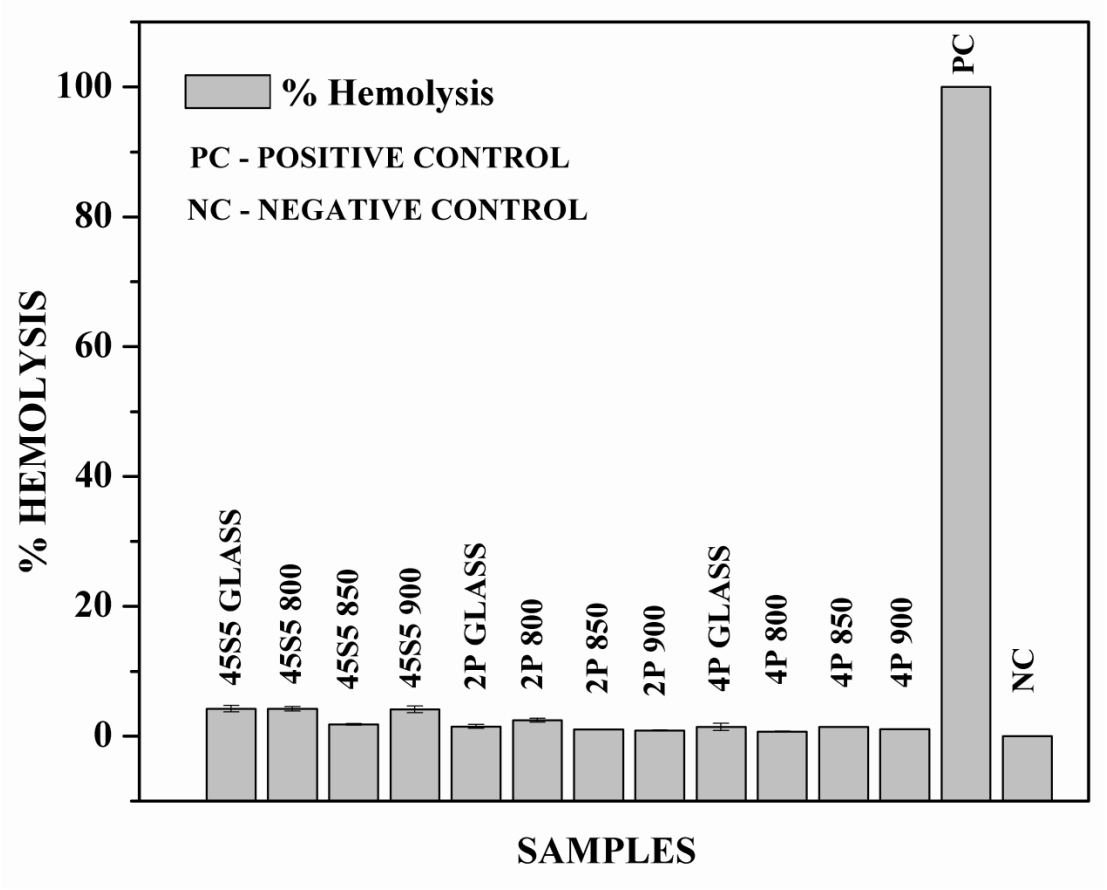

Fig – 4.8 Hemolysis Study of bioactive glass and glass ceramics

On all the samples, % Hemolysis is less than 5% and greater than the Negative control. This ensures that all the samples are highly hemocompatible. The highest % Hemolysis had been observed in 45S5 800 & the least % Hemolysis had been recorded by 4P 800. In the case of 2P based glass and glass ceramics, the % hemolysis is less than 45S5 based glass and glass ceramics. But the amount of hemolysis in 2P based glass and glass ceramics had occurred more than 4P based glass and glass ceramics.

4.8 PROTEIN ABSORPTION STUDIES

Bovine Serum Albumin (BSA) had been used as a reference protein for the evaluation of protein absorption of bioactive glasses and glass ceramics. Fig – 4.9 shows the protein absorption profiles of bioactive glasses and glass ceramics.

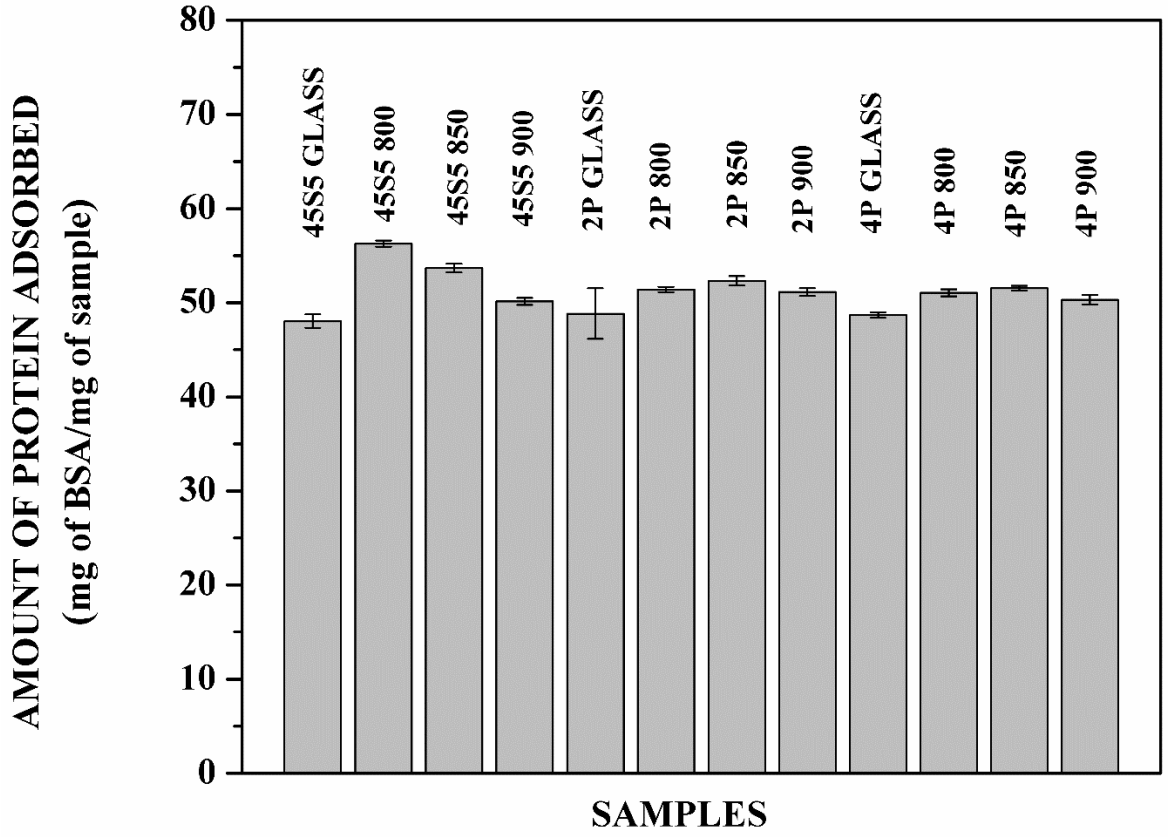

Fig – 4.9 Protein Adsorption studies of Bioactive glass and glass ceramics

All protein adsorption profiles had been recorded within the range of 45-60 mg/ mg of the sample. All the glass ceramic samples adsorbs more than the corresponding glass samples. Among the all other samples, 45S5 850 adsorbs 53.67 mg of BSA per mg of itself. The least adsorption had been registered by 45S5 bioactive glass; almost 48.04 mg of BSA/mg. 2P based glass ceramics shown a moderate adsorption capability.

4.9 APPARENT POROSITY & BULK DENSITY OF SINGLE LAYER SCAFFOLDS

By using naphthalene as a pore former (0wt.%, 30wt.% & 50wt.%), fabrication of single layer bioactive glass ceramic scaffolds had been done by uniaxial pressing and sintering method. As mentioned earlier, the single layer scaffolds had been sintered at 800°C, 850°C and 900°C. Fig – 4.10.1 (a), Fig – 4.10.1(b) & Fig – 4.10.1(c) illustrates the apparent porosity & bulk density of Single layer - 45S5 porous bioactive glass ceramic scaffolds with 0 wt.%, 30wt.% and 50wt.% of naphthalene respectively.

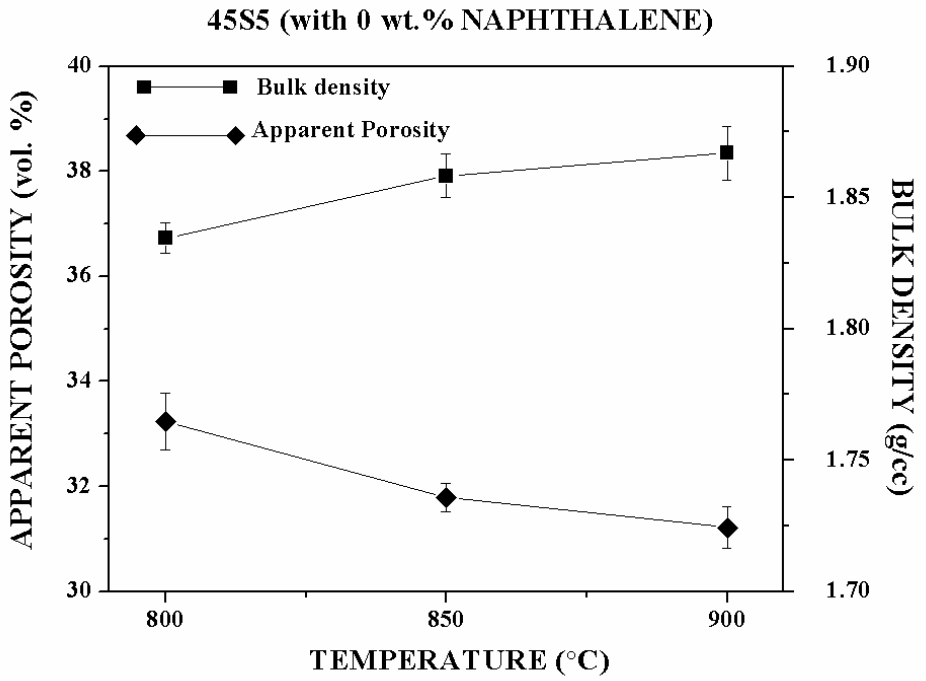

Fig – 4.10.1(a) Apparent porosity and bulk density of 45S5 single layer scaffold with 0 wt. % naphthalene

Without pore former (0 wt.% naphthalene), 45S5 single layer scaffolds had been fabricated. The maximum bulk density had been attained at 800°C itself. There is no significant increase in bulk density had been noticed when the temperature rises from 800°C to 900°C. The Apparent porosity had been saturated within 31-33 vol.% and the bulk density had been attained within the range of 1.83g/cc-1.87g/cc.

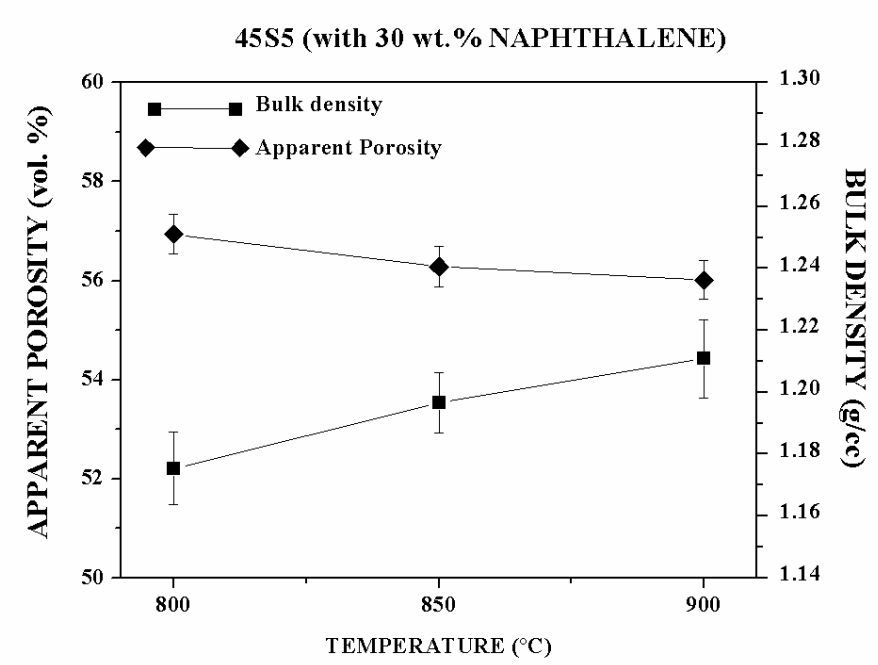

Fig – 4.10.1(b) Apparent porosity and bulk density of 45S5 single layer scaffold with 30 wt. % naphthalene

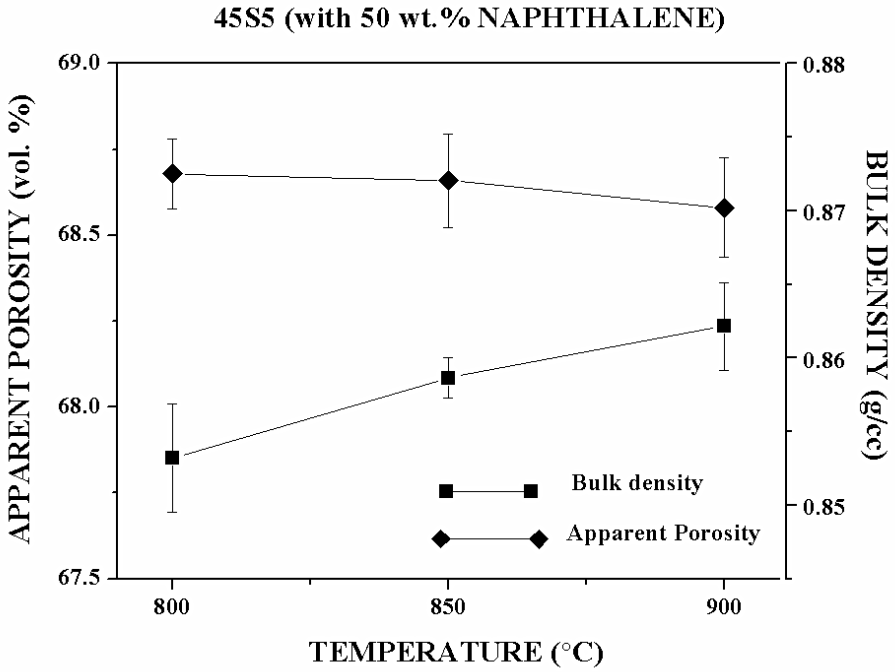

Fig – 4.10.1(c) Apparent porosity and bulk density of 45S5 single layer scaffold with 50 wt. % naphthalene

Even in the case of 45S5 single layer scaffolds with 30 wt.% and 50 wt.% of naphthalene, the maximum strength had been attained at 800°C itself. There is no substantial increase in bulk density when the sintering temperature from 800°C to 850°C and 900°C. Table 4.1 illustrates the apparent porosity and bulk density attained by Porous 45S5 single layer scaffolds sintered at 800°C to 850°C and 900°C.

Table – 4.1 Apparent Porosity (A.P) and Bulk density (B.D) of Porous 45S5 Single layer scaffolds

Sintering Temperature (°C)	45S5 (0 wt.% Naphthalene)		45S5 (30 wt.% Naphthalene)		45S5 (50 wt.% Naphthalene)	
	A.P (vol.%)	B.D (g/cc)	A.P (vol.%)	B.D (g/cc)	A.P (vol.%)	B.D (g/cc)
800	33.23	1.83	56.94	1.17	68.67	0.853
850	31.78	1.85	56.28	1.19	68.65	0.858
900	31.21	1.86	56.01	1.21	68.58	0.862

Fig – 4.10.2 (a), Fig – 4.10.2 (b) & Fig – 4.10.2 (c) shows the Apparent Porosity and bulk density of 2P based bioactive glass ceramics with 0wt.%, 30wt.% & 50wt.% Naphthalene respectively.

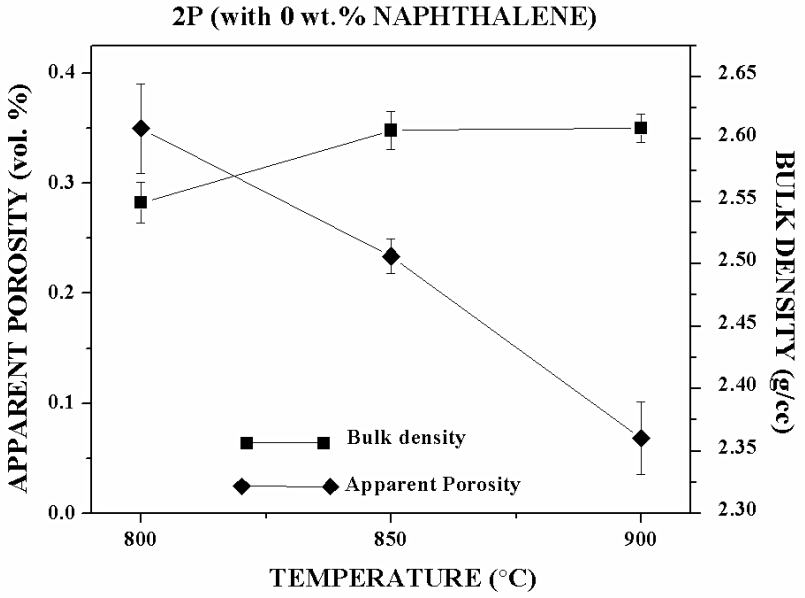

Fig – 4.10.2(a) Apparent porosity and bulk density of 2P single layer scaffold with 0 wt. % naphthalene

2P single layer scaffolds, when sintered without pore former, minimum apparent porosity of less 0.5 vol.% had been attained. It had recorded a bulk density of about 2.6 g/cc, which is considered to be the highest dense among the other scaffolds tested. A drastic increase in bulk density had been noticed when the sintering temperature increases from 800°C to 850°C. When the sintering temperature increases to 900°C, the rate of increase in density had been saturated.

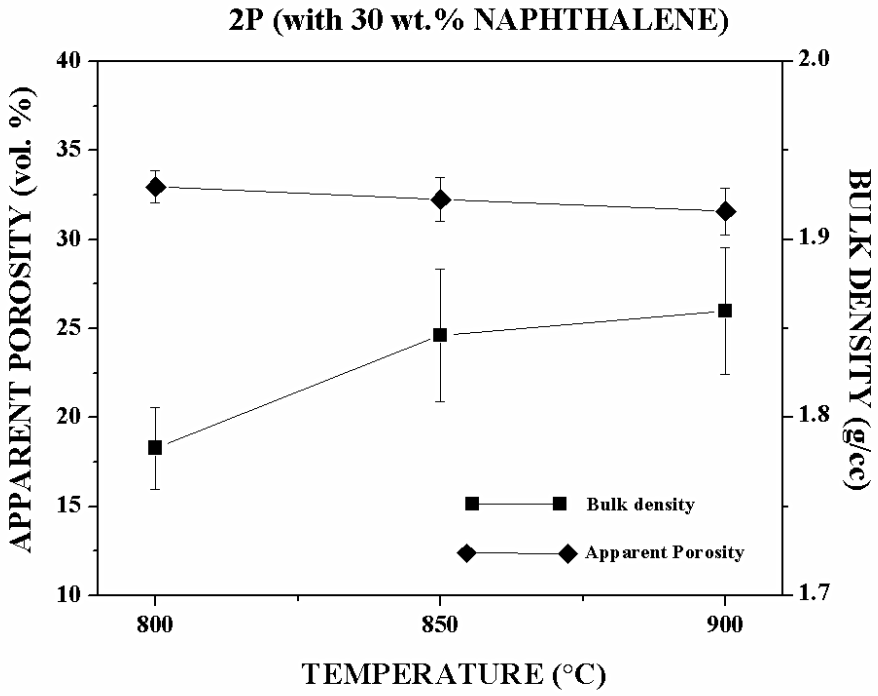

Fig – 4.10.2(b) Apparent porosity and bulk density of 2P single layer scaffold with 30 wt. % naphthalene

Similar behavior had been observed with 2P Single layer scaffolds with 30wt.% naphthalene. There is a commendable increase in bulk density when the sintering temperature increases from 800°C to 850°C. Then the value of bulk density had been saturated when the scaffolds had been fired at 900°C. The attained apparent porosity is very much close to the volume of naphthalene incorporated into the scaffolds. Even the same sintering behavior had been observed with 2P single layer scaffolds with 50wt.% naphthalene.

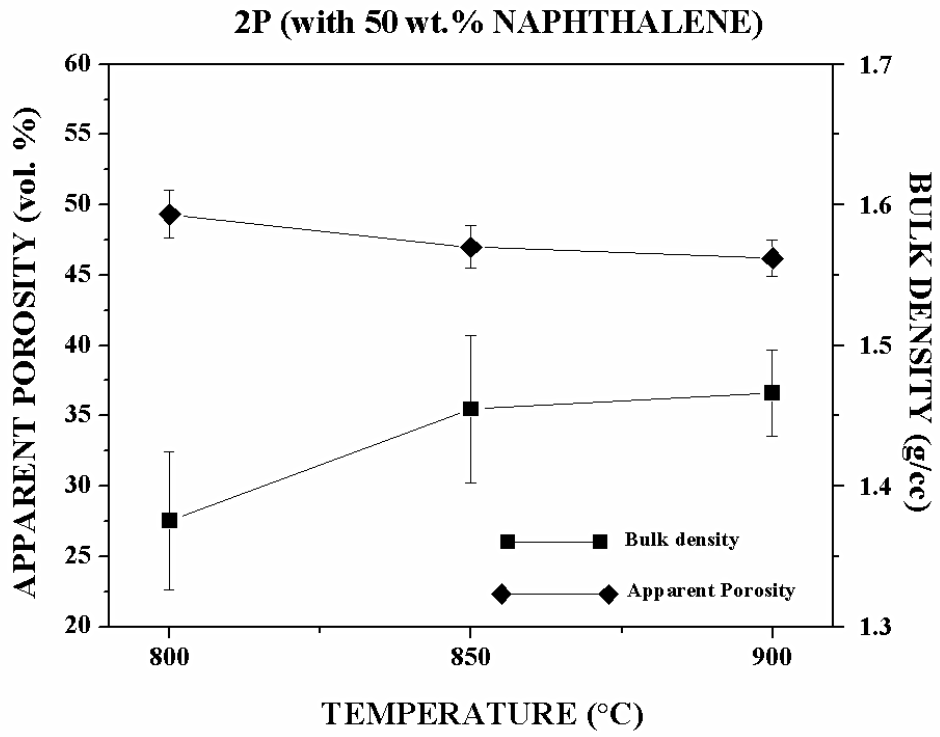

Fig – 4.10.2(c) Apparent porosity and bulk density of 2P single layer scaffold with 50 wt. % naphthalene

The values of Apparent Porosity and bulk density attained by 2P single layer scaffolds with different amount of naphthalene addition had been tabulated in the Table – 4.2.

Table – 4.2 Apparent Porosity (A.P) and Bulk density (B.D) of Porous 2P Single layer scaffolds

Sintering Temperature (°C)	2P (0 wt.% Naphthalene)		2P (30 wt.% Naphthalene)		2P (50 wt.% Naphthalene)	
	A.P (vol.%)	B.D (g/cc)	A.P (vol.%)	B.D (g/cc)	A.P (vol.%)	B.D (g/cc)
800	0.34	2.349	32.96	1.78	49.33	1.37
850	0.23	2.607	32.25	1.84	46.98	1.45
900	0.06	2.609	31.57	1.85	46.20	1.46

Fig – 4.10.3 (a), Fig – 4.10.3 (b) & Fig – 4.10.3 (c) shows the Apparent Porosity and bulk density of 4P glass ceramics with 0wt.%, 30wt.% & 50wt.% Naphthalene addition respectively.

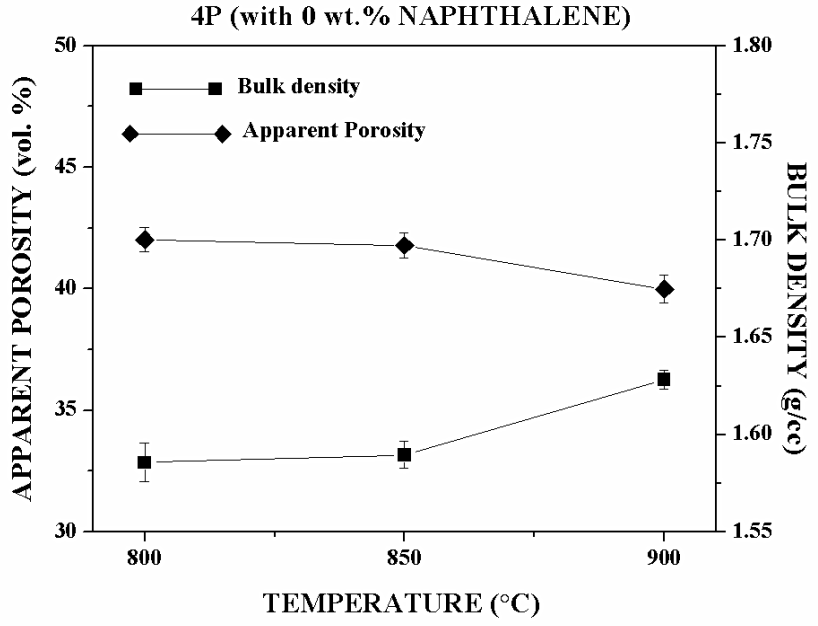

Fig – 4.10.3(a) Apparent porosity and bulk density of 4P single layer scaffold with 0 wt. % naphthalene

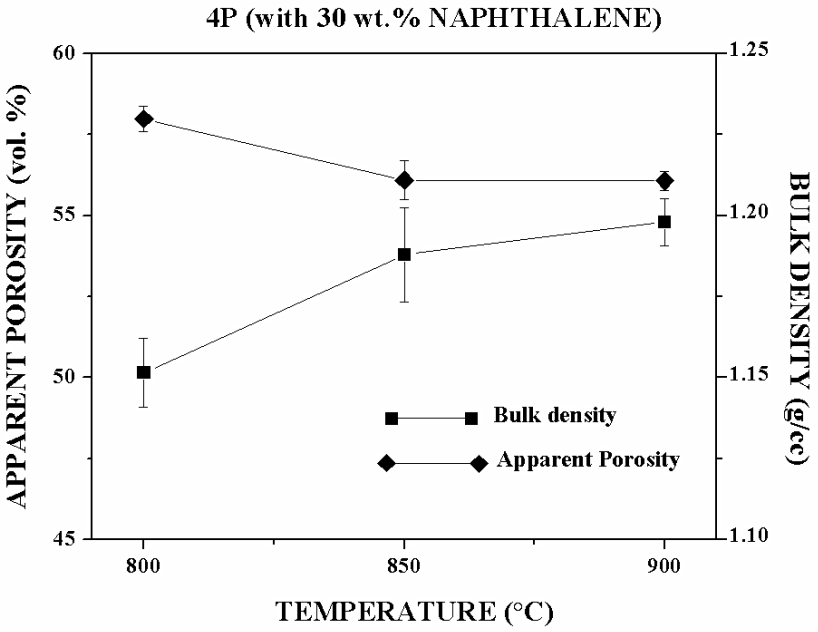

Fig – 4.10.3(b) Apparent porosity and bulk density of 4P single layer scaffold with 30 wt. % naphthalene

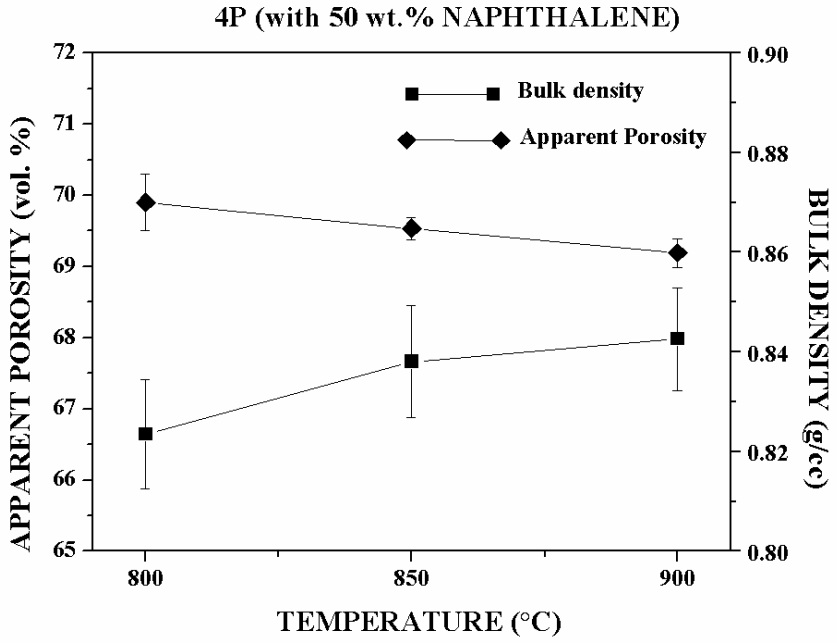

Fig – 4.10.3(c) Apparent porosity and bulk density of 4P single layer scaffold with 50 wt. % naphthalene

4P based porous single layer scaffolds had been considered as highly porous scaffolds among the other single layer scaffolds. Apparent Porosity of 39-42vol.%, 56-58 vol.% & 69-70 vol.% had been recorded for 2P single layer scaffolds with 0wt.%, 30wt.% & 50wt.% of naphthalene respectively. 4P single layer scaffold with 0 wt.% naphthalene attained its maximum density at 800°C. A little marginal increase of bulk density had been observed when the sintering temperature increases to 850°C. When the sintering temperature proceeds to 900°C, it tends to increase its bulk density, but not to a greater extent. In the case of 4P single layer scaffolds with 30wt.% naphthalene, there was a drastic increase in bulk density when the sintering temperature increases from 800°C to 850°C. Then the rate of increase in bulk density had been suppressed when the sintering temperature proceeds towards 900°C. A gradual increase in bulk density had been observed with 4P (50wt.% naphthalene) single layer scaffolds, when the sintering temperature proceeds from 800°C to 850°C and goes on to 900°C. The tabulated results of apparent porosity and bulk density for 4P single layer scaffolds had been drafted in the table 4.3.

Table – 4.3 Apparent Porosity (A.P) and Bulk density (B.D) of Porous 4P Single layer scaffolds

Sintering Temperature (°C)	4P (0 wt.% Naphthalene)		4P (30 wt.% Naphthalene)		4P (50 wt.% Naphthalene)	
	A.P (vol.%)	B.D (g/cc)	A.P (vol.%)	B.D (g/cc)	A.P (vol.%)	B.D (g/cc)
800	42.01	1.58	57.97	1.15	69.90	0.82
850	41.78	1.59	56.08	1.18	69.53	0.83
900	39.98	1.62	56.07	1.19	69.19	0.84

Each glass composition behaves differently, when compacted and sintered at 800°C, 850°C & 900°C, due to emergence of degree of polymerization at different temperature ranges, as discussed in the dilatometric analysis via section 4.3. The average degree of polymerization eventually occurs during the course of liquid phase formation and phase separation. This had been characteristically illustrated by a plateau of drastic increase in linear shrinkage on the dilatometric profiles [Fig – 4.4 (a), Fig – 4.4 (e) & Fig – 4.4 (i)]. Due to less amount of P_2O_5 in the 2P bioactive glass composition, as mentioned earlier (section 4.2), the glass compacts attains the degree of polymerization well before 650°C. This polymerization, at this temperature range triggers the liquid phase formation, which actually promoted viscous flow sintering. As a result, the densification mechanism was rigorous and 2P bioactive glass scaffold (without pore former) attained maximum bulk density of 2.34 g/cc (0.34 vol. % of apparent porosity), at sintering temperature of 800°C. Similar strategy had been followed by 2P based porous scaffolds (30 & 50 wt. % of Naphthalene), when sintered at 800°C. The attained apparent porosity on 2P based porous scaffolds, when sintered at 800°C, where approximately equal to the amount of Naphthalene (pore former) incorporated. Beyond this temperature, i.e when 2P based scaffolds sintered at 850°C and 900°C, incremented bulk density had been achieved, but the performance of viscous flow sintering had been more rigorous. Thus for 2P based scaffolds, 800°C had been considered as an optimum sintering temperature.

In this section, as per the tabulated results of bulk density, the next better dense bodies had been achieved by 45S5 bioglass composition. With reference of the dilatometric profile of 45S5 bioglass composition [Fig – 4.4 (a)], it can be concluded that the degree of polymerization originates within the temperature - 650°C to 700°C. Hence the prominent densification mechanism happens during this period.

Furthermore, apart from liquid phase formation and phase separation, simultaneous crystallization took place, which lags the densification mechanism, when compared with 2P based scaffolds. Thus the amount of pore former incorporated into the 45S5 based scaffolds approximately equalizes with the attained apparent porosity, when the sintering temperature is beyond 800°C (Table 4.1). With this it can be concluded that the optimum level of sintering had been attained by 45S5 based scaffolds, when the sintering temperature is 850°C.

Among these three bioglass composition, 4P based scaffolds were considered as the weakest one. As per the dilatometric profile of 4P bioglass composition [Fig – 4.4 (i)], the degree of polymerization emerges beyond 690°C. This is a delayed happening when compared with 45S5 and 2P bioglass composition. Additional to that, as per the dilatometric profile of 4P bioglass composition, the linear shrinkage had not been saturated even at 900°C. As a result sintering mechanism had been considerably postponed to higher sintering temperature. 2P based scaffolds achieves better sintering at 800°C itself due to less amount of P_2O_5. But 45S5 bioglass composition, even though possessed higher amount of P_2O_5 than 4P bioglass composition, the optimum sintering temperature was 850°C only. This is due to the excess amount of SiO_2 present in 4P bioglass composition than 45S5 bioglass composition. Higher amount of SiO_2 delays the polymerization and also drags the liquid phase formation. Hence sintering mechanism had been retarded on 4P based scaffolds and also by the matter of fact, apparent porosity is also higher than the other scaffolds. Thus 4P based scaffolds demands for higher temperature than 900°C, to attain an optimum level of sintering.

In this section, the optimum sintering temperature had been decided based on two preliminary requirements. As per the application point of view, scaffolds requires better dense bodies, at the same, they should retain some appreciable amount of porosity on it, on post sintering, to favor osteogenesis. And hence the above conclusions had been illustrated.

4.10 DIAMETRAL TENSILE STRENGTH OF POROUS SINGLE LAYER SCAFFOLDS

As the main objective of this work is majorly focused on Porosity gradient bioactive glass ceramic scaffolds, evaluation of tensile strength plays a pivotal role. Fig – 4.10.1, Fig – 4.10.2 & Fig – 4.10.3 illustrates the Diametral Tensile strength (DTS) of Porous 45S5, 2P & 4P single layer scaffolds respectively.

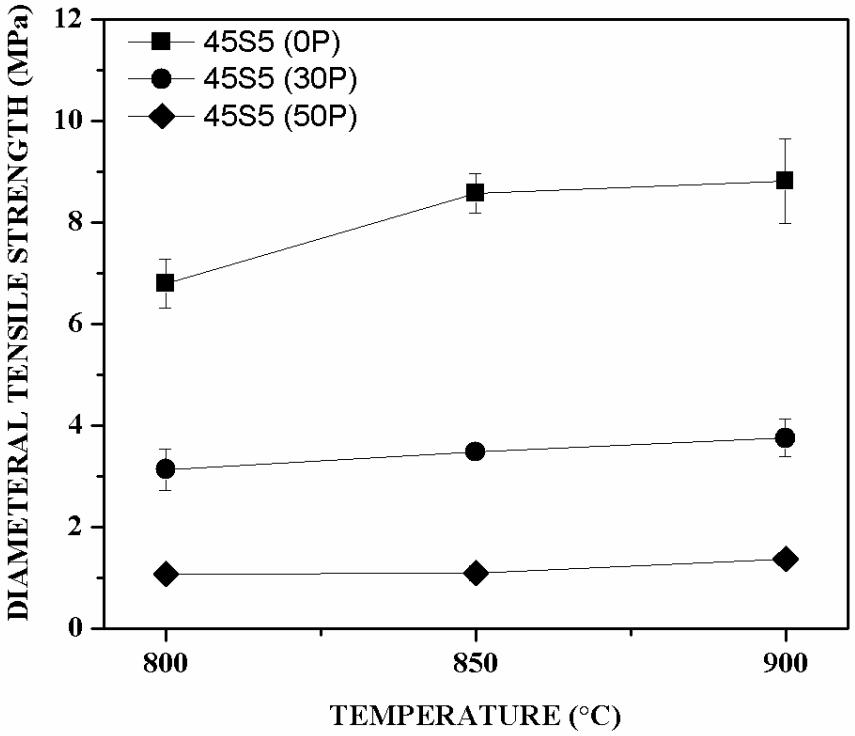

Fig – 4.11.1 Diametral Tensile strength of Porous 45S5 Single Layer scaffolds

Diametral Tensile Strength of 45S5 (0P) had been recorded as 6.78MPa, 8.57MPa & 8.81MPa on sintering temperatures 800°C, 850°C & 900°C. A drastic increase in DTS from 800°C to 850°C had been observed and the rate of increase is reduced when the sintering temperature proceed to 900°C. This feature had not shown with 45S5 (30P) & 45S5 (50P).

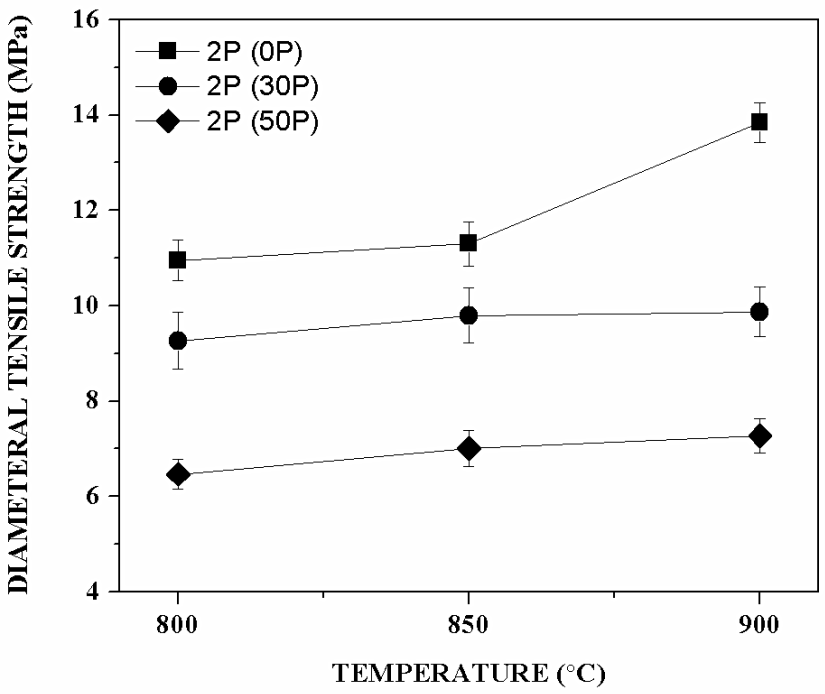

Fig – 4.11.2 Diametral Tensile strength of Porous 2P Single Layer scaffolds

Sudden increase in DTS had been observed with the scaffold 2P (0P) when the sintering temperature rises from 850°C to 900°C. On rest of the 2P based porous single layer scaffolds, a normal increase in DTS had been observed on increase in sintering temperature. Since 2P based porous scaffolds are the highly dense when compared with 45S5 and 4P based porous single layer scaffolds, they results with better diametral tensile strength than the other single layer scaffolds.

The diametral tensile strength of porous 4P single layer scaffolds had been illustrated in the Fig – 4.11.3. In the case of 4P based porous single layer scaffolds, the rate of increase in DTS is comparatively high for 4P (0P) & 4P (30P) than 4P (50P). A large increase in DTS had been seen with the samples 4P (0P) at 800°C to 850°C and 4P (30P) at 850°C to 900°C. On rest of the 4P based porous single layer scaffolds, a linear increase in DTS had been recorded.

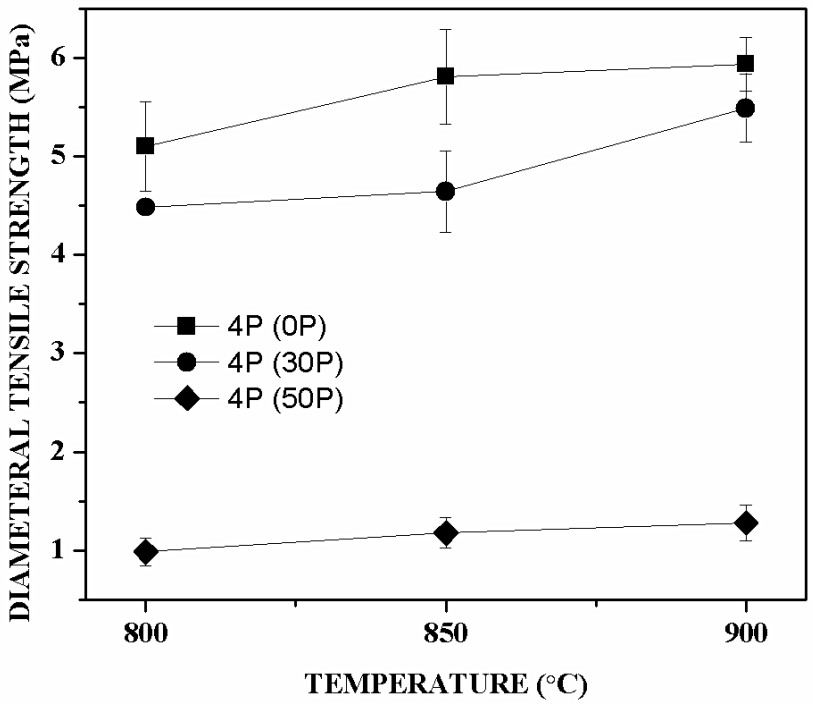

Fig – 4.11.3 Diametral Tensile strength of Porous 4P Single Layer scaffolds

The tabulated results for the Diametral Tensile Strength of Porous Single layer scaffolds had been drafted in the table 4.4.

Table – 4.4 Diametral Tensile strength of Single Layer Bioactive glass ceramic scaffolds

Sintering Temperature (in °C)	Diametral Tensile Strength (MPa)								
	45S5			2P			4P		
	0P	30P	50P	0P	30P	50P	0P	30P	50P
800	6.78	3.13	1.07	10.94	9.26	6.46	5.09	4.48	0.98
850	8.57	3.48	1.09	11.30	9.79	7.00	5.80	4.64	1.17
900	8.81	3.75	1.37	13.84	9.87	7.27	5.93	5.48	1.27

4.11 FLEXURAL STRENGTH OF POROUS SINGLE LAYER SCAFFOLDS

The three point bending moment test on Porous Single layer scaffolds indulges in the evaluation of flexural strength of the scaffolds. Fig – 4.12.1, Fig – 4.12.2 & Fig – 4.12.3 shows the flexural strength of porous 45S5, 2P & 4P single layer scaffolds respectively for the corresponding sintering temperatures.

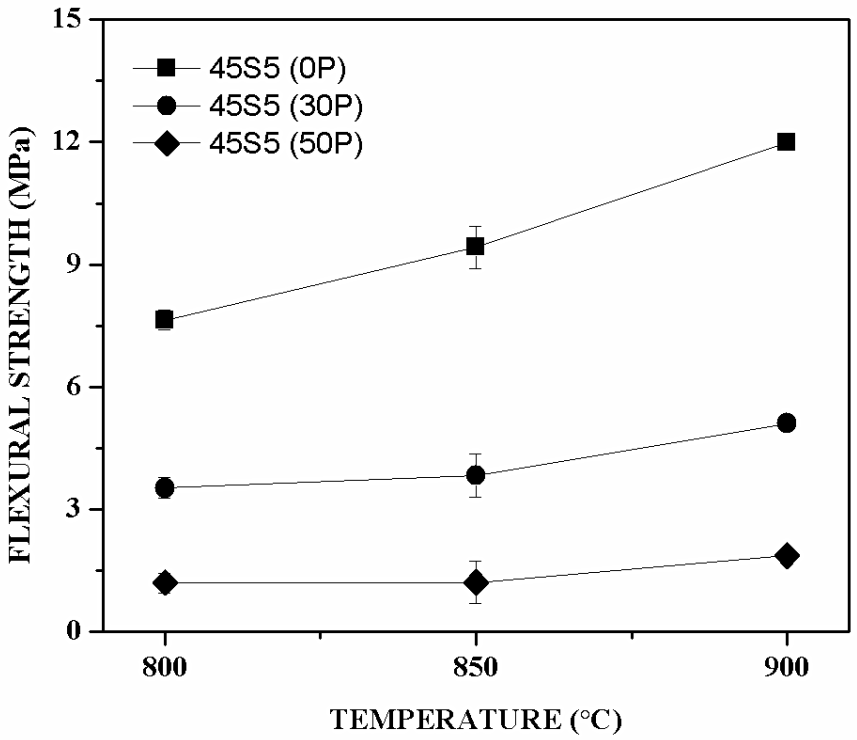

Fig – 4.12.1 Flexural strength of Porous 45S5 Single Layer scaffolds

Porous 45S5 single layer scaffolds shows a steady state increase in flexural strength, when the sintering temperature increases from 800°C to 900°C. As the porosity increases, the corresponding amount of strength had been reduced.

A drastic increase in Flexural strength had been recorded when the sintering temperature rises from 800°C to 850°C for 2P (0P) sample. When the temperature proceeds to 900°C a normal increase in Flexural strength had been observed on 2P (0P) sample. Rest of the 2P porous based single layer scaffolds registered a linear increase in flexural strength as the sintering temperature increases.

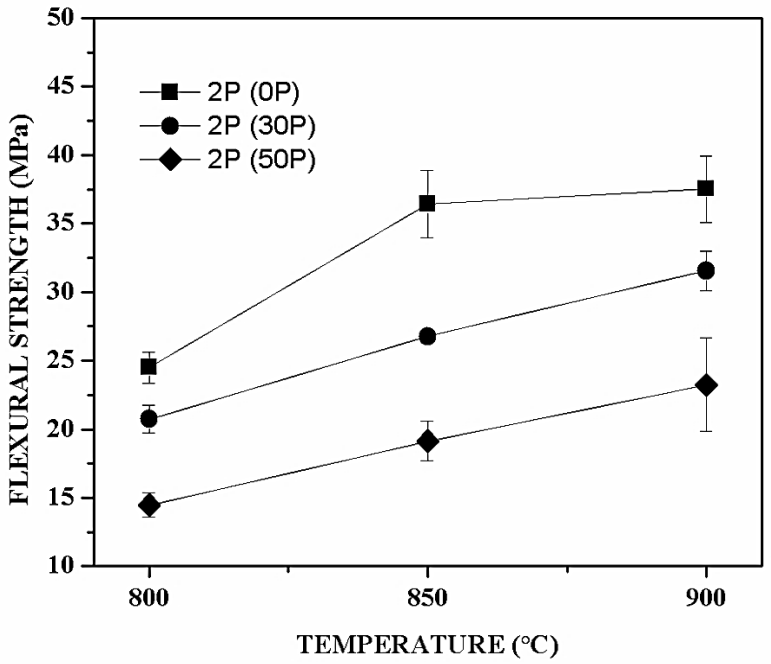

Fig – 4.12.2 Flexural strength of Porous 2P Single Layer scaffolds

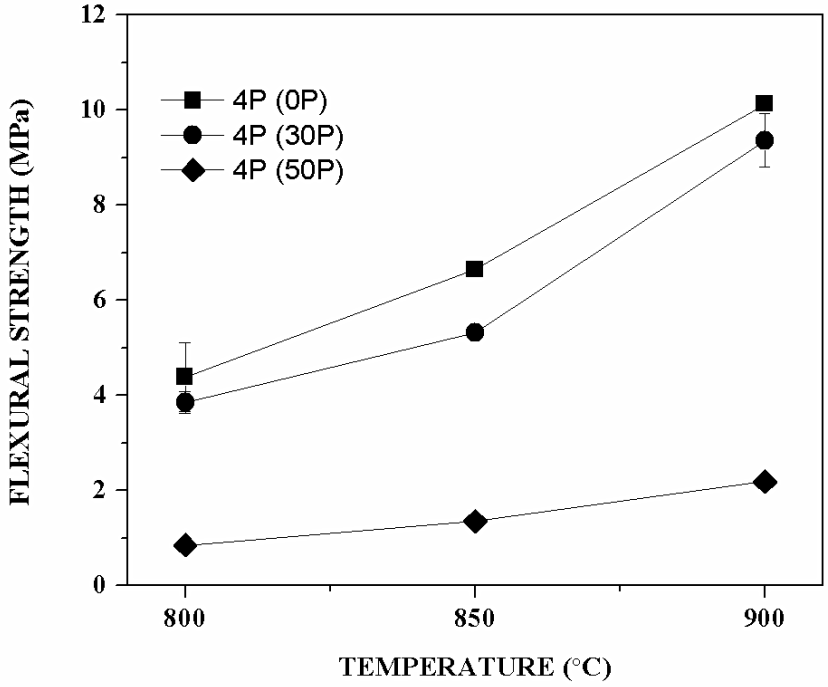

Fig – 4.12.3 Flexural strength of Porous 4P Single Layer scaffolds

In the case of 4P based porous single layer scaffolds, rate of increase in flexural strength was high, when the temperature increases from 800°C to 850°C. When the temperature increases to 900°C, the flexural strength increases more than the samples of previous sintering temperatures. These observations had been observed with the samples 4P (0P) & 4P (30P). 4P (50P) registered a linear increase in flexural strength when the temperature increases from 800°C to 900°C. The flexural strength values for the corresponding sintering temperatures had been tabulated in the table – 4.5.

Table – 4.5 Flexural strength of Single Layer Bioactive glass ceramic scaffolds

Sintering Temperature (in °C)	Flexural strength (MPa)								
	45S5			2P			4P		
	0P	30P	50P	0P	30P	50P	0P	30P	50P
800	7.63	3.52	1.19	24.50	20.73	14.47	4.37	3.84	0.84
850	9.42	3.83	1.21	36.40	26.75	19.13	6.64	5.31	1.34
900	11.98	5.10	1.86	37.52	31.55	23.24	10.12	9.36	2.18

On an overall comparison of the flexural strength of porous single layer scaffolds, 2P based scaffolds attains better flexural strength than the other single layer scaffolds. As mentioned in the section 4.9, this is again due to less amount of P_2O_5 present in 2P bioglass composition and viscous flow sintering.

4.12 APPARENT POROSITY & BULK DENSITY OF FGS

With 45S5, 2P & 4P glass composition and by uniaxial pressing and sintering method, porosity gradient or functionally graded bioactive glass ceramic scaffolds had been fabricated as per the protocol drafted in the section __. The fabricated green porosity gradient bioactive glass scaffolds had been sintered at 800°C, 850°C & 900°C. Fig – 4.13.1 shows the polished surface of porosity gradient bioactive glass ceramic scaffold.

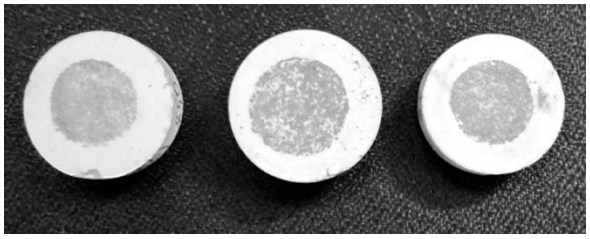

Fig – 4.13.1 Polished surface of porosity gradient scaffolds

Two types of porosity gradient bioactive glass ceramic scaffolds had been prepared which had been represented by (0,30) and (0,50). (0,30) represents 0wt.% naphthalene added for outer layer and 30wt.% naphthalene added for inner layer. Similarly (0,50) represents 0wt.% naphthalene added for outer layer and 50wt.% naphthalene added for inner layer.

The apparent porosity & bulk density of the entire porosity gradient scaffold had been evaluated. Fig – 4.13.2, Fig – 4.13.3, Fig – 4.13.4, Fig – 4.13.5, Fig – 4.13.6 & Fig – 4.13.7 shows the Apparent porosity & Bulk density of 45S5(0,30), 45S5(0,50), 2P(0,30), 2P(0,50), 4P(0,30) & 4P(0,30) bioactive glass ceramic scaffolds respectively.

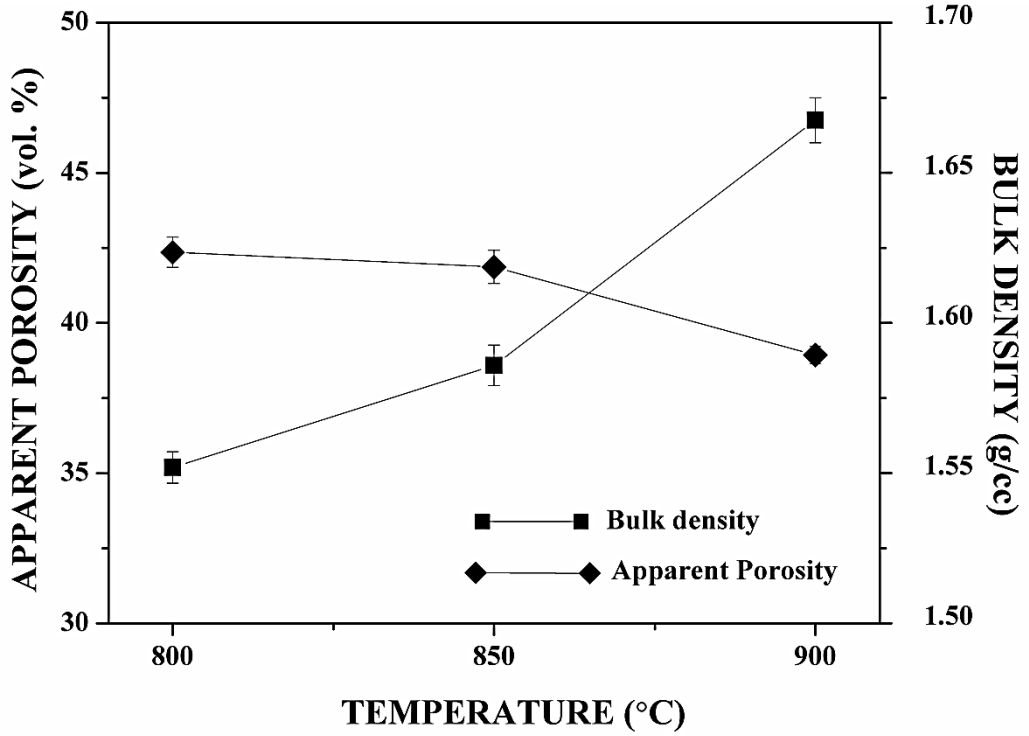

Fig – 4.13.2 Apparent Porosity & Bulk density of FGS-45S5 (0,30)

The overall apparent porosity of the entire FGS scaffold, FGS 45S5 (030) achieved from 42 vol.% to 38 vol.% for the sintering temperatures 800°C, 850°C & 900°C. The bulk density had been achieved within the range of 1.55 g/cc to 1.66g/cc.

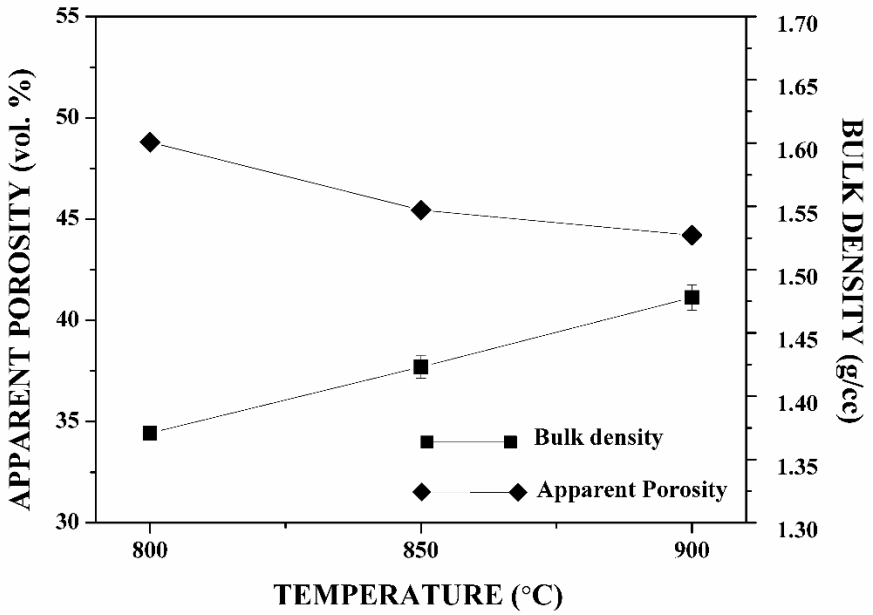

Fig – 4.13.3 Apparent Porosity & Bulk density of FGS-45S5 (0,50)

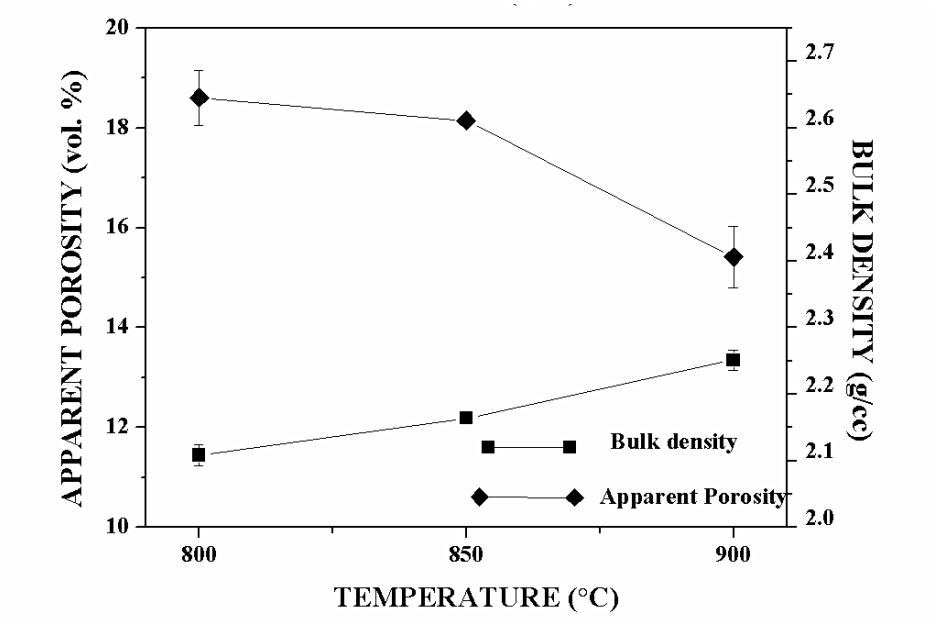

Fig – 4.13.4 Apparent Porosity & Bulk density of FGS-2P (0,30)

In the case of FGS – 45S5(0,50), a gradual reduction of apparent porosity had been achieved, from 48 vol.% to 44 vol.% on increasing sintering temperatures. And 1.37 g/cc to 1.47 g/cc of bulk density had been recorded.

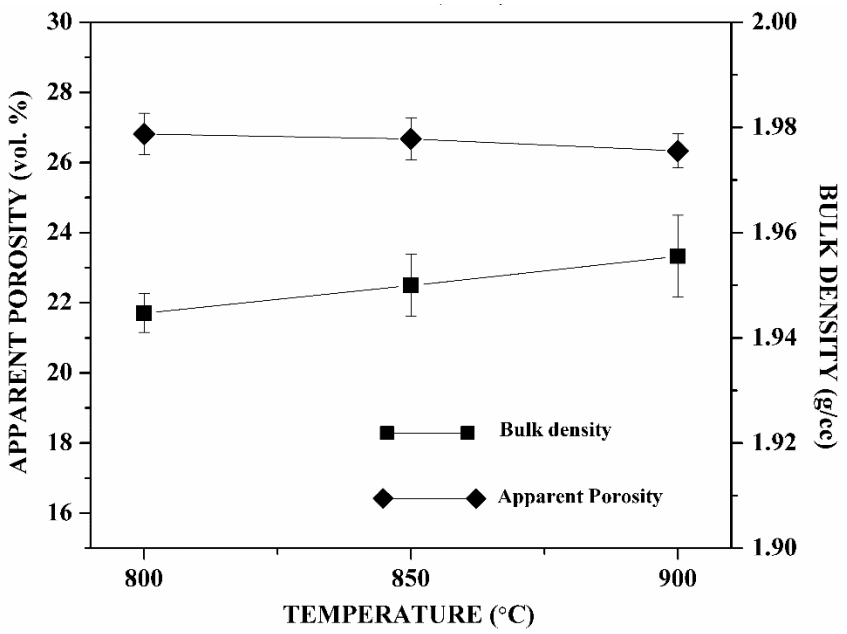

Fig – 4.13.5 Apparent Porosity & Bulk density of FGS-2P (0,50)

FGS 2P (0,30) observes a sudden drop in apparent porosity when the sintering temperature rises from 850°C to 900°C. Approx. 18 vol.% to 15 vol.% of apparent porosity and 2.10 g/cc to 2.25 g/cc of bulk density had been recorded on different sintering temperatures.

For FGS 2P (050), major amount of pore reduction had been attained at the sintering temperature of 800°C itself. When the sintering temperature increases from 850°C to 900°C, less amount of apparent porosity had been dropped.

FGS 4P (030) possess a gradual reduction of apparent porosity, which had been attained when the sintering temperature increases from 800°C to 850°C and then to 900°C.

The rate of reduction of apparent porosity had been totally reduced when the sintering temperature increases from 850°C to 900°C in FGS 4P (050)

.

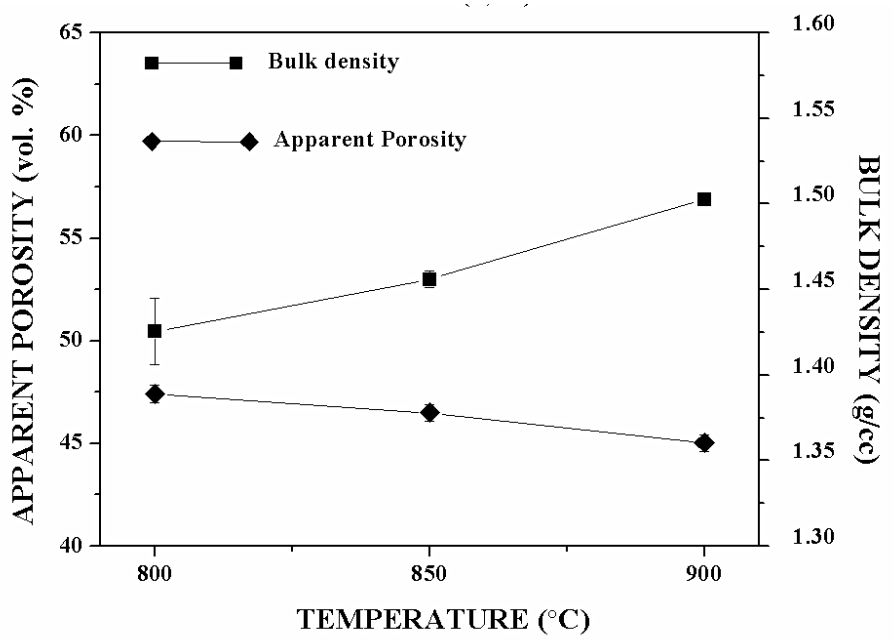

Fig – 4.13.6 Apparent Porosity & Bulk density of FGS-4P (0,30)

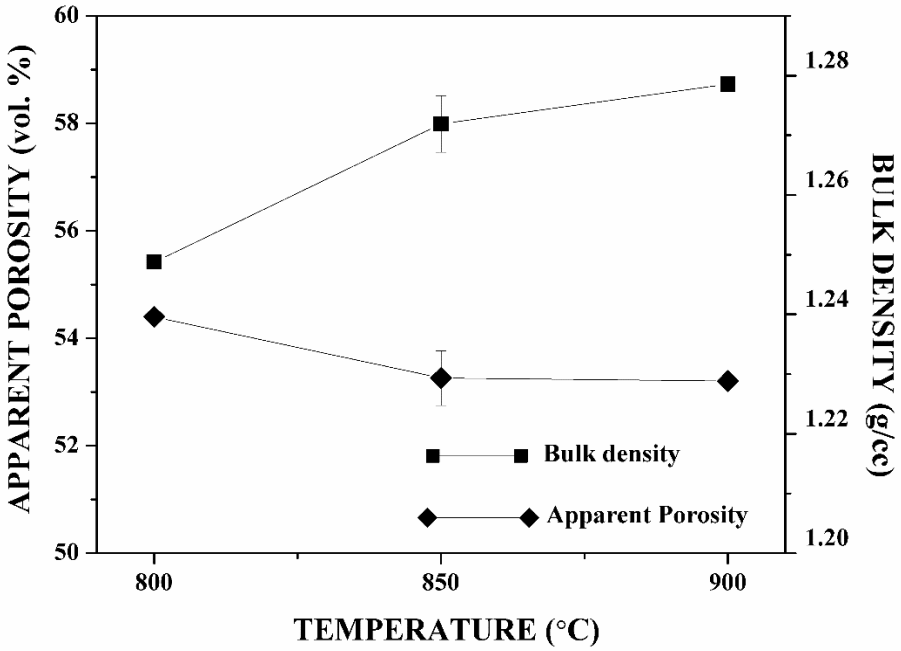

Fig – 4.13.7 Apparent Porosity & Bulk density of FGS-4P (0,50)

Table – 4.6 Apparent Porosity (A.P) & Bulk density (B.D) of Entire FGS

Sintering Temp. (°C)	45S5				2P				4P			
	(0,30)		(0,50)		(0,30)		(0,50)		(0,30)		(0,50)	
	A.P (vol.%)	B.D (g/cc)	A.P (vol.%)	B.D (g/cc)	A.P (vol.%)	B.D (g/cc)	A.P (vol.%)	B.D (g/cc)	A.P (vol.%)	B.D (g/cc)	A.P (vol.%)	B.D (g/cc)
800	42.36	1.55	48.79	1.37	18.60	2.10	26.81	1.94	47.41	1.42	54.39	1.24
850	41.86	1.58	45.43	1.42	18.14	2.16	26.67	1.95	46.49	1.45	53.25	1.27
900	38.93	1.66	44.20	1.47	15.41	2.25	26.33	1.96	45.03	1.50	53.20	1.28

On reviewing the consolidated results drafted in Table – 4.5, it had been confirmed that FGS 2P (0,30) attains better overall bulk density than the other FGS scaffolds. FGS 4P (0,50) performs as a highly porous scaffold when compared with other FGS scaffolds.

4.13 APPARENT POROSITY & BULK DENSITY OF GRADED LAYERS

The evaluation of apparent porosity and bulk density on each and every layer is mandatory for the characterization of functionally graded scaffolds. Three small regions from outer layer and inner layer had been cut and carved out. Then the apparent porosity and bulk density of those samples had been calculated. This evaluation clearly shows the gradient in porosity attained by uniaxial pressing and sintering method. In other words, the results obtained in the previous section can be called as effective Apparent Porosity and bulk density values of the graded layers. Fig – 4.14.1(a) & Fig – 4.14.1(b) shows the apparent porosity & bulk density of outer and inner layers of 45S5 (0,30) scaffold respectively. Without any drastic fall in apparent porosity, there was a gradual reduction in apparent porosities of outer and inner layers of 45S5 (030) scaffold. Table – 4.5 shows the corresponding tabulated results.

Table – 4.7 Apparent Porosity & Bulk density of graded layers of 45S5 (0,30)

Sintering Temperature (in °C)	45S5 (0,30) – Outer Layer		45S5 (0,30) – Inner Layer	
	Apparent Porosity (vol.%)	Bulk Density (g/cc)	Apparent Porosity (vol.%)	Bulk Density (g/cc)
800	32.16	1.82	52.33	1.250
850	30.99	1.84	52.31	1.261
900	29.64	1.89	52.21	1.262

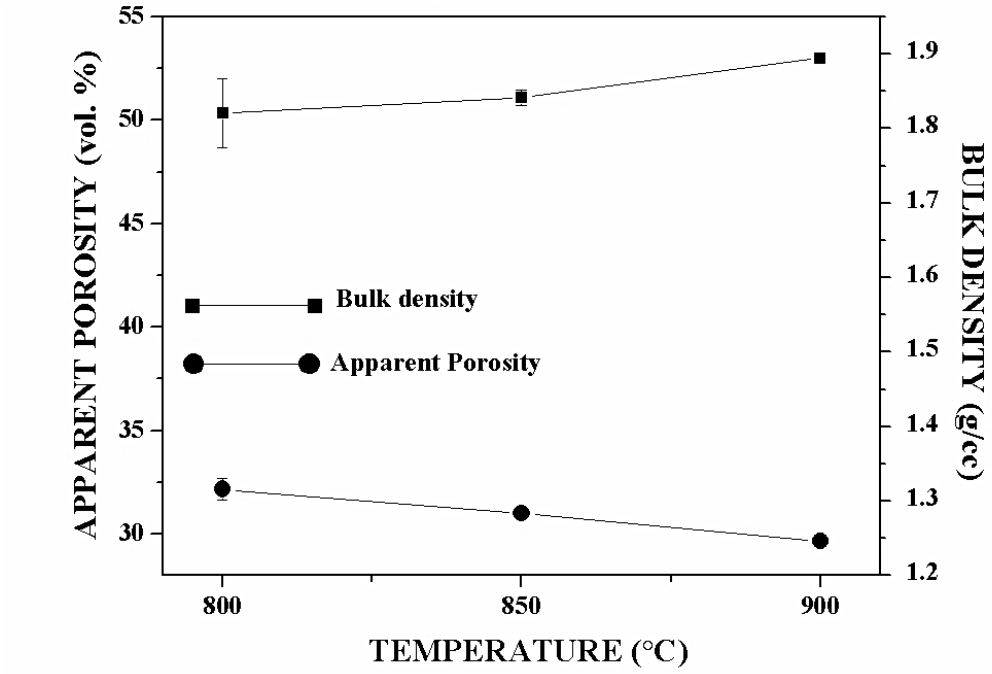

Fig – 4.14.1(a) Apparent Porosity & Bulk density of Outer Layer of 45S5 (0,30) scaffold

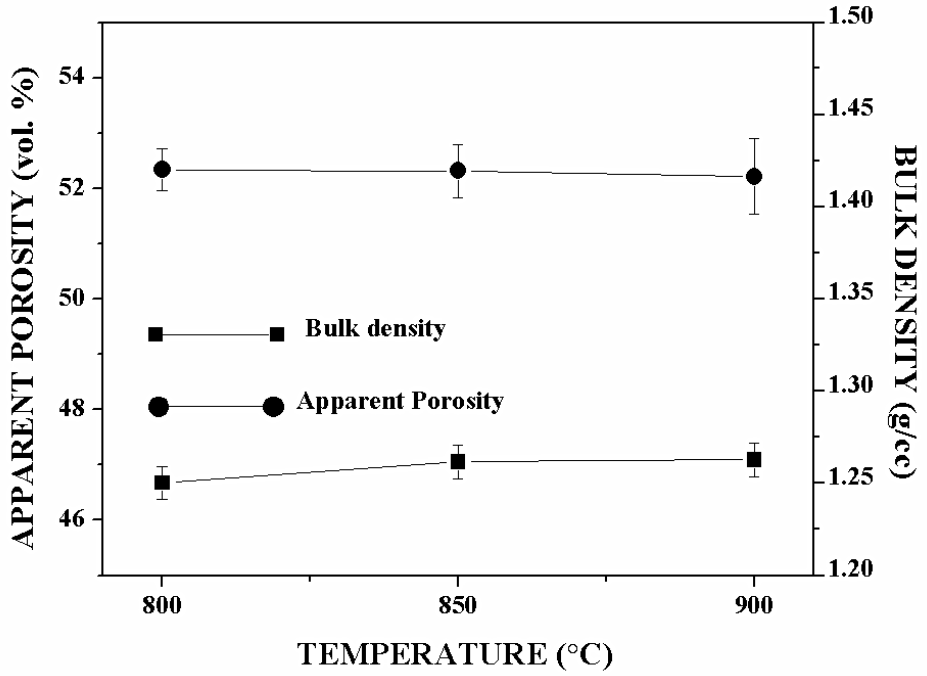

Fig – 4.14.1(b) Apparent Porosity & Bulk density of Inner Layer of 45S5 (0,30) scaffold

Fig – 4.14.2 (a) and Fig – 4.14.2(b) shows the apparent porosity and bulk density of outer and inner layers respectively of 45S5 (0,50) scaffold. The outer layer achieved a maximum bulk density of about 1.9g/cc and inner layer attains a bulk density of 1.28 g/cc at 900°C. In the case of 45S5(0,50), pore reduction proceeds even till sintering temperature reaches 900°C. The densification of outer layer is comparatively less than the inner layer of 45S5 (050). Table 4.6 shows the Apparent porosity and bulk density values of graded layers of 45S5 (0,50).

Table – 4.8 Apparent Porosity & Bulk density of graded layers of 45S5 (0,50) scaffold

Sintering Temperature (in °C)	45S5 (0,50) – Outer Layer		45S5 (0,50) – Inner Layer	
	Apparent Porosity (vol.%)	Bulk Density (g/cc)	Apparent Porosity (vol.%)	Bulk Density (g/cc)
800	34.67	1.71	63.02	0.98
850	32.15	1.81	61.54	1.01
900	28.58	1.91	58.02	1.05

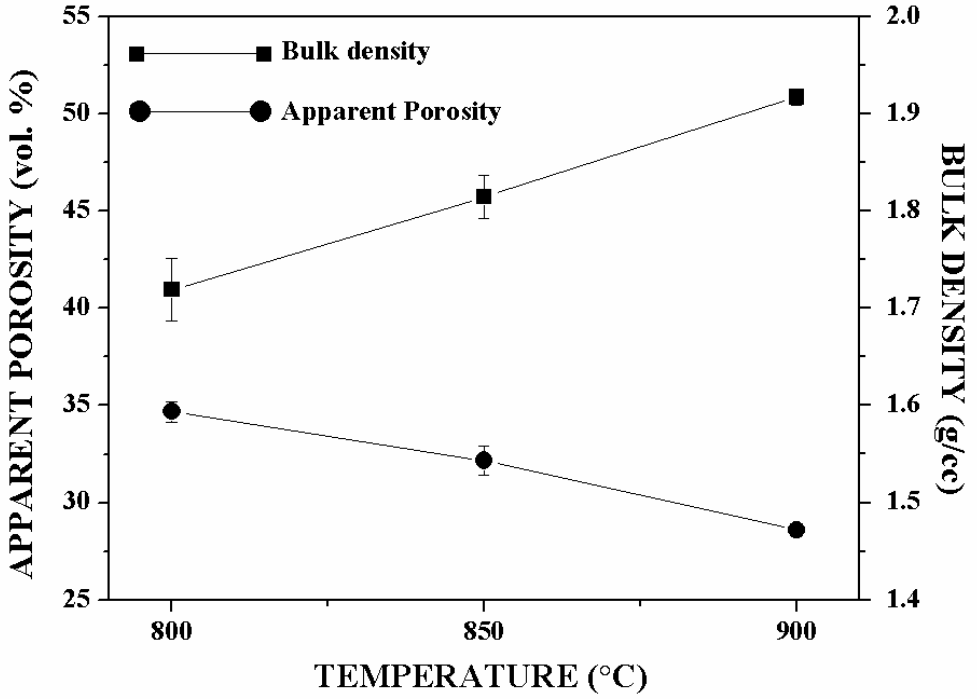

Fig – 4.14.2(a) Apparent Porosity & Bulk density of Outer layer of 45S5 (0,50) scaffold

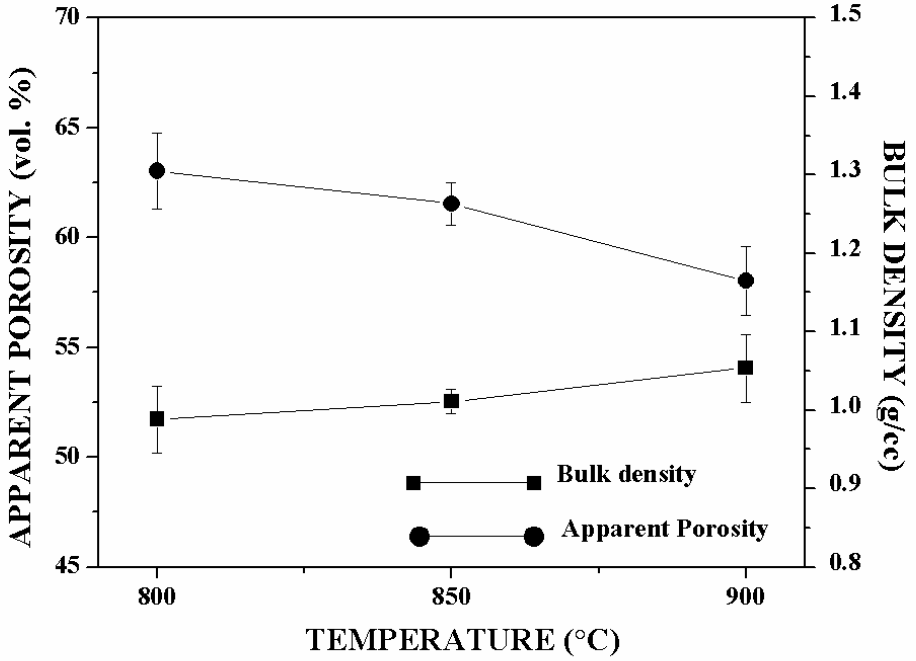

Fig – 4.14.2(b) Apparent Porosity & Bulk density of Inner layer of 45S5 (0,50) scaffold

Fig – 4.14.3(a) & Fig – 4.14.3(b) shows the apparent porosity and bulk density of outer and inner layers of 2P (0,30) scaffold respectively. In the case of outer layer of 2P (0,30), the maximum pore reduction had been attained at 800°C and not much pore reduction had been observed when the sintering temperature proceeds to 850°C and 900°C. In the inner layer of 2P(0,30), maximum pore reduction took place within 850°C itself. Table – 4.7 shows the apparent porosity and bulk density values of graded layers of 2P (0,30) scaffold.

Table – 4.9 Apparent Porosity & Bulk density of graded layers of 2P (0,30) scaffold

Sintering Temperature (in °C)	2P (0,30) – Outer Layer		2P (0,30) – Inner Layer	
	Apparent Porosity (vol.%)	Bulk Density (g/cc)	Apparent Porosity (vol.%)	Bulk Density (g/cc)
800	5.77	2.46	54.15	1.15
850	3.95	2.47	48.73	1.76
900	3.13	2.55	34.10	1.34

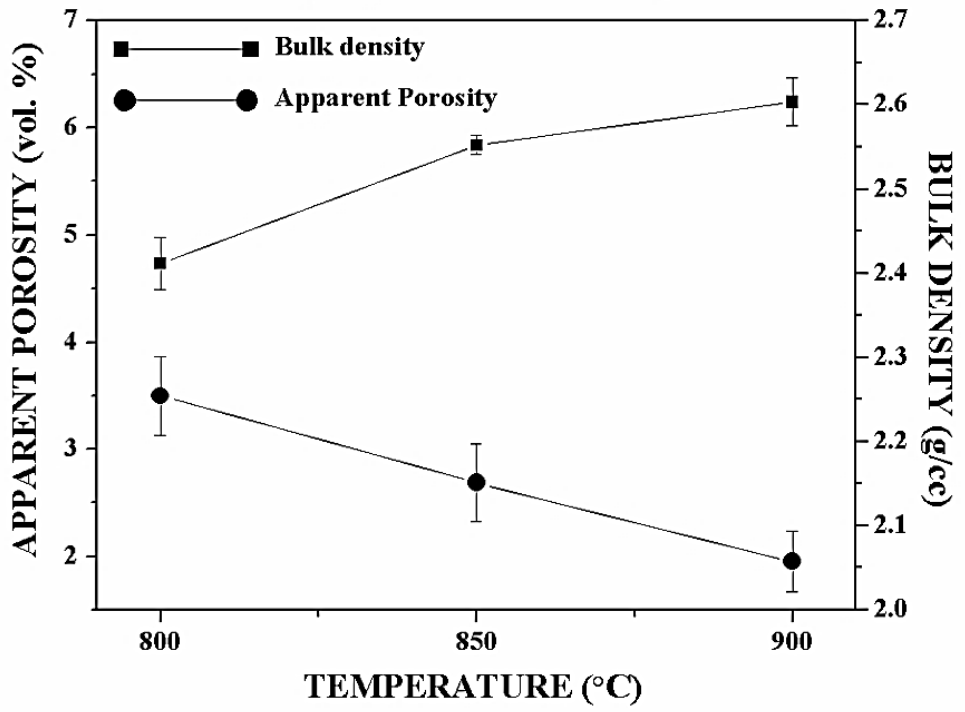

Fig – 4.14.3(a) Apparent Porosity & Bulk density of Outer layer of 2P (0,30) scaffold

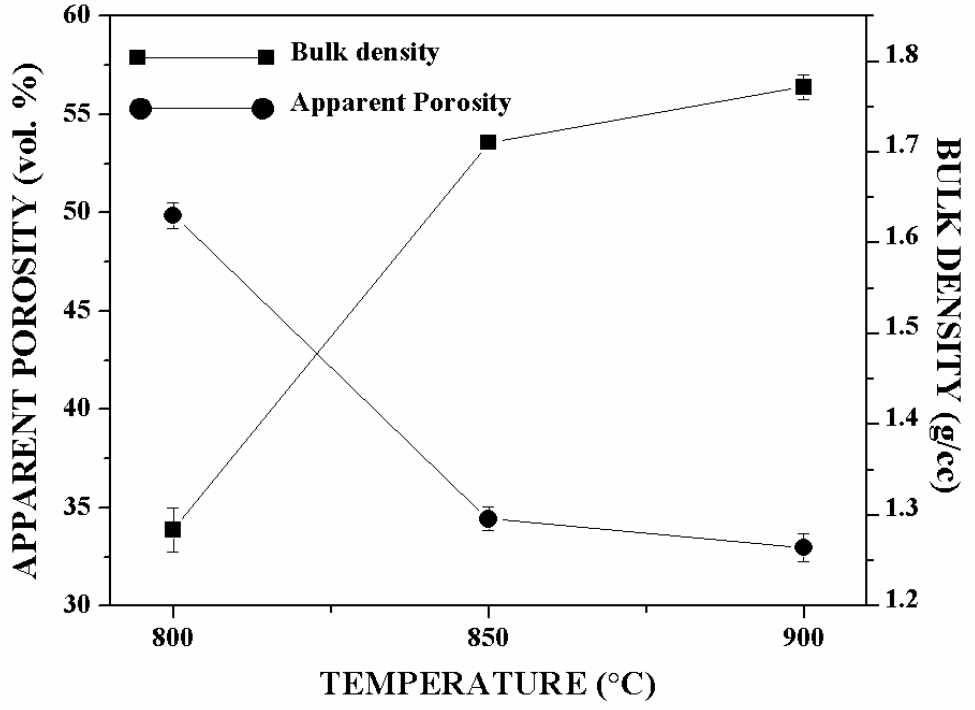

Fig – 4.14.3(b) Apparent Porosity & Bulk density of Inner layer of 2P (0,30) scaffold

Fig – 4.14.4 (a) & Fig – 4.14.4(b) shows the Apparent porosity and bulk density of outer and inner layers of 2P (0,50) respectively. At 800°C, a large amount of pore reduction had been carried out in the outer layer. But at the same time, pore reduction had been continued till the sintering temperature reaches 900°C for inner layer. The apparent porosity and bulk density values of graded layers of 2P(0,50) with corresponding temperature had been drafted in the table – 4.8.

Table – 4.10 Apparent Porosity & Bulk density of graded layers of 2P (0,50) scaffold

Sintering Temperature (in °C)	2P (0,50) – Outer Layer		2P (0,50) – Inner Layer	
	Apparent Porosity (vol.%)	Bulk Density (g/cc)	Apparent Porosity (vol.%)	Bulk Density (g/cc)
800	3.49	2.41	49.85	1.28
850	2.68	2.55	34.43	1.71
900	1.95	2.60	32.98	1.77

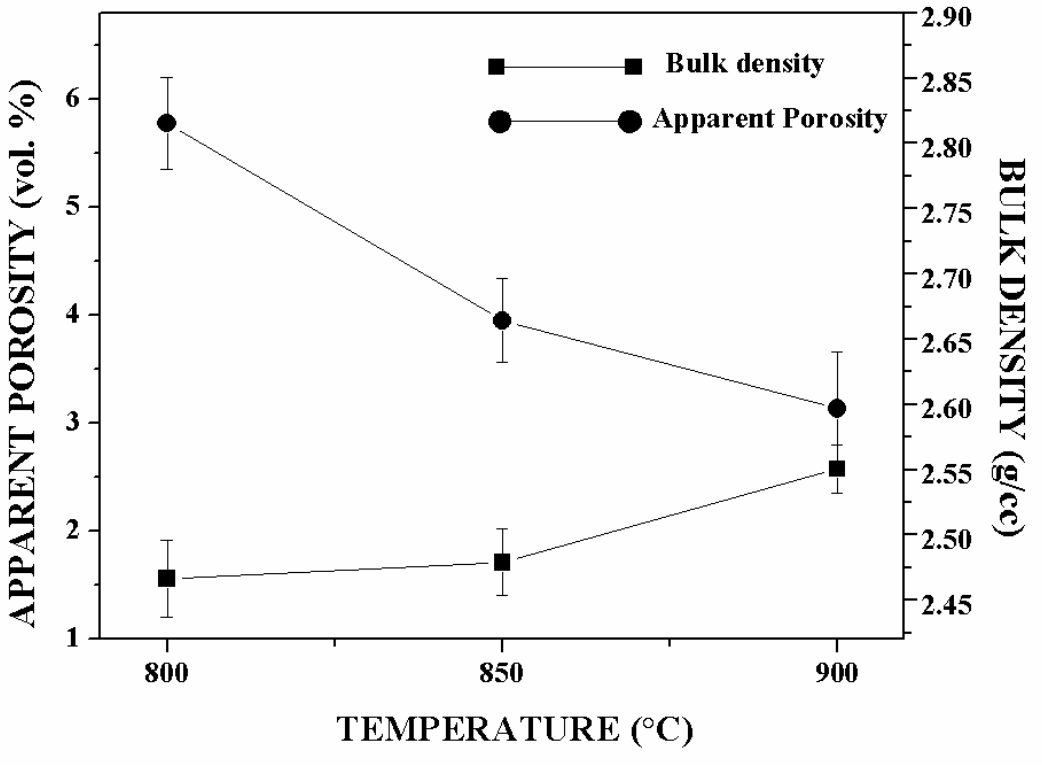

Fig – 4.14.4(a) Apparent Porosity & Bulk density of Outer layer of 2P (0,50) scaffold

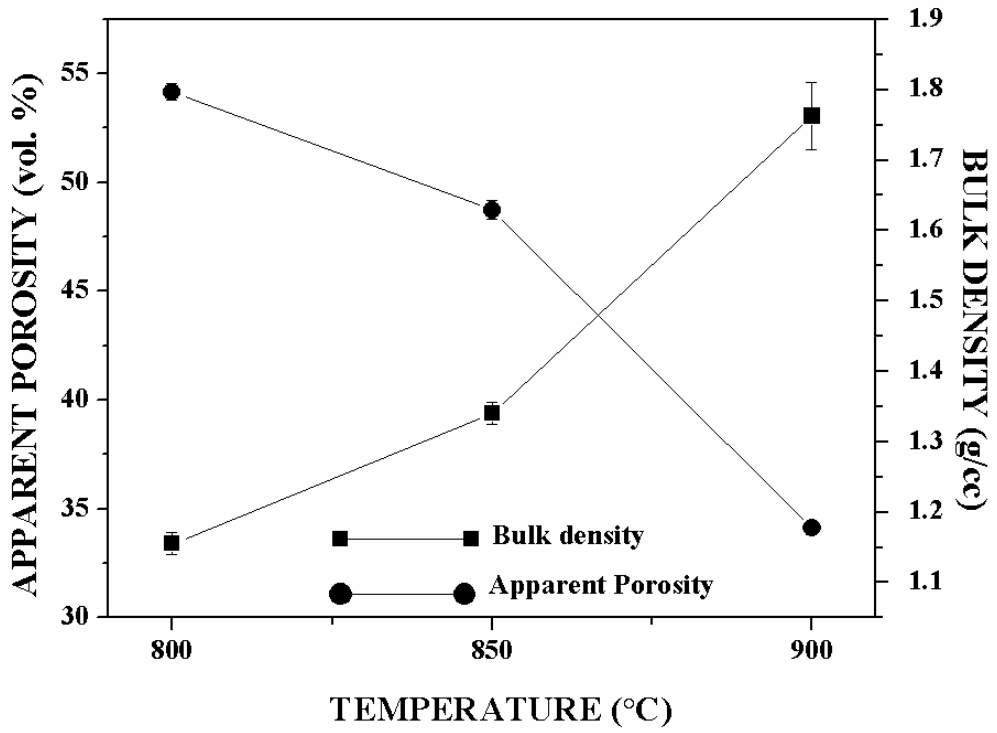

Fig – 4.14.4(b) Apparent Porosity & Bulk density of Inner layer of 2P (0,50) scaffold

Fig – 4.13.5(a) and Fig – 4.13.5(b) shows the apparent porosity and bulk density of outer and inner layer of 4P(0,30) respectively. The outer bone layer registered apparent porosity within the range of 36vol.% to 38vol.%, which is the highest among the outer bone layers of 45S5 (030) and 2P (030). A gradual increase in bulk density had been attained when the temperature increases from 800°C to 900°C. Table – 4.9 illustrates the corresponding apparent porosity and bulk density values of graded layers of 4P(0,30) scaffold.

Table – 4.11 Apparent Porosity & Bulk density of graded layers of 4P (0,30) scaffold

Sintering Temperature (in °C)	4P (0,30) – Outer Layer		4P (0,30) – Inner Layer	
	Apparent Porosity (vol.%)	Bulk Density (g/cc)	Apparent Porosity (vol.%)	Bulk Density (g/cc)
800	37.86	1.66	53.27	1.25
850	37.82	1.68	51.96	1.26
900	36.68	1.72	50.72	1.29

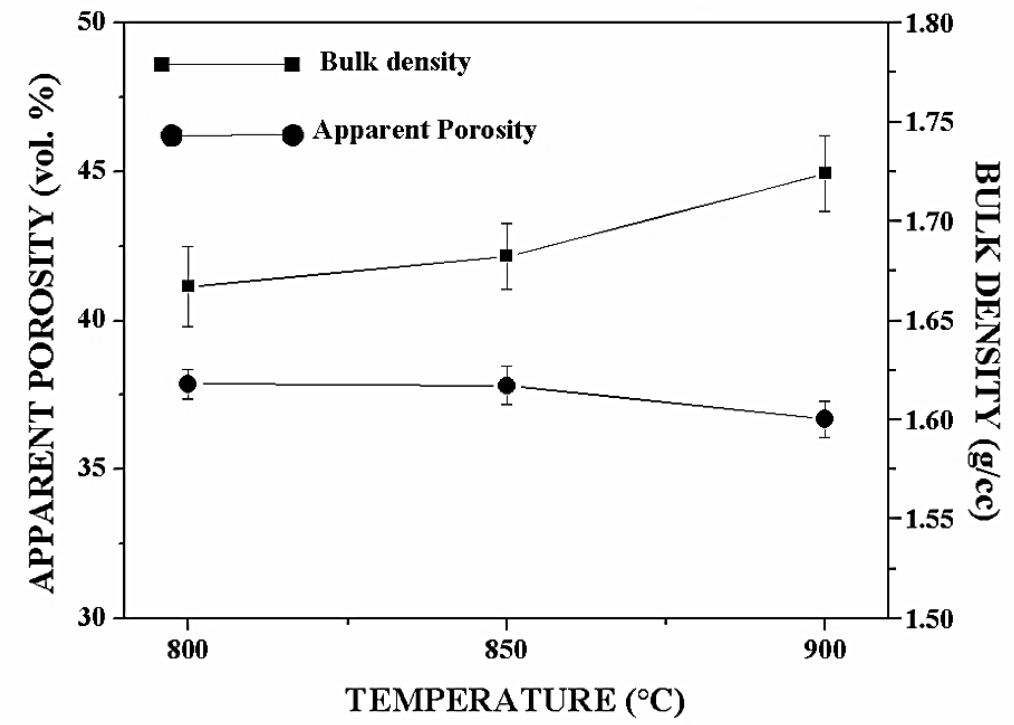

Fig – 4.14.5(a) Apparent Porosity & Bulk density of Outer layer of 4P (0,30) scaffold

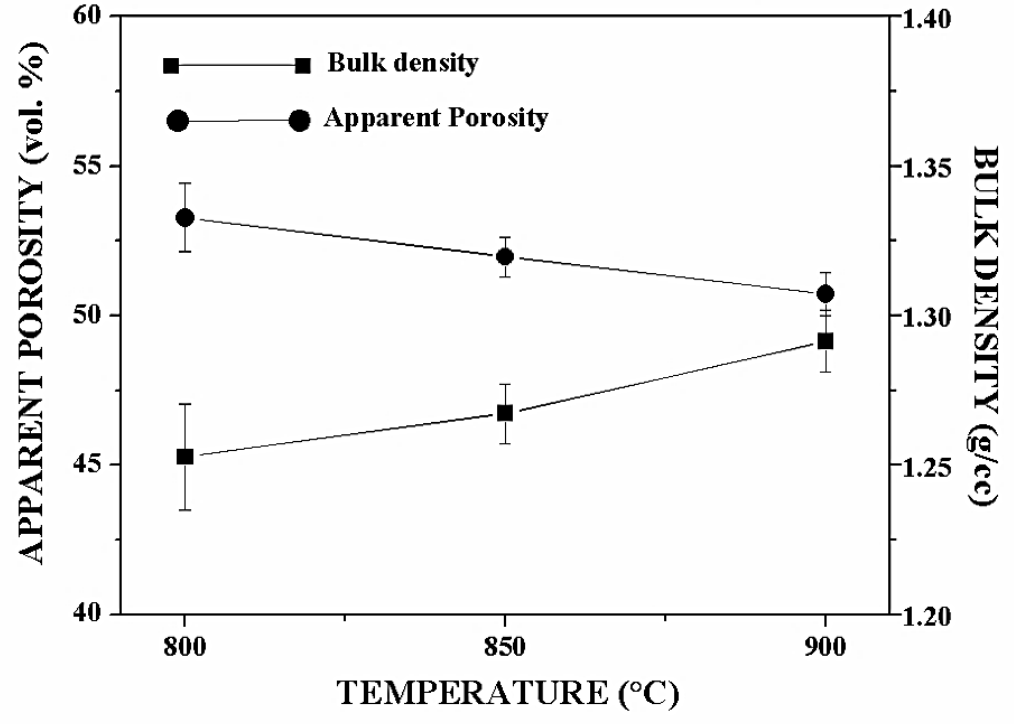

Fig – 4.14.5(b) Apparent Porosity & Bulk density of Inner layer of 4P (0,30) scaffold

Fig – 4.14.6(a) and Fig – 4.14.6(b) shows the apparent porosity and bulk density of outer and inner layer of 4P(0,50) respectively. 4P (050) had been considered to be the highly porous scaffolds among the other scaffolds. 52 to 64 vol.% and 38 to 42 vol.% of apparent porosity had been attained with the outer and inner layers respectively. A drastic decrease in apparent porosity had been observed on the inner layer, when the temperature increases from 800°C to 850°C. Table – 4.10 illustrates the apparent porosity and bulk density values of graded layers of 4P(0,50) scaffold.

Table – 4.12 Apparent Porosity & Bulk density of graded layers of 4P (0,50) scaffold

Sintering Temperature (in °C)	4P (0,50) – Outer Layer		4P (0,50) – Inner Layer	
	Apparent Porosity (vol.%)	Bulk Density (g/cc)	Apparent Porosity (vol.%)	Bulk Density (g/cc)
800	41.93	1.55	64.16	0.88
850	41.16	1.60	53.17	1.10
900	38.98	1.61	52.32	1.13

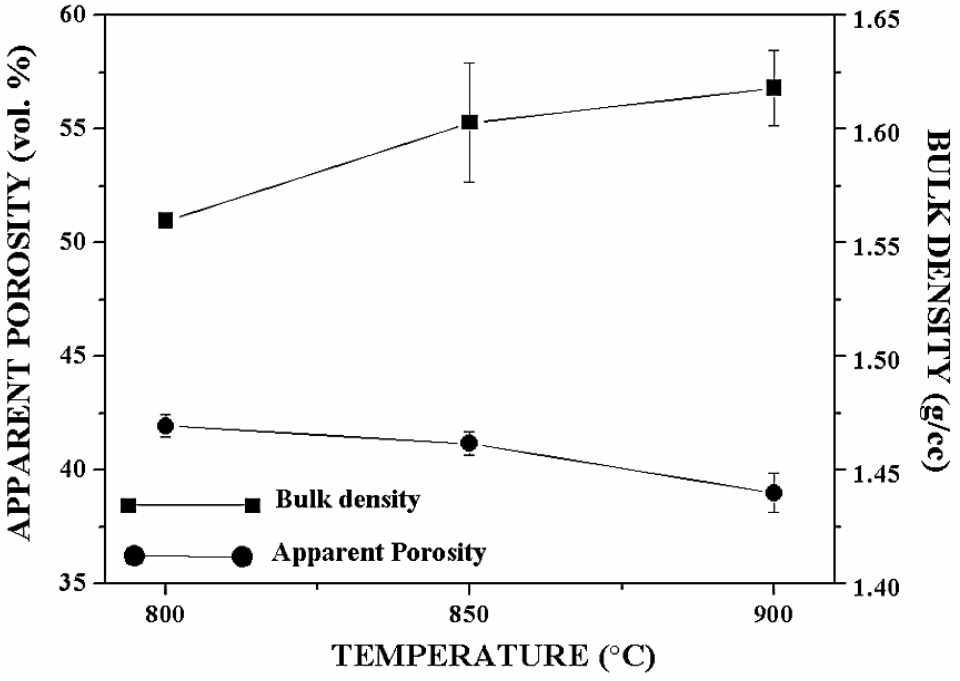

Fig – 4.14.6(a) Apparent Porosity & Bulk density of Outer layer of 4P (0,50) scaffold

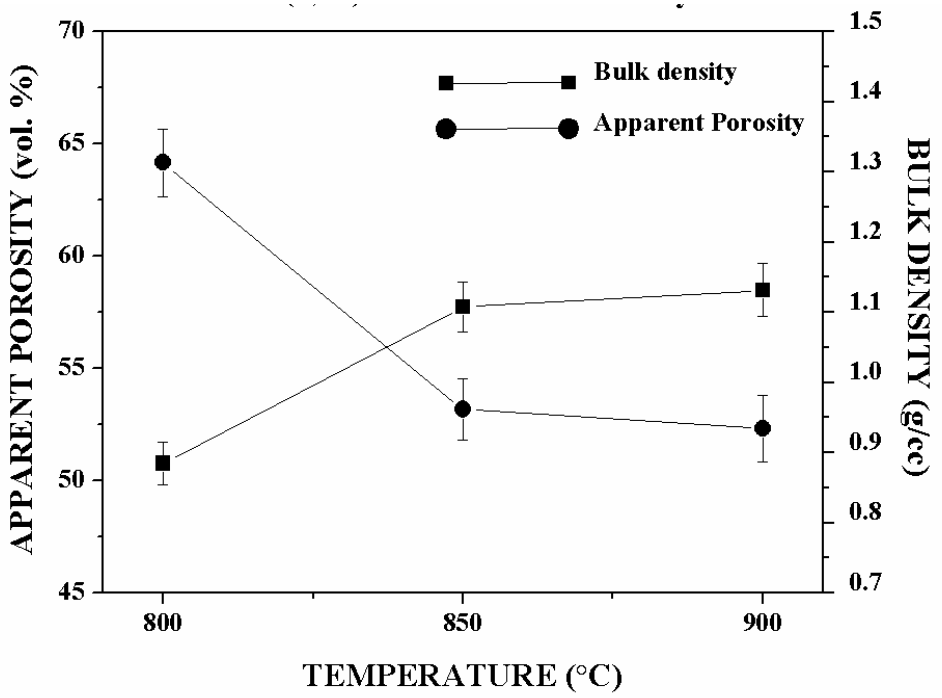

Fig – 4.14.6(b) Apparent Porosity & Bulk density of Inner layer of 4P (0,50) scaffold

4.14 COMPARATIVE STUDY OF SINGLE LAYER AND FUNCTIONALLY GRADED SCAFFOLDS – Apparent Porosity & Bulk density

Single layer porous scaffolds had been fabricated on addition of 0wt.%, 30wt.% & 50wt.% naphthalene which had been represented as 0P, 30P & 50P respectively. As given in the table – 3.2, two types of functionally graded scaffolds – (0,30) and (0,50) had been prepared. The Outer layer (without pore former – 0wt.%) of the functionally graded scaffolds and 0P – single layer scaffolds resembles with same composition. Similarly, the inner layer (30wt.% & 50wt.%) depicts the similar composition of the single layer scaffolds – 30P & 50P. Single layer scaffold compositions had been uniaxial pressed and sintered. But the functionally graded scaffolds are co-compacted and co-sintered with outer and inner layer compositions. Even the compositions of the single layer scaffolds resemble with the composition of the graded layers, the compaction and sintering environments are different. Comparing the properties of single layer scaffolds with graded layers of functionally graded scaffolds fetches a better understanding of sintering behavior of functionally graded scaffolds. In this section, the apparent porosity and bulk density of single layer scaffolds and graded layers had been compared.

Fig – 4.15.1 illustrates the apparent porosity and bulk density of 45S5 (0,30), 45S5(0P) & 45S5(30P).

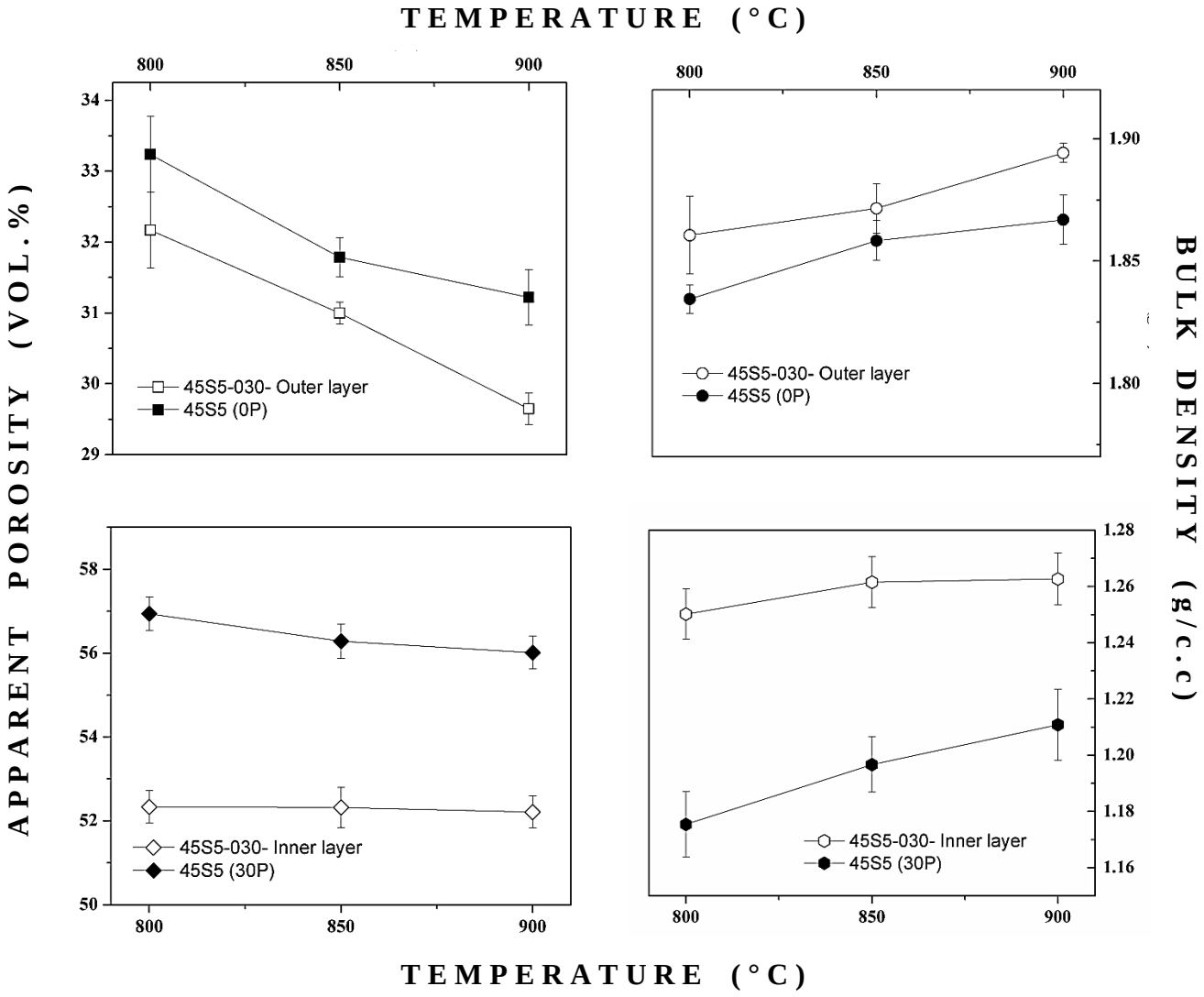

Fig – 4.15.1 Graded Layers of 45S5(0,30) vs 45S5(0P) & 45S5(30P)

Apparent Porosity of Outer Layer of 45S5 (030) FGS is comparatively less than the 45S5(0P). Apparent Porosity of Inner Layer of 45S5 (030) FGS is comparatively less than the 45S5(30P). Difference in Apparent porosities of Inner Layer of 45S5 (030) FGS and 45S5(30P) is too high when compared with the difference in Apparent porosities of Outer Layer of 45S5 (030) FGS and 45S5(0P).

Fig – 4.15.2 illustrates the apparent porosity and bulk density of the graded layers of 45S5 (0,50), 45S5(0P) & 45S5(50P).

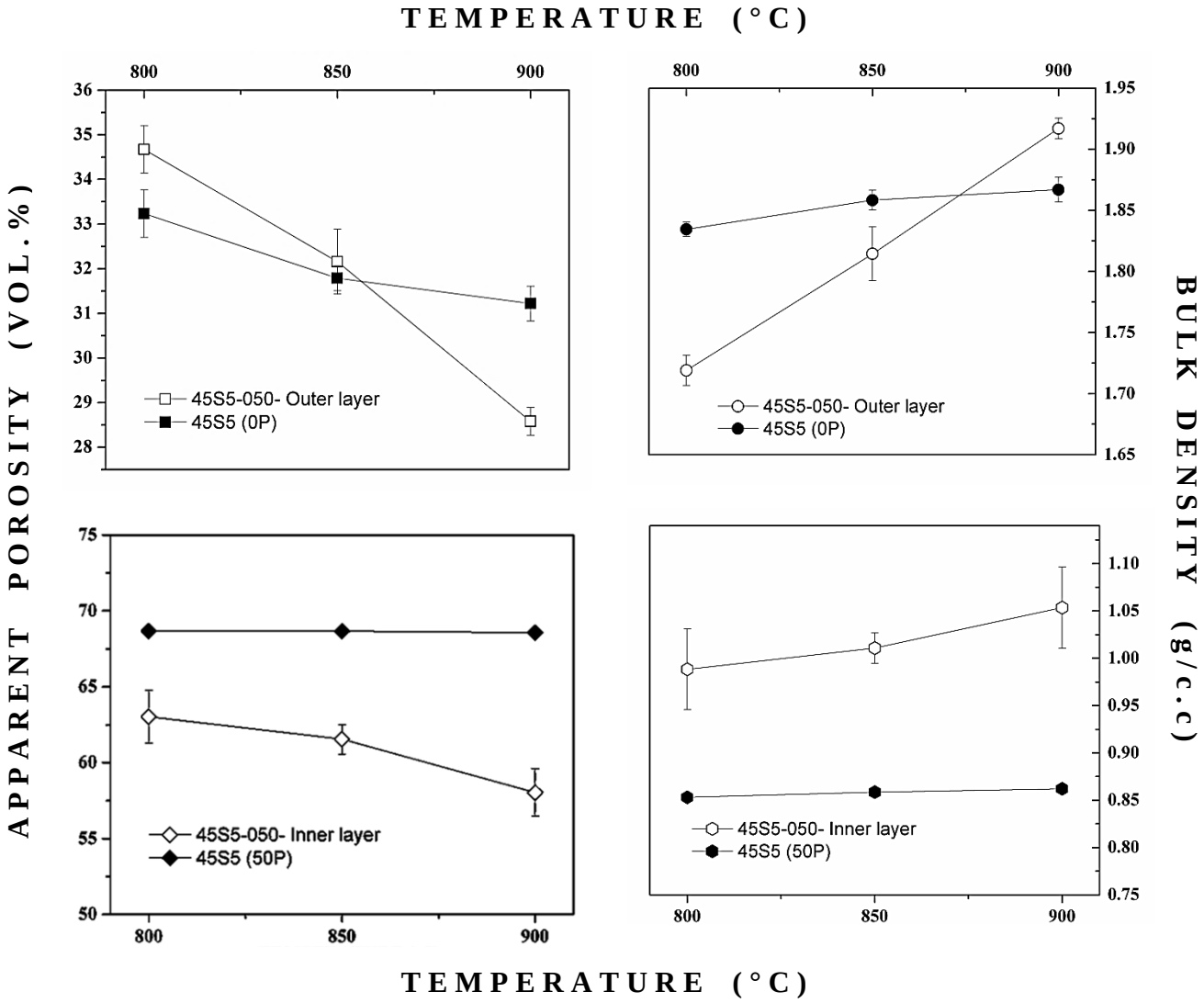

Fig – 4.15.2 Graded Layers of 45S5(0,50) vs 45S5(0P) & 45S5(50P)

Apparent Porosity of Outer Layer of 45S5 (050) FGS is higher than the 45S5 (0P) for the scaffolds sintered at 800°C & 850°C. But there was a drastic decrease in the Apparent Porosity of Outer Layer of 45S5 (050) FGS, when they had sintered at 900°C. This drastic decrease recorded a lower Apparent Porosity than the 45S5 (0P). Apparent porosity of Inner Layer of 45S5 (050) FGS is relatively lower than the 45S5 (50P) scaffolds. From 800°C to 850°C, there was a linear decrease in apparent porosity. But at 900°C, a huge reduction in apparent porosity of Inner Layer of 45S5 (050) FGS & 45S5 (50P) had been observed.

Fig – 4.15.3 illustrates the apparent porosity and bulk density of 2P (0,30), 2P(0P) & 2P(30P).

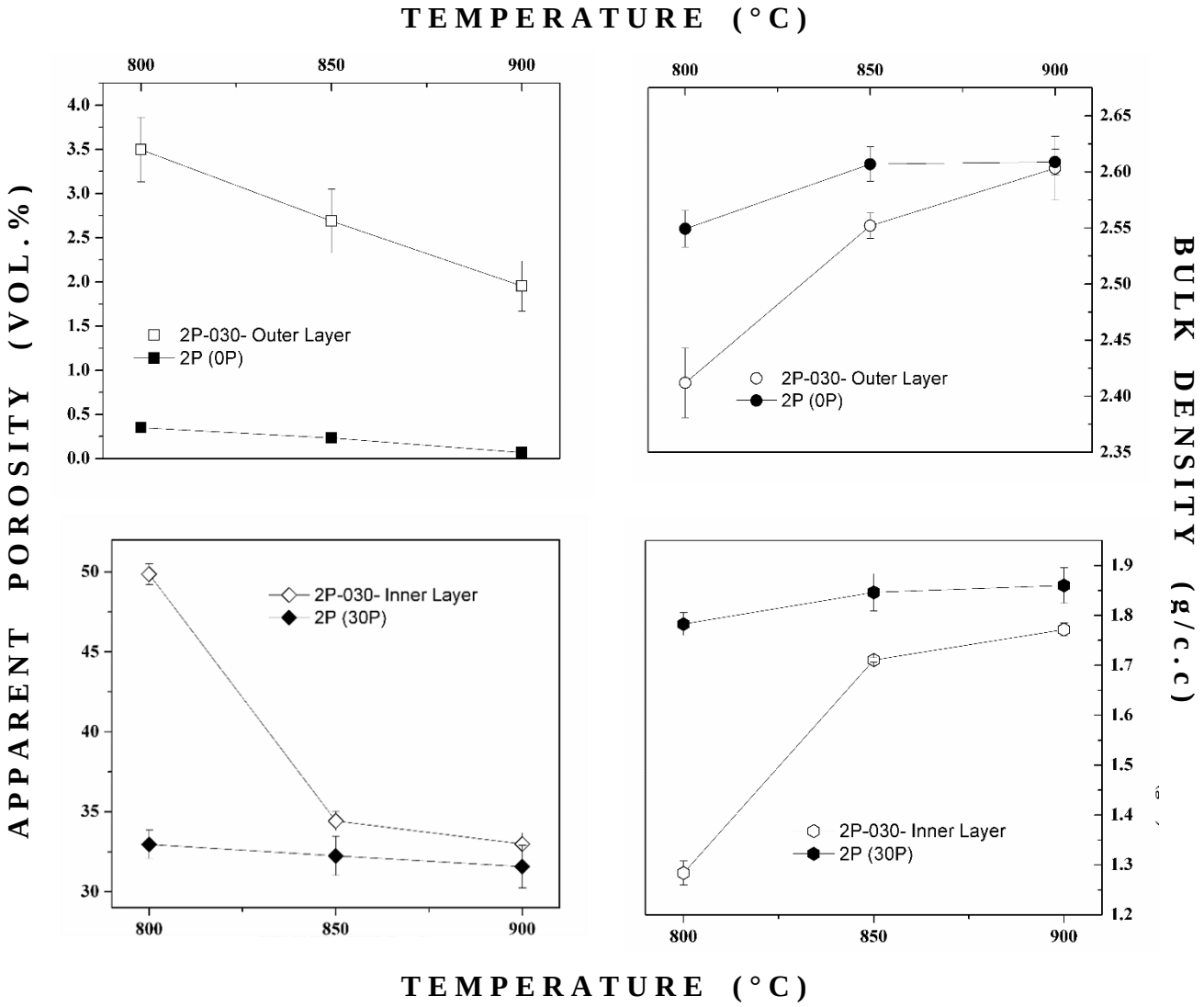

Fig – 4.15.3 Graded Layers of 2P(0,30) vs 2P(0P) & 2P(30P)

A gradual decrease in Apparent porosity had been observed for Outer Layer of 2P (030) FGS and 2P (0P), when sintered from 800°C to 900°C. The bulk density for Outer Layer of 2P (030) FGS and 2P (0P) were almost similar when sintered at 900°C. A drastic decrease in Apparent porosity of Inner Layer of 2P (030) FGS had been observed when sintered from 800°C to 850°C. Then a linear reduction of apparent porosity had been observed on the Inner layer of 2P (030) when fired at 900°C. A linear reduction of apparent porosity had been observed for 2P (30P) from 800°C to 900°C. Similar phenomena had been observed in the bulk density of 2P(30P) and Inner layer of 2P (030) FGS.

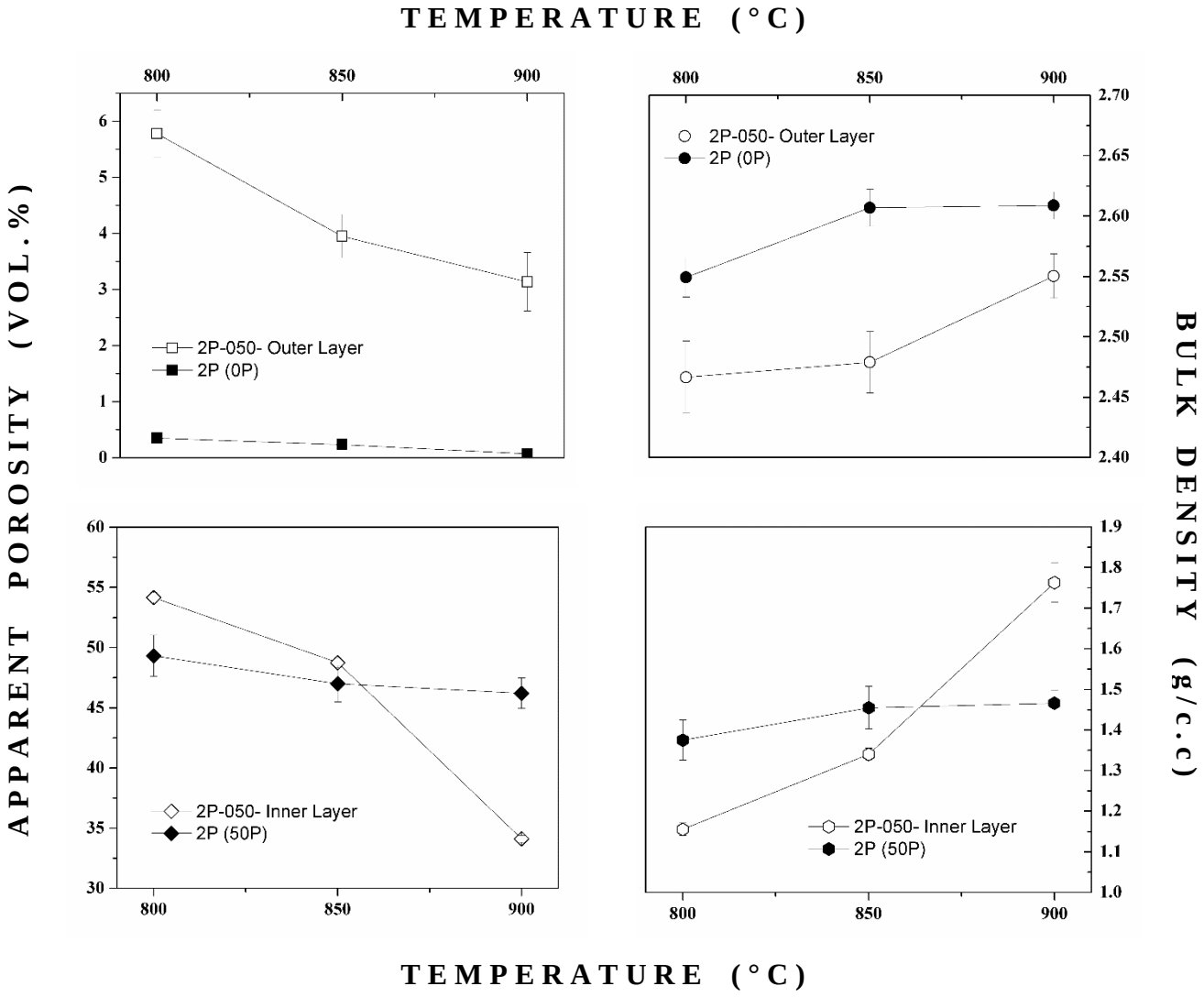

Fig – 4.15.4 Graded Layers of 2P(0,50) vs 2P(0P) & 2P(50P)

Fig – 4.15.4 illustrates the apparent porosity and bulk density of 2P (0,50), 2P(0P) & 2P(50P). From 800°C to 850°C, gradual reduction in apparent porosity for Outer Layer of 2P (050) had been attained. But the rate of reduction in apparent porosity had been reduced, when the temperature proceeds to 900°C. The apparent porosity of 2P (0P) is comparatively less than the outer layer of the 2P (050) FGS. At sintering temperatures 800°C & 850°C, the apparent porosity for Inner Layer of 2P (050) was relatively high than the 2P (50P) scaffold. But at 900°C, a drastic decrease in apparent porosity of Inner Layer of 2P (050) had been noticed whose apparent porosity is less than the 2P (50P).

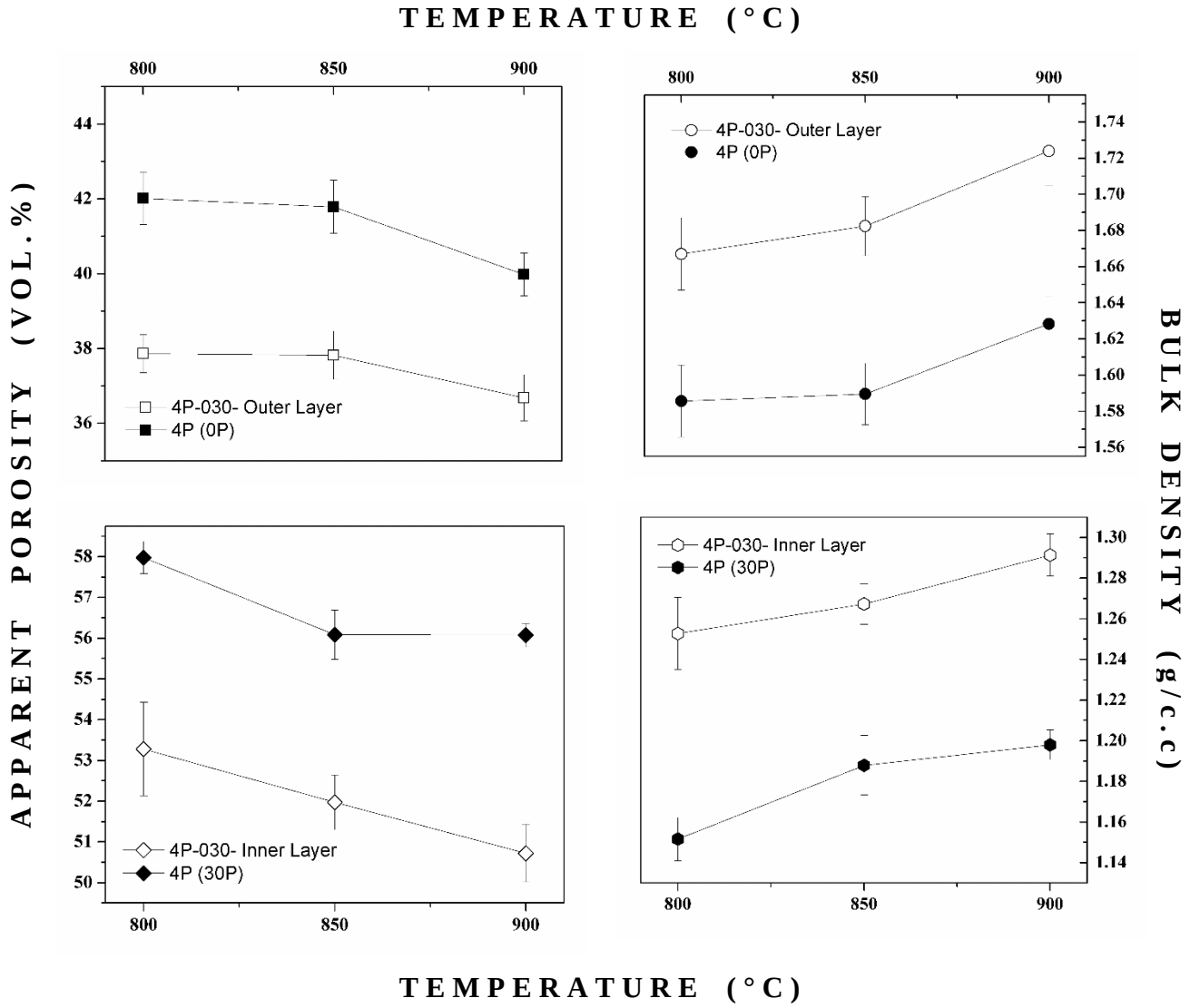

Fig – 4.15.5 Graded Layers of 4P(0,30) vs 4P(0P) & 4P(30P)

Fig – 4.15.5 illustrates the apparent porosity and bulk density of 4P (0,30), 4P(0P) & 4P(30P). The apparent porosity of the FGS parts are less when compared with the Single layer scaffolds – 4P (0P) & 4P (30P) on all temperatures. Similar characteristic feature had been observed on all the cases. Fig – 4.15.6 illustrates the apparent porosity and bulk density of 4P (0,50), 4P(0P) & 4P(50P).The graded parts had attained less apparent porosity when compared to the single layer scaffolds – 4P (0P) & 4P (50P).

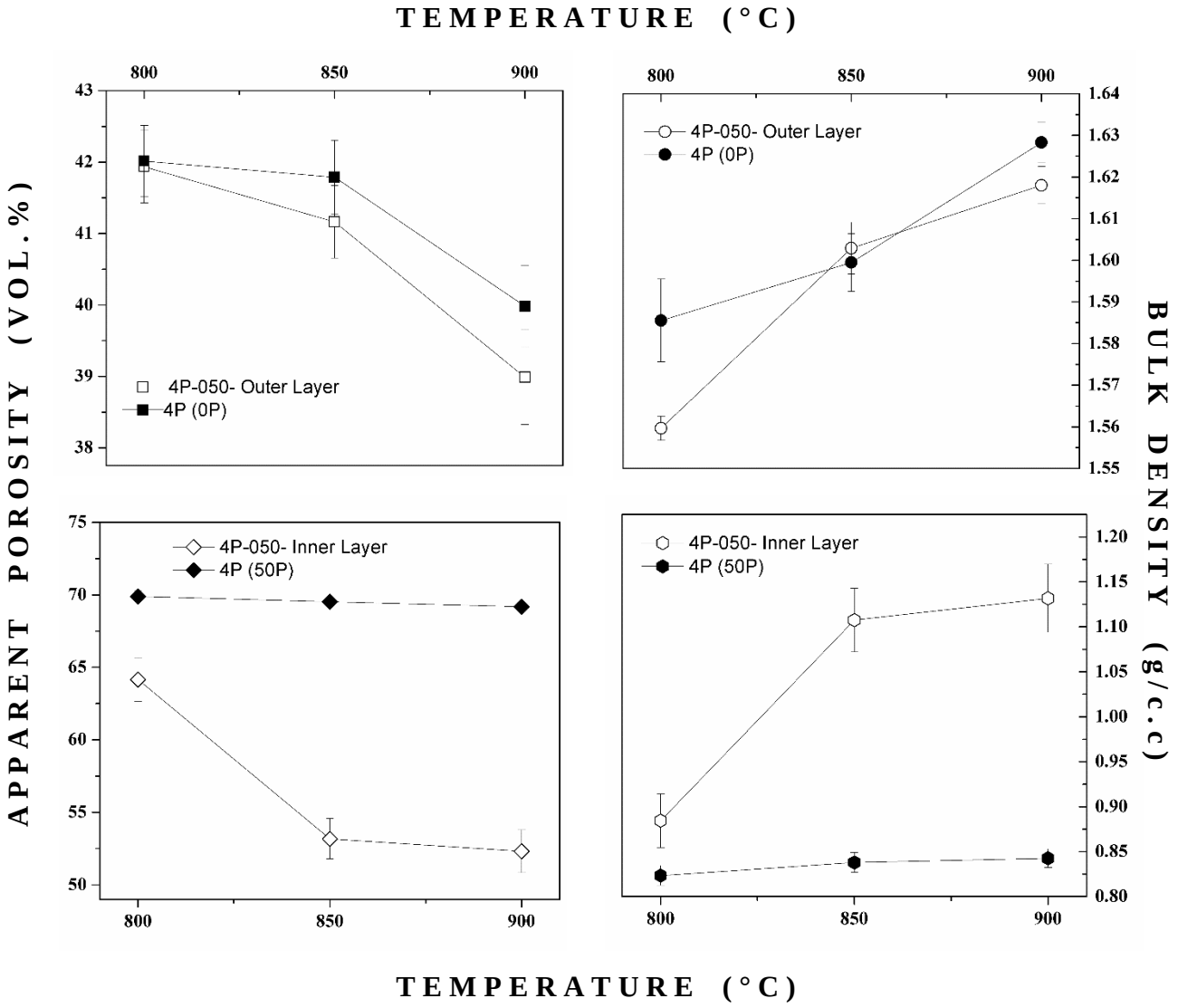

Fig – 4.15.6 Graded Layers of 4P(0,50) vs 4P(0P) & 4P(50P)

A drastic decrease in the reduction of apparent porosity had been observed on the graded parts, from 800°C to 850°C. When the temperature proceeds to 900°C, the linear reduction of apparent porosity had been attained. The oscillation had not been seen with the single layer scaffolds - 4P (0P) & 4P (50P).

4.15 FUNCTIONALLY GRADED MICROSTRUCTURES

On reviewing the results of apparent porosity and bulk density, it had been decided that optimum porosity and density is required for functionally graded scaffold. Thus the intermediate sintering temperature of 850°C had been fixed for the further characterization of the current work. The interface joining the outer and inner layer of the functionally graded scaffold is the critical point of the fabrication technique, on post sintering. In order to view the interface, it is necessary to take microstructures with least magnification. From the fabricated scaffolds, the samples had been cut in such a way that both dense (outer layer) and the porous (inner layer) regions are present. Fig – 4.16.1, Fig – 4.16.2, Fig – 4.16.3, Fig – 4.16.4, Fig – 4.16.5 & Fig – 4.16.6 shows the SEM microstructures of the 45S5(0,30), 45S5(0,50), 2P(0,30), 2P(0,50), 4P(0,30) and 4P(0,50) graded scaffolds, which had been sintered at 850°C.

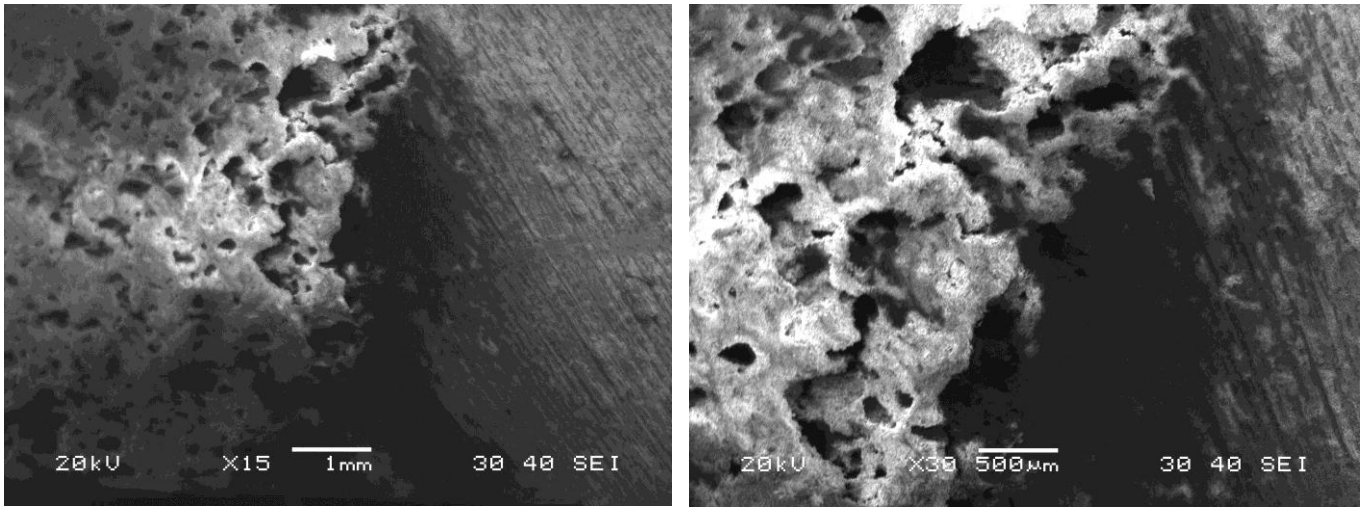

Fig – 4.16.1 SEM Microstructures of 45S5(0,30) scaffolds sintered at 850°C

Fig – 4.16.1 shows the SEM microstructures of 45S5(030) at 850°C. In order to possess clear microstructure showing the interface, dense and porous regions, these kinds of microstructures had been taken with 1mm and 500µm scale.

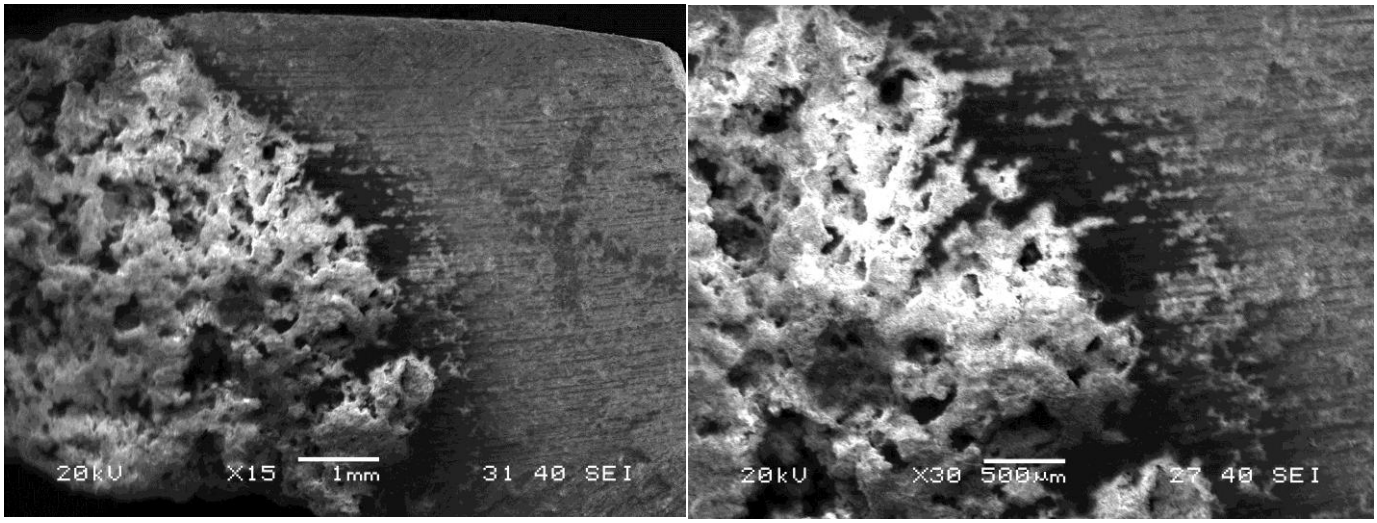

Fig – 4.16.2 SEM Microstructures of 45S5(0,50) scaffolds sintered at 850°C

The Fig – 4.16.2 shows the microstructures of 45S5 (050) functionally graded scaffold. Including the microstructure of 45S5 (030) , the porous region seems to be fibrous like structure. These samples had been carved out from the center region of the FGS.

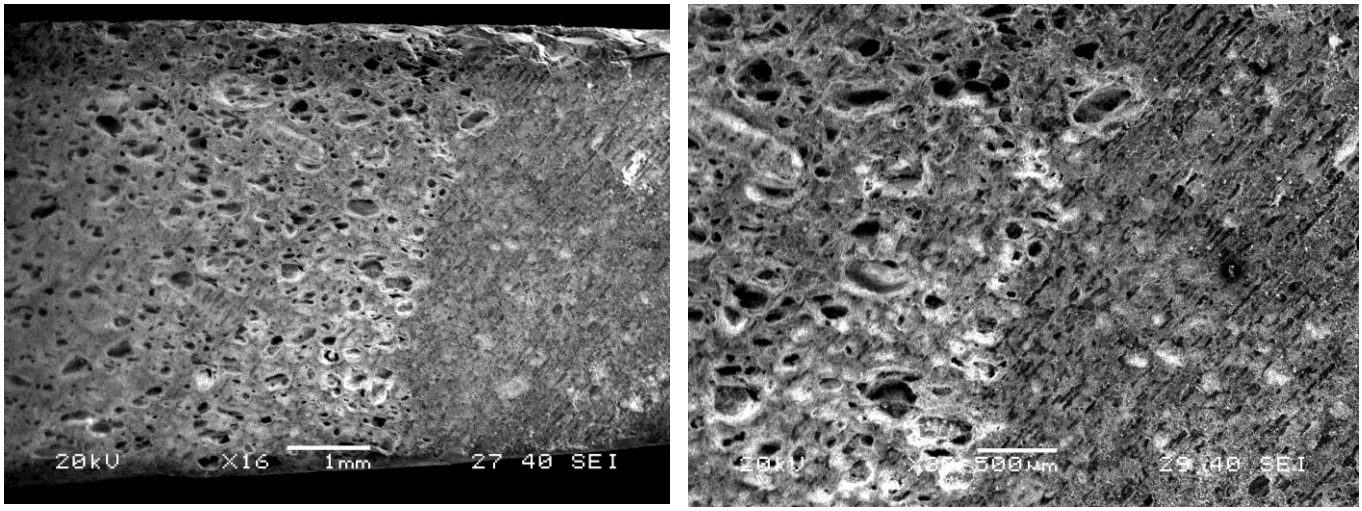

Fig – 4.16.3 SEM Microstructures of 2P(0,30) scaffolds sintered at 850°C

Fig – 4.16.3 shows the SEM microstructure of 2P(030) scaffold. Since the sintering behavior of 2P based scaffolds are better than the 45S5 and 4P, the interface is perfectly is joined without any major cracks.

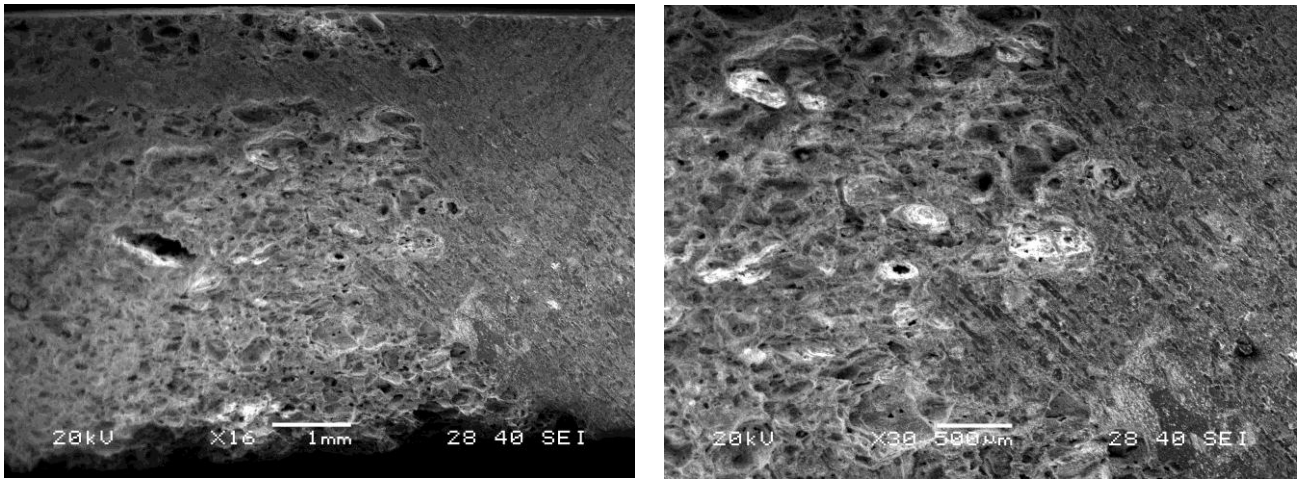

Fig – 4.16.4 SEM Microstructures of 2P(0,50) scaffolds sintered at 850°C

The microstructure of the cross section of 2P (030) looks prominent in pore arrangement. In the case of 2P(050), the porous and dense region merges and makes it undistinguishable. This may be due to larger shrinkage, as pore former is deliberately high.

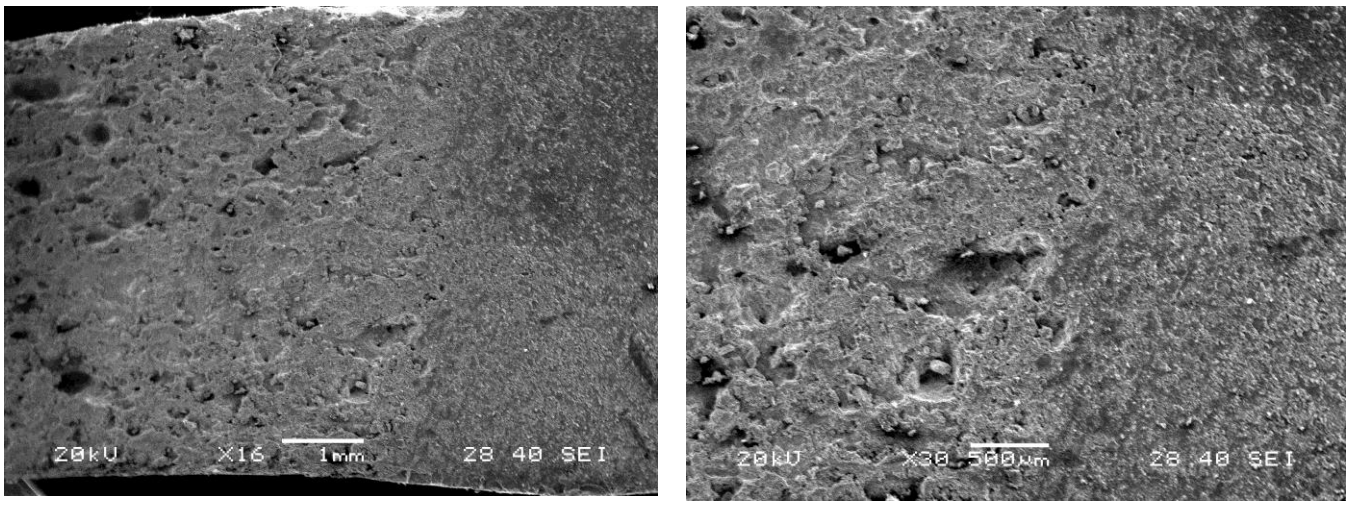

Fig – 4.16.5 SEM Microstructures of 4P(0,30) scaffolds sintered at 850°C

Due to restricted densification, the 4P(030) microstructure shows the irregular arrangement of pore compared with the other scaffolds. Even though the interface is joined well, due to insufficient densification, weak interface will be formed.

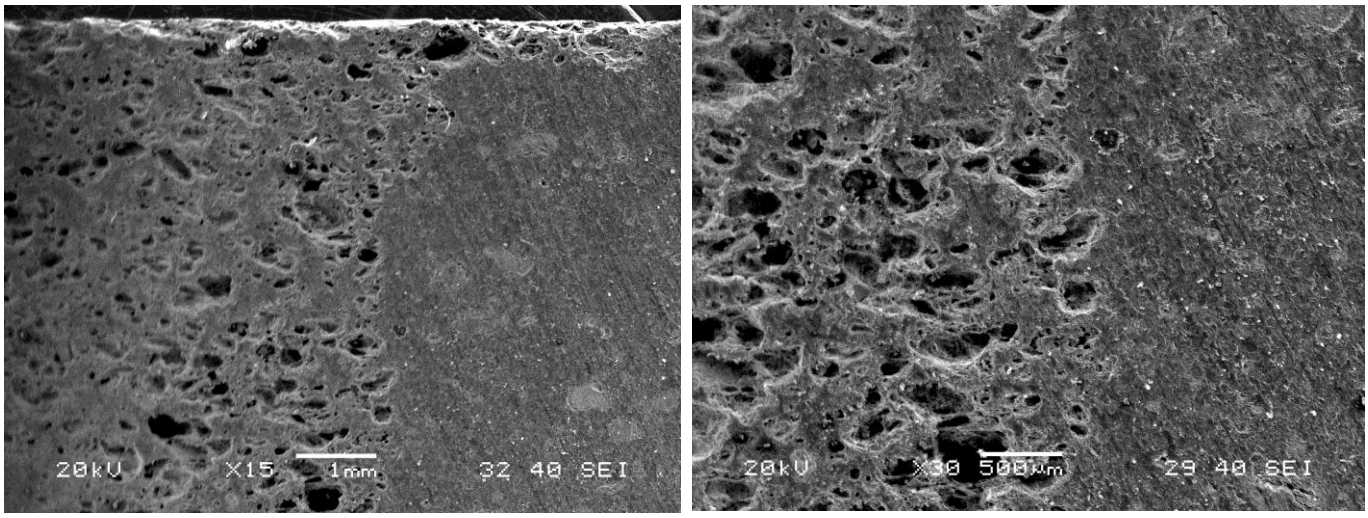

Fig – 4.16.6 SEM Microstructures of 4P(0,50) scaffolds sintered at 850°C

As per the microstructure of 4P(050), the pore size is quite large when compared with other microstructures of functionally graded scaffolds. As per the Apparent porosity and bulk density results, 4P (050) are highly porous scaffolds which is clearly evident with the microstructure. Some of the other microstructures of 45S5, 2P & 4P based functionally graded scaffolds, which had been sintered at 850°C, which had been taken from different regions of the scaffolds had been illustrated in Fig – 4.16.7, Fig – 4.16.8 & Fig – 4.16.9 respectively.

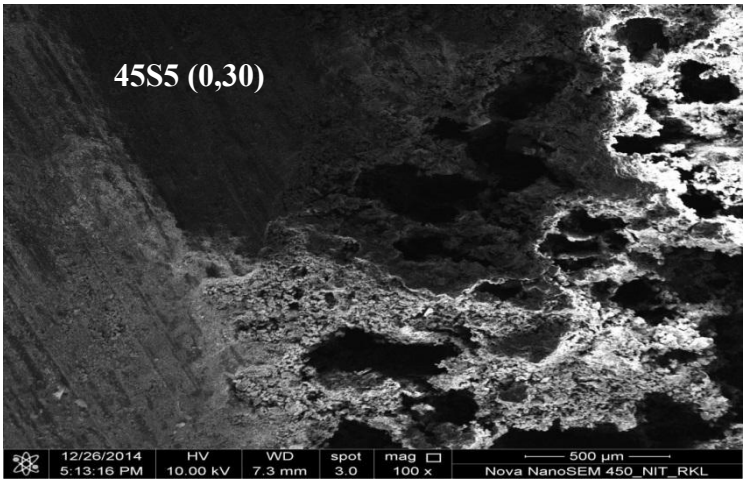

Fig – 4.16.7 (a) 45S5 based functionally graded microstructures

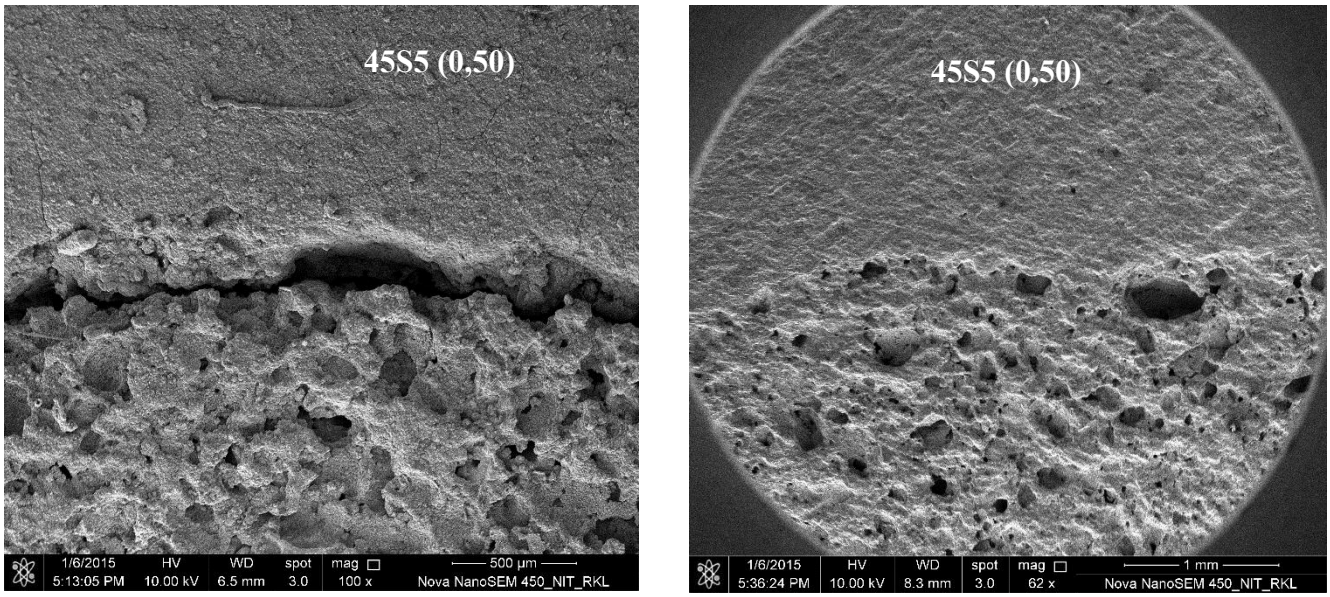

Fig – 4.16.7 (b) 45S5 based functionally graded microstructures

Fig – 4.16.7 (a) shows the microstructure of 45S5 (030) FGS. It clearly illustrates the longitudinal section of the interface between dense and porous region.

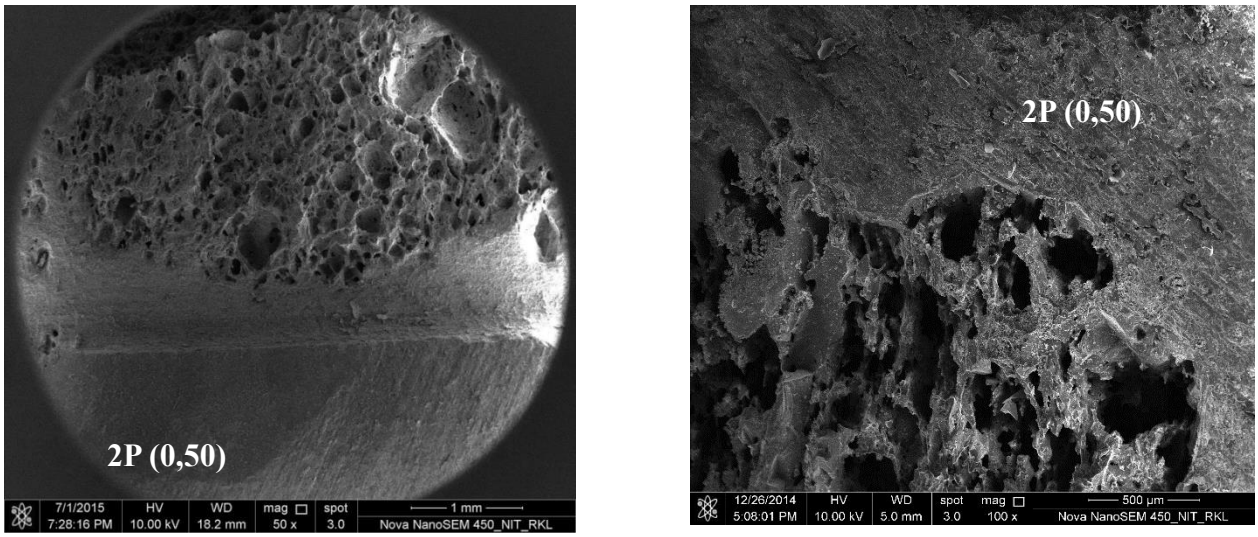

Fig – 4.16.8 2P based functionally graded microstructures

Fig – 4.16.8 shows the microstructures of 2P (050) scaffolds. The pore population and pore channel morphology can be clearly seen on these microstructures.

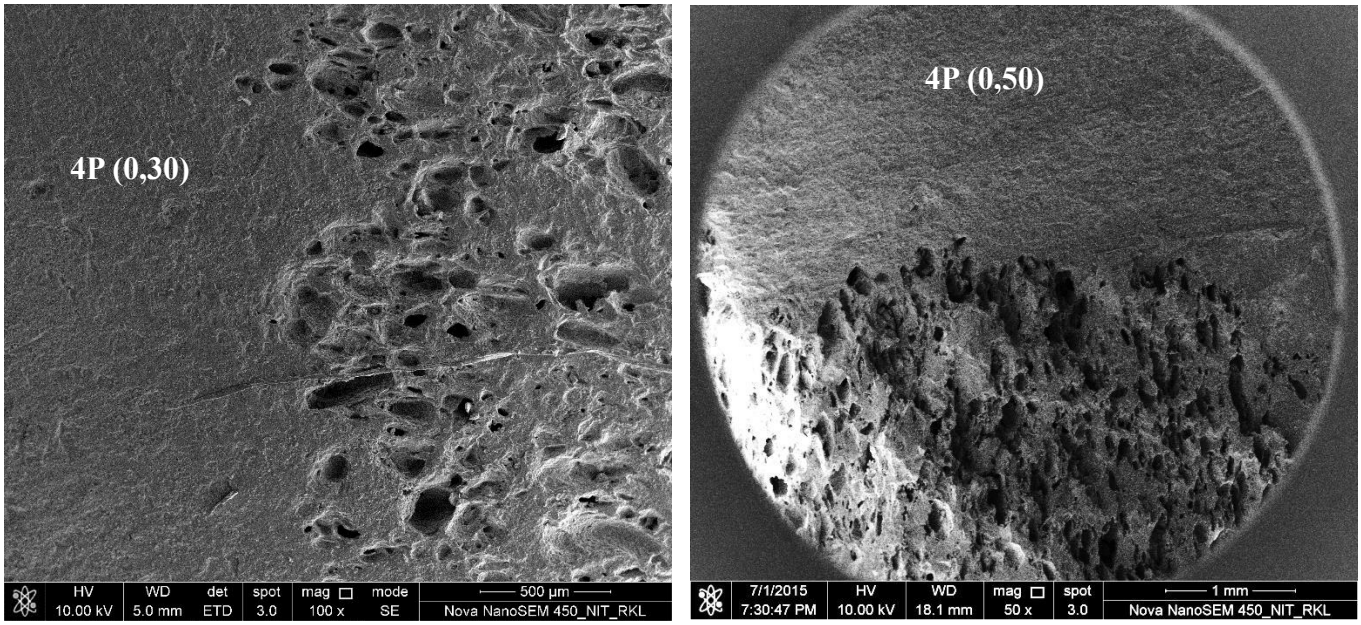

Fig – 4.16.9 4P based functionally graded microstructures

4.16 BRAZILIAN DISC ANALYSIS

The architecture of the scaffold is functionally graded, with dense layer at the outer region and porous layer at the inner region. As mentioned earlier in the section 3.16, splitting tensile strength is measured for gradient microstructures, as per the theory of rock mechanics. During tensile strength measurement on functionally graded scaffolds, the applied continuous uniaxial loading instigates the propagated crack to travel from outer - dense region to the inner - porous region. Since the scaffolds were not isotropic, the measured tensile strength is called us splitting tensile strength **[69]**.

Splitting tensile strength of the functionally graded scaffolds had been evaluated by making a Brazilian disc specimen and undergoing Brazilian Disc analysis. The functionally graded scaffolds, which had been sintered at 850°C, had been cut with a diamond tool to make Brazilian disc specimen as shown in the Fig – 4.17.1.

On the Brazilian disc specimen, uniaxial loading had been given as per the specifications mentioned in the section 3.16. When the uniaxial loading is given, the applied force increases continuously. When the crack originates within the specimen, the applied force drops and the propagated crack travels from the dense region, further enters the porous region.

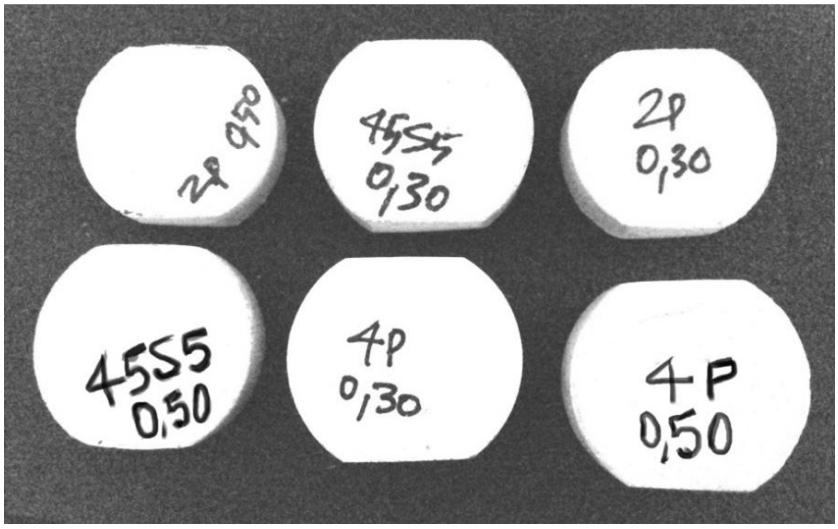

Fig – 4.17.1 Functionally graded scaffolds as Brazilian disc specimens

After crossing the porous region, when the crack reaches the dense region, the applied force again tends to increase. Once the specimen is completely fractured, the applied force again drops. This kind of phenomena had been noticed with the functionally graded – Brazilian disc specimens. Fig – 4.17.2 shows the fractured Brazilian disc specimens.

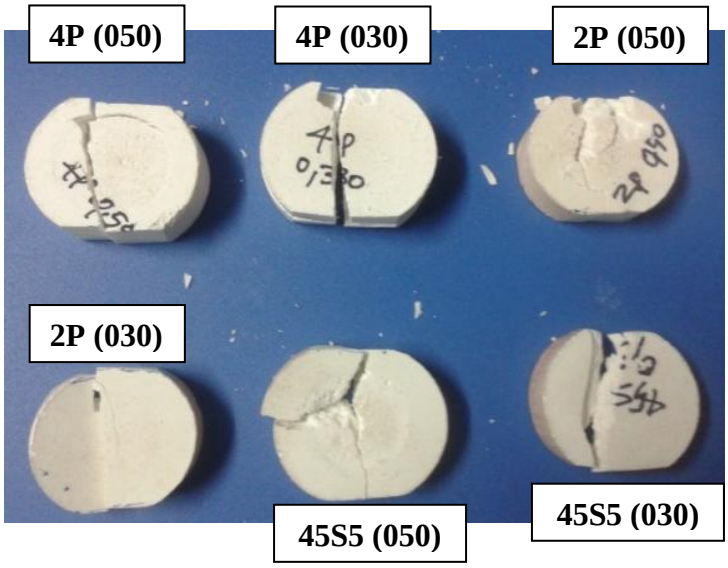

Fig – 4.17.2 Fractured functionally graded - Brazilian Disc specimens

After the uniaxial loading of the functionally graded - Brazilian disc specimens, different ranges of fractures had been encountered. But a common scenario had been encountered within the specimens in terms of cracks.

The Brazilian disc specimens with low amount of porosity in the inner layer, (i.e) (030) based scaffolds, propagates the cracks within the region of central diameter of the specimen. The specimen with high amount of porosity, (i.e) (050) based scaffolds, tends to get fractured in irregular modes.

Fig – 4.17.3 illustrates the Force vs. Extension curve evolved during the uniaxial loading on functionally graded Brazilian disc specimens.

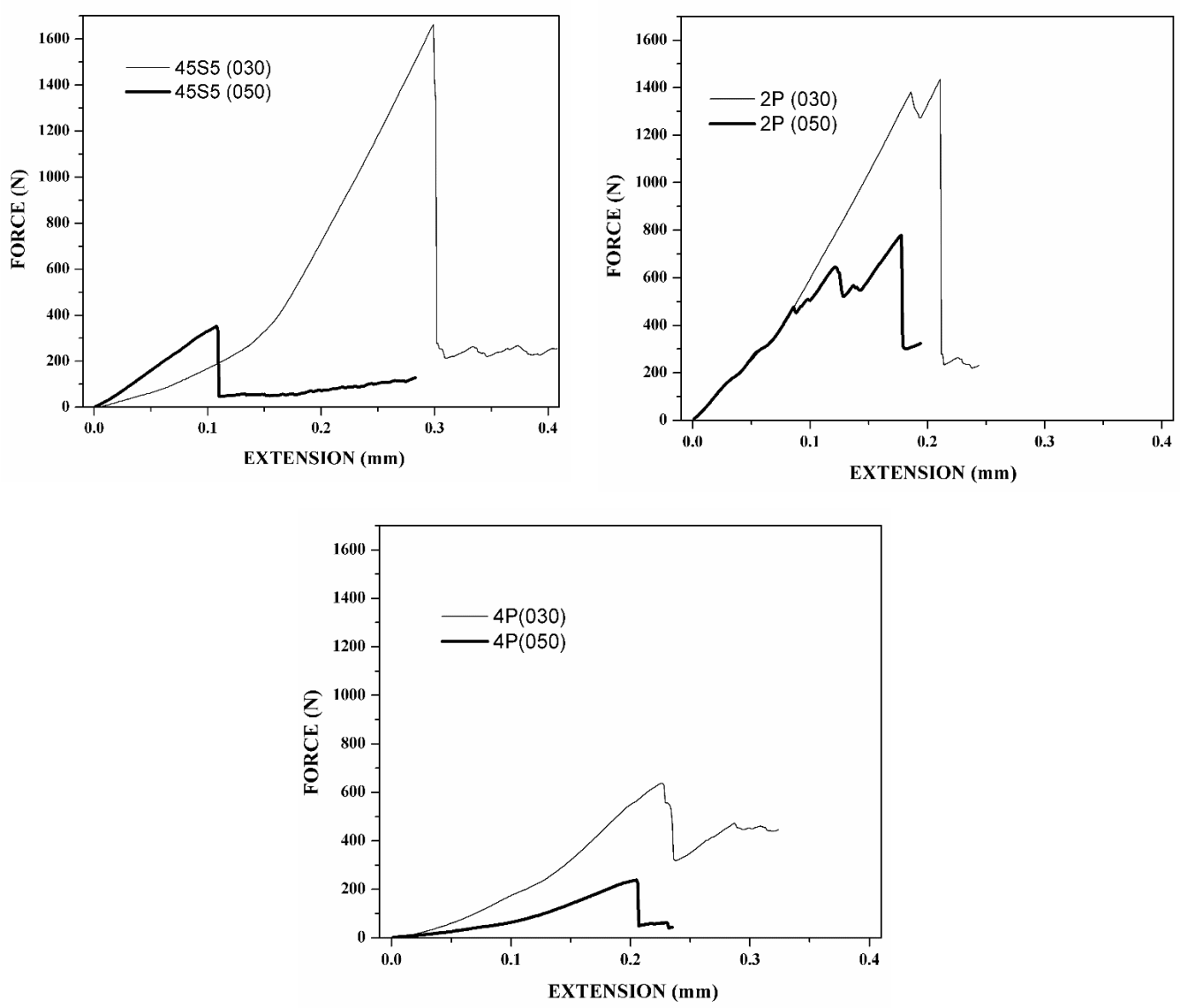

Fig – 4.17.3 Force vs. Extension curves on Fractured functionally graded - Brazilian Disc specimens

From the Force vs. Extension curves, the peak load had been noted and the splitting tensile strength of the functionally graded scaffolds had been calculated as given in the section 3.16. The average disc diameter had been calculated from the three diameters marked in the Fig – 4.17.4.

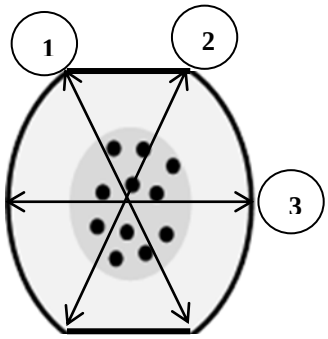

Fig – 4.17.4 Measurement of Average Brazilian Disc diameter

As per the formula mentioned in the section 3.16, the splitting tensile strength of the functionally graded Brazilian disc specimens had been calculated. The test results of the Brazilian disc analysis had been tabulated in the table – 4.11.

Table – 4.11 Brazilian disc analysis of functionally graded scaffolds

S.No:	FGS Scaffolds	Applied Peak Load (N)	Average Disc Diameter (mm)	Splitting Tensile Strength (MPa)
1.	45S5 (0,30)	1662	26.84	6.15
2.	45S5 (0,50)	350	26.91	1.31
3.	2P (0,30)	1434	24.87	6.59
4.	2P (0,30)	776	24.80	3.69
5.	4P (0,30)	636	26.86	2.13
6.	4P (0,50)	238	26.79	0.81

The splitting tensile strength is purely based on the average diameter of brazilian disc specimen obtained apart from the applied peak load. For a better comparative study, within the scaffolds, the evaluated splitting tensile strength had been plotted in the Fig – 4.17.5.

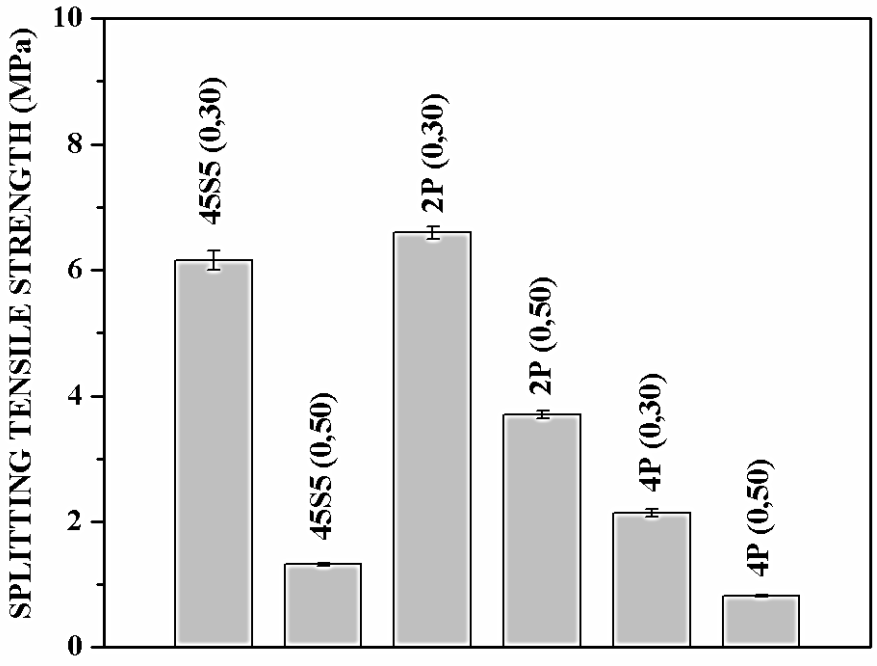

Fig – 4.17.5 Splitting Tensile Strength of Functionally graded scaffolds (sintered at 850°C)

2P (0,30) attained high tensile strength than the other functionally graded scaffolds. 45S5 (0,30) possess a tensile strength much close to 2P (0,30) scaffolds. The high porous 2P(0,50) is stronger than both 4P(0,30) and 4P(0,50).

4.17 COMPARATIVE STUDY OF SINGLE LAYER AND FUNCTIONALLY GRADED SCAFFOLDS – Tensile Strength

In the section 4.14, the apparent porosity and bulk density of single layer scaffolds and functionally graded scaffolds had been compared and discussed. As mentioned earlier, since the composition of single layer bioactive glass ceramic scaffolds (with or without pore former) occupies a layer in functionally graded bioactive glass ceramic scaffolds, the comparison becomes fruitful. It is appropriate to study the performance of a particular bioactive glass ceramic composition, which occupies a region in single layer and functionally graded scaffolds. As similar to the section – 4.14, in this section, the tensile strength of the single layer and layers of functionally graded scaffolds had been compared.

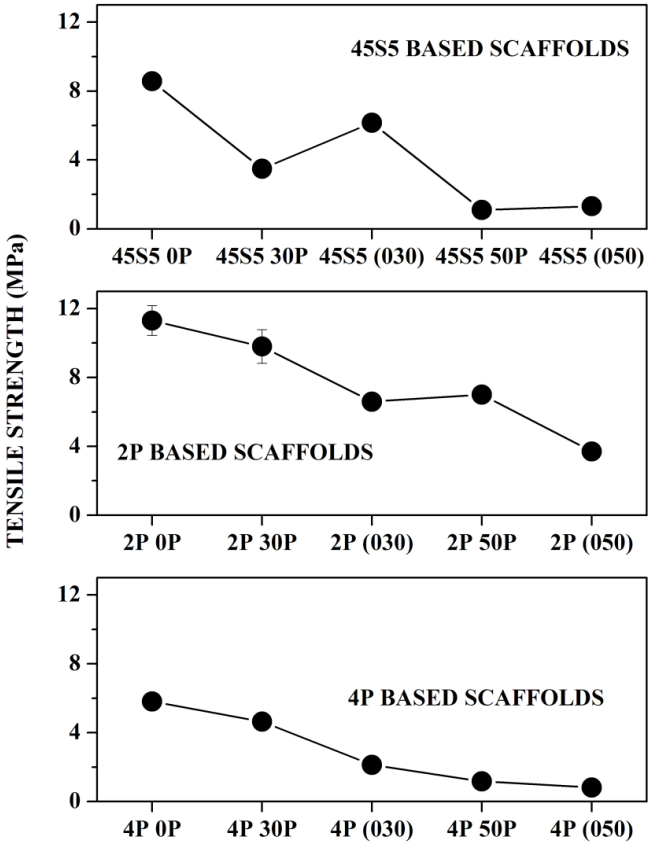

Fig – 4.18 Comparison of Tensile Strength of Single Layer Scaffolds and Functionally graded scaffolds

Fig – 4.17.1 illustrates the comparison of tensile strength of single layer scaffolds and functionally graded scaffolds. The 45S5 based functionally graded scaffolds, (i.e) 45S5(030) and 45S5(050) scaffolds, bears tensile strength better than the porous single layer scaffolds - 45S5 30P and 45S5 50P respectively. This shows that during sintering of functionally graded scaffolds, the bonding between the outer layer and the inner layer are strong. Fig – 4.14.1 clearly illustrates that the bulk density of Inner Layer of 45S5 (030) scaffold is better than the bulk density of 45S5 30P. Similarly, the bulk density of outer layer of 45S5 (030) is better than the bulk density of 45S5 0P. This shows that the outer layer shrinks and acts as a driving force for the shrinkage of inner layer. When the porosity is increased in the inner layer, (i.e) the 45S5 (050), the bulk density of 45S5 0P and outer layer of 45S5 (050) are more or less same.

But the inner layer of 45S5 (050) and 45S5 50P retains the similar behavior of 45S5 30P and inner layer of 45S5 (030). These types of architectural considerations had reflected on the corresponding tensile strength of the scaffolds. As mentioned earlier in the section - 4.3, due to low amount of P_2O_5 in 2P glass composition, the degree of polymerization of Si-network decreases. This leads to undergo actual densification mechanism at the low temperature itself. Since the process of densification starts early and takes a long to time to end, the impact of differential shrinkage had been neutralized. At the same time, since there is no interruptions of differential shrinkage in single layer scaffolds, better densification mechanism had been carried out. This is the reason for the porous single layer scaffolds - 2P 30P and 2P 50P, which attains better tensile strength than 2P (030) and 2P (050) scaffolds.

In the case of 4P based scaffolds, the amount of P_2O_5 is 4wt.%, which provides an intermediate performance between 2P and 45S5 based scaffolds. Due to the similar phenomena of degree of polymerization, 4P based scaffolds starts the densification mechanism even before 45S5 based scaffolds. This lengthy densification mechanism was capable to handle the differential shrinkage interruptions of 4P (030) but not 4P (050). It requires some more time for the sintering of 4P (050). That's the reason, 4P 30P attains better tensile strength than 4P (030). Due to less efficiency in controlling differential shrinkage issues of highly porous scaffold – 4P (050), 4P 50P is stronger than 4P (050).

4.18 INVITRO ANALYSIS OF FGS BY USING SBF

The functionally graded scaffolds, 45S5 (050), 2P(050) & 4P(050), which had been sintered at 850°C, had been immersed as mentioned in the section 3.17. The immersed scaffolds had been undergone surface phase analysis and microstructure analysis to ensure the formation of carbonated hydroxyapatite. Fig – 4.19.1(a), Fig – 4.19.1(b) & Fig – 4.19.1(c) shows the microstructures of 45S5 (050) scaffolds immersed after 1 day, 7 days and 14 days of incubation respectively. After one day of immersion, spherical shaped carbonated hydroxyapatite particles had been deposited on the surface of the 45S5 (050) FGS [Fig – 4.19.1(a)]. Fig – 4.19.1(a) – 1 shows the porosity gradient functionally graded structure of 45S5 (050) FGS. Fig – 4.19.1(a) – 2, Fig – 4.19.1(a) – 3, Fig – 4.19.1(a) – 4 & Fig – 4.19.1(a) – 7 shows the spherical particle morphology and Fig – 4.19.1(a) – 5 shows the deposition on the porous region.

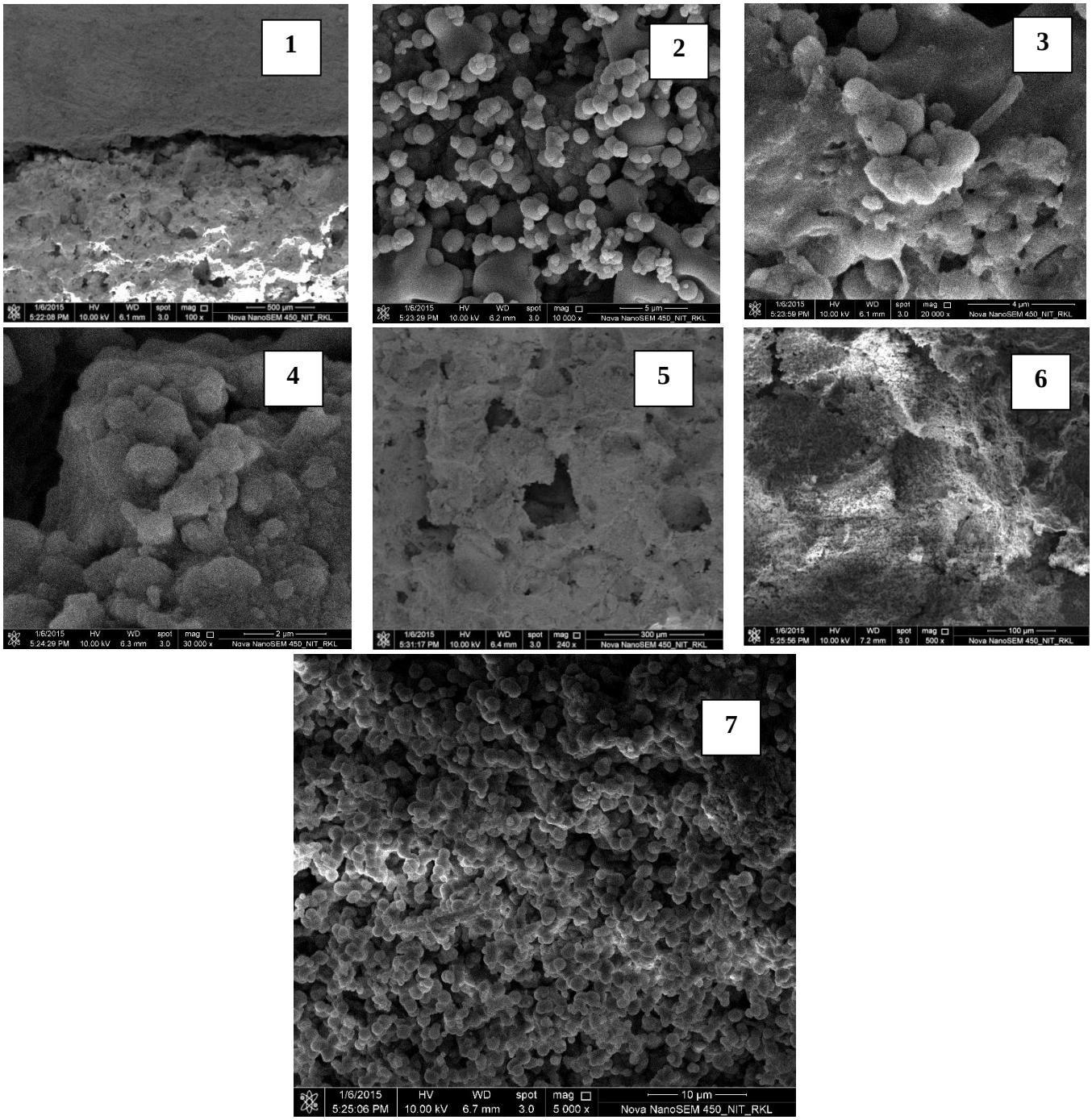

Fig – 4.19.1 (a) Microstructures of 45S5 (050) immersed in SBF for 1 day incubation

These spherical particles are the functional morphology for the development of carbonated hydroxyapatite formation. Fig – 4.19.1 (b) shows the Microstructures of 45S5 (050) FGS immersed in SBF for 7 days.

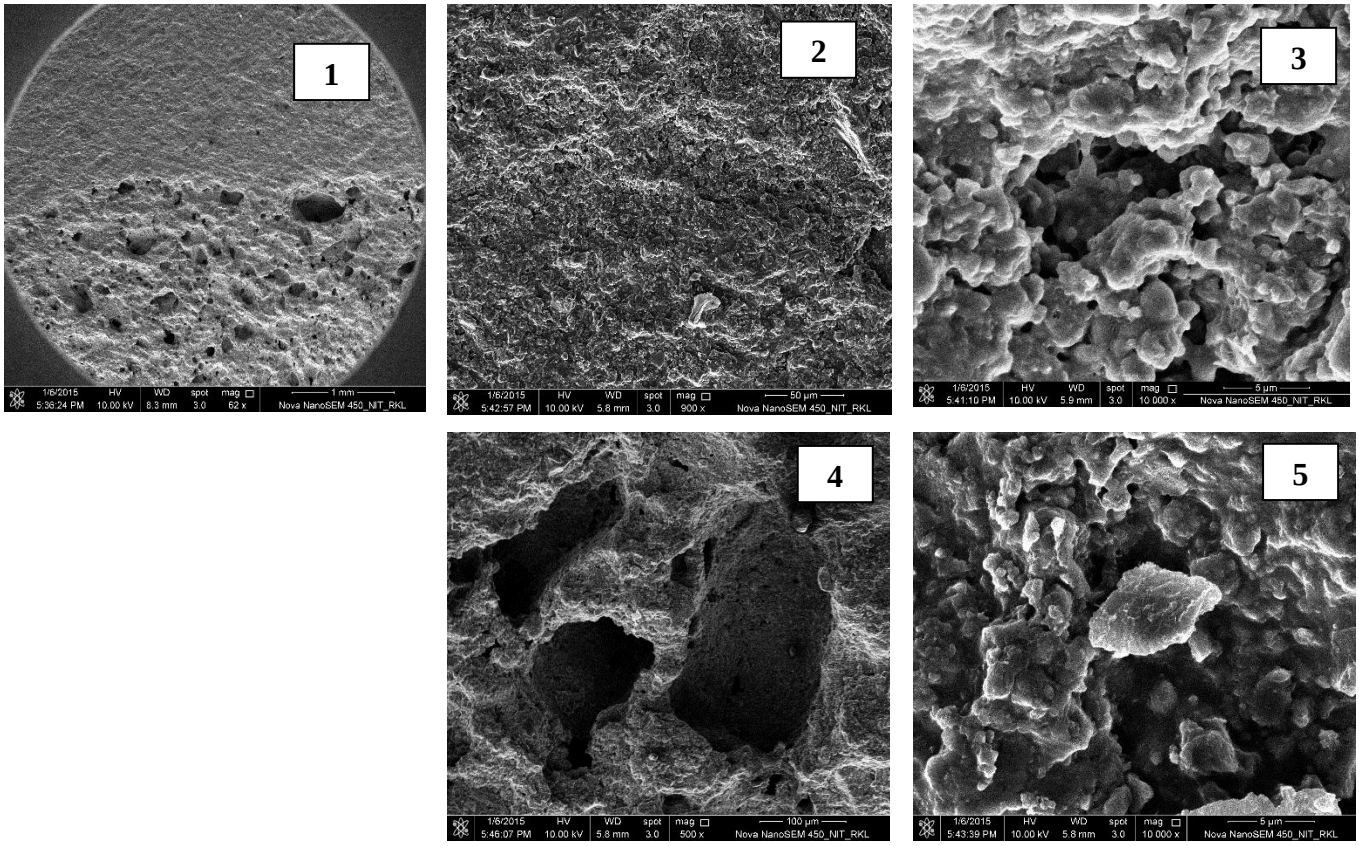

Fig – 4.19.1 (b) Microstructures of 45S5 (050) immersed in SBF for 7 days incubation

Fig – 4.19.1 (b) Microstructure of 45S5(050) FGS immersed in SBF for 7 days. Fig – 4.19.1(b) – 1 shows the functionally graded microstructure. After 7 days of immersion, the spherical particle tends to get fused with each other. This kind of mechanism had been observed after 7 days of immersion. Fig – 4.19.1(b) – 2&3 shows the fused particles on the dense region. Fig – 4.19.1(b) – 4&5 shows the fused particle deposition on the porous region. Fig – 4.19.1 (c) shows the microstructures of 45S5 (050) immersed in SBF for 14 days.

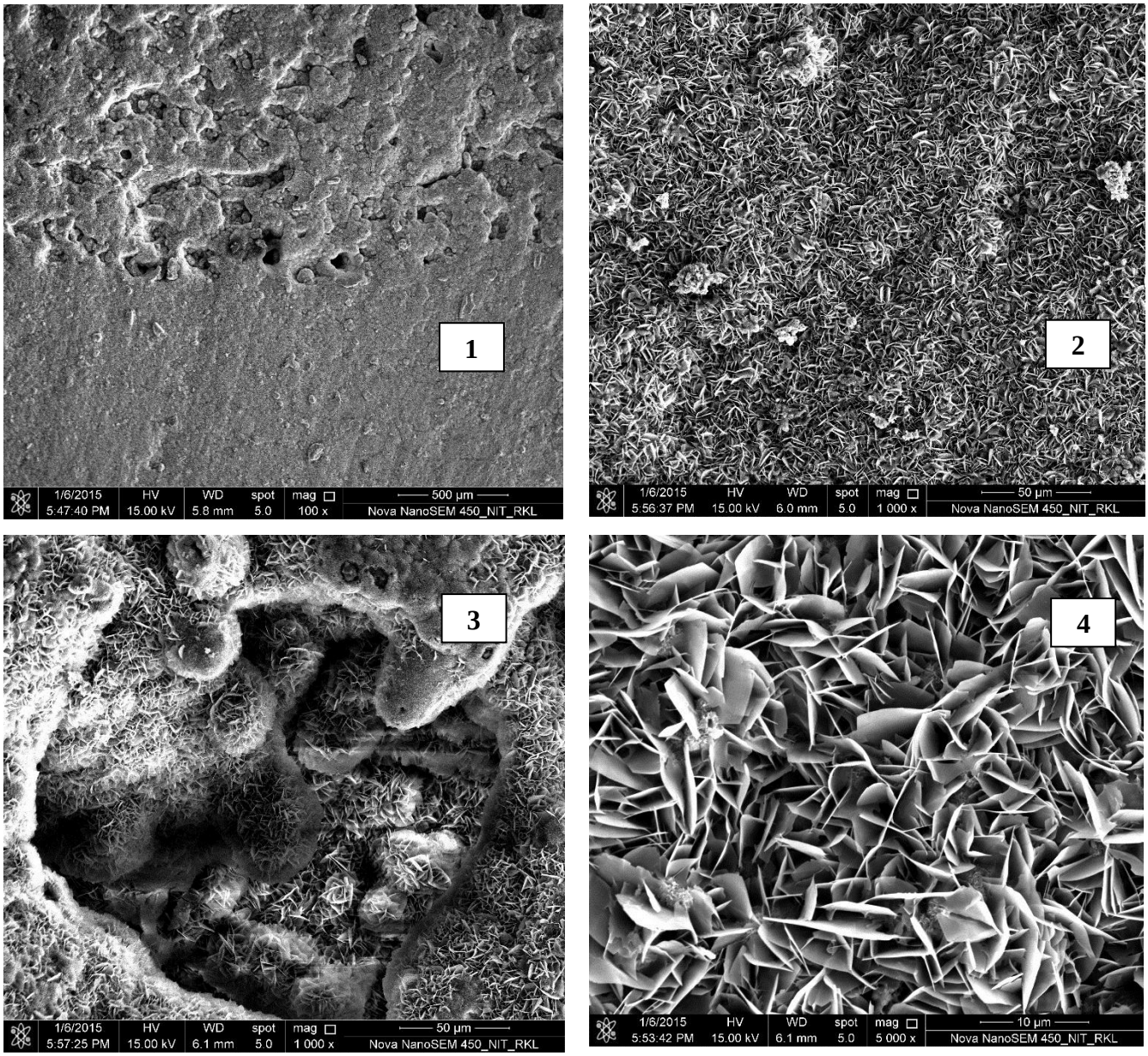

Fig – 4.19.1 (c) Microstructures of 45S5 (050) immersed in SBF for 14 days incubation

Fig – 4.19.1 (c) – 1 shows the microstructure of gradient state of 45S5 (050) scaffold after immersion. Fig – 4.19.1 (c) – 2 shows the carbonated hydroxyapatite deposition on the dense region of FGS. Fig – 4.19.1 (c) – 3 shows the carbonated hydroxyapatite deposition on the porous region of FGS. Fig – 4.19.1 (c) – 4 shows the morphology of the deposited carbonated hydroxyapatite.

Fig – 4.19.2 (a) shows the microstructure of 2P(050) scaffold immersed in SBF for 1 day.

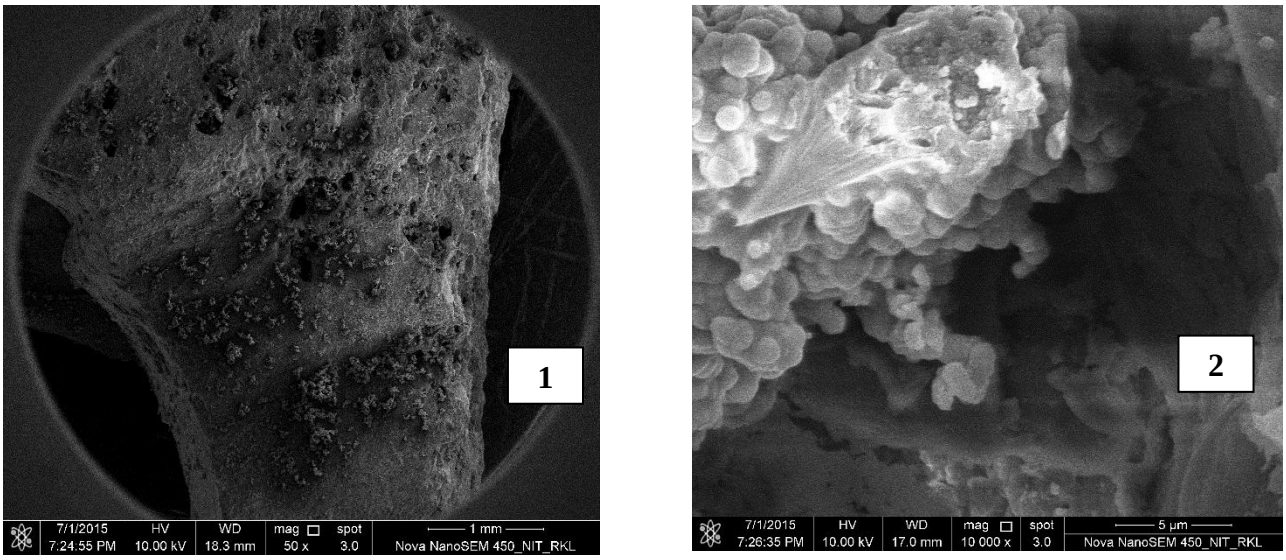

Fig – 4.19.2(a) Microstructures of 2P (050) immersed in SBF for 1 day incubation

4.19.2(a) – 1 shows the 2P(050) gradient structure of 2P(050) immersed in SBF for 1 days. 4.19.2(a) – 2 shows minimum deposition as spherical particles. The morphology of those deposition is not prominent as observed with 45S5 (050) FGS immersed in SBF for 1 day. 4.19.2(b) shows the microstructures of 2P(050) immersed in SBF for 4 days.

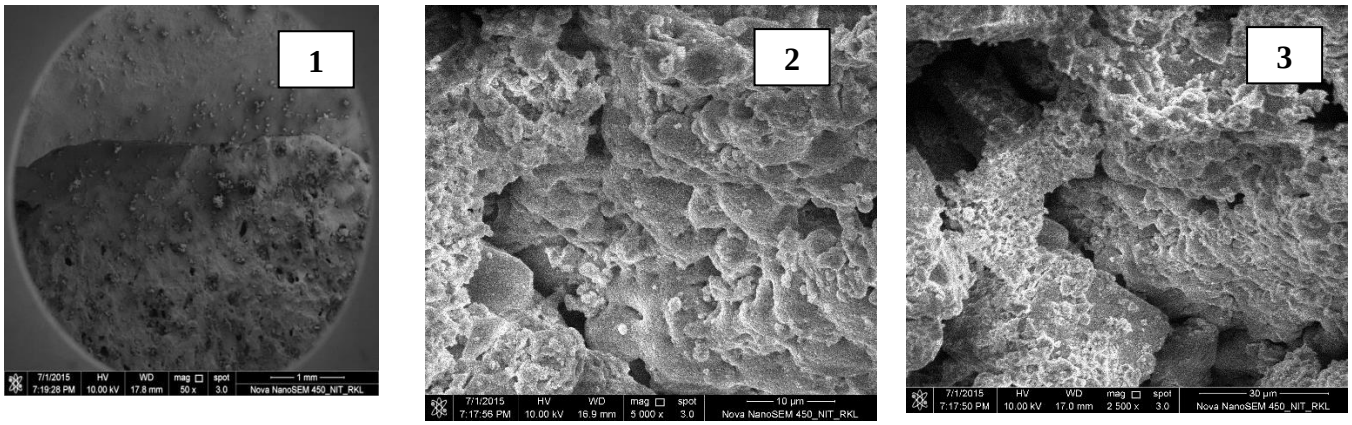

Fig – 4.19.2(b) Microstructures of 2P (050) immersed in SBF for 4 days incubation

Fig – 4.19.2 (b) – 1 shows the functionally graded structure. Fig – 4.19.2 (b) – 2 shows that no major development in the morphology of the deposition on the dense region of FGS. Fig – 4.19.2 (b) – 3 shows the deposition on the porous region of FGS

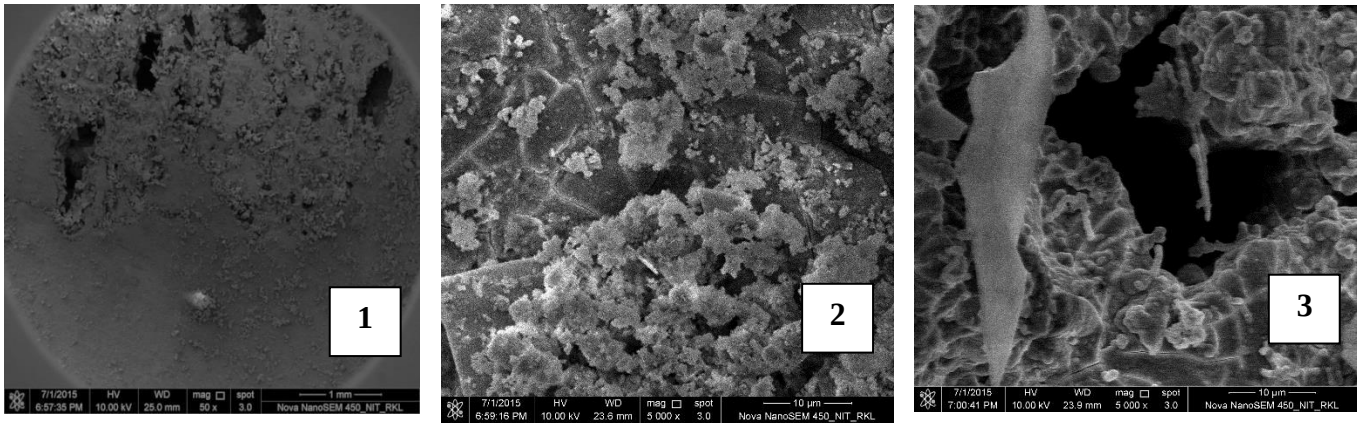

. **Fig – 4.19.2(c) Microstructures of 2P (050) immersed in SBF for 7 days incubation**

Fig – 4.19.2 (c) shows the microstructures of 2P (050) FGS immersed in SBF for 7 days. No further development from the previous interval had been on these microstructures. Fig – 4.19.2 (c) -1 shows the gradient nature of the scaffold. Fig – 4.19.2 (c) – 2 shows the deposition on the dense region of FGS. Fig – 4.19.2 (c) – 3 shows the deposition on the porous region of the FGS.

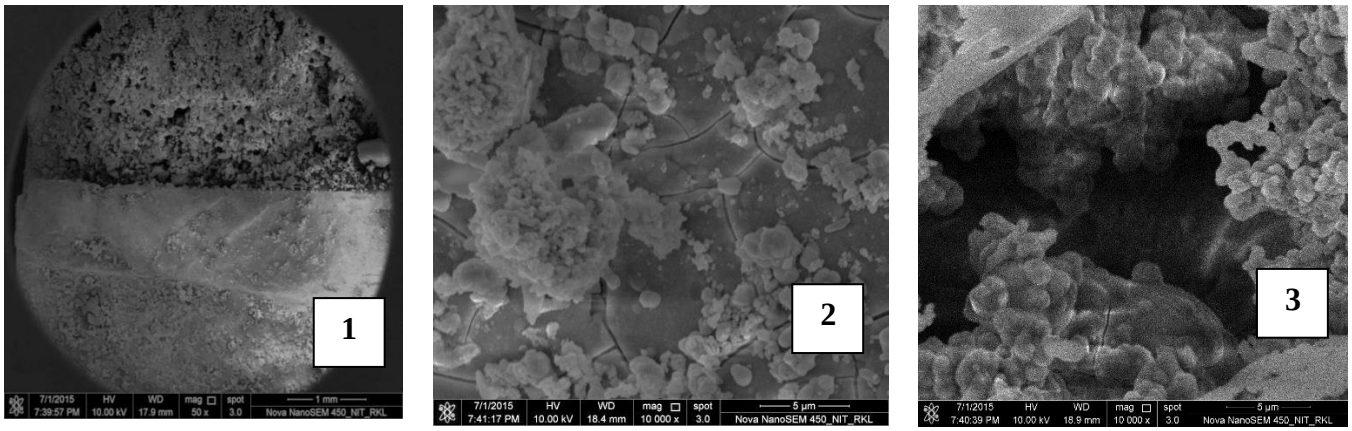

Fig – 4.19.2(d) Microstructures of 2P (050) immersed in SBF for 14 days incubation

Fig -4.19.2 (d) shows the microstructures of 2P(050) immersed in SBF for 14 days. Fig -4.19.2(d) – 2 shows the deposition on the dense region of the scaffold. Fig -4.19.2(d) – 3 shows the deposition on the porous region of the scaffold. Carbonated Hydroxyapatite formation is not evident with the microstructures even after immersion in SBF for 14 days. But the spherical particles indicates that they are in the under developed stage of carbonated hydroxyapatite.

Fig -4.19.3 illustrates the microstructures of 4P(050) immersed in SBF for 1,4,7 &14 days.

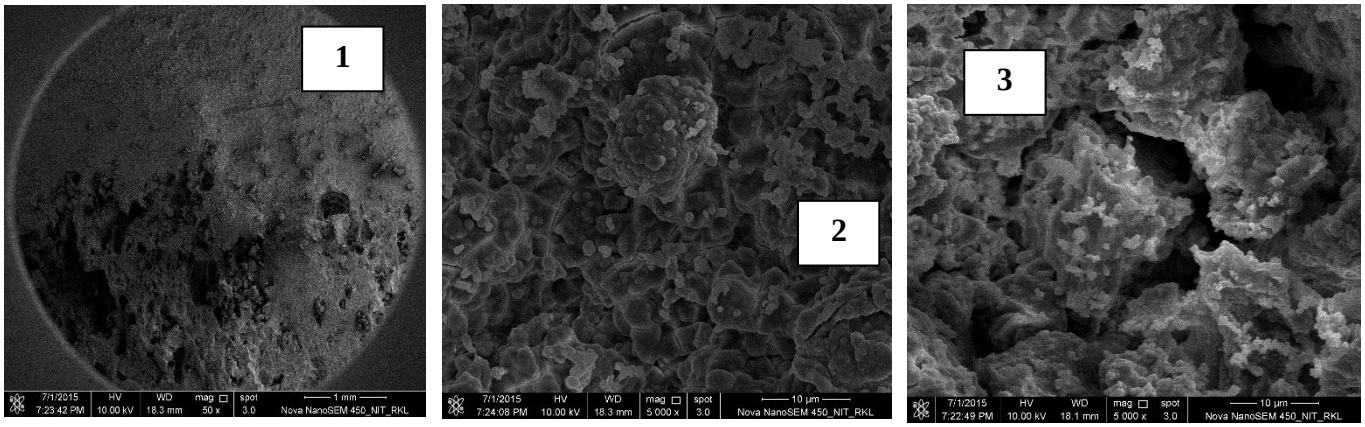

Fig – 4.19.3(a) Microstructures of 4P (050) immersed in SBF for 1 day incubation

Fig – 4.19.3 (a) shows the microstructure of 4P(050) FGS immersed in SBF for 1 day. Fig – 4.19.3 (a) – 1 show the graded layers of the scaffolds immersed. Fig – 4.19.3 (a) – 1 shows the deposition on the dense region and Fig – 4.19.3 (a) – 2 shows the deposition on the porous region of the scaffold. Some fused particles had been deposited on the surface of the scaffold.

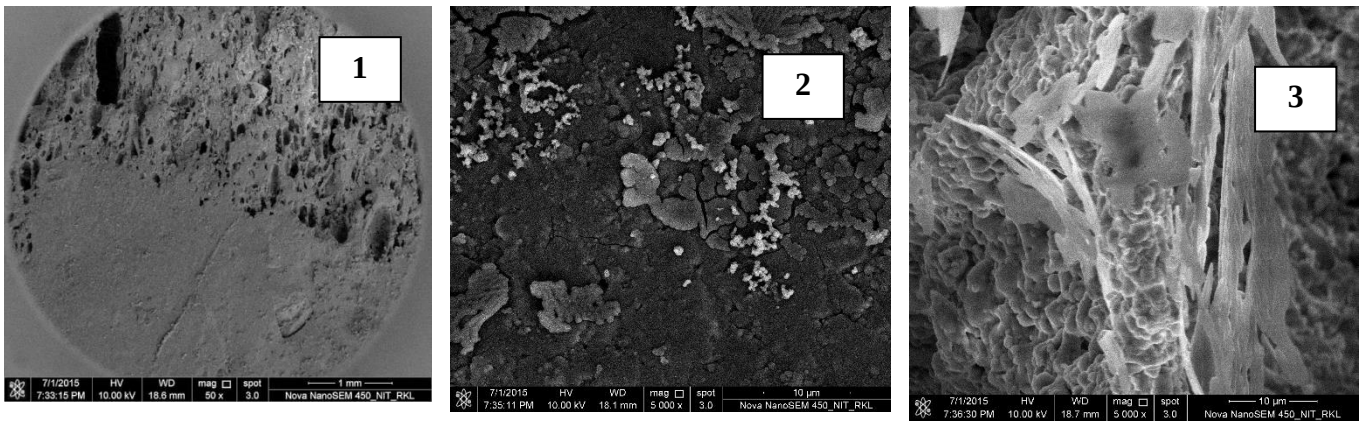

Fig – 4.19.3(b) Microstructures of 4P (050) immersed in SBF for 4 days incubation

Fig – 4.19.3(b) shows the microstructure of 4P(050) immersed in SBF for 4 days. Fig – 4.19.3(b) – 1 shows the gradient structure of the scaffold immersed in SBF. Fig – 4.19.3(b) – 2 shows the deposition on the dense region of the scaffold. Fig – 4.19.3(b) – 3 shows the deposition on the porous region of the scaffold. With minimal deposition and no major development had been observed.

Fig – 4.19.3(c) shows the microstructure of 4P(050) immersed in SBF for 7 days.

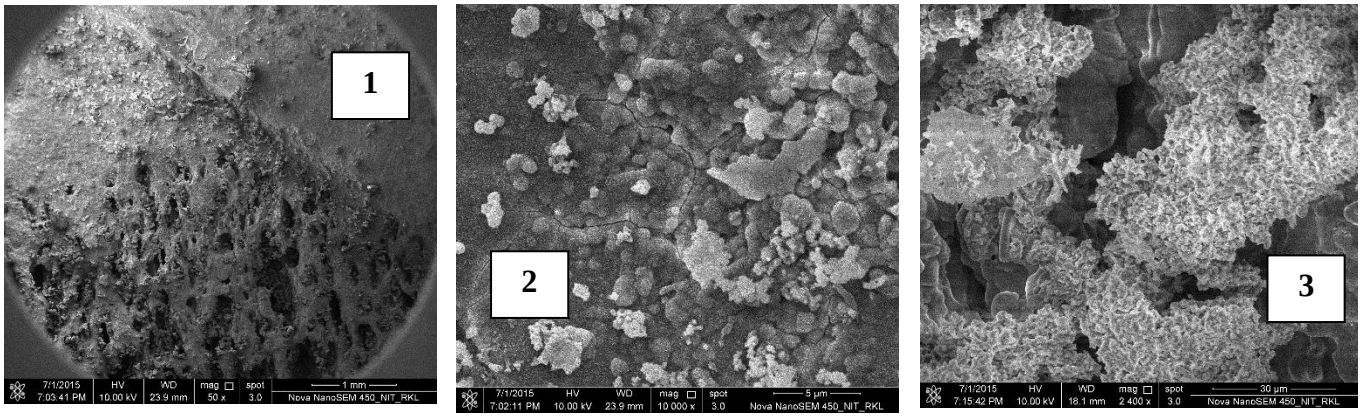

Fig – 4.19.3(c) Microstructures of 4P (050) immersed in SBF for 7 days incubation

Fig – 4.19.3(c) - 1 shows the microstructure of 4P(050) gradient nature. Fig – 4.19.3(c) – 2 shows the deposition on the dense region and Fig – 4.19.3(c) – 3 shows the deposition on the porous region. This microstructure shows the under developed stage of carbonated hydroxyapatite formation.

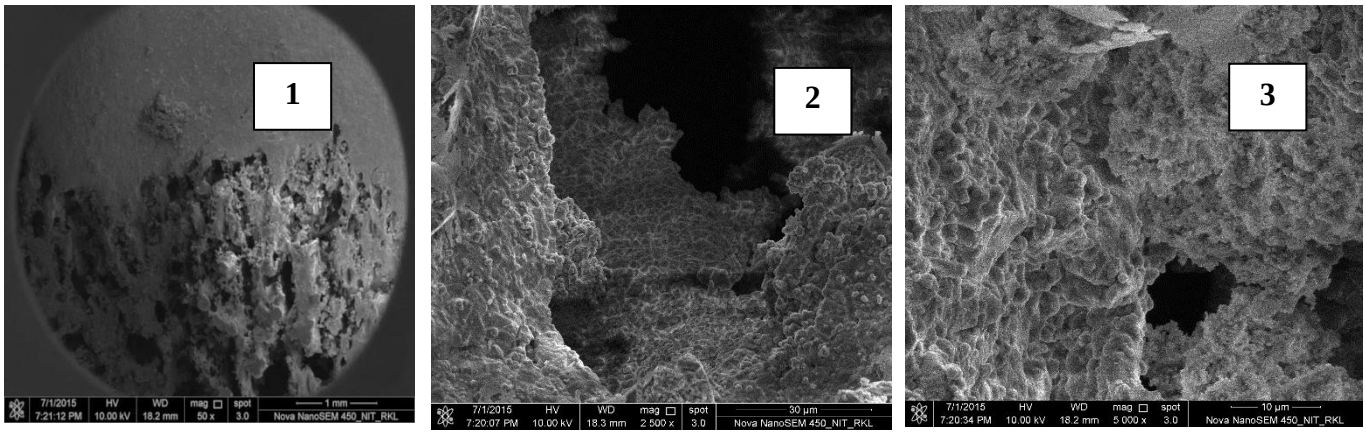

Fig – 4.19.3(d) Microstructures of 4P (050) immersed in SBF for 14 days incubation

Fig – 4.19.3(d) shows the microstructure of 4P(050) FGS immersed in SBF for 14 days. There is no traces of development and retains in the previous interval of observation. Fig – 4.19.3(d) – 1 shows the gradient nature of the 4P(050) after immersion. Fig – 4.19.3(c) – 2 shows the deposition on the porous cavity of the scaffold. Fig – 4.19.3(d) – 3 shows the microstructure of deposition on the dense region of the scaffold. To determine the phases formed on the surface of the scaffold, XRD analysis of the SBF soaked had been carried out. Fig – 4.19.4 shows XRD analysis of SBF soaked 45S5 (050) scaffolds.

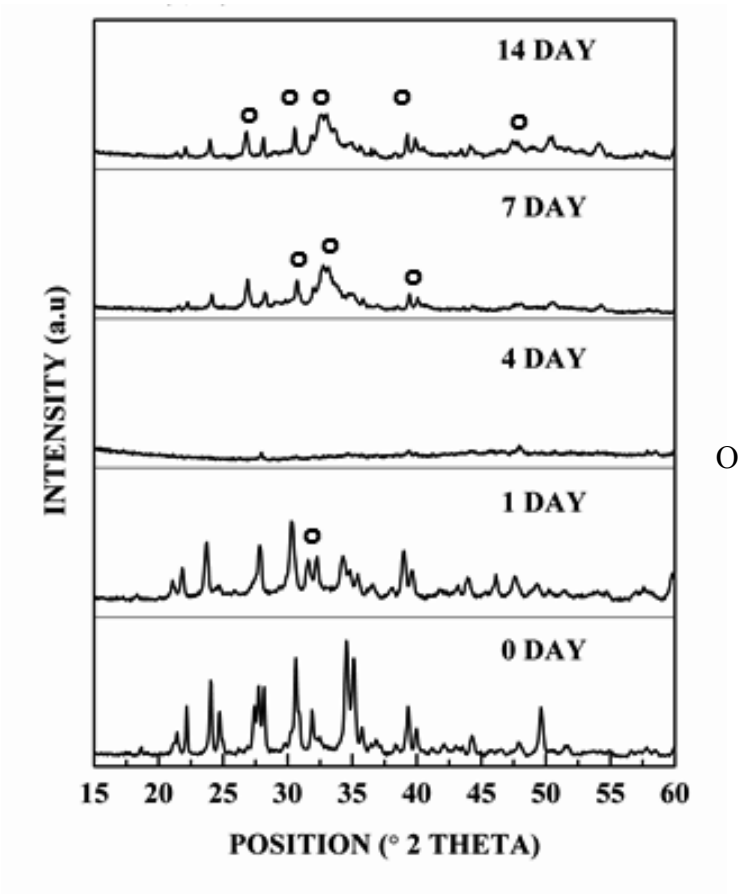

Fig – 4.19.4 (a) Surface phase analysis of SBF immersed 45S5 (050) scaffolds

Fig -4.19.4 (a) shows the surface phase analysis of 45S5 (050) scaffolds immersed in SBF for 1, 4, 7 & 14 days. After first day of immersion, a minor trace of carbonated hydroxyapatite phase had been identified. On the fourth day, the surface of the 45S5 scaffold becomes amorphous due to the formation of amorphous calcium phosphate. Due to crystallization, after 7 days of immersion, carbonated hydroxyapatite phase is formed. After 14 days of immersion, the carbonated hydroxyapatite phase is predominantly distributed all over the surface of the 45S5 (050) scaffold. The carbonated hydroxyapatite - **$Ca_{10}(PO_4)_3(CO_3)_3(OH)_2$** had been matched by the JCPDS pattern 19-0272.

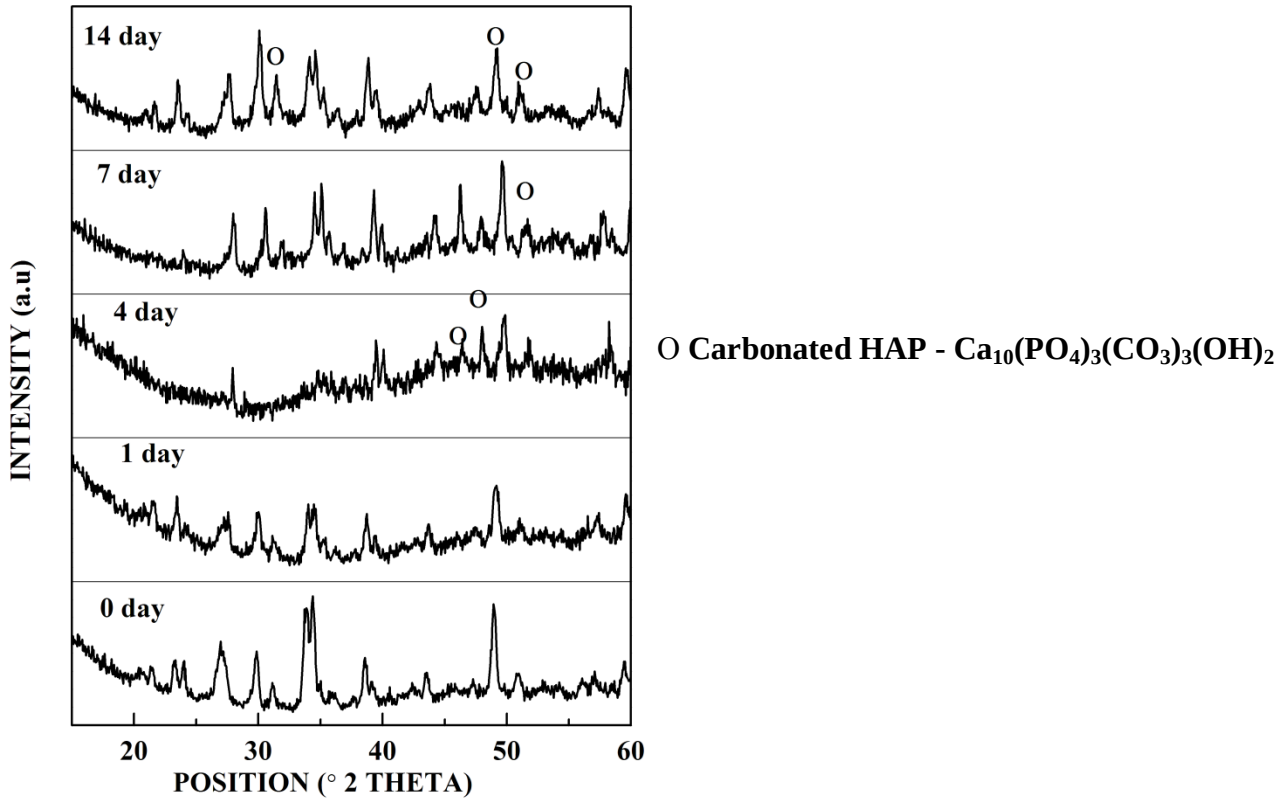

Fig – 4.19.4 (b) Surface phase analysis of SBF immersed 2P (050) scaffolds

Fig – 4.19.4 (b) shows the phase analysis of SBF soaked 2P (050) scaffolds. The carbonated hydroxyapatite phase had originated after 4 days of immersion in SBF. The phase after the 4^{th} day of immersion shows partial amorphous calcium phosphate formation. After 7 days of immersion, there is no development in the growth and regeneration, which results with a minor phase of carbonated hydroxyapatite phase. After 14 days of immersion, the carbonated hydroxyapatite phase had been increased, but still it is in the development stage. The carbonated hydroxyapatite - $\mathbf{Ca_{10}(PO_4)_3(CO_3)_3(OH)_2}$ had been matched by the JCPDS pattern 19-0272.

Fig – 4.19.4 (c) shows the phase analysis of SBF soaked 4P (050) scaffolds.

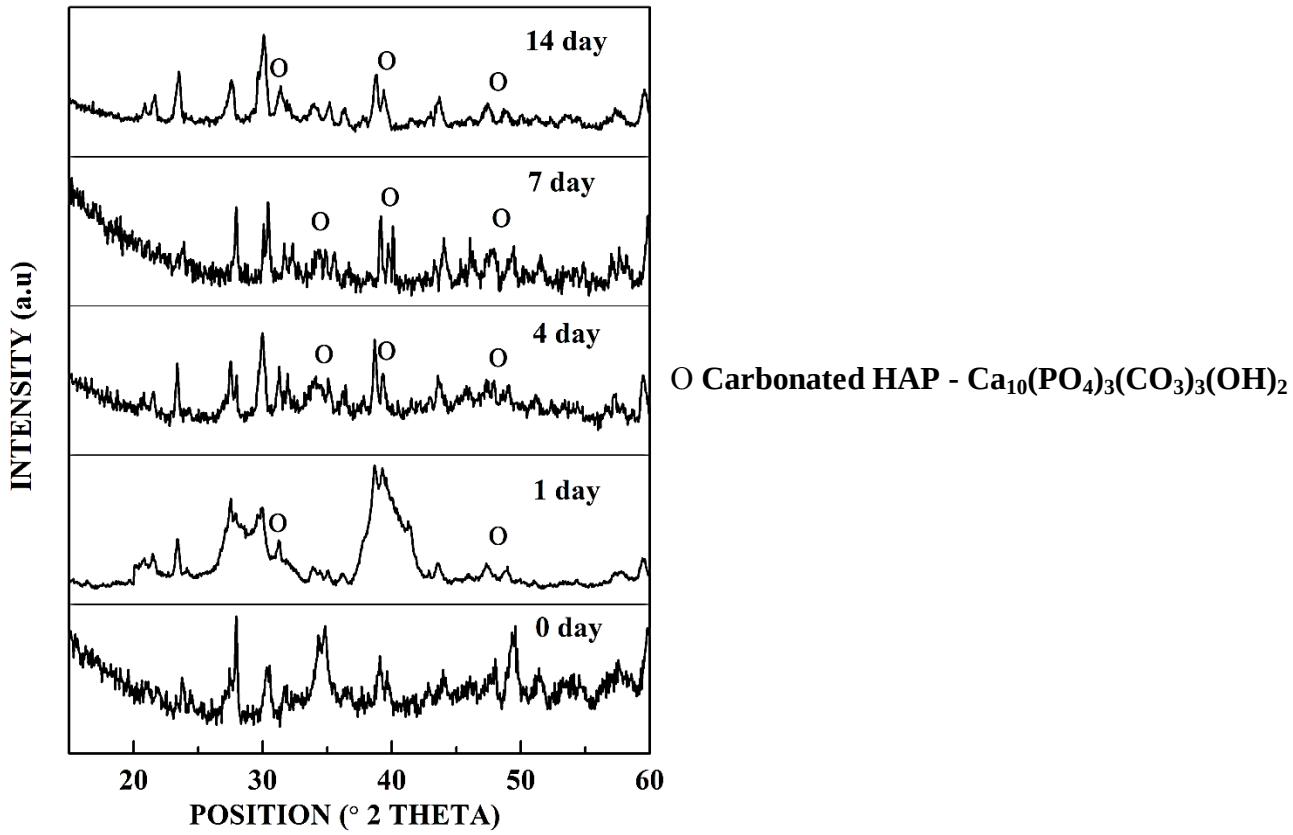

Fig – 4.19.4 (c) Surface phase analysis of SBF immersed 4P (050) scaffolds

Fig – 4.19.4 (c) shows the surface phase analysis of SBF immersed 4P(050) scaffolds. After first day of immersion, minor phase of carbonated hydroxyapatite phase had been formed. Partial amorphous calcium phosphate formation is evident after the first day of immersion. After 4 days, there is no development or growth of phase had been formed. The carbonated hydroxyapatite - **$Ca_{10}(PO_4)_3(CO_3)_3(OH)_2$** had been matched by the JCPDS pattern 19-0272.

On an overall comparison, 45S5 based functionally graded scaffolds shown highly matured carbonated hydroxyapatite morphology in its microstructure, at the end of 14 days, in invitro - SBF analysis. Whereas the growth of the carbonated hydroxyapatite on 4P and 2P based scaffolds is not distinctly evident as in 45S5. The phase analysis had shown the deposition of carbonated hydroxyapatite on all the three glass compositions.

O.Peitl et al **[78]** had clearly illustrated that amount of phosphate ions present in the solid solution (during invitro analysis) plays the vital role on the rate of Carbonated Hydroxyapatite deposition. Hence due to insufficient P_2O_5, we can conclude that carbonated hydroxyapatite formation on 4P and 2P based scaffolds are immature or it can be said that they are under development.

4.19 INVITRO ANALYSIS ON FGS BY USING MG-63 CELL LINE

MG-63 cells had been seeded on the functionally graded scaffolds to determine cell viability and cell adherence. By using MTT Assay, the cell viability on the FGS had been determined.

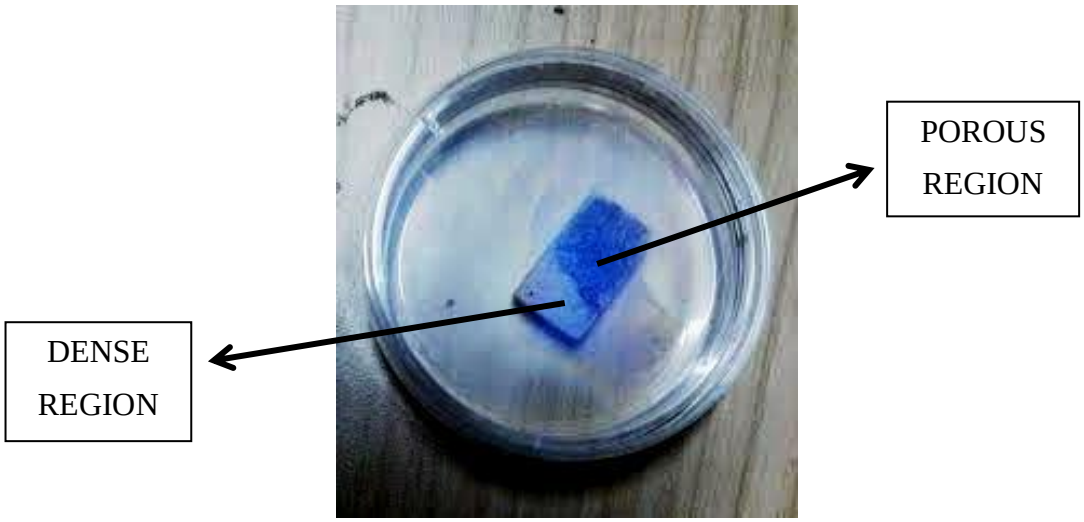

Fig – 4.20 (a) MG – cell seeded FGS after addition of MTT Assay

When the MTT Assay is added on the cell seeded scaffolds, due to mitochondrial reductase, farmazon compounds had been formed, which had been indicated by blue color precipitates on the scaffolds. Since the farmazon compound formation had been initiated by the viable mitochondria, the optical densities of the farmazon compounds are directly proportional to the viable cells. Fig – 4.20 (a) shows the condition of the MG- 63 cell seeded scaffold after addition of MTT Assay. The blue color intensity is predominantly high in the porous region than the dense region. This clearly shows that the cell viability is more in the porous region than the dense region of the FGS. In the biological systems, cell proliferation is restricted on the cortical bone layer; rather it provides attachment points for the adsorption of proteins and other biomolecules. The cancellous bone layer provides feasibility for cell proliferation and cell growth due highly porous architecture. The same scenario had been depicted with this FGS. The effective cell viability of entire FGS had been evaluated and illustrated in Fig – 4.20 (b).

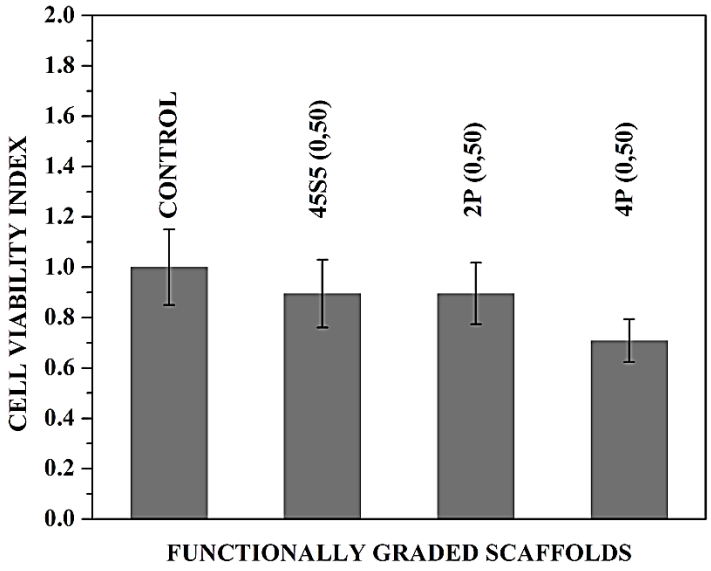

Fig – 4.20 (b) Cell viability of functionally graded scaffolds

All the functionally graded scaffolds showed cell viability less than the control. This is due to the restriction cell movement through the dense region. 2P (050) scaffold survived with more or less equal amount of viable cells. But in the case of 4P (050) scaffold, it had shown less cell viability than the others. The phase contrast microscopic images of cell seeded scaffolds had been illustrated in fig – 4.20 (c).

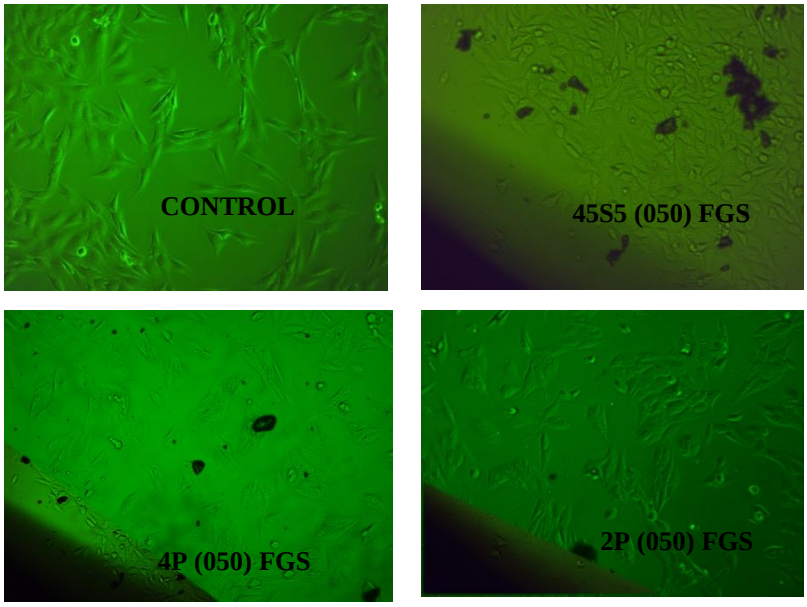

Fig – 4.20 (c) Phase contrast images of MG-63 cell seeded FGS

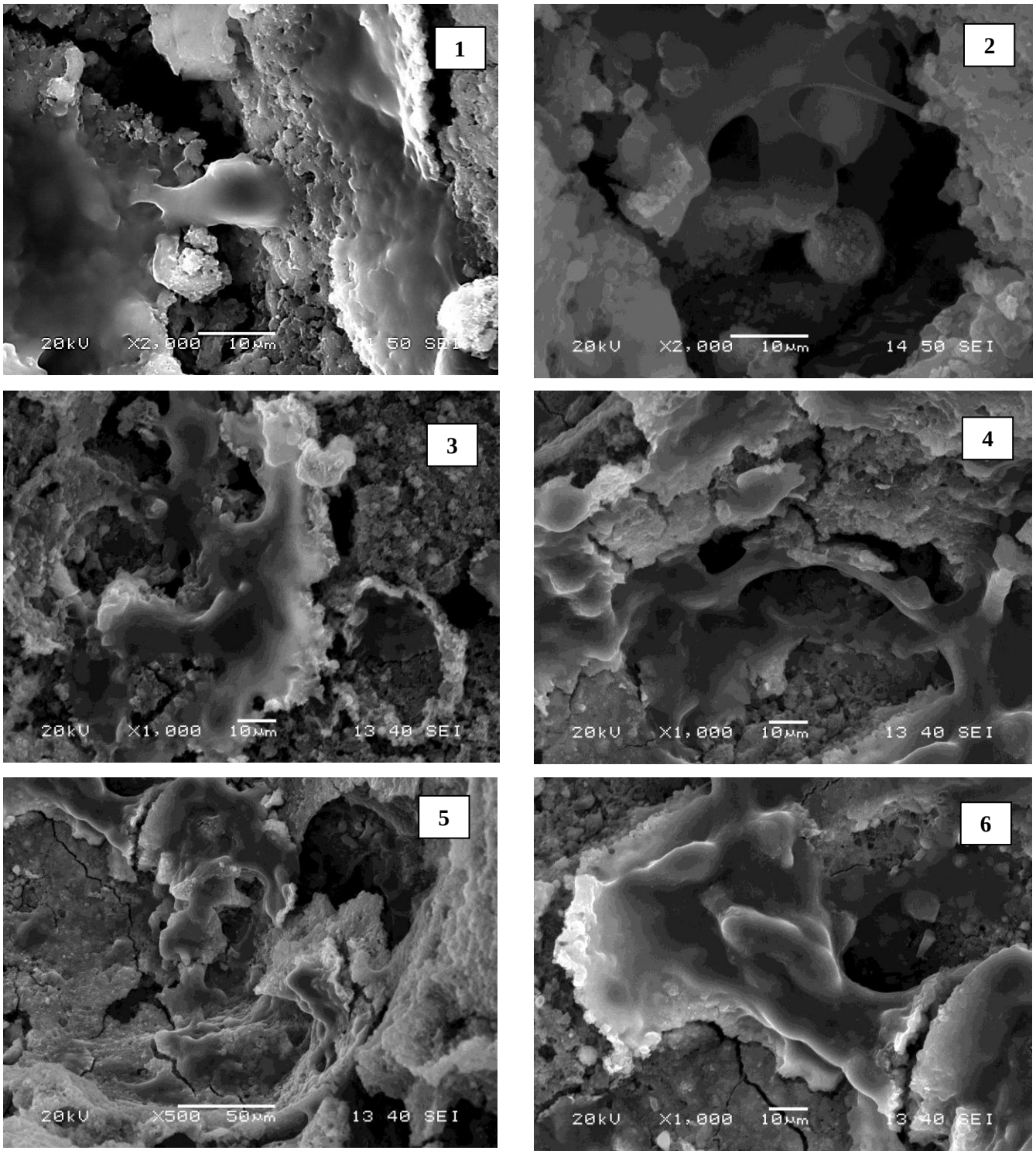

Fig – 4.20 (d) SEM images of MG-63 cell seeded 45S5(050) FGS

After incubation for 1 day, the MG-63 cell seeded functionally graded scaffolds had been fixed with glutraldehyde. Fig – 4.20(d) shows the SEM images of cell seeded on 45S5 (050) scaffolds. These microstructures show that the cells are adhered perfectly on the surface of the scaffolds. The Fig-4.20(d) -1 shows the penetration of cells into the pores. Fig-4.20(d) -2 depicts the development of tail and attaching itself via the circumference of the pore. Fig-4.20(d) -3 shows the cell adherence on the dense surface of the scaffold. Fig-4.20(d) -4 shows the cells entering the pore interconnectivity. Fig-4.20(d) -5 & Fig-4.20(d) – 6 shows the cell to cell attachment within the pores.

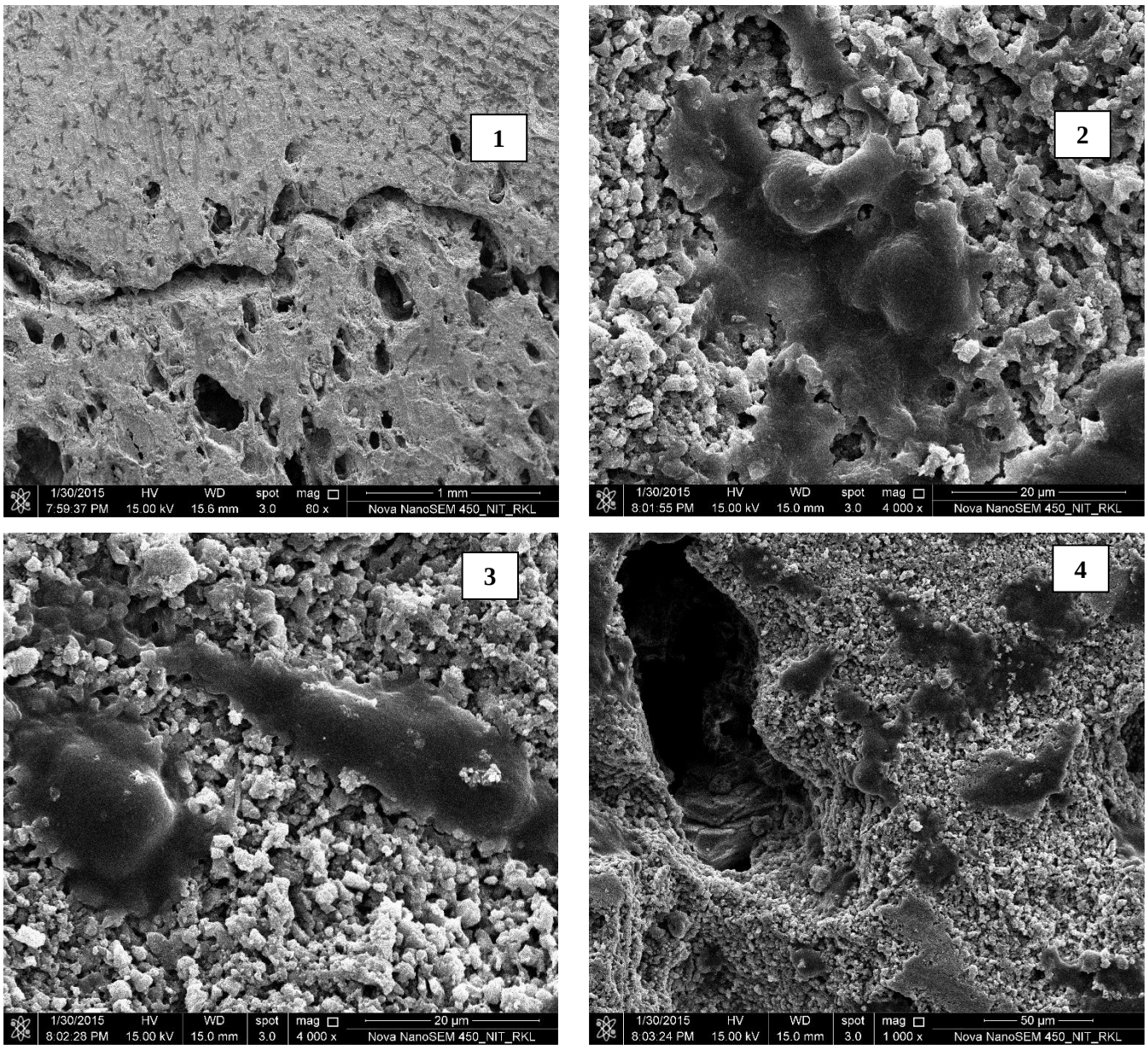

Fig – 4.20 (e) FESEM images of MG-63 cell seeded 45S5(050) FGS

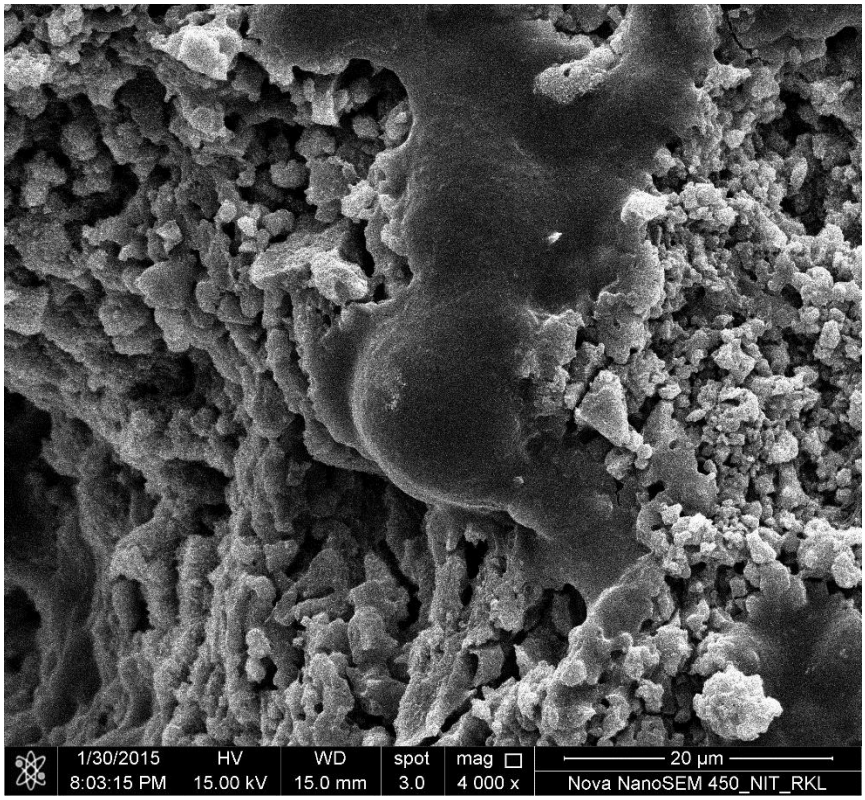

Fig – 4.20 (f) FESEM image of MG-63 cell travelling into the pores of 45S5(050) FGS

Fig – 4.20 (e) - 1 shows the FESEM image of MG-63 cell seeded 45S5 (050) FGS. Fig – 4.20 (e) – 2 shows the cells adhered on the rough surface of the scaffolds. Fig – 4.20 (e) – 3 shows the spherical and elongated cells adhered on the dense region. Fig – 4.20 (e) – 4 shows the cells trying to enter into the pores of the scaffold. Fig – 4.20 (f) depicts the cells travelling into the pore cavity. These microstructures clearly illustrates that the architecture of the scaffolds had not interrupted the cell movement. Due to the high biocompatible environment provided by the scaffold, pronounced cell adherence and cell movements had been observed.

4.20 CONCLUSIONS

In this present work, three bioactive glass compositions had been taken namely 45S5 (6wt. % P_2O_5), 2P (2wt. % P_2O_5) and 4P (4wt. % P_2O_5). These bioactive glass compositions had been prepared by using melt quench method. For the first time, Functionally graded scaffolds had been prepared with these bioactive glass compositions by using simple uniaxial pressing and sintering method. The architecture of the functionally graded bioactive glass ceramic scaffolds had been designed in such a way that the porous region and the dense region are at the center and the periphery respectively.

Before evaluating the performance of functionally graded bioactive glass ceramic scaffolds, each bioactive glass compositions had been fabricated as single layer – dense and single layer - porous scaffolds. By using Naphthalene as a pore former (0 wt.%, 30 wt.% and 50 wt.%) the single layer scaffolds had been uniaxial pressed and sintered at 800°C, 850°C and 900°C. Apparent Porosity, Bulk density, diametral tensile strength and flexural strength had been evaluated for single layer porous bioactive glass ceramic scaffolds. Then the functionally graded bioactive glass ceramic scaffolds had been prepared by uniaxial pressed and sintered at 800°C, 850°C and 900°C. During the course of the fabrication and characterization of single layer and FGS, the following conclusions had be made:

- The melt derived bioactive glasses – 45S5, 2P and 4P had undergone DSC-TG analysis. It had been observed from the thermal analysis that when the amount of P_2O_5 increases, the proportion of Q3 species had also increases, which results in pronounced crystallization.
- The sintering behavior of 45S5, 2P and 4P bioactive glass compacts had been investigated by dilatometric analysis. The degree of polymerization aroused early on 2P bioactive glass than the other two bioactive glass compositions, which results in better densification for 2P than 45S5 and 4P. The sintering had been initiated within 750°C to 800°C for all the three bioactive glass compositions
- Sintering had been carried out at 800°C, 850°C and 900°C to observe different glass ceramic phase formation. $Na_4Ca_4Si_6O_{18}$ (75-1686) and $Na_2Ca_3Si_6O_{16}$ (77-0386) are the major crystallization phases observed on post sintering. $Na_2Ca_4(PO_4)_2SiO_4$ (33-1229) phase had also been appeared as a minor phase of the glass ceramic system due to phase separation and simultaneous crystallization. No major phase transformation had been occurred when the sintering temperature rises from 800°C to 850°C and 900°C.

- On post sintering, without pore formers, approximately 31-33 vol.% of Apparent porosity had been recorded for Single layer - 45S5 bioactive glass ceramic scaffolds. Whereas in the case of 2P and 4P, approximately 0-0.5 vol.% and 39-42 vol.% of apparent porosity had been attained respectively. Due to the delayed polymerization in 45S5 and 4P bioactive glass scaffold, the efficient densification had not been attained.
- The diametral tensile strength of Single layer – 45S5 bioactive glass ceramic scaffolds, without pore former, had been observed approximately 6-9 MPa on different sintering temperatures. With 30wt.% pore former, on post sintering, they attained 3-4 MPa of diametral tensile strength. Similarly, with 50wt.% of pore former, it attained 1-1.4 MPa. Approximately (10-14) MPa, (9-10) MPa & (6-7.5) MPa of diametral tensile strength had been recorded for 2P bioactive glass ceramic scaffolds with 0 wt.%, 30wt.% & 50wt.% of pore former inclusion respectively. Approximately (5-6) MPa, (4-5.5) MPa and (0.9-1.3) MPa of diametral tensile strength had been recorded for the 4P bioactive glass ceramic scaffolds with 0 wt.%, 30wt.% & 50wt.% of pore former respectively. On a whole, 2P based porous single layer scaffolds registered a better diametral tensile strength than the 45S5 and 4P based scaffolds.
- The similar trend of diametral tensile strength had been followed with flexural strength of 45S5, 2P and 4P based single layer porous scaffolds. On different sintering temperatures, (7.5-12) MPa, (3.5-5.1) MPa and (1.1-1.9) MPa of flexural strength had been observed with 45S5 porous single layer scaffolds with 0wt.%, 30wt.% and 50wt.% pore former addition respectively. Similarly, (24.5-37.5) MPa, (20-32) MPa and (14.4-23.3) MPa of flexural strength had been recorded for 2P bioactive glass ceramic scaffolds with 0wt.%, 30wt.% and 50wt.% pore former addition respectively. Approximately, (4.35-10.15) MPa, (3.8-9.4) MPa & (0.8-2.2) MPa of flexural strength had been observed with 4P based single layer porous scaffolds with 0wt.%, 30wt.% and 50wt.% pore former addition respectively. The better flexural strength had been observed with 2P based porous single layer scaffolds.
- These bioactive glass and glass ceramics are highly hemocompatible, as all the samples recorded hemolysis of less than 5%. The cell viability of MG-63 cells on these bioactive glass and glass ceramics are better than the cell viability of the control. The protein adsorption profiles of the bioactive glass and glass ceramics recorded within the range of 45-60mg of BSA per mg of sample.

On a whole, the biological invitro characterization shows better compatibility results, which ensures that better biological recognition can be attained when the scaffolds had been made out of these materials.

- As the characterization of single layer scaffolds had been carried out, the fabrication of FGS had been done by uniaxial pressed and sintering method. The apparent porosity and bulk density of the entire FGS had been evaluated. This evaluation provides effective apparent porosity and effective bulk density of both dense and porous regions. Approximately (38-42) vol.% and (44-48) vol.% of effective apparent porosities had been observed on 45S5 (030) and 45S5(050) FGSs respectively. (15-18) vol.% and (26-27)vol.% of effective apparent porosities had been recorded on 2P(030) and 2P(050) FGSs respectively. Approximately (45-47.5) vol.% and (53-54.5) vol.% of apparent porosities had been observed with 4P(030) and 4P(050) FGSs respectively. 2P(030) is FGS with low porosity and 4P(050) FGS attains high amount of porosity.
- The outer dense and inner porous regions had been cut and carved out. The apparent porosity and bulk density of those scaffold parts had been evaluated. Approximately, (29.6-32.2) vol.% and (52.2-52.35) vol.% of apparent porosity had been recorded in outer and inner regions of 45S5 (030) FGS respectively. For 45S5 (050) FGS, (28.5-34.7) vol.% and (58-63) vol.% of apparent porosity had been recorded in outer and inner region of the scaffold respectively. Approximately (3.1-5.7) vol.% and (34.1-54.1) vol.% of apparent porosity had been attained on outer and inner region of 2P (030) FGS respectively. For 2P (050) FGS, (1.9-3.5) vol.% of apparent porosity on outer layer and (32.9-49.8) vol.% of apparent porosity on inner layer had been observed. In the case of 4P (030) FGS, (36.6-37.9) vol.% and (50.7-53.2) vol.% of apparent porosities had been recorded on outer layer and inner layer respectively. Almost (38-42) vol.% and (52-64) vol.% of apparent porosities had been recorded on the outer and inner layer of the 4P(050) FGS respectively.
- The composition of Single layer 45S5 (0 wt.%) scaffold occupies the outer layers of 45S5(030) and 45S5(050) FGS. Thus, the apparent porosity of single layer scaffolds can be compared with the graded layers with a similar composition. And again 2P (0wt.%) can be compared with the outer layers of 2P (030) and 2P (050) FGS scaffolds. Similarly, single layer scaffolds are compared with the graded layers of similar composition. Even though the sintering mechanism of single layer scaffolds and FGS are different, as FGS has differential shrinkage issues, there is no drastic difference between these apparent porosities.

- To determine splitting tensile strength of the FGSs, Brazilian disc analysis had been carried out. Beyond the peak load, the applied force drops and again tends to increase. This feature had been seen due to the porosity gradient architecture. The crack propagates and the deflection travels from dense region to the porous region and again enters a dense region. 6.15MPa, 1.31 MPa, 6.59 MPa, 3.69 MPa, 2.13 MPa and 0.81 MPa are the calculated splitting tensile strength for 45S5(030), 45S5(050), 2P(030), 2P(050), 4P(030) and 4P(050) respectively. Among these 2P based FGSs have better splitting tensile strength than the other FGSs.
- Invitro analysis of FGSs, by immersing in SBF, had been carried out. Better stage by stage morphological development of carbonated hydroxyapatite had been observed with 45S5 based FGS, within a period of 14 days. 2P and 4P based FGS scaffolds shows minimal deposition of carbonated hydroxyapatite. Here it can be concluded that 45S5 shows better deposition of carbonated hydroxyapatite particles than the 2P and 4P based scaffolds.
- By using MG-63 cell line, the invitro analysis on FGSs had been carried out. After addition of MTT on MG-63 seeded FGS, the surface of the scaffolds will change into blue color due to the formation of farmazon compounds. The optical density of the Farmazon compound will be directly proportional to the viable cells present in the well. The intensity of the blue color is high in the porous region than the dense region. This shows that the cell viability is high in the porous region than the dense region of the FGSs. And hence the biomimetic approach is well established with these FGSs.
- MG-63 cells had been seeded on FGS and microstructures had been taken. The cell adherence, cell penetration via the pores had been evidently visible with the microstructures. This shows that the porosity evolved in the FGS had established a better feasibility for biological mechanisms.
- On comparing the 45S5, 2P and 4P based FGSs, 2P based FGSs performs better in mechanical characterization and 45S5 based FGSs performs better in overall biological characterization.

4.21 FUTURE WORKS

- Increasing the overall strength of the FGS
- To study the relationship between the degree of interconnectivity and bioactivity on FGS.
- Incorporation of dissimilar materials for outer and inner layers of FGS
- Introduction of more than two layers to the FGS

4.22 REFERENCES

1. Principles of Human Anatomy, G. J.Tortora & Mark T. Nielson, 12th edition, ISBN 13 978-0470-56705-0
2. Athanasiou KA, Zhu C-F, Lanctot DR, Agrawal CM, Wang X, Tissue Eng 2000; 6: 361-381
3. J.O.Hollinger & J.C.Kleinschmidt, Journal of Craniofacial Surgery,vol.1,no.1,pp.60–68,1990
4. L.L.Hench, 2nd edition, ISBN 978-1-908977-15-1, World Scientific, 1993.
5. L.L.Hench, Biomaterials 19 (1998) 1419—1423
6. Basic Knowledge of Bone grafting, N.N.Hung, Ch-2 (2012), ISBN: 978-953-51-0324-0, InTech.
7. http://www.uofmchildrenshospital.org/index.htm
8. http://www.nlm.nih.gov/medlineplus/ency/imagepages/18023.htm
9. R.P.Lanza, R.Langer & Joseph Vacanti, Academic Press, 2000, ISBN 9780080539676
10. L.L.Hench, D.E.Day et al, Int J of Appl Glass Sci 1 [1] 104–117 (2010)
11. T. V. Thamaraiselvi & S. Rajeswari, Trends Biomater. Artif. Organs, Vol 18 (1), pp 9-17 (2004)
12. L.L.Hench, Int. J. Non-Cryst. Sol. **1** (1970) 250
13. Kelly Alvarez & Hideo Nakajima, Materials 2009,2, 790-832; ISSN 1996-1944
14. S.Bose & G.Fielding et al, Trends in Biotechnology, October 2013, Vol. 31, No. 10
15. M. Navarro, A.Michiardi, O.Castano & J.A.Planell, J. R. Soc. Interface (2008)5, 1137–1158
16. A.R.Amini, C.T.Laurencin & S.P.Nukavarapu, Crit Rev Biomed Eng. 2012; 40(5): 363–408.
17. A.M.Martins, C.M.Alves et al, J. Mater. Chem., 2010, 20, 1638–1645
18. R.Murugan & S.Ramkrishna, TISSUE ENGINEERING Volume 12, Number 3, 2006
19. L.L.Hench, R. J. Splinter, T. K. Greenlee & W.C.Allen, J. Biomed. Mater. Res. (1971) 117
20. L.L.Hench, A. E. Clark Jr & and H.F.Schaake, Int.J. Non-Cryst. Sol. 8–10, **(**1972)837
21. L.L.Hench & Ethridge EC, New York: Academic Press, 1982.
22. Greenspan, D.C., 1999, Medical Device and Diagnostics Industry, p. 150
23. L.L.Hench, J Mater Sci: Mater Med (2006) 17:967–978
24. P.N.De Aza et al, Bol. Soc. esp. Ceram. V., 46 [2]45-55 (2007)
25. J.R.Jones, Acta Biomaterialia 9 (2013) 4457–4486
26. Jacques Livage, Current Opinion in Solid State & Materials Science 1997, 2:132-138
27. A.L.Girot, F.Z.Mezahi et al, Journal of Non-Crystalline Solids 357 (2011) 3322–3327
28. D.W.Hutmacher, Biomaterials 21 (2000) 2529}2543
29. Fergal J. O'Brien, Materials Today (March 2011) Vol 14: No-3; ISSN:1369 7021
30. Brekke JH, Tissue Eng 1996;2(2):97}114
31. B. P. Chan & K. W. Leong, Eur Spine J (2008) 17 (Suppl 4):S467–S479.
32. C. Mauli Agrawal & Robert B. Ray, J Biomed. Mat. Res. 2001, 55(2): 141-150.

33. Felicity R. A. J. Rose & Richard O. C. Oreffo, Biochem & Biophy Res Comm 292,1–7 (2002).
34. Kuboki Y, Takita H, Kobayashi D, Tsuruga E et al, J Biomed. Mater. Res. 1998;39(2):190–9.
35. J.R.Jones & L.L.Hench, Current Opinion in Solid State and Materials Science, 7 (2003) 301–307.
36. Vassilis Karageorgiou & David Kaplan, Biomaterials 26 (2005) 5474–5491.
37. J.R. Jones, Lisa M. Ehrenfried & L.L.Hench, Biomaterials 27 (2006) 964–973.
38. K. Rezwan, Q.Z. Chen, J.J. Blaker & Aldo Roberto Boccaccini, Biomaterials 27 (2006) 3413–3431
39. Q.Z. Chen, Yuan Li, Li-Yu Jin, J.M.W.Quinn & P.A.Komesaroff, Acta Biomaterialia 6 (2010) 4143–415
40. A.Balamurugan, G.Sockalingum, J.Michel, J.Fauré et al, Materials Letters 60 (2006) 3752–3757
41. A.L.Girot, F.Z.Mezahi, M.Mami, H.Oudadesse et al, J of Non-Cryst.Solids 357 (2011) 3322–3327
42. P. Sepulveda, J. R. Jones & L.L. Hench, J Biomed Mater Res. 2001;58(6):734-40.
43. P. Sepulveda, J. R. Jones & L.L. Hench, J Biomed Mater Res. 2002 Aug;61(2):301-11.
44. Marivalda M. Pereira, Arthur E. Clark and Larry L. Hench, J Am Ceram Soc. 1995;78(9):2463–8
45. L.L.Hench & Michael M. Walker, Patent no: US4171544 A, 1979.
46. Qiang Fu, Eduardo Saiz, M.N.Rahaman & A.P.Tomsia, Mat Sci and Eng C 31 (2011) 1245–1256
47. Qiang Fu, Rahaman MN, Bal BS, Huang W & Day DE, J Biomed. Mater. Res. 2007;82A:222–9
48. Li P, Zhang F & Kokubo T, J Mater Sci Med 1992;3:452–6.
49. Oscar Peitl Filho, Guy P. LaTorre & L.L.Hench, J Biomed Mat Res, Vol. 30, 509-514 (1996)
50. Francesco Baino & Chiara Vitale-Brovarone, J Biomed. Mat. Res. A|15 Jun 2011 Vol. 97A, Issue 4.
51. Qizhi Z. Chen, Ian D. Thompson & Aldo R. Boccaccini, Biomaterials 27 (2006) 2414–2425
52. W. Pompea, H. Worch, M. Epple, W. Friess et al, Materials Science and Engineering A362 (2003) 40–60
53. Tampieri A, Celotti G, Sprio S, Delcegliano A, Franzese S., Biomaterials 2001;22:1365–70.
54. Cevat Erisken, Dilhan M. Kalyon*& Hongjun Wang, Biomaterials 29 (2008) 4065–4073.
55. Young-Mi Soon, Kwan-Ha Shin, Young-Hag Koh et al, J of the Euro Cera Society 31 (2011) 13–18.
56. Changqing Hong, Jiancong Du, Jun Liang et al, Ceramics International 37 (2011) 3717–3722
57. Y. H. Hsu, I. G. Turner & A. W. Miles, J Mater Sci: Mater Med (2007) 18:2251–2256
58. Lydia Helena Wong & Betty Tio, Xigeng Miao, Materials Science and Engineering C 20 (2002) 111– 115
59. C.vitale-brovarone, F.Baino & E.Verne, J Biomater Appl 2010 24:693.
60. J. Wernera, B.Linner-Krcmar, W.Friess & P.Greil, Biomaterials 23 (2002) 4285–4294
61. Oscar Peitl, E.D.Zanotto, F.C.Serbena & L.L.Hench, Acta Biomaterialia 8 (2012) 321–332
62. X.Xiang Xu, Xing-hua Gao, R.Pan, Dan Lu & Yue Dai, Cytotechnology (2010) 62:17–2
63. P.A. Ramires, A. Romito, F. Cosentino & E. Milella, Biomaterials, 22 (2001) 1467-1474
64. K.Kandori, T.Shimizu, A.Yasukawa & T.Ishikawa, Coll & Surfa B: Biointerfaces 5(1995) 81- 87
65. E.Mavropoulos, A.M.Costa, L.T.Costa, C.A.Achete et al, Coll & Surfa B: Biointerfaces, 83 (2011) 1-9
66. D. Gan & L.A.Lyon, Macromolecules, 35 (2002) 9634-9639

67. K. Pal, S. Pal, Materials and Manufacturing processes, 21 (2006) 325-328.
68. E.G.Mota, H.M.S.Oshima, L.H.Burnett Jr et al, Stomat. Baltic Dent & Maxillo Jo 8:67- 9, 2006
69. ASTM International, designation D3967-08.
70. T. kokubo, Acta. Mater. 46 (1998) 2519-2527.
71. T. Kokubo & H.Takadama, Biomaterials 27 (2006) 2907-2915
72. A.C. Tas, Biomaterials 21 (2000) 1429-1438.
73. J.E.Gough, J.R.Jones & L.L.Hench, Biomaterials 25 (2004) 2039–2046
74. A.Aline, R.Oliveira, D.Alves de Souza et al, Biomed. Mater. 8 (2013) 025011
75. C. Rey, M. H. Kim, L. Gerstenfeld, and J. M. Glimcher, Connect Tissue Res. 35, 343 (1996).
76. I. Rehman and W. Bonfield, J. Mater. Sci., Mater. Med. 8, 1 (1997).
77. Socrates, G. (2001). Infrared and Raman Characteristic Group Frequencies—Tables and Charts, John Wiley & Sons Inc., ISBN 978-0-470-09307-8, Hoboken, USA
78. Peitl O, Zanotto ED, Hench LL. Highly bioactive P_2O_5–Na_2O–CaO–SiO_2 glass–ceramics. J Non-Cryst Solids 2001;292:115–26.
79. N.A. Zarifah a, W.F. Limb et al, Journal of Non-Crystalline Solids 412 (2015) 24–29